

Development of A Dynamic Model For Vibration During Turning Operation And Numerical Studies

Thesis submitted in accordance with the requirements of the
University of Liverpool for the degree of Doctor in Philosophy

By

Nurhafizzah Hassan

March 2014

To Khairil and Faris

Abstract

Turning operation is a very popular process in producing round parts. Vibration and chatter noise are major issues during turning operation and also for other machining processes. Some of the effects of vibration and chatter are short tool life span, tool damage, inaccurate dimension, poor surface finish and unacceptable noise. The basic dynamic model of turning operation should include a rotating work piece excited by a force that moves in the longitudinal direction. Dynamic interaction between a rotating work piece and moving cutting forces can excite vibration and chatter noise under certain conditions. This is a very complicated dynamic problem. Vibration and chatter in machining is one example of moving load problems as the cutter travels along the rotating work-piece. These moving cutting forces depend on a number of factors and regenerative chatter is the widely accepted mechanism and model of cutting forces which then introduce time delays in a dynamic model.

In this investigation, the work piece is modelled as a rotating Rayleigh beam and the cutting force as a moving load with time delay based on the regenerative mechanism. The mathematical model developed considers work piece and cutting tools both as a flexible. Without doubt, this dynamic model of vibration of work piece in turning operation is more realistic than previous ones as the dynamic model has multiple-degrees-of-freedom and considers the vibration of the cutter with regenerative chatter. It is found that the cutting force model of regenerative chatter which introduces time delay in a dynamic model leads to interesting dynamic behaviour in the vibration of rotating beams and a sufficient number of modes must be included to sufficiently represent the

dynamic behaviour. The effects of depth of cut, cutting speed and rotational speed on the vibration and chatter occurrence are obtained and examined. Simulated numerical examples are presented. These three different parameters are vital and definitely influence the dynamic response of deflection in the y and z directions. The depth of cut is seen to be the most influential on the magnitude of the deflection. In addition, higher cutting speed combined with high depth of cut promotes chatter and produces a beating phenomenon whereas rotational speeds have a moderate influence on the dynamic response. Furthermore, several turning experiments are conducted that demonstrate vibration and chatter in the machining operations. There is fairly good qualitative agreement between the numerical results and the experimental ones.

Acknowledgements

The author is extremely grateful and appreciative to all the contributions made and advices given that has made this work possible. In particular acknowledgements are given to the following people and organisations.

First and foremost, to my supervisors, **Professor Huajiang Ouyang**, whose encouragement, guidance and invaluable supports from the very beginning of my PhD study. Without his continuous encouragement and support, this doctoral thesis would not have been possible. His wide knowledge and logical way of thinking have been great value for me.

I would also like to thank my second supervisor **Prof. Westley Cantwell**, for his encouragement. My thanks also go to **Dr Simon James** and **Mr Steve Bode** for their great help on all the experimental works. Many thanks as well to **Mr. Xiangou Han**, **Mr. Eric** and **Professor Minjie Wang** for their valuable helps providing the experimental results. Without that the numerical results could not be validated properly.

Thanks must also go to my fellow researchers in the Dynamic and Control Group, including **John, Shahrir, Hamid and Yazdi** for giving me an outlet for my frustration.

Special appreciation for my husband, **Dr Rd. Khairilhijra** and my beloved son, **Rd. Faris Izharkhalish** as well as my family especially my parents who endured this long process with me, for constant support and unwavering faith throughout my PhD.

And finally, I would like to greatly acknowledge the support by the **Ministry of Education of Malaysia** and the **University of Tun Hussein Onn Malaysia (UTHM)**.

Contents

Abstract	iii
Acknowledgements	v
Contents	vii
List of Figures	xi
List of Tables	xiv
List of Symbols	xv
List of Abbreviations	xvii
1 INTRODUCTION	1
1.1 Introduction	1
1.2 Motivations	3
1.3 Research aim	5
1.4 Scope of the thesis	7
1.5 Organization of the thesis	9
2 LITERATURES REVIEW AND THEORY	11
2.1 Introduction	12
2.2 Turning operation	12
2.3 Vibration in machining	16
2.4 Chatter noise in machining	17
2.4.1 Mode coupling	21
2.4.2 Regenerative chatter	21
2.5 Regenerative chatter mechanism in turning operation	23
2.5.1 Chatter modelling theory	26
2.6 Introduction to moving loads problem	31
2.6.1 Moving loads with regenerative chatter in turning operation	32
2.7 Dynamic model of rotating beam subjected to moving loads	33

2.7.1	Introduction to beam theories	34
2.7.1.1	Euler-Bernouli beam	34
2.7.1.2	Rayleigh beam	35
2.7.1.3	Timoshenko beam	35
2.7.2	Previous dynamic model of a rotating beam/shaft	36
2.8	Factors influencing surface finish of turned metals	42
2.9	Chatter suppression in turning operation	50
2.10	Machining of composite	53
2.11	Factors influencing surface finish of turned composites	55
2.12	Chapter Summary	57
3	DYNAMIC MODEL OF TURNING OPERATION	59
3.1	Introduction	59
3.2	Development of mathematical formulation of Rotating Beam Subjected to Three Directional Moving Loads with Regenerative Chatter	60
3.2.1	Boundary Conditions	60
3.2.2	Energy method	63
3.2.3	Lagrange's equation	65
3.2.4	Three directional moving cutting forces with regenerative chatter mechanism	69
3.2.5	Improved dynamic model by adopting Insperger's cutting force model	73
3.2.6	Cutting Tool Equation of Motion	76
3.3	Elastic boundary condition	78
3.4	Methodology for Chatter Analysis / Numerical Integration methods in vibration analysis	84
3.4.1	Frequency Response Analysis	85
3.4.2	Transient Response Analysis	86
3.4.2.1	Runge-Kutta Method	87
3.4.2.2	Delay Differential Equations	89
3.5	Chapter Summary	91
4	EXPERIMENTAL MODAL ANALYSIS	93
4.1	Introduction	93
4.2	Basic components of experimental modal analysis (EMA)	97
4.2.1	Excitation of structure	98
4.2.2	Mechanism of sensing	100
4.2.3	Data acquisition and processing mechanism	101
4.3	Experimental modal analysis of metal and composite work piece	101
4.3.1	Free-free boundary	102
4.3.2	Clamped pinned boundary	109

4.4	Experimental modal analysis during machining of cylindrical metal work piece at DUT	116
4.5	Chapter summary	120
5	NUMERICAL SIMULATION RESULTS	122
5.1	Overview	122
5.2	Parametric studies	123
5.2.1	Clamped pinned (metal work piece)	123
5.2.1.1	Convergence test	123
5.2.1.2	Effect of depth of cut	127
5.2.1.3	Effect of cutting speed	135
5.2.1.4	Effect of rotational speed	140
5.2.2	Elastic boundary (chuck pinned for metal work piece)	144
5.2.2.1	Introduction	144
5.2.2.2	Convergence test	144
5.2.2.3	Effect of depth of cut	147
5.2.2.4	Effect of cutting speed	155
5.2.2.5	Effect of rotational speed	159
5.2.3	Clamped pinned (composite work piece)	166
5.3	Vibration test during turning operation	168
5.4	Chapter summary	173
6	ANALYSIS AND DISCUSSION	175
6.1	Parametric Studies	175
6.1.1	Clamped pinned (metal work piece)	175
6.1.1.1	Effect of depth of cut	176
6.1.1.2	Effect of cutting speed	177
6.1.1.3	Effect of rotational speed	178
6.1.2	Elastic boundary (chuck pinned – metal work piece)	178
6.1.2.1	Effect of depth of cut	179
6.1.2.2	Effect of cutting speed	180
6.1.2.3	Effect of rotational speed	180
6.2	Validation between numerical and experimental results	181
7	CONCLUSIONS AND FUTURE WORKS	183
7.1	Summary of Findings of the Investigation	183
7.2	Contribution to New Knowledge	186
7.3	Recommendations for Further Investigation	187
7.4	List of Publications	188
	REFERENCES	189
	APPENDIX	201

i.	Appendix A1 - Calculation of deflection, v and w for clamp-pinned boundary	207
ii.	Appendix A2 - Derivation of Delay Differential equation for clamp-pinned boundary	208
iii.	Appendix A3 - Time delay function	211
iv.	Appendix A4 - Determination of mode shape function for clamp-pinned boundary	212
v.	Appendix A5 - First derivation of mode shape function for clamp-pinned boundary	213
vi.	Appendix A6 - Second derivation of mode shape function for clamp pinned boundary	214
vii.	Appendix A7 - Calculation of cutting speed	215
viii.	Appendix A8 - Calculation of deflection, v and w for elastic Boundary	216
ix.	Appendix A9 - Derivation of Delay Differential equation for elastic boundary	219
x.	Appendix A10 - Determination of mode shape function for elastic boundary	221
xi.	Appendix A11 - First derivation of mode shape function for elastic boundary	222
xii.	Appendix A12 - Second derivation of mode shape function for elastic boundary	223
xiii.	Appendix A13 - Calculation of C_1 , C_2 , C_3 and C_4 variables	225

List of Figures

2.1	Conventional lathe machine at University of Liverpool.....	13
2.2	Schematic illustration of a turning operation	15
2.3	(a) Chatter mark	18
2.3	(b) Chatter mark on turned work piece.....	18
2.4	(a) Segmented chips	19
2.4	(b) Discontinuous chips	19
2.5	Regenerative chatter mechanism	24
2.6	Rotating shaft subjected to a moving load with three perpendicular forces	33
2.7	Torque and bending moment generated from P_x and P_z force components translated to the neutral axis	33
2.8	Elements of surface machine surface texture	43
3.1	Comparison between current dynamic model coordinate system and Insperger's coordinate system (a) current dynamic model coordinate system (b) Insperger's coordinate system	74
3.2	Example of one value of β_n showing the beam classical mode Shape	81
3.3	Graph of new fitted theoretical (marked by red) and measured (marked by blue) mode shapes for the chuck-tailstock	84
4.1	Route to vibration analysis	95
4.2	General layout of EMA	98
4.3	Impact Hammer	100
4.4	Accelerometer	101
4.5	Experimental set up for the cylindrical metal work piece of	

	free-free boundary	102
4.6	Apparatus used for modal testing (a) PCB impact hammer (b) Kistler accelerometer (c) 12 channels LMS system	103
4.7	A cylindrical metal work piece with its five measured locations	103
4.8	The experimental mode shapes of the cylindrical metal work piece for free-free boundary.....	106
4.9	The experimental mode shapes of the cylindrical composite work piece for free-free boundary	108
4.10	Modal test setup for cylindrical work piece in clamped-pinned boundary condition	109
4.11	Kistler accelerometer and Micro-epsilon laser sensor	110
4.12	The experimental mode shapes of the cylindrical metal work piece for clamp-pinned boundary	112
4.13	Responses from laser sensor showing the noise	113
4.14	Modal test setup for clamped-pinned boundary in y and z direction	115
4.15	Schematic illustration of the vibration test set-up	117
4.16	Two views of the experimental rig	118
5.1	Dynamic response of deflection, v (y direction) with (a) one mode (b) two modes (c) three modes (d) four modes (e) five modes. Note that the unit for x axis is time, t (s) and y axis is the dynamic response, m.....	125
5.2	Dynamic response of deflection, w (z direction) with (a) one mode (b) two modes (c) three modes (d) four modes (e) five modes. Note that the unit for x axis is time, t (s) and y axis is the dynamic response, m.....	126
5.3	Dynamic response of deflection, v at different depths of cut with one mode (cutting speed = 0.2228 m/s, the rotational speed = 1250 rev/min and the feed rate = 0.3 mm/rev).....	128
5.4	Dynamic response of deflection, w at different depths of cut with one mode (cutting speed = 0.2228 m/s, the rotational speed = 1250 rev/min and the feed rate = 0.3 mm/rev)	129
5.5	Dynamic response of deflection, v at different depths of cut with two modes (cutting speed = 0.2228 m/s, the rotational speed =	

	1250 rev/min and the feed rate = 0.3 mm/rev)	130
5.6	Dynamic response of deflection, w at different depths of cut with two modes (cutting speed = 0.2228 m/s, the rotational speed = 1250 rev/min and the feed rate = 0.3 mm/rev)	131
5.7	Phenomenon of beats	133
5.8	Dynamic response of deflection, v at different depths of cut with three modes (cutting speed = 0.2228 m/s, the rotational speed = 1250 rev/min and the feed rate = 0.3 mm/rev)	133
5.9	Dynamic response of deflection, w at different depths of cut with three modes (cutting speed = 0.2228 m/s, the rotational speed = 1250 rev/min and the feed rate = 0.3 mm/rev).....	134
5.10	Dynamic response of deflection, v at different depths of cut with four modes (cutting speed = 0.2228 m/s, the rotational speed = 1250 rev/min and the feed rate = 0.3 mm/rev).....	135
5.11	Dynamic response of deflection, w at different depths of cut with four modes (cutting speed = 0.2228 m/s, the rotational speed = 1250 rev/min and the feed rate = 0.3 mm/rev)	136
5.12	Dynamic response of deflection, v at different cutting speeds with one mode (depth of cut = 3.00 mm, rotational speed = 1250 rev/min and the feed rate = 0.3 mm/rev)	137
5.13	Dynamic response of deflection, w at different cutting speeds with one mode (depth of cut = 3.00 mm, rotational speed = 1250 rev/min and the feed rate = 0.3 mm/rev)	138
5.14	Dynamic response of deflection, v at different cutting speeds with two modes (depth of cut = 3.00 mm, rotational speed = 1250 rev/min and the feed rate = 0.3 mm/rev)	139
5.15	Dynamic response of deflection, w at different cutting speeds with two modes (depth of cut = 3.00 mm, rotational speed = 1250 rev/min and the feed rate = 0.3 mm/rev)	139
5.16	Dynamic response of deflection, v at different cutting speeds with three modes (depth of cut = 3.00 mm, rotational speed = 1250 rev/min and the feed rate = 0.3 mm/rev)	140
5.17	Dynamic response of deflection, w at different cutting speeds with three modes (depth of cut = 3.00 mm, rotational speed = 1250	

	rev/min and the feed rate = 0.3 mm/rev)	140
5.18	Dynamic response of deflection, v at different cutting speeds with four modes (depth of cut = 3.00 mm, rotational speed = 1250 rev/min and the feed rate = 0.3 mm/rev)	141
5.19	Dynamic response of deflection, w at different cutting speeds with four modes (depth of cut = 3.00 mm, rotational speed = 1250 rev/min and the feed rate = 0.3 mm/rev)	142
5.20	Dynamic response of deflection, v at different rotational speeds with one mode (depth of cut = 3.00 mm, cutting speed = 0.2228 m/s and the feed rate = 0.3 mm/rev)	143
5.21	Dynamic response of deflection, w at different rotational speeds with one mode (depth of cut = 3 mm, cutting speed = 0.2228 m/s and the feed rate = 0.3 mm/rev)	144
5.22	Dynamic response of deflection, v at different rotational speeds with two modes (depth of cut = 3.00 mm, cutting speed = 0.2228 m/s and the feed rate = 0.3 mm/rev)	145
5.23	Dynamic response of deflection, w at different rotational speeds with two modes (depth of cut = 3.00 mm, cutting speed = 0.2228 m/s and the feed rate = 0.3 mm/rev)	146
5.24	Dynamic response of deflection, v (y direction) with (a) one mode (b) two modes (c) three modes (d) four modes (e) five modes. Note that the unit for x axis is time, t (s) and y axis is the dynamic response, m	149
5.25	Dynamic response of deflection, w (z direction) with (a) one mode (b) two modes (c) three modes (d) four modes (e) five modes. Note that the unit for x axis is time, t (s) and y axis is the dynamic response, m	150
5.26	Dynamic response of deflection, v at different depths of cut with one mode (1250 rev/min, cutting speed = 2.228m/s and feed rate is 0.3 mm/rev)	152
5.27	Dynamic response of deflection, w at different depths of cut with one mode (1250 rev/min, cutting speed = 2.228m/s and feed rate is 0.3 mm/rev)	153
5.28	Dynamic response of deflection, v at different depths of cut with	

	two modes (1250 rev/min, cutting speed = 2.228m/s and feed rate is 0.3 mm/rev)	154
5.29	Dynamic response of deflection, w at different depths of cut with two modes (1250 rev/min, cutting speed = 2.228m/s and feed rate is 0.3 mm/rev)	155
5.30	Dynamic response of deflection, v at different depths of cut with three modes (1250 rev/min, cutting speed = 2.228m/s and feed rate is 0.3 mm/rev)	156
5.31	Dynamic response of deflection, w at different depths of cut with three modes (1250 rev/min, cutting speed = 2.228m/s and feed rate is 0.3 mm/rev)	157
5.32	Dynamic response of deflection, v at different depths of cut with four modes (1250 rev/min, cutting speed = 2.228m/s and feed rate is 0.3 mm/rev)	158
5.33	Dynamic response of deflection, w at different depths of cut with four modes (1250 rev/min, cutting speed = 2.228m/s and feed rate is 0.3 mm/rev)	159
5.34	Dynamic response of deflection, v at different cutting speed with one mode (depth of cut = 3.00 mm, rotational speed = 1250 rev/min and feed rate is 0.3 mm/rev)	160
5.35	Dynamic response of deflection, w at different cutting speed with one mode (depth of cut = 3.00 mm, rotational speed = 1250 rev/min and feed rate is 0.3 mm/rev)	161
5.36	Dynamic response of deflection, v at different cutting speed with two modes (depth of cut = 3.00 mm, rotational speed = 1250 rev/min and feed rate is 0.3 mm/rev)	162
5.37	Dynamic response of deflection, w at different cutting speed with two modes (depth of cut = 3.00 mm, rotational speed = 1250 rev/min and feed rate is 0.3 mm/rev)	162
5.38	Dynamic response of deflection, v at different cutting speed with three modes (depth of cut = 3.00 mm, rotational speed = 1250 rev/min and feed rate is 0.3 mm/rev)	163
5.39	Dynamic response of deflection, w at different cutting speed with three modes (depth of cut = 3.00 mm, rotational speed = 1250	

	rev/min and feed rate is 0.3 mm/rev)	163
5.40	Dynamic response of deflection, v at different cutting speed with four modes (depth of cut = 3.00 mm, rotational speed = 1250 rev/min and feed rate is 0.3 mm/rev)	164
5.41	Dynamic response of deflection, w at different cutting speed with four modes (depth of cut = 3.00 mm, rotational speed = 1250 rev/min and feed rate is 0.3 mm/rev)	164
5.42	Dynamic response of deflection, v at different rotational speed with one mode (depth of cut = 3.00 mm, cutting speed = 2.228 m/s and feed rate = 0.3 mm/rev)	165
5.43	Dynamic response of deflection, w at different rotational speed with one mode (depth of cut = 3.00 mm, cutting speed = 2.228 m/s and feed rate = 0.3 mm/rev)	166
5.44	Dynamic response of deflection, v at different rotational speed with two modes (depth of cut = 3.00 mm, cutting speed = 2.228 m/s and feed rate = 0.3 mm/rev)	167
5.45	Dynamic response of deflection, w at different rotational speed with two modes (depth of cut = 3.00 mm, cutting speed = 2.228 m/s and feed rate = 0.3 mm/rev)	168
5.46	Dynamic response of deflection, v at different rotational speed with three modes (depth of cut = 3.00 mm, cutting speed = 2.228 m/s and feed rate = 0.3 mm/rev)	169
5.47	Dynamic response of deflection, w at different rotational speed with three modes (depth of cut = 3.00 mm, cutting speed = 2.228 m/s and feed rate = 0.3 mm/rev)	170
5.48	Dynamic response of deflection, v at different rotational speed with four modes (depth of cut = 3.00 mm, cutting speed = 2.228 m/s and feed rate = 0.3 mm/rev)	171
5.49	Dynamic response of deflection, w at different rotational speed with four modes (depth of cut = 3.00 mm, cutting speed = 2.228 m/s and feed rate = 0.3 mm/rev)	172
5.50	Dynamic response of deflection, w at one mode (depth of cut = 0.25 mm, cutting speed = 0.2228 m/s, rotational speed = 1250 rev/min and feed rate = 0.3 mm/rev)	174

5.51	Dynamic response of deflection, w at one mode (depth of cut = 0.25 mm, cutting speed = 0.2228 m/s, rotational speed = 1250 rev/min and feed rate = 0.3 mm/rev)	174
5.52	Dynamic response of deflection, v at one mode (depth of cut = 3.0 mm, cutting speed = 0.2228 m/s, rotational speed = 1250 rev/min and feed rate = 0.3 mm/rev)	175
5.53	Dynamic response of deflection, w at one mode (depth of cut = 3.0 mm, cutting speed = 0.2228 m/s, rotational speed = 1250 rev/min and feed rate = 0.3 mm/rev)	175
5.54	The being machined work piece of experiment 1	177
5.55	Deflections in time domain of experiment 1	177
5.56	The being machined work piece of experiment 2 shown chatter occurrence	178
5.57	Deflections in time domain of experiment 2	179

List of Tables

2.1	Factors affecting surface roughness and their major investigators	47
2.2	Factors affecting surface roughness and major investigators	56
3.1	Possible boundary conditions	61
3.2	Matching table for both coordinate systems	74
3.3	Tabulated measured mode shapes, frequencies and β_n	80
3.4	Example calculation for fitting the mode shape of 2Z	83
3.5	A technique of solving DDEs by reducing them to a sequence of ODEs	90
4.1	Nominal material properties of cylindrical metal work piece	104
4.2	The three measured natural frequencies of the cylindrical metal work piece	104
4.3	Nominal material properties of cylindrical composite work piece	106
4.4	The three measured natural frequencies of the cylindrical composite work piece	107
4.5	The five measured clamped-pinned natural frequencies of the cylindrical metal work-piece	110
4.6	Properties of the cylindrical metal work piece used in the DUT test ...	114
4.7	Free-free boundary condition for cylindrical metal work piece	114
4.8	Clamped-pinned boundary condition for metal work piece (y direction)	115
4.9	Clamped-pinned boundary condition for metal work piece (z direction)	116
4.10	Cutting conditions and work piece characteristics	118
5.1	Cutting parameters and work piece characteristics used during	

	turning operation	176
6.1	Comparison between theoretical and experimental of dynamic responses at both v and w	189

List of Symbols

A	Cross-sectional area (mm^2)
$\mathbf{Bl}(t)$	A time varying matrix
c_y	Damping
d	Work piece diameter in mm
E	Young's Modulus (kg/m^3)
f	Feed rate (m/rev)
$f(t)$	Driving force
$f.f. S$	Speed of the feed
$F(s)$	Laplace's Transform
F_f	Feed cutting force (N)
$F_f(t)$	A time varying dynamic force due to cutting process
h	Instantaneous depth of cut (mm)
$h(t)$	Instantaneous chip thickness
h_o	Intended cut (mm)
I	Moment of inertia (kgm^2)
k_y	Stiffness of the cutting tool
K_x	Cutting force coefficient (unitless)
K_y	Cutting force coefficient (unitless)
K_z	Cutting force coefficient (unitless)
l	Length (mm)
m_y	Mass
M_z	Bending moment
N	Spindle speed in rev/min
P_x	Feed force

P_y	Tangential force
$P_y(t)$	The magnitude of tangential cutting force
P_z	Radial force
\dot{q}_j	A generalized velocity
Q	A generalize cutting force component
$Q_j^{(n)}$	A non-conservative generalized force
$s(t)$	Variable length from the spindle end to the location of the cutter
$s^2X(s)$	Laplace's Transform of acceleration
t	Time (s)
T	Kinetic energy (J)
T	Torque
v	Deflection in z direction (mm)
V	Strain energy of the beam
V	Cutting speed in m/min or ft/min
w	Deflection in y direction (mm)
w	Depth of cut in mm
$W(x)$	A normal mode or characteristic function of the beam
y	Displacement
$y(t - \tau)$	Outside surface
$y(t)$	Inside surface
Z	Measured mode shape
$\alpha_i(t)$	Corresponding modal coordinate
$\beta_i(t)$	Corresponding modal coordinate
δ	Logarithmic decrement
ρ	Mass density (GPa)
σ	Root mean square
τ	Time delay (s)
ϕ	Shear plane angle
ω	Angular rotation (rad/s)
ω_n	Theoretical frequency (Hz)
$\varphi_i(x)$	A spatial function that satisfies the boundary condition of the beam
Ω	Rotary speed (rev/min)

List of Abbreviations

1D	One-dimensional
3D	Three-dimensional
DD	Dimensional deviations
DDEs	Delay differential equations
DOF	Degree of freedom
DUT	Dalian University of Technology
EMA	Experimental modal analysis
FFT	Fast Fourier Transform
FRFs	Frequency response functions
FRP	Fibre reinforced polymer
GFRP	Glass fibre reinforced polymer
IRFs	Impulse response functions
MDOF	Multiple degree of freedoms
ODEs	Ordinary differential equations
SDOF	Single degree of freedom
TDOF	Two degrees of freedom

Chapter 1

Introduction

1.1 Introduction

This chapter contains a general introduction of the research (Section 1.1), motivations for the work (Section 1.2), research aim (Section 1.3) and scope of the thesis (Section 1.4). Section 1.5 describes the organisation of the thesis.

There are many different ways in which a product can be manufactured. Conventional techniques encompass processes such as machining, metal forming, injection moulding, die casting, stamping and many others. Machining is one of the basic and most widely used operations necessary to cut things to size and to finish off edges, dimensions and other aspect of a finished assembly part. Machining is a term that covers a large collection of manufacturing processes designed to remove unwanted material, usually in the form of chips, from a work piece. Machining is also used to convert basic geometrical shapes or shapes manufactured using different technologies (castings, forgings) into desired shapes, with size and finish specified to fulfil design requirements. A blank work piece is converted into a final product by cutting extra material away by turning, milling, drilling, boring or grinding operation. Generally, it can be said that most of manufactured product has components that require machining.

Therefore, this collection of processes is one of the most important among the basic manufacturing processes because of the value added to the final product.

In general, work pieces used in machining are made of metals due to their popular physical and mechanical properties in most engineering applications. In automotive industry for example, most of the parts are made from metals and their alloys. In cars, steel can crumple to absorb different impacts and hence are used to create the underlying chassis or cage beneath the body that forms the skeleton of the vehicle, door beams, roofs, and other parts. A large number of manufacturers these days are gradually trying to substitute metals due to their shortcomings such as weight, and corrosion (for some metals) if not painted or coated. Plastic materials especially composites become prominent to avoid these drawbacks.

Over the years, manufacturers begin to explore other materials that cost less and perform better, being lighter, for instance or more corrosion resistant. Metals have been steadily incorporated with composite materials as they offer special advantages mentioned earlier. Although composite parts may be produced by other fabrication techniques like near net shape forming and modified casting, they still require further subsequent machining to facilitate precise dimensions to the part. Composites, unlike metals, are not isotropic and consist of both unique resins and fibres. Therefore machining composites in any post processing operation to get to the final part is indeed different.

Machining of composite has become an exciting subject in recent years since the use of composite materials has increased tremendously in various areas in science and technology. With regard to the increase use of composites in many industries such as aerospace sector, the need to machine composite materials adequately has increased enormously. Typically composites are layered construction unite a resin matrix with normally discrete layers of brittle fibre reinforcement. In comparison to metals, composite react very differently and not so predictably during machining. The tool encounters continuously alternate fibres and matrix, which response differently. In composite, the material behaviour is not only inhomogeneous, but also depends on diverse fibre

and matrix properties, fibre orientation at the point of contact, and the relative volumes of fibre and matrix (Basavarajappa *et al.*, 2006)

1.2 Motivations

One of the most-known machining processes is turning. Turning operation is one of the oldest and most versatile conventional ways to produce round parts by means of a single point cutting tool. Typical products made include parts as small as miniature screws for eyeglass frame hinges and as large as rolls for rolling mills, cylinders, gun barrels and turbine shafts for hydroelectric power plants. Normally turning is performed on a lathe machine where one end of the work piece is fixed to the spindle and the other end pin mounted to the tails stock. The tool is fed either linearly in the direction parallel or perpendicular to the axis of rotation of the work piece. The work piece will experience a rotary motion whereas the cutting tool will experience a linear translation.

Work piece and cutting tool come in contact with each other during turning operation. This dynamic interaction between a rotating work piece and moving cutting forces will suppress vibration and occasionally under certain conditions it will excite chatter noise. The growing vibrations increase the cutting forces and may chip the tool and produce a poor surface finish. Harder regulations in terms of the noise levels also affected the operator environment. This is a very complicated dynamic problem. Vibration and chatter noise are major issues not just for turning operation but for any other machining processes. Short tool life span, tool damage, inaccurate dimension, poor surface finish are some distinctive adverse effects of vibration during machining. In addition, noise is a nuisance and unacceptable noise to the well-being of the operator. Manufactured products or components should have a good surface finish for better quality, reliability, excellent performance and meet customer requirements. In most cases poor surface finish contributes to irregularities in the surface and may form nucleation sites of cracks or corrosion.

There are two groups of researchers who study on vibration and chatter noise in turning operation which are the structural dynamicists and manufacture engineers. The structural dynamicists studied on vibration of a shaft spinning about its longitudinal axis subjected to moving load (Ouyang, 2011). Vibration and chatter noise in turning operation is one example of the moving load problems as the cutter travels along the rotating work piece and this generate three directional moving cutting forces. The rotating work piece (usually treated as a beam or shaft) can be modelled in more than one beam theory. In general there are four beam theories used which are Euler-Bernoulli, Rayleigh, shear and Timoshenko. The more sophisticated beam theories employed into the dynamic model of the turned work piece, the more accurate is the model. On the other hand, it is time consuming during computational work since sophisticated theories consider numerous interactions between several known variables. From the established dynamic model, vibration of the work piece during turning operation can be simulated.

The second group is from manufacturing engineers. Most of the manufacture engineers use simplified dynamic models for the work piece and do not treat it as well as structural dynamicists. The cutting tools often modelled as a lumped mass having one or two degrees of freedom (for describing motions of the cutting tool in the main cutting force direction). On the other hand, the manufacture engineer's cutting forces models are more realistic as they usually model the cutting tool as a single degree of freedom (SDOF) or two degree of freedom (TDOF) with regenerative chatter mechanism. Mode coupling and regeneration of chatter are two common chatter mechanisms occur during machining. Moving cutting forces in turning operation depend on a number of factors and regenerative chatter is the widely accepted mechanism which then introduces time delays in the established dynamic model. The length of this delay in turning operation is the time period for one revolution of the work piece.

A substantial amount of research on dynamic model of vibration for turned metal had been investigated over the years but unfortunately there has been less research on this area especially in turning of composites. The dynamic

models developed in this study assumed a straightforward and common behaviour which captures some basic features of a turning operation in machining, in which a cutting tool is moved in the axial direction against a work piece that is rotating rapidly. This dynamic model should work well for both of the work piece, metal and composite. In the past, most studies of dynamic model of turning operation have generally assumed the work piece to be rigid and have, therefore, ignored work piece deformation. However, in practice, the work piece undergoes deformation as a result of an external force by the cutting tool. This deformation affects and changes the chip thickness. In this thesis, the main contribution is to combine both dynamic models concept from those two groups; structural dynamicists and manufacturing engineers and develop a new mathematical model considering the work piece and cutting tools as a flexible work piece and flexible cutting tools. In addition the effect of the deflection-dependence of the moving cutting forces with regenerative chatter on the dynamic behaviour of the system at various travelling cutting speeds is also investigated.

1.3 Research Aim

The reliability of the developed dynamic model of turning operation is required to be simulated first for metal work piece. This has to be done right before considering simulating the composite material into the established dynamic model. There are two boundary conditions simulated in the developed dynamics model for metal work piece; clamp pinned and elastic boundary (chuck-tail stock) boundary. Each boundary condition was simulated to determine the work piece natural frequency and mode shapes. The results from the simulation are needed to be validated with the experimental results to realize the reliability of the dynamics model. In the beginning, the dynamic responses are set to be measured by laser sensor but unfortunately the laser is not sensitive enough. From the initial results, it is found that they had big differences compared to the numerical results (The details of the result were discussed in Chapter 4). Due to lack of the equipment in measuring the deflection of the

work piece and the moving cutting forces, the produced data could not be used. Instead, a collaboration data from a collaborator in China had to be used. However, there has not been a reduced quality of the research. In addition, the dynamic model developed is originally aimed to be used for work pieces made from composite materials but since enough original work on metal work pieces has been done, the thesis is focused on metals. Composites are studied only during the preliminary stage of this research. Previous works on composites and their characteristics are also discussed in the literature review in the context of vibration and chatter noise during turning of composite as they can be useful in future.

Due to several encountered problems mentioned earlier, the focus of the research had to be changed slightly to the development of mathematical aspect of coding and numerical simulation after consultation with the supervisor. Thus, the main aim of this study is to develop a dynamic model for turning metal work pieces which considers flexible work piece and flexible cutting tool with the regenerative chatter effects. This can be achieved by pursuing several tasks: (1) to understand what affect the vibration and chatter noise during turning in a quantitative manner and then find ways of alleviating this problem by parametric studies, (2) to develop the mathematical model which is then will be validated against experimental results from a collaborator from China due to lack of equipment and technical support within the student's own school. The validated model will be used to simulate structural modifications in order to identify means of design improvements and vibration reduction. The developed models permit a full analysis and discussion of the interaction between the work piece and the tool.

1.4 Scope of the thesis

The scope of the research covers several key areas which are given as follows:

i. Identify the main factors that influence vibration and chatter noise of turned metal and composite work pieces

One step towards a solution to the vibration and chatter noise problems is to investigate what kind of vibration that is present during turning operation. Thus, it is vital to investigate and identify several factors that will influence this vibration and chatter noise of turned metals and composites.

ii. Literatures review on dynamic model of turned metal with regenerative chatter

The next scope is to provide a brief but comprehensive survey on the currently available dynamic models of turned metal and composite.

iii. Develop a dynamic model for the vibration of rotating Rayleigh beam subjected to three directional moving cutting forces with regenerative chatter and flexible cutting tool and code it in MATLAB software

Develop a mathematical model for the behaviour of turning operation and validate the realistic dynamic model through experiments. The work piece is modelled as a rotating shaft (Rayleigh beam) subjected to a three directional moving cutting forces with regenerative chatter. The dynamic response of a rotating shaft is based on two boundary conditions which are the clamped pinned and elastic boundaries. This dynamic model of vibration of work piece in turning operation is more realistic as the dynamic model has multiple degrees of freedom and considers the

vibration of the cutter with regenerative chatter mechanism. It will involve great effort since the dynamic model for turning is very complicated in mathematics. Simulation is then needed to imitate the dynamic behaviour of the turning process subjected to moving cutting forces with regenerative chatter mechanism prior to actual machining and numerical examples are analysed accordingly.

iv. Numerical simulation of reducing vibration by parametric studies of machining parameters

One has to predict and visualize the effect of several cutting and machine parameters to the turned metal parts so that a good finished product can be achieved. It is known that several machining parameters such as cutting speed, depth of cut, feed rate and rotational speed affect the surface finish of turned work piece. By means of the dynamic model established above, these machining parameters and work piece characteristics are simulated to observe how they influence surface finish and vibration of turned work piece. The effects of depth of cut, the rotational speed and cutting speed of the cutter on the vibration and chatter occurrence are examined. Unfortunately due to the lack of equipment, most of the work is done in the form of numerical simulation and the validation of the developed dynamic model is made by using and comparing the data from the collaborate group in China. Only modal testing of metal and composite work pieces has been conducted. Ideally, experiments will be performed to test the machinability of metal according to the recommended cutting and machining parameters and validate the established dynamic model.

1.5 Organization of the thesis

The thesis consists of seven chapters describing all the works done in the research. These chapters are structured as follows:

Chapter 1 described the introduction and background of the research. The motivation behind the research was also stressed out in this chapter. In addition, the aim of the research was also laid out. The scopes of the research as well were also highlighted as a framework of the research.

Chapter 2 presents a brief literature review on the background of metal cutting especially turning operation and machining of composite. The influence factors contributing to the surface finish of the turned metals and composites were also explained. The introduction to vibration and chatter noise in machining and what would contribute to the occurrence of chatter noise in turning of metals or composites are also presented. Two different mechanisms of chatter noise usually occurred in machining process were also discussed. The basic vibration/chatter theory of 1-2 degree of freedom (DOF) used by most manufacturing people is discussed. The classical beam theories used in this research were also explained. Lastly, the methods to suppress vibration and chatter noise in turning operation by means of active and passive controlled were also reviewed in this chapter.

Chapter 3 presents the theory and development details of dynamic model employed in turning operation. The classical beam theories used in this research were also explained. A number of regenerative chatter models developed were also presented. This chapter also introduces the dynamic models of a rotating shaft subjected to three directional moving cutting forces with regenerative chatter mechanism. The sequence of improved mathematical formulation developed was also presented and discussed.

Chapter 4 explains the experimental modal analysis and discuss several experiments done to determine the natural frequency and mode shapes for the

work piece. Some cutting tests were also carried out on metals to identify the cutting force coefficient and cutting parameter effects.

Chapter 5 describes the numerical simulation works done and discuss the outcomes of the simulation which includes the parametric studies done to evaluate the effect of different cutting parameters on vibration.

Chapter 6 explained the detail analysis and discussion on the results from the parametric studies. Explanation on how the dynamic model developed is validated is also stated.

Chapter 7 concludes the research on numerical studies of vibration in turning operation. In addition, the contribution of the research are summarised and future research directions are proposed. Published journal and conference proceeding papers are also listed.

Chapter 2

Literatures Review and Theory

The organisation of this literature review is as follows; Section 2.2 presents the fundamental knowledge of turning operation cutting parameters such as cutting speed, depth of cut and feed rate. Section 2.3 describes the vibration in turning operation and Section 2.4 explains the phenomena of chatter noise in turning operation. Two different chatter mechanisms are described and discussed. Section 2.5 discusses the mechanism of regenerative chatter and some of the equations involved. In the meantime, Section 2.6 introduces some fundamental concepts of moving load dynamics problem. A number of dynamic responses of a rotating shaft subjected to moving load are reviewed in Section 2.7 with references for readers to explore at their own time. Several factors that influence the vibration and surface finish of turned metal are discussed in section 2.8. In Section 2.9, machining of composite will be discussed briefly and some factors contributing to the vibration and surface finish of turned composites is explained in Section 10. Last but not least in section 2.11, various chatter suppression methods in turning operation are discussed. Lastly, section 2.12 draws conclusions and presents an outlook of this research.

2.1 Introduction

Most machining today is carried out to shape metals and alloys. Many composites and plastic products are also machined. As regards to size, components from watch parts to aircraft wing parts are machined. In the engineering industry, the term machining is used to cover chip forming operations. Machining is an operation in which a thin layer of metal is removed by a wedge shaped tool from a larger body (Trent and Wright, 2000). It includes various processes in which a piece of raw material is cut into a desired final shape and size by a controlled material removal process. Machining also is one of the most widely used methods of producing the final shape of the manufactured products.

2.2 Turning Operation

There are three principals of machining process which are turning, drilling and milling. Other operations fall into miscellaneous categories such as shaping, planing, boring, broaching and sawing. The focus of this thesis is on turning operation. Turning operation is one of the oldest and most versatile conventional ways of producing parts that are basically in round shape. Turning means that the work piece is rotating while it is being machined. The starting material is usually a work piece that has been made by other processes such as casting, forging or extrusion.

A conventional lathe which normally turning is performed is illustrated in Figure 2.1. One end of the work piece is fixed to the spindle by chuck and the other end is pin mounted to the tails stock as can be seen in Figure 2.1. The machine consists of a headstock which is mounted on the lathe bed. The headstock contains the spindle that rotates the cylindrical work piece that is held in the chuck. The single point cutting tool is placed at the tool holder that is mounted on the cross slide. The cross slide is in turn mounted on the carriage.

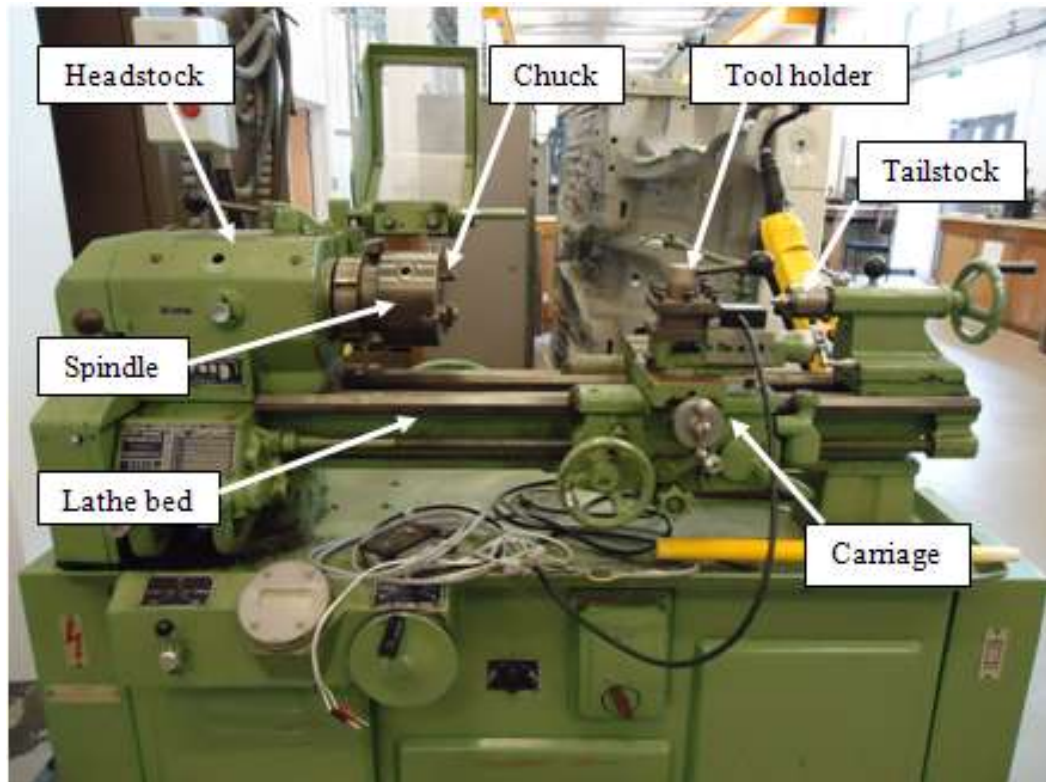


Figure 2.1: Conventional lathe machine at University of Liverpool

On a lathe, the tool is held rigidly in a tool post and moved at a constant rate along the axis of the work piece, cutting away a layer of metal to form a cylinder as shown in Figure 2.2. The tool is fed either linearly in the direction parallel or perpendicular to the axis of rotation of the work piece. The work piece will experience a rotary motion whereas the cutting tool will experience a linear translation. The three components of the cutting force acting on the rake face of the tool are also depicted in Figure 2.2. Normal to the cutting edge is called the tangential force, P_y . This usually is the largest of the three components and acts in the direction of cutting velocity. The force component acting on the tool, parallel with the direction of feed, is referred to as feed force, P_x . This force acts in the normal direction to the main cutting forces P_y . The third component, P_z , tend to push the tool away from the work in the radial direction, is the smallest of the force components in simple turning operation.

Figure 2.2 also shows the cutting parameters involved in turning operation such as depth of cut, feed rate and cutting speed. A thorough

knowledge of the variable factors of cutting speeds, feed rate and depth of cut must be understood (Trent and Wright, 2000) and below are the definitions for each of the turning process parameters.

The *cutting speed* (V) is the rate at which the uncut surface of the work passes the cutting edge of the tool, usually expressed in units of m/min or ft/min. The cutting speed of a tool is the speed at which the metal is removed by the tool from the work piece. Cutting speed is usually between 3 and 200 m/min (10 and 600 ft/min) (Trent and Wright, 2000). The cutting speed can be calculated using the equation 2.1 below:

$$V = \frac{N \pi d}{1000} \quad (2.1)$$

where V is the cutting speed (m/min), N is the spindle speed (rev/min) and d is the work piece diameter. Since πd is constant, thus the cutting speed depends on the spindle speed in which it is usually being determined first before actual turning operation according to Trent and Wright (2000).

The *feed rate* (f) is the distance moved by the tool in an axial direction at each revolution of the work piece. The feed rate may be as low as 0.0125 mm (0.0005 in) per revolution and with very heavy cutting, it can go up to 2.5 mm (0.1 in) per revolution as mentioned by Trent and Wright (2000). Equation 2.2 is normally used to calculate the feed rate;

$$Feed\ Rate = feed \times N \quad (2.2)$$

where N is the spindle speed (rev/min), $feed$ is in mm/rev and the unit of feed rate is in mm/min.

The *depth of cut* (w) is the thickness of the metal removed from the work piece, measured in radial direction. A depth of cut is the perpendicular distance measured from the machined surface to the uncut surface of the work piece. A

depth of cut may vary from zero to over 25 mm (1 in). Equation 2.3 is sometimes used to define a depth of cut;

$$\text{Depth of cut} = \frac{d_1 - d_2}{2} \quad (2.3)$$

where d_1 is diameter of the work surface before cutting and d_2 is the diameter of the machined surface. The unit of a depth of cut is in mm.

The *rotational speed* (ω) or sometimes called speed of revolution is the number of complete rotations, revolutions, cycles, or turns per time unit. It is a cyclic frequency, measured in radians per second or in hertz or in revolutions per minute (rev/min or min^{-1}) or revolutions per second in everyday life. Equation 2.4 is used to define a rotational speed;

$$\omega = \frac{v}{r} \quad (2.4)$$

where v is a tangential speed and r is a radial distance.

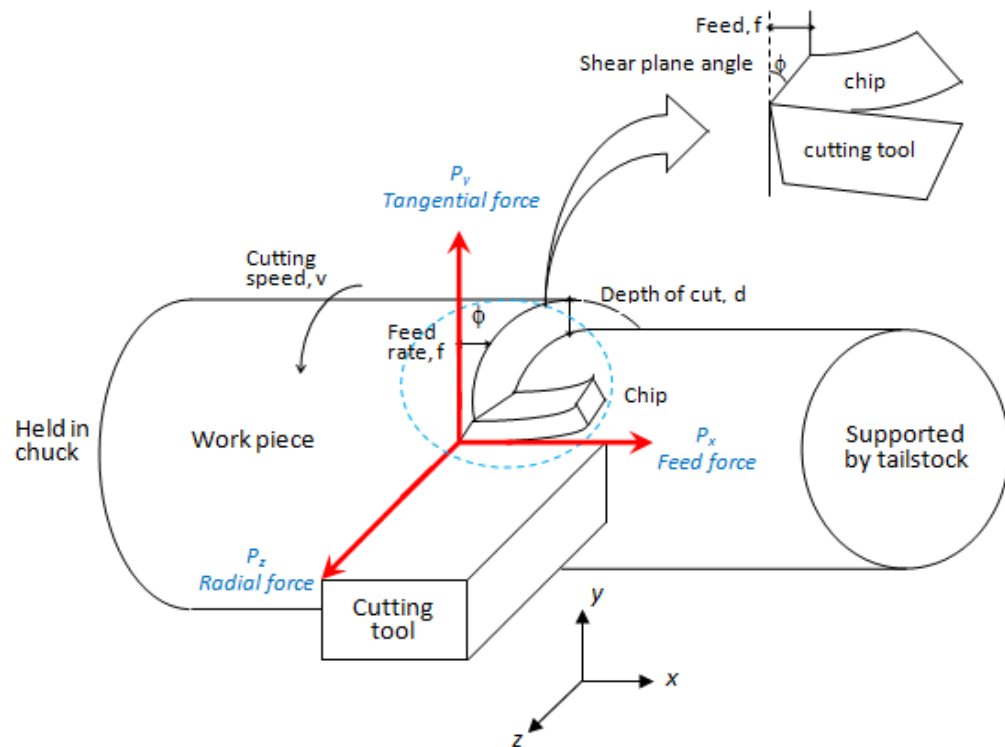


Figure 2.2: Schematic illustration of a turning operation

2.3 Vibration in Machining

Vibrations in machining are complex phenomena. During machining, work pieces are being cut and remove in discrete chunks. Each time the cutting tool takes a bite, it exerts a force on the work piece that was not there an instant ago. The work piece responds to this force by deflecting or by molecules compressing closer together, and generate mechanical stress. This mechanical stress travels through the work piece as a whole and the work piece acts like a spring to deflect and then return into shape. This explains vibration phenomenon during machining process.

Vibration is defined as any motion that repeats itself after interval of time and can be classified in several ways (Rao, 1995). There are two type of vibrations occurred during machining; forced and self-excited vibration. Forced vibration is generally caused by some periodic applied force present in the machine tool, such as that from gear drives, imbalance of the machine tool components, misalignment, and motors and pumps (Altintas, 2000). The basic solution to forced vibration is to isolate or remove the forcing element. If the forcing frequency is at or near the natural frequency of a component of a machine tool system, one of the frequencies may be raised or lowered. The amplitude of vibration can be reduced by increasing the stiffness or by employing a damping system.

The force acting on a vibrating system is usually external to the system and independent of the motion. However, there are systems for which the exciting force is a function of the motion parameters of the system, such as displacement, velocity or acceleration. Such systems are called self-excited vibrating systems, since the motion itself produces the exciting force (Rao, 1995). In machining, self excited vibration comes from the dynamic interaction of dynamics of chip removal process and structural dynamics of machine tool. Chatter is one of the examples of self excited vibrations that feeds on itself as the cutting tool moves across the work piece and generate distinctive loud and

unwanted noise. This unwanted noise is known in machining world as chatter noise.

2.4 Chatter Noise in Turning Operation

Chatter noise in machining is complex phenomena too similar to the vibration in machining. Chatter is an abnormal tool behaviour which it is one of the most critical problems in machining process and must be avoided to improve the dimensional accuracy and surface quality of the product. Chatter is a harmonic imbalance that occurs between the tool and the work piece because they are bouncing against each other. Chatter can be caused by the tool bouncing in or out of the work piece or the work piece bouncing against the tool, or both. It is not always easy to determine why chatter is happening.

Chatter needs to be taken into account during machining as it causes serious problems in machining instability. One of the most detrimental phenomena to productivity in machining is unstable cutting or chatter. To ensure stable cutting operations, cutting parameters must be chosen in such a way that they lie within the stable regions. Ideally, cutting conditions are chosen such that material removal is performed in stable manner. However, sometimes chatter is unavoidable because of the geometry of the cutting tool and work piece. Unless avoided, chatter marks leaves unacceptable vibration mark on the cut surface finish and may damage the cutting tool as can be seen in Figure 2.3 (a). A clearer picture of the chatter mark on turned metal work piece is illustrated in Figure 2.3 (b).

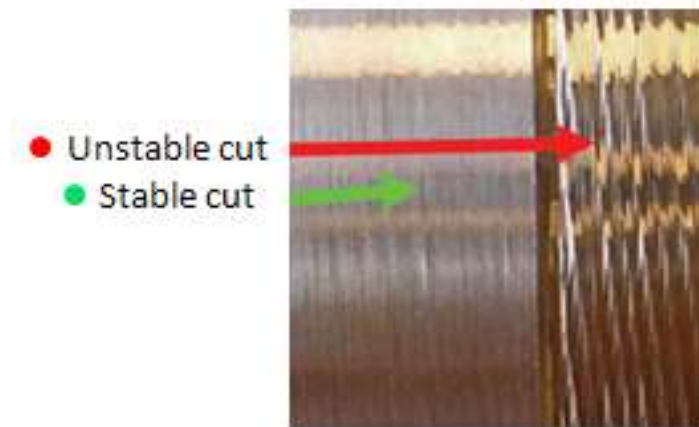


Figure 2.3 (a): Chatter mark (Budak and Wiercigroch, 2001)

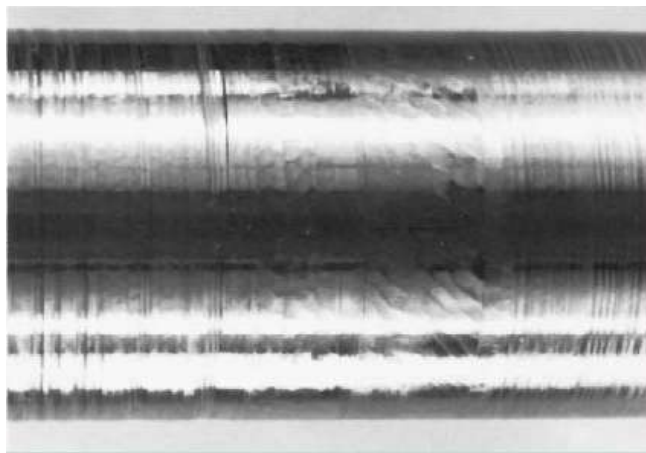


Figure 2.3 (b): Chatter mark on turned work piece (Tlusty, 2000)

According to Tlusty (2000), chatter can easily be recognized by the noise associated with self-excited vibrations. It also can be seen from the appearance of the chips as depicted in Figure 2.4 (a) and Figure 2.4 (b). Clearly from Figure 2.4 (a), the chip is short and segmented and it is caused by the chatter amplitude and the average chip thickness which will set different chip forms. With high amplitudes and a small average chip thickness, the chip will be broken. Meanwhile in Figure 2.4 (b) shows the chip is discontinuous with varied thickness.

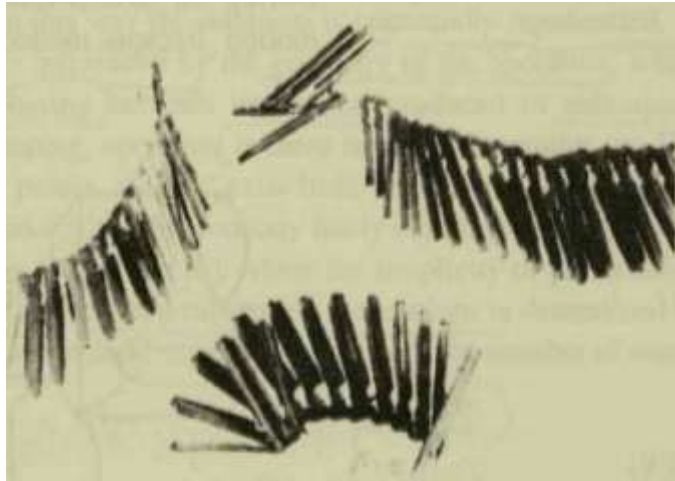


Figure 2.4 (a): Segmented chips (Tlustý, 2000)



Figure 2.4 (b): Discontinuous chips (Birhan, 2008)

Machine tool chatter has long been studied as interesting phenomenon. Chatter is self excited vibration that occurs in metal cutting if the chip width is too large with respect to the dynamic stiffness of the system (Altintas, 2000). Meanwhile, dynamic stiffness is defined as the ratio of the amplitude of the force applied to the amplitude of the vibration (Rao, 1995). A machine tool has different stiffness values at different frequencies and changing cutting parameters can affect chatter. Under such conditions the vibration starts and quickly grows. The cutting force becomes periodically variable, reaching considerable amplitudes and when the magnitude of this vibration keeps

increasing, the machine tool system becomes unstable. The machined surface becomes undulated, and the chip thickness varies in the extreme so much that it becomes dissected. In general, self excited vibrations can be controlled by increasing the dynamic stiffness of the system and damping (Birhan, 2008). Almost 100 years ago, Taylor (1907) described machine tool chatter or chatter as the most obscure and delicate of all problems faced by the machinist. Chatter significantly affects work piece surface finish, dimensional accuracy, and cutting tool life (Stephenson and Agapiou, 1996). In an attempt to achieve high material removal rates, aggressive cutting strategy is often employed in industry. This practice may cause chatter to occur more often in a competitive production environment, and makes chatter research imperative.

Such phenomena of chatter occurs during machining is due to material removal process in turning operation, both cutting tool and work piece are in contact with each other. Vibration and chatter noise are suppressed under certain conditions by this dynamic interaction between a rotating work piece and moving cutting forces from the tool. The cutting tool is subjected to a dynamic excitation due to the deformation of the work piece during cutting. The relative dynamic motion between the cutting tool and the work piece produce vibration and chatter thus affect the surface finish. Poor surface finish and dimensional accuracy of the work piece, possible damage to the cutting tool and irritating noise from excessive vibration are the results of uncontrolled vibration and chatter. Thus vibration related problems are of great interest in turning operations.

Furthermore, machine tool chatter is thought to occur for a variety of reasons. Mode coupling and regenerative chatter are two basic mechanisms that cause machine tool chatter and will be explained in the following sections. Tobias (1965) and Tlusty (2000) had documented much of the pioneering work in the field. In addition, Tobias and Fishwick (1958) were the first to identify the mechanisms known as regeneration chatter. On the other hand, mode coupling was studied by Koeingsburger (1970) and Tlusty (2000).

Another factor that should be considered in machining is machine stiffness. Machine stiffness is recognized as one of the important parameter during machining since low machine stiffness affects the magnitude of vibration during machining (milling, turning, drilling etc). It can have adverse effects on product surface finish where surface finish is directly affected by a dynamic displacement (vibration) between cutting tool and work piece according to Rao, (1995).

2.4.1 Mode Coupling

Mode coupling is recognized as one of the causes of chatter which is often called primary chatter. Mode coupling is a mechanism of self excitation that can only be associated with situations where the relative vibration between the tool and the work piece can exist simultaneously in at least two directions in the plane of the cut. Usually mode coupling occurs without any interaction between the vibration of the system and undulated surface of work piece. It acts only within vibratory systems with at least two degrees of freedom, which is due to the fact that the system mass vibrates simultaneously in the directions of the degrees of freedom of the system, with different amplitudes and phase.

Mode coupling is very complex and is inherently related to the dynamics of the cutting process. It may arise from different physical causes such as the dynamical effects of the geometry of the cutting tool on the cutting process. According to Huang and Wang (2009), the rotation direction of chatter vibration is an important feature to determine whether mode coupling chatter occurs or not.

2.4.2 Regenerative Chatter

Regenerative chatter is renowned as a secondary chatter and it is a self excited vibration. It is caused by the regeneration of waviness of the surface of

the work piece or by the oscillating cutter running over the wavy surface produced from the previous cut. It occurs whenever cuts overlap and the cut produced at time leaves small waves in the material that are regenerated with each subsequent pass of the tool on the previous cut surface (Kashyzadeh and Ostad-Ahmad-Ghorabi, 2012).

The tool in the next pass encounters a wavy surface and removes a chip periodically. The chip thickness produced varies after each successive cut. This will produce vibration and depending on conditions derived further on, these vibrations may be at least as large as in the preceding pass. Thus, the cutting force, which is a function of the chip thickness, depends not only on the current position of the tool and work piece but also on the delayed value of the work piece displacement. The newly created surface is again wavy in this way the waviness is continually regenerated.

Regenerative chatter is considered to be the dominant mechanism of chatter in turning operations. If regenerative tool vibrations become large enough that the tool loses contact with the work piece, then a type of chatter known as multiple regenerative chatter occurs. This mechanism has been the subject of study by Shi and Tobias (1984).

The occurrence and mechanism of chatter in machining has been first investigated by Tobias (1958) and Tlustý (1963). They found that the regenerative chatter is caused by instability of the system. Meanwhile chatter prediction models have a long history that began with work by Tobias (1958) and Tlustý (1963, 1971). These early efforts recognized that the regenerative effect was the main cause of instability, which leads to the development of chatter. Tlustý and Polacek (1963) and Merrit (1965) had discovered that the main sources of chatter come from stability condition of cutter, investigated conditions of stability for the cutter, structural dynamics of machines and feedback of subsequent cuts on the surface of the work piece as the main sources of chatter.

Several theories have been proposed to explain the occurrence of chatter instability for optimizing certain combination of process parameters such as feed rate, depth of cut, rotational speed, variation of chip thickness and variation of cutting force. In the work by Tobias and Fishwick (1958), the dynamics of the cutting process were modelled and effects such as process damping were included in their stability model. Tlusty and Polacek (1963) created a stability condition in which stability limits can be calculated based upon the system dynamics for orthogonal machining. Several dynamic models for regenerative chatter have been put forward, for example in the studies of Altintas (2000) and Tlusty (2000). Early stability lobe diagrams were created by Merrit (1965) based upon feedback control theory to model regenerative chatter. These early studies provided insight into the elementary chatter mechanisms.

In the past, by choosing the appropriate combination of cutting parameters for example, the feed rate, depth of cut, rotational speed, different chip thickness and variation of cutting force to prevent the occurrence of chatter during turning operation.

2.5 Regenerative Chatter Mechanism in Turning Operation

Regenerative chatter is a principal mechanism of chatter in turning operations. Tobias (1965) developed a regenerative machine tool chatter theory where the cutting force is considered to be a function of both the current and previous cuts. The theory is widely accepted as the most appropriate to describe the regenerative type chattering phenomenon, and it has become a foundation of many theoretical and experimental researches regarding cutting processes.

In this section the underlying mechanism of regenerative chatter in turning operation is explained. This regenerative chatter mechanism has been the subject of studies by Tobias (1965), Shi and Tobias (1984), and Stepan and Nagy (1997). Tobias (1965), Tlusty (2000), Budak (2006) and Altintas (2000)

are among the first to study regenerative chatter in turning operation. Figure 2.5 can be used to illustrate one degree of freedom of regenerative chatter in turning operation.

The work piece is supported at one end by chuck and the other end by tailstock on lathe machine. The chuck is often represented with linear spring. During turning process, the work piece will rotate as it is being machined. The cutting tool movement is parallel to the longitudinal axes of the work piece and depending on the depth of cut. When the cutting tool makes contact with the work piece, it will deflect. As the cutting tool moves along its direction, there will be a variation in the magnitude and the direction of cutting forces because the previous cut leaves a wavy surface finish due to structural vibrations. The developing vibrations will lead to the increase of cutting force thus, resulting poor surface finish (Altintas, 2000).

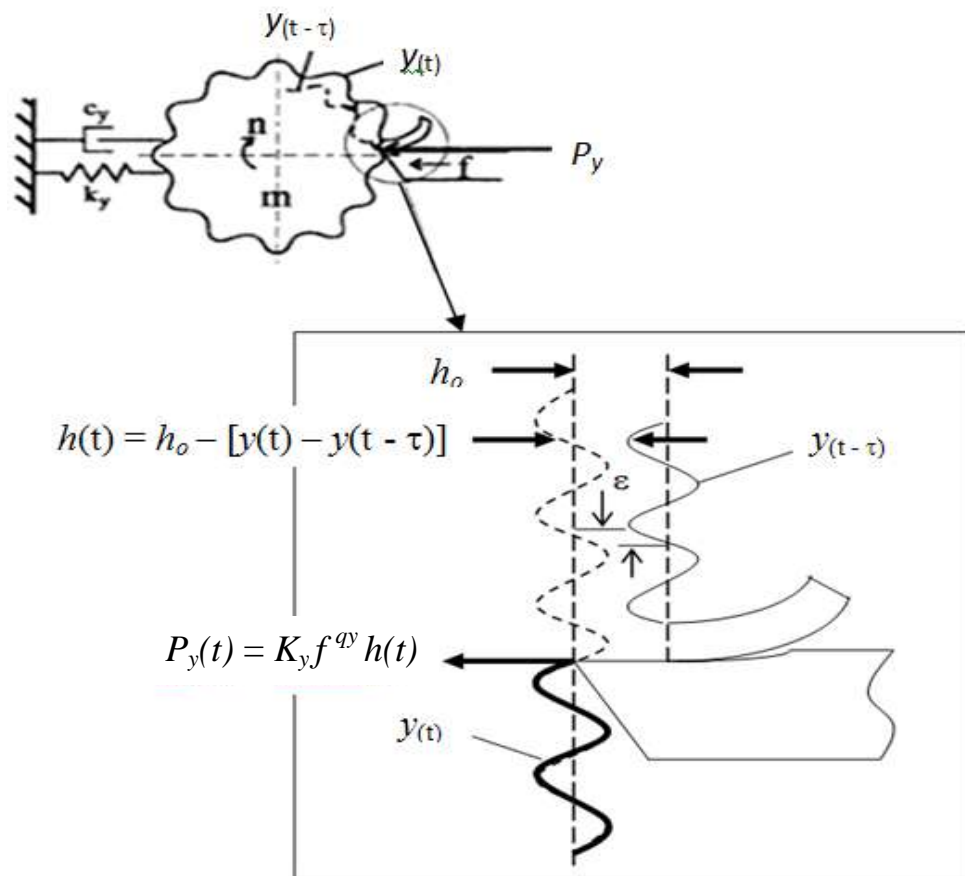


Figure 2.5: Regenerative chatter mechanism (Altintas, 2000)

The work piece is free to move in the feed direction and the feed cutting force, P_y applied causes the work piece to vibrate. Presume a single point cutter is fed perpendicular to the axis of cylindrical shaft. During the first revolution, the surface of the work piece is smooth which is without waves but due to the bending vibration of the work piece it will initially leave a wavy surface in the feed cutting force, P_y direction. As a second revolution takes place, the previous surface now has two waves at the inside and outside surface of the work piece. The inside surface denoted as $y(t)$ is originated from the cut made by the tool whereas the outside surface indicated by $y(t - \tau)$ is the effect of the vibrations during the previous revolution of cutting. The wavy surface leads to variable chip thickness, cutting force and vibration. This regeneration of chatter mechanism can be represented in the mathematical form below;

$$h(t) = h_o - [y(t) - y(t - \tau)] \quad (2.5)$$

where $h(t)$ is instantaneous chip thickness, h_o is the intended cut, $[y(t) - y(t - \tau)]$ is the dynamic of chip thickness and ω is a rotation speed of the shaft (rev/s). The associated time delay is the time period τ of one revolution of the work piece

$$\tau = \frac{2\pi}{\omega} \quad (2.6)$$

By assuming the work piece is a one single degree of freedom in the radial direction which consists of mass and spring system, the corresponding equation of motion can be written as below;

$$m_y \ddot{y}(t) + c_y \dot{y}(t) + k_y y(t) = F_f(t) \quad (2.7)$$

The magnitude of tangential cutting force $P_y(t)$ is proportional to the instantaneous chip thickness $h(t)$.

$$P_y(t) = K_y f^{q_y} h(t) \quad (2.8)$$

where K_y is the cutting force coefficient, f is feed rate (m/rev) and q_y is the exponents determined from Han *et al.* (2010) and h is the instantaneous depth of cut. This tangential cutting force not only depends upon the present cut $y(t)$, but also on a delayed value of displacement of the previous cut of the tool $y(t - \tau)$.

2.5.1 Chatter Modelling Theory

To set up a system of dynamic equations for studying chatter onset conditions, a reliable cutting force model, a mechanistic chatter model, and an accurate work piece deformation model are required. Depending on the relative flexibility of the work piece and the cutting tool, different chatter models may be developed. If the flexibility of the tool structure is predominant, the work piece may be considered rigid. Rigid is meant by the work piece is properly tightened at the chuck and deflection is assumed to be zero for simplification of the results. Flexible tool is defined as the ability to deflect in the main cutting force direction or in both directions. This happen due to the tool shank is only tighten by screw at the tool post (deflection is inevitable).

A large body of work has been published in chatter modelling over the last fifty years. Traditional models of the turning process consider a rigid work piece and vibration of the machine tool structure are studied by a few early researcher such as Tobias and Fischwick (1948), Nathan (1959), Merrit (1965), and Marui (1983). Numerous researchers investigated single degree of freedom regenerative tool models such as Tobias (1965), Hanna and Tobias (1974), Shi and Tobias (1984), Fofana (1993), Johnson (1996), Nayfeh *et al.* (1998), Kalmar-Nagy *et al.* (2001), Stepan (2001), Kalmar-Nagy (2002), Stone and Campbell (2002) and Stepan *et al.* (2003).

Basically, the turning cutting tools are often modelled as a lumped vibration system having one or two degrees of freedom according to Merrit (1965), Marui (1983) and Lin (1990) for describing motions of the cutting tool in the main cutting force direction or in both radial and main cutting force

directions working over rigid work piece. These chatter models developed on the basis of rigid work piece assumption are generally valid for cutting tools having a long tool shank in turning operations.

Chiou and Liang (1997) established a dynamic turning model for cutting rigid work piece with a flexible cutting tool. A comprehensive expression of the equation of motion for the dynamic cutting system incorporating the effects of cutting and contact forces is established. Machining experiments were conducted on a conventional lathe with the use of a specially designed flexible tool which can only vibrate parallel to the feed and perpendicular to the cutting velocity direction. The work piece is cut so as to observe the mechanism of the cutting tool chatter stability corresponding to the continuous variation of width of cut and cutting speed. The chatter stability was observed in verification of the analytical solutions over a range of cutting velocities and width of cuts. Among these cutting conditions, flank wear has been shown to have a significant effect on the chatter stability.

The simplest model that models the tool as a one degree of freedom is underdamped linear oscillator excited by the variation in undeformed chip thickness from one revolution to another (Tobias and Fishwick, 1948). The vast majority of these investigations employ a single degree of freedom (SDOF), representing the lumped mass behaviour of the cutting tool at the cutting zone. Equation (2.9) describes the motion during cutting for a SDOF cutting tool and a rigid work piece, given as

$$m_y \ddot{y}(t) + c_y \dot{y}(t) + k_y y(t) = F_f(t) \quad (2.9)$$

where y is the displacement, $F_f(t)$ is a time varying dynamic force due to cutting process, m_y is the mass, c_y is the damping and k_y is the stiffness of the cutting tool. Typically, the work piece is assumed to be rigid and the cutting tool to be vibrates.

On the other hand, if the work piece flexibility is predominant, the tool structure may be considered rigid. The work piece is considered flexible since

the tool will exert force on the work piece, there will be work piece deflection and the chip thickness will be changed. In addition, most of the work pieces used are long and slender having a smaller ratio of diameter over length, d/l (ratio is equal to less than 1). Due to this, deflection is likely to occur during cutting even though one side of the end is supported by tailstock as weight factor contributes to the deflection.

Chen and Tsao (2006) considered flexible work piece in his model and discussed a stability analysis of regenerative chatter for turning a cantilever beam. In the past studies, the work piece was assumed to be rigid, and only the tool vibration was considered. The research is focus on the regenerative chatter where a flexible work piece is considered rather than a rigid assumption. Such flexibility will affect the cutting force due to work piece deflection and will result in a smaller real chip thickness and larger critical chip width. Two models are used for the work piece and the tool, which correspond to a second order partial differential equation and a second order ordinary differential equation, respectively. The interaction between the work piece and the tool can be discussed and analysed based on these models. The effect of the critical chip width under different spindle speed is also discussed. By considering the deformation of the work piece under different conditions, the results show that the critical chip width of the deformed case is always larger than the rigid body case. Under the same natural frequency, both the work piece deflection and the critical chip width will become larger. Under the same work piece deflection, the smaller the natural frequency, the larger the critical chip width

Chen and Tsao (2006) as well presented a dynamic model of cutting tool with and without tailstock supported work piece using beam theory. Here, the effects of work piece parameters are studied on the dynamic stability of turning process by treating the work piece as a continuous system. In contrast to the most of the previous studies which considered the work piece to be a rigid body, the current stability analysis focuses on the regenerative chatter generated during the cutting of a flexible work piece supported with a tailstock. To provide a full description of the vibration behaviour, this study had developed two models; one for the work piece and one for the tool. These two models are in the form of a

second order partial differential equation and a second order ordinary differential equation, respectively. The developed models permit a full analysis and discussion of the interaction between the work piece and the tool. The results have shown that the deflection of the work piece affects the cutting force. It has also been shown that the larger the work piece deflection, the larger the critical chip width. In addition for a constant work piece deflection, the smaller the natural frequency, the larger the critical chip width. When the slenderness ratio of the work piece and the spindle speed are not excessive, work piece deformation considerations can be ignored without affecting the stability analysis significantly. However, the smaller slenderness ratio of work pieces and higher spindle speeds associated with many modern precision machining processes lead to significant deformation of the work piece. Hence, the stability analysis of turning processes should take deformation effects into consideration. Studies of chatter based on the rigid tool assumption and the flexible work piece modelled as the Euler–Bernoulli beams include those of Lu and Kamecki (1990), Kato and Marui (1974), Jen and Magrab (1996), and Shawky and Elbestawi (1998).

Moreover, a two-degree of freedom (TDOF) is defined by a system that requires two independent coordinates to describe their motion. In chatter model, the tool and work piece are modelled as two separate single degree of freedom spring mass damper systems. They are generally in the form of coupled differential equations that is each equation involves all the coordinates. If a harmonic solution is assumed for each coordinate, the equations of motion lead to a frequency equation that gives two natural frequencies of the system. If suitable initial excitation is applied, the system vibrates at one of these natural frequencies. During free vibration at one of the natural frequencies, the amplitudes of the two degrees of freedom (coordinates) are related in a specified manner and the configuration is called a normal mode, principle mode, or natural mode of vibration. Thus a two degree of freedom system has two normal modes of vibration corresponding to two natural frequencies (Kashyzadeh and Ostad-Ahmad-Ghorabi, 2012). There are some investigations reported previously employing two degree of freedom (SDOF) model of cutting tool to

represent the dynamics of chatter. Chandiramani and Pothala (2006) depicted dynamics of chatter with two degrees of freedom model of cutting tool.

Sekar *et al.* (2009) proposed an analytical scheme for stability analysis in turning process by considering the motion of tailstock supported work piece using a compliance model of tool and work. A dynamic cutting force model based on relative motion between the cutting tool and work piece is developed to study the chatter stability. Linear stability analysis is carried out in the frequency domain and the stability charts are obtained with and without considering work piece flexibility. The research proposed a compliant two degrees of freedom dynamic cutting force model by considering the relative motion of work piece with cutting tool. Tool and work piece were modelled as two separate single degree of freedom spring-mass-damper systems. The model allows selection of different operating conditions with and without a tailstock support by accounting the fundamental natural frequency of the work piece. Effect of cutting position, work piece dimensions, cutter flexibility, and cutter damping on the dynamic stability have been presented with the proposed dynamic model.

Dassanayake (2008) investigated different stages of stability of the work piece and tool by simulating three dimensional (3D) models of work piece cutter deflections in response to a nonlinear regenerative force with a method of rotor dynamics. Tool chatter in turning process is addressed with a new perspective. Turning dynamics is investigated using a 3D model that allows for simultaneous work piece tool deflections in response to the exertion of nonlinear regenerative force. The work piece is modelled as a system of three rotors, namely, unmachined, being machined and machined, connected by a flexible shaft. Such a configuration enables the work piece motion relative to the tool and tool motion relative to the machining surface to be three dimensionally established as functions of spindle speed, instantaneous depth of cut, material removal rate and whirling. The equations of motion for the model are coupled through the nonlinear cutting force. The model is explored along with its one-dimensional (1D) counterpart, which considers only tool motions and disregards work piece vibrations. Different stages of stability for the work piece and the tool subject to

the same cutting conditions are studied. Numerical simulations reveal diverse, oftentimes inconsistent, tool behaviours described by the two models. Most notably, observations made with regard to the inconsistency in describing machining stability limits raise the concern for using 1D models to obtain stability charts.

2.6 Introduction to Moving Loads Problem

The moving loads problem is a fundamental problem in structural dynamics. Engineers have been investigating the potential hazard produced by the moving loads on structures for many years. The dynamic response of structures carrying moving masses is a problem of widespread practical significance. For instance, a lot of hard works have been accounted during the last ten decades relating with the dynamic response of railway bridges and later on highway bridges under the effect of moving loads.

Moving loads dynamic problems are very common in engineering and daily life. The peculiar features of moving loads are they are variable in both space and time. The majority of the engineering structures are subjected to time and space varying loads. Any structures or machines subjected to loads which move in space and excite the structures or machines into vibration are such problems (Ouyang, 2010). The dynamic effect of moving loads was not known until mid-nineteenth century. When the Stephenson's bridge across river Dee Chester in England in 1847 collapsed, it motivates the engineers for research of moving loads problem. Moving loads have a great effect on the bodies or structures over which it travels. It causes them to vibrate intensively, especially at high velocities. Moving loads have substantial effects on the dynamic behaviour of the engineering structures. The simplest case of a moving load investigation is the case of a simple beam over which a concentrated load is moving, that is represented with a Fourth order partial differential equation.

2.6.1 Moving Loads with Regenerative Chatter in Turning Operation

Vibration problem in turning operation can be modelled as a beam subjected to moving loads and these moving loads come from the cutting tool. Treating vibration in turning operation as moving loads problem involves more sophisticated mathematics and exhausting computational works.

Generally, turning operation has two moving components; a cutter and a work piece that is fixed to the spindle and pin-mounted at the tailstock. The work piece spins about its longitudinal axis while the cutter moves axially along the work piece. The moving loads from the cutter is considered as a concentrated load which has three normal components and travels in the axial direction on the surface of the work piece, as shown in Figure 2.6. As the equilibrium of a beam is established on the neutral axis, the loads acting on the beam surface have to be translated to the neutral axis (also the longitudinal spinning axis in this example). When axial force P_x is translated to the neutral axis x , a bending moment, M_z must be added as shown in Figure 2.7 and is generated as

$$M_z = -P_x r \quad (2.10)$$

When P_z is translated to the neutral axis x , a torque, T must be added, also shown in Figure 2.7. On the other hand, P_y can be translated to the neutral axis x without adding anything. $s(t)$ is the variable length from the spindle end to the location of the cutter. The virtual work done by components of the cutting force P_y and P_z and the moment M_z are

$$\delta W = -P_y \delta v(s, t) - P_z \delta w(s, t) + M_z \left. \frac{\partial \delta v}{\partial x} \right|_{x=s(t)} \quad (2.11)$$

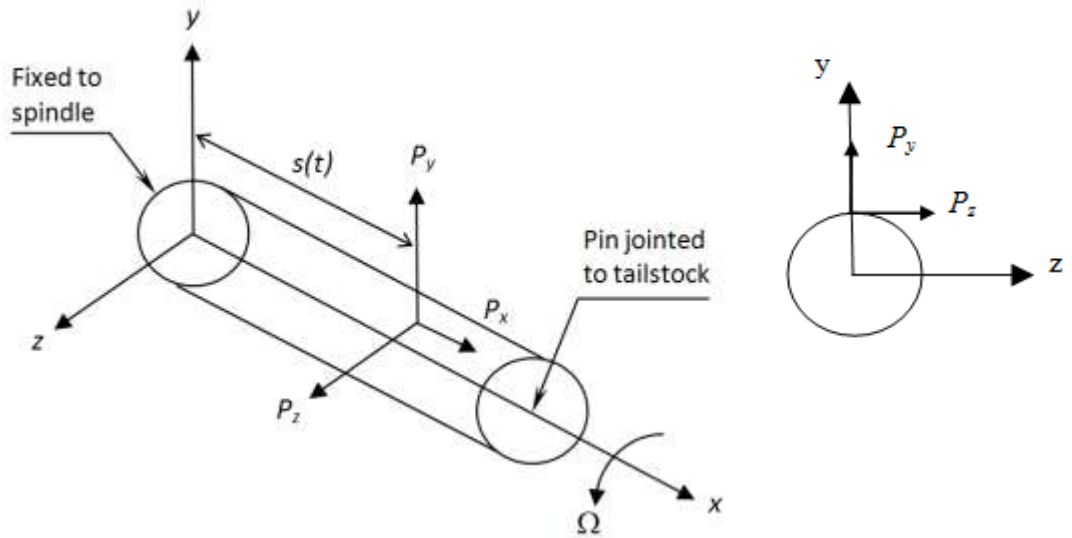


Figure 2.6: Rotating shaft subjected to a moving load with three perpendicular forces (Ouyang and Wang, 2007)

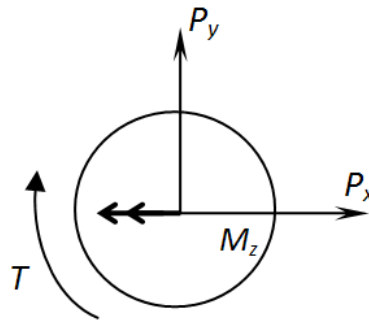


Figure 2.7: Torque and bending moment generated from P_x and P_z force components translated to the neutral axis (Ouyang and Wang, 2007)

2.7 Dynamic Model of Rotating Beam Subjected to Moving Load

Generally, a dynamic model is used to express and model the behaviour of a system over time. In the study of machining dynamics, it is vital to model the dynamics of cutting forces and machining system vibrations such as the vibrations of the tool and work assemblies. The machining dynamics model can

be used for the prediction of the machining system vibration and chatter, the simulation of machining process, the prediction of the machine surface roughness and waviness, the prediction of the machining accuracy, and the optimization of the machining process for a maximum production rate.

2.7.1 Introduction to Beam Theories

Beam is an important structural and fundamental component in mechanical engineering. Members that are slender and support loadings that are applied to their longitudinal axis are called beams. In general, beams are long, straight bars having a constant cross sectional area. Often they are classified as to how they are supported. For example, a simply supported beam is pinned at one end and roller supported at the other, a cantilever beam is fixed at one end and free at the other, and an overhanging beam has one or both of its ends freely extended over the supports.

Free-free, pinned-pinned, fixed-fixed, fixed-free, fixed-pinned and pinned-free are the most common boundary conditions for beam. It was recognized by the early researchers that the bending effect is the single most important factor in a transversely vibrating beam. There are four models for transversely vibrating uniform beam which are Euler-Bernoulli, shear, Rayleigh and Timoshenko. The model of the beam in this research is considered a Rayleigh beam and it is assumed that its boundary condition is a clamped-pinned.

2.7.1.1 Euler-Bernoulli Beam

The Euler-Bernoulli beam theory, sometimes called the classical beam theory, Euler beam theory, Bernoulli beam theory, is the most commonly used because it is simple and provides reasonable engineering approximations for many problems. The Euler-Bernoulli model includes strain energy due to the

bending and kinetic energy due to the lateral displacement. The Euler-Bernoulli model dates back to the 18th century. Jacob Bernoulli (1604 – 1705) first discovered that the curvature of an elastic beam at any point is proportional to the bending moment at that point. Daniel Bernoulli (1700 – 1782) nephew of Jacob, was the first one who formulated the differential equation of motion of a vibrating beam. Later, Jacob Bernoulli's theory was accepted by Euler in his investigation of the shape of elastic beams under various loading conditions. Many advances on the elastic curves were made by Euler (1750).

2.7.1.2 Rayleigh Beam

Rayleigh came up with a method of solving complex oscillations for mass spring system based on the fact during an oscillation the maximum kinetic energy of the oscillating mass is equal to the maximum strain (spring) energy. Rayleigh method is based on finding the fundamental natural frequency of vibration using the principle of conservation of energy. The Rayleigh beam theory provides a marginal improvement on the Euler-Bernoulli theory by including the effect of rotation of the cross-section. It particularly adds the rotary inertia effects to the Euler-Bernoulli beam describing the flexural and longitudinal vibrations of beams by showing the importance of this correction (Rayleigh, 2003). As a result, it partially corrects the overestimation of natural frequencies in the Euler-Bernoulli model. The resulting equation is found to be more accurate in representing the propagation of elastic waves in beam (Shabana, 1996). The equation of transverse motion for Rayleigh beam is a fourth order partial differential in space and second order in time (Bottega, 2006).

2.7.1.3 Timoshenko Beam

Timoshenko's theory of beams constitutes an improvement over the Euler-Bernoulli theory and Rayleigh theory. The Timoshenko's beam theory is

an extension of the Euler-Bernoulli beam theory which allows for the effect of transverse shear deformation. In addition, the theory adds the effect of shear as well as the effect of rotation to the Euler-Bernoulli beam (Timoshenko, 1921 - 1922). In other words, the model takes into account of shear deformation and rotational inertia effects, making it suitable for describing the behaviour of short beams, sandwich composite beams or beams subject to high-frequency excitation when the wavelength approaches the thickness of the beam. The resulting equation is of 4th order, but unlike ordinary beam theory (Euler–Bernoulli beam theory) there is also a second order spatial derivative present. The latter effect is more noticeable for higher frequencies as the wavelength becomes shorter, and thus the distance between opposing shear forces decreases. The model is a major improvement for non-slender beams and for high-frequency responses where shear or rotary effects are not negligible. If the shear modulus of the beam material approaches infinity, and thus the beam becomes rigid in shear, and if rotational inertia effects are neglected, Timoshenko beam theory converges towards ordinary beam theory. More recently, the Timoshenko beam theory accounting for the transverse shear effect was used by Erturka *et al.* (2006) in chatter studies.

2.7.2 Previous Dynamic Model of a Rotating Beam/Shaft

A substantial amount of researches has been made over the past decades in modelling the vibration in machining including turning operation. There is a number of turning operation dynamic models developed in recent years. The basic dynamic model of turning operation should include a rotating work piece excited by a force that moves in the longitudinal direction. Among the first dynamic model of rotating beam or shaft subjected to an axially moving load are established by Lee *et al.* (1987) and Katz *et al.* (1988). In general, there are three beam theories employed to model vibration of rotating beams or shafts as mentioned earlier. They are Euler, Rayleigh and Timoshenko beam theories

Lee *et al.* (1987) and Katz *et al.* (1988) are the first researchers to establish such a model and studied the vibration of a rotating shaft as a beam based on Euler, Rayleigh and Timoshenko beam theories under a constant transverse load, moving at constant velocity. Lee *et al.* (1987) used modal analysis technique is used to investigate force response analysis of an undamped distributed parameter rotating shaft. The shaft model includes rotary inertia and gyroscopic effects, and various boundary conditions (not only the simply supported case). In addition to the modal analysis, Galerkin's method is also used to analyse the forced response of an undamped distributed parameter rotating shaft. Both methods (modal analysis and Galerkin's) are illustrated in a numerical example and the calculations of the shaft response to a moving load in the plane of the moving load and in the perpendicular plane, are in a very good agreement.

Meanwhile, Katz *et al.* (1988) studied the dynamic behaviour of a rotating shaft subject to a constant moving load. The Euler-Bernoulli, Rayleigh (which includes rotary inertia effects) and Timoshenko (which includes rotary inertia and shear deformation effects) beam theories are used to model the rotating shaft. The shaft, which is simply supported, rotates at a constant rotational speed and is subject to a constant velocity moving load. The influence of parameters such as load speed, rotational speed of the shaft, the axial velocity of the load and the dimensions of the shaft are included and discussed for each shaft model. It is found that the maximum deflections of the shaft under the moving loads are dependent on the values of the load speed parameter. Later the results were also compared with the available solutions of a non-rotating beam subject to a moving load.

Katz *et al.* (1988) as well had introduced a dynamic cutting force model for turning of slender work pieces. The model is based on a flexible work piece and rigid machine tool, and a work piece displacement dependent cutting force. The model is described and studied theoretically as well as experimentally. The model is used to predict expected changes in the work piece natural frequencies during cutting. In the cutting experiments, only one typical natural frequency was consistently measured. This frequency was lower than the natural frequency

of the work piece without cutting. The experimental studies utilise both cutting force and work piece vibration measurements in two orthogonal directions. This data is obtained for both cutting and non cutting conditions, and analysed in the frequency domain. The experimental procedure represents a new method for determining the cutting process damping ratio, based on differences in the measured work piece natural frequencies with and without cutting.

Huang and Chen (1990) studied the dynamic response of a rotating orthotropic beam subjected to a moving harmonic load using an Euler-beam model. The individual and combined effects of rotation, moving load, and harmonic frequency on the system response are examined, emphasizing the resonant conditions. The influence of the orthotropic properties of the beam cross section on the dynamic response is also considered. In addition, Argento and Morano (1995) are the first who used deflection-dependent forces of Katz *et al.* (1987) for the moving load considered a random force according to work done by Zibdeh and Juma (1999). As mentioned by Zibdeh and Juma (1999), the problem of transverse vibrations of homogeneous isotropic rotating beams due to the passage of different types of loads is of considerable practical interest. Using analytical and numerical methods, this paper investigates the stochastic dynamic response of a rotating simply supported beam subjected to a random force with constant mean value moving with a constant speed along the beam. The beam is modelled by Euler-Bernoulli, Rayleigh, and Timoshenko beam models. The problem is formulated by means of partial differential equations. Closed form solutions for the mean and variance of the response for the three models are obtained. The effects of load speed, rotational speed of the beam and the Rayleigh beam coefficient on the dynamic coefficient are studied. The results show the effect of load speed, beam rotating speed, and geometrical size of the beam on the random response of the beam represented by some random dynamic coefficients. Comparisons with known solutions of random loads moving with uniform velocity are made.

Argento and Scott (1982) investigated the dynamic response of a rotating beam subjected to an axially distributed load acting normally to the top surface. The load has constant magnitude and accelerates axially along the beam surface.

The beam is pinned and rotates with constant angular velocity. The beam model used is based on the Timoshenko theory as this model includes the displacement component transverse to the load direction, which is gyroscopically induced by interaction between the displacement in the direction of the load and the beam rotation. A general method has been developed to treat an accelerating fixed direction distributed surface force on a rotating, pinned Timoshenko beam. Comparisons are made between the beam response to a constant velocity load and its response to a load which accelerates to the same velocity. The results show that the effect of varying speed load on the beam maximum displacement under the load is highly dependent on the asymptotic speed being approached by the load. In general, the transverse displacement has been found to be effected more than the displacement in the direction of the load. The varying speed load function used here usually leads to smaller overall peak displacements under the load

In the meantime, Han and Zu (1992) also examined a rotating Timoshenko beam subjected to moving loads with general boundary conditions. The dynamics of a simply supported, spinning Timoshenko beam subjected to a moving load is solved analytically using a modal analysis technique. In addition to obtaining the system transient response, this method also yields eigenquantities such as natural frequencies and mode shapes. Unlike the spinning Euler-Bernoulli and the simply supported spinning Rayleigh beams which have only one pair of natural frequencies corresponding to each mode shape, simply supported spinning Timoshenko beams possess two pairs of natural frequencies. It is also shown that the coupled differential equations are of the eighth-order which for most cases, can be reduced to a set of uncoupled, fourth-order equations without introducing any significant errors. Closed-form expressions for natural frequencies and the system transient response are presented using this simplified theory. A linearized expression for the computation of natural frequencies, which retains the essential features of the Timoshenko beam theory, is also proposed here.

According to Lee (1994), the dynamic response of a rotating shaft subject to axial force and moving loads is analysed by using Timoshenko beam

theory and the assumed mode method. The deformations of the shaft are expressed in terms of an inertial reference frame. The kinetic and potential energy are then expressed in matrix form by using the assumed mode method. The influences of the rotational speed of the shaft, the axial speed of the loads, and the Rayleigh coefficient are investigated and compared with the available reported results. The effects of compressive axial forces and perturbation of the axial velocity of the moving loads are also included in the analysis. Results of numerical simulations have been presented for various combinations of constant and non constant axial speeds of the moving load and axial forces. An increase in the rotational speed of the shaft is found to have minimal effect on the deflection in the direction of the applied load. However, the deflection in the orthogonal direction of the applied load is found to increase steadily with increased rotational speed.

El-Saeidy (2000) introduced bending moments and pioneered the study of rotating members subjected to moving loads using the finite element method. He presented finite element formulation for the dynamic analysis of a rotating or non rotating beam with or without nonlinear boundary conditions subject to a moving load. The formulation handles classical boundary conditions as well, namely, simply supported, clamped-clamped, cantilevered, and clamped-pin. The nonlinear end conditions arise from nonlinear rolling bearings (both the nonlinear stiffness and clearance(s) are accounted for) supporting a rotating shaft. The shaft finite element model includes shear deformation, rotary inertia, elastic bending moment, and gyroscopic effect. The analyses are implemented in the finite-element program 'DAMRO 1'. The results of the simulation of a simply supported non rotating shaft under a moving force are in excellent agreement with the exact solution and other formulations reported in the literature and thus validate the formulation for non rotating beams. However, for a simply supported rotating shaft, the first natural frequency in bending dominates the response spectrum

Recently, the dynamic response of a rotating Rayleigh beam with mass eccentricity under a moving stationary load was investigated by Sheu and Yang (2005). The bending moment produced from the axial surface force component

had a significant influence on dynamic response of the beam according to Ouyang and Wang (2007) who developed a dynamic model for vibration of a Rayleigh beam subjected to a three directional moving load. They had studied the vibration of a rotating Rayleigh beam subjected to a three directional moving load acting on the surface of the beam and moving in the axial direction. The model takes into account the axial movement of the axial force component and bending moment produced by this force component is included in the model. Lagrange's equations of motion for the modal coordinates are derived based on the assumed mode method and then solved by a fourth-order Runge-Kutta algorithm. It is found that the bending moment induced by the axial force component has a significant influence on the dynamic response of the shaft, even when the axial force and speed are low and, hence, must be considered in such problems as turning operations. When the axial force induced moving moment is included, the deflection of the beam may increase by a large amount under compression and the contributions from the higher frequency components become significant. In comparison small realistic values of axial force and speed are used, there is no moving load effect if the moment is ignored and there can be considerable moving load effect if the moment is considered

Ouyang and Wang (2010) as well investigated the vibration of a rotating Timoshenko beam subjected to a three directional load moving in the axial direction. A dynamic model for a rotating Timoshenko beam subjected to a moving surface load of three force components (two transverse and one axial) is established. The axial force component acting on the surface of the beam must be translated to the longitudinal axis of the beam and as a result a bending moment is generated and included in the dynamic model. The two transverse force components of the moving load are modelled as of constant magnitude or a linear function of the local deflection of the beam. The effects of the axial force component and its induced bending moment, and the deflection dependence of the moving forces on the dynamic behaviour of the system at various travelling speeds are investigated. The constant and non moving axial force had a significant effect on the magnitude of the dynamic response and it has been established and included by Lee *et al.* (1987).

Huang and Hsu (1990) developed a modal expansion technique and used this approach to investigate the dynamic response of a rotating cylindrical shell, with a predominant axial length, subjected to an axially moving harmonic load. A modal expansion method in which in plane membrane effects are neglected is adopted to solve for, analytically, the forced response of the shell to harmonic travelling loading. The closed form solution can be use to simulate a dynamic problem in machining, where the tool provides a moving load with an amplitude varying harmonically or periodically and the work piece rotates at a constant speed. The dynamic response of the shell is affected by three parameters: coupling of rotation, moving load speed and harmonic frequency and effects upon the resonant conditions of the shell.

In this thesis, Rayleigh beam theory has been adopted to develop the mathematical model of turning process with regenerative chatter mechanism. Rayleigh method has been employed due to it is more robust and accurate as mentioned by Shabana, 1996 in which the method particularly adds the rotary inertia and gyroscopic effects to the Euler-Bernoulli beam describing the flexural and longitudinal vibrations of beams. It is found to be more accurate in representing the propagation of elastic waves in beams. It partially corrects the overestimation of natural frequencies in the previous method (Euler-Bernoulli model). Rayleigh method is based on finding the fundamental of natural frequency of vibration using the principle of conservation of energy which has been mentioned earlier.

2.8 Factors Influencing Surface Finish of Turned Metals

Machining is often the manufacturing process that determines the final geometry and dimensions of the part. It also determines the part's surface texture. In general, machining will produce a smoother surface texture and a hand finishing process is no longer needed, and thus save time and improve the quality and therefore it is widely used.

The quality of machined surface is characterized by the accuracy of its manufacture with respect to the dimensions specified by the designer. Every machining operation leaves characteristic evidence on the machined surface. This evidence in the form of finely spaced micro irregularities left by the cutting tool. Each type of cutting tool leaves its own individual pattern which therefore can be identified. This pattern is known as surface finish or surface roughness (Figure 2.8).

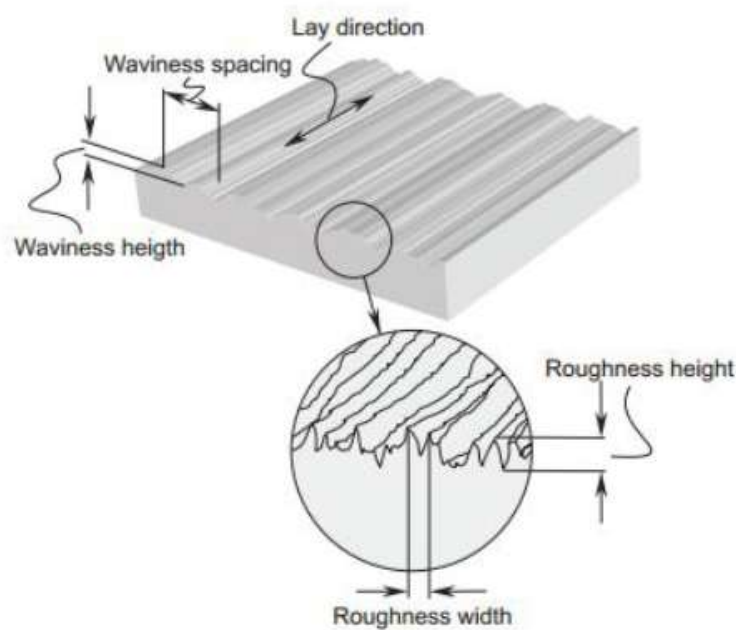


Figure 2.8: Elements of surface machine surface texture (Azouzi and Guillot, 1997)

Surface finish is defined as the characteristics of a surface. Surface finish of a machined surface depends on: (a) geometrical factors (b) work material factors and (c) vibrations and machine tool factors. Surface finish is also a widely used index of product quality and in most cases a technical requirement for mechanical products (Azouzi and Guillot, 1997). In machining, the interaction of the cutting edges and the microstructure of the material being cut both contribute to the final surface finish. Achieving the desired surface quality is of great importance for the functional behaviour of a part as it has formulated

an important design feature in many situations such as parts subject to fatigue loads and precision fits.

As competition grows fiercer, customers now make higher demands on quality, making surface finish become one of the most competitive aspects in today's manufacturing industry. The demand for high quality and fully automated production focuses on the surface condition of the product, especially the roughness of the machined surface, because of its effect on product appearance, function, and reliability. For these reasons it is important to maintain consistent tolerances and surface finish. It also reflects aesthetical value of the product besides its functionality. Also, the quality of the machined surface is useful in diagnosing the stability of the machining process, where a deteriorating surface finish may indicate work piece material non-homogeneity, progressive tool wear, cutting tool chatter and others. Greater surface finish also affects fatigue strength as mentioned by Nishitani and Imai (1983). The majority of engineering failures are caused by fatigue failure. Fatigue failure is defined as tendency of a material to fracture by means of progressive brittle cracking under repeated alternating or cyclic stresses.

Surface finish has received serious attention for many years. It has formulated an important design feature in many situations such as parts subject to fatigue loads, precision fits, fastener holes, and aesthetic requirements. In addition to tolerances, surface finish imposes one of the most critical constraints for the selection of machines and cutting parameters in process planning. A considerable number of studies had investigated the general effect of the cutting speed, feed rate, depth of cut, nose radius and other major factors on the surface finish of turned metal.

Lambert and Taraman (1974) described that a mathematical model for the surface finish in a turning operation was developed in terms of the cutting speed, feed and depth of cut. The model was used to generate contours of surface finish in planes containing the cutting speed and feed at different levels of depth of cut. The surface finish contours were used to select the machining conditions at which an increase in the rate of metal removal was achieved

without sacrifice in surface finish. Petropoulos (1974) had studied the process variability with respect to surface finish as measured by R_a and $-R_{max}$ values in single point oblique finish turning of carbon steel. The effect of tool wear on surface finish is considered. Furthermore, cumulative distributions of R_a and $-R_{max}$ values are presented to illustrate how well the observed data fits the theoretical.

Beside, Sundaram and Lambert (1981) outlined the experimental development of mathematical models for predicting the surface finish of AISI 4140 steel in fine turning operation using TiC coated tungsten carbide throw away tools. In their research, the variables included in the model are: cutting speed, feed, depth of cut and time of cut of the tool. Meanwhile, Miller *et al.* (1973) had conducted a statistical designed experiment for both wet and dry turning of 380 and 390 aluminium casting alloys with sharp and dull carbide and polycrystalline diamond cutting tools. Surface finish data for each alloy, tool material and coolant condition were mathematically related to cutting speed, feed rate and depth of cut.

Azouzi and Guillot (1997) examined the feasibility for an intelligent sensor fusion technique to estimate on-line surface finish (R_a) and dimensional deviations (DD) during machining. In the case studied, it appeared that the cutting feed, depth of cut and two components of the cutting force (the feed and radial force components) provided the best combination to build a fusion model for on-line estimation of R_a and DD in turning process. Meanwhile, Risbood *et al.* (2003) in his work found that using neural network; surface finish can be predicted within a reasonable degree of accuracy by taking the acceleration of radial vibration of tool holder as a feedback. It is also possible to utilise the fitted network for predicting the surface finish in turning with a tool of same material but different geometry provided coolant situation is the same. It was observed that while turning the steel rod with TiN coated carbide tool, surface finish improves with increasing feed up to some feed where from it starts deteriorating with further increase of feed.

In addition, Mital and Mehta (1988) developed the surface finish prediction models, as a function of cutting speed, feed, and tool nose radius. A general purpose surface finish prediction model is also proposed for ductile cast iron, medium carbon leaded steel, and alloy steel. Statistical analysis of experimental data indicated that surface finish is strongly influenced by the type of metal, speed and feed of cut, and tool nose radius. While the effects of feed and tool nose radius on surface finish were generally consistent for all materials, the effect of cutting speed was not.

Furthermore, Xavier and Adithan (2009) had determined the influence of cutting fluids on tool wear and surface finish during turning of AISI 304 with carbide tool. Further attempt has been made to identify the influence of coconut oil in reducing the tool wear and surface finish during turning process. According to Ozel and Karpaz (2005), there are various machining parameters that influence the surface roughness, but those effects have not been adequately quantified. In order for manufacturers to maximize their gains from utilising finish hard turning, accurate predictive models for surface roughness and tool wear must be constructed. Decrease in the feed rate resulted in better surface finish but slightly faster tool wear development, and increasing cutting speed resulted in significant increase in tool wear development but resulted in better surface finish. Increase in the work piece hardness resulted in better surface finish but higher tool wear. Overall, CBN inserts with honed edge geometry performed better both in terms of surface roughness and tool wear development.

In the meantime, Singh and Rao (2007) had conducted an experiment to determine the effects of cutting conditions and tool geometry on the surface finish in the finish hard turning of the bearing steel (AISI 52100). The study revealed that the feed is the dominant factor determining the surface finish followed by nose radius and cutting velocity. Though, the effect of the effective rake angle on the surface finish is less, the interaction effects of nose radius and effective rake angle are considerably significant. Mathematical models for the surface finish were developed by using the response surface methodology.

A representative summary of these studies is shown in Table 2.1.

Table 2.1: Factors affecting surface finish and their major investigators

Investigators	Major Factors	Material studied
Lambert and Taraman (1974)	Speed, feed, depth of cut	Steel SAE 1018
Petropoulos (1974)	Tool wear, surface finish distribution	Steel
Sundaram and Lambert (1981)	Speed, feed, nose radius, depth of cut	Steel 4140
Miller <i>et al.</i> (1983)	Speed, feed, tool condition, cutting fluid	Alloy, cast iron
Azouzi and Guillot (1997)	Feed, depth of cut, feed and radial force components	Low carbon steel
Risbood <i>et al.</i> (2003)	Feed	Steel rod
Mital and Mehta (1998)	Cutting speed, feed, and tool nose radius	Aluminium alloy 390, ductile cast iron, medium carbon leaded steel 10L45, medium carbon alloy steel 4130 and inconel 718
Xavior and Adithan (2009)	Cutting fluids	Hardened AISI 304 steel
Ozel and Karpat (2005)	Cutting speed, feed rate, work piece hardness	Hardened AISI 52100 steel
Singh and Rao (2007)	Feed, nose radius and speed	Bearing steel

It is obvious to conclude from the table that the most factors contributing to surface finish are cutting parameters such as cutting speed, depth of cut and feed rate.

Generally in machining, by changing the cutting parameters, one should be more careful and consider the cutting condition used is within recommended range to prevent unstable cutting condition. This is true according to Stephenson and Agapiou (1996) where in an attempt to achieve high material removal rates; aggressive cutting strategy (without considering recommended cutting condition) is often employed in industry. This practice may cause chatter to occur more often in a competitive production environment. Chatter significantly affects work piece surface finish, dimensional accuracy and cutting tool life.

In addition, according to Faassen *et al.* (2003), for the efficiency of the milling process (high-speed milling is widely used in the manufacturing industry) high demands on the material removal rate and the surface generation rate are posed. The process parameters, determining these two rates, are restricted by the occurrence of regenerative chatter. During the milling process, chatter can occur at certain combinations of axial depth of cut and spindle speed. This is an undesired phenomenon, since the surface of the work piece becomes non-smooth as a result of heavy vibrations of the cutter. Moreover, the cutting tool and machine wear out rapidly and a lot of noise is produced when chatter occurs. Chatter is an undesired instability phenomenon, which causes both a reduced product quality and rapid tool wear.

Furthermore, according to Lacerda and Lima (2004) in milling, one of the machine tool work piece system structural modes is initially excited by cutting forces. The waved surface left by a previous tooth is removed during the succeeding revolution, which also leaves a wavy surface due to structural vibrations. The cutting forces become oscillatory whose magnitude depends on the instantaneous chip dynamic thickness, which is a function of the phase shift between inner and outer chip surface. The cutting forces can grow until the system becomes unstable and the chatter vibrations increase to a point when the cutter jumps out of the cut or cracks due the excessive forces involved. These vibrations produce poor surface finishing, noise and reduce the life of the cutter. In order to avoid these undesirable effects, the feed rate and the depth of cut are chosen at conservative values, reducing the productivity. They concluded that the depth of cut is the main parameter relative to chatter vibrations: selecting a

spindle speed and increasing the depth of cut, a limit is found when these vibrations start with the characteristic sound and work piece surface marks. The feed rate modifies only the chip thickness static component, which is removed from the equations, because it does not contribute to the dynamic chip load regeneration mechanism, origin of chatter vibrations.

According to Budak (2005), chatter is one of the most common limitations for productivity and part quality in milling operations. Poor surface finish with reduced productivity and decreased tool life are the usual results of chatter. Additional operations, mostly manual, are required to clean the chatter marks left on the surface (low surface finish). Thus, chatter vibrations result in reduced productivity, increased cost and inconsistent product quality. Rivin (1995) also mentioned that the cutting of metals is frequently accompanied by violent vibration of work piece and cutting tool which is known as machine tool chatter. Chatter is a self excited vibration which is induced and maintained by forces generated by the cutting process. It is highly detrimental to tool life and surface finish, and is usually accompanied by considerable noise. Chatter adversely affects the rate of production since, in many cases its elimination can be achieved only by reducing the rate of metal removal.

Thrusty and Polacek (1963) and Merrit (1965) had discovered that the main sources of chatter come from stability condition of cutter, investigated conditions of stability for the cutter, structural dynamics of machines and feedback of subsequent cuts on the surface of the work piece as the main sources of chatter. In the past, by choosing the appropriate combination of cutting parameters for example, the feed rate, depth of cut, rotational speed, different chip thickness and variation of cutting force to prevent the occurrence of chatter noise during turning.

Besides, a machine tool has different stiffness at different frequencies and changing cutting parameters can affect chatter. Under such conditions these vibration start and quickly grow. The cutting force becomes periodically variable, reaching considerable amplitudes and when the magnitude of this vibration keeps increasing, the machine tool system becomes unstable. The

machine surface becomes undulated, and the chip thickness varies in the extreme so much that it becomes dissected. In general, self excited vibrations can be controlled by increasing the dynamic stiffness of the system and damping as mentioned by Frangoudis *et al.* (2013).

Chatter not only limits productivity of cutting processes but also causes poor surface finish and reduced dimensional accuracy, increases the rate of tool wear, results in a noisy workplace and reduces the life of a machine tool. Chatter can be avoided by keeping a low depth of cut; however this leads to low productivity. Over the years, various methods have been developed to avoid regenerative chatter without reducing the depth of cut. The basic principle of these techniques is to prevent the dynamic of the machining process from locking on the most favorable phase for chatter (Al-Regib *et al.*, 2003).

In addition, during material removal process in turning operation, both cutting tool and work piece are in contact with each other. Vibration and chatter noise are suppress under certain conditions by this dynamic interaction between a rotating work piece and moving cutting forces from the tool. The cutting tool is subjected to a dynamic excitation due to the deformation of the work piece during cutting. The relative dynamic motion between the cutting tool and the work piece produce vibration and chatter thus affect the surface finish. Poor surface finish and dimensional accuracy of the work piece, possible damage to the cutting tool and irritating noise from excessive vibration are the results of uncontrolled vibration and chatter. Thus vibration related problems are of great interest in turning operations.

2.9 Chatter Suppression in Turning Operation

A great deal of research has been carried out since the late 1950s to solve the chatter problems. Researchers have studied how to detect, identify, avoid, prevent, reduce, control or suppress regenerative chatter. Analysis and suppression of chatter has received great attention during the past two decades.

The aim is to suppress chatter instability by reducing the relative displacements between the tool and work piece. Methods can involve active, semi-active or passive control. Active control systems do not require external assistance. They depend essentially upon a source of power to drive ‘active device’ which may be electro mechanical, electro hydraulic or electro pneumatic actuators. In contrast, passive vibration control involves modification of the stiffness, mass and damping of vibrating system to make the system less responsive to its vibratory environment. Passive control, compared to active control, exhibit the advantages of easy implementation, low cost and no need for external energy.

There are a number of chatter suppression methods established for turning operation such as those reported by Tarng *et al.* (2000) and Al Regib *et al.* (2003) who discovered that selecting suitable spindle speeds certainly eliminated regenerative chatter. Online chatter recognition and cutting speed control principles were introduced by Tlustý (1965). These systems detect the occurrence of chatter via sound or vibration sensor, and then automatically choose a new speed for cutting which is less chatter prone. Changes in system damping are one of the effects of different spindle speeds, which are found by Ganguli *et al.* (2007). They proposed active damping with velocity feedback as a chatter control strategy.

An alternative, modern way to reduce chatter is by actively detecting and suppressing the unwanted vibration with a control algorithm and an actuator which uses active materials. Active materials are materials that exhibit a coupling between two or more of their physical properties. Piezoelectrics, for example, experience an elastic strain when exposed to an electric field and are excellent candidates for vibration control because they can be driven at high frequencies with high force by electrical signals. Mounting a piezoelectric inertia actuator on the cutting tool as a vibration absorber was another method of chatter suppression recommended by Tarng *et al.* (2000). Furthermore, an analytical tuning method with vibration absorbers to suppress regenerative chatter was established by Sims (2007). Another method of using a magnetic bearing connected with cutter was suggested by Chen and Knopse (2007) to prevent the onset of chatter. Wang and Fei (1999) proposed a method based on

variable stiffness in boring bars to suppress chatter. This is based on the principle of avoidance of self excited vibrations by continuously varying the natural frequency of a structure over a range.

Slavicek (1965) and Vanherck (1967) proposed the use of milling cutters with non-uniform tooth pitch and Stone (1970) used end mills with alternating helix. Effectiveness of these methods in chatter suppression has been verified by simulation and experiments (Doolan *et al.*, 1975, Fu *et al.*, 1984 and Thusty *et al.*, 1983). These techniques can be applied to the design of a non-uniform pitch cutter for a specific cutting condition, but cannot be applied to single point machining. By the way, Weck *et al.* (1975) utilised an on-line generated stability lobes to select a spindle speed, and thus maximized the depth-of-cut limit. Later, Smith and Thusty (1992), Delio *et al.* (1992) and Tarng *et al.* (1996) avoided the need for the knowledge of the stability lobes and proposed that the best tooth passing frequency be made equal to the chatter frequency. This minimizes the phase between the inner and outer modulations. This approach is adaptive in the sense that the spindle speed is changed based on feedback measurement of the chatter frequency. This method is practical for high spindle speed machining when the stability lobes are well separated.

Another technique to suppress regenerative chatter is by sinusoidal spindle speed variation (S^3V) around the mean speed to disturb the regenerative mechanism. Since this technique was introduced by Stoferle and Grab (1972), there have been many research efforts to verify its effectiveness on machining stability by numerical simulation and experiments in turning (Hoshi *et al.*, 1977, Inamura and Sata, 1974, Sexton and Stone, 1978-1980, Takemura *et al.*, 1974 and Zhang, 1996) and in milling (Altintas and Chan, 1992, Inamura and Sata, 1974, Lee and Liu, 1991). Despite the above research efforts, this technique has not been implemented widely in industry because there is no systematic way to select the proper amplitude and frequency of the sinusoidal forcing signal. The selection of these parameters depends on the dynamics of the machining system and is constrained by the spindle-drive system response and its ability to track the forcing speed signal.

In addition, variable speed machining can result in an adverse effect and may even cause chatter in an otherwise stable process (Engelhardt *et al.*, 1989, Lin *et al.*, 1990, Sexton and Stone, 1978 and Soliman and Ismail, 1997). This usually occurs when this method is applied to high speed machining. Recently, Soliman and Ismail (1997) proposed using fuzzy logic to select on-line the amplitude and frequency of the forcing speed signal. Yilmaz *et al.* (1999) generalized sinusoidal spindle speed variation technique by introducing multi-level random spindle speed variation, where the spindle speed is varied in random fashion within the maximum amplitude ratio allowed by the spindle-drive

2.10 Machining of Composites

By definition, a composite is a structural material that consists of two or more combined constituents that are combined at a macroscopic level and are not soluble in each other. Composites have been seen as early as 1940s where glass reinforced resin matrix composites were first introduced. Composite materials have gained popularity in high performance products that need to be lightweight, yet strong enough to take harsh loading conditions such as aerospace component (tails, wings, and propellers), boats and scull hulls, bicycle frames and racing car bodies. Other uses include fishing rods and storage tanks. Carbon composites are a key material in today's vehicles and spacecraft. Owing to increasing use of composites in engineering, machining of composites becomes a new research topic and novel research may be done. Machining of composites is briefly reviewed in this chapter since it is in very interesting and it will be the research topic of the student in near future.

Since then, the use of composites like glass fibre reinforced polymer (GFRP) composites are increased in its applications including aerospace, aircraft, automobile engineering, sporting goods, off-shore drilling platforms, appliances. With regards to the increasing use of composites in the aeronautical,

aerospace, nuclear, biomedical and automotive industries, the need to machine composite materials adequately increases.

Machining of composites predominantly uses milling, turning or drilling operations have become an exciting subject in recent years since the use of composites has increased tremendously in various areas of science and technology. It differs significantly in many aspects from machining of conventional metals and their alloys due to their special mechanical and physical properties such as good corrosive resistance and high specific strength and stiffness. Composite also has been considered as an advanced material in which they are characterized by a combination of light weight, very high specific strength, high modulus and a high stiffness.

Besides, it is an engineered material made from two or more constituent materials with significantly different physical or chemical properties and which remain separate and distinct on a macroscopic level within the finished structure. Composites have replaced conventional materials in various fields of applications such as aeronautical, aerospace, automotive, biomechanical and mechanical engineering, as well as in other industries. In composites, the material behaviour is not only inhomogeneous, but also depends on diverse fibre and matrix properties, fibre orientation, and the relative volumes of fibre and matrix. The tool encounters continuously alternate fibres and matrix, which response differently to machining.

Several attempts have been made to eliminate machining of composite by fabrication techniques like near net shape forming and modified casting, but the scope of these techniques is limited by Basavarajappa *et al.*, (2006). Although composite parts may be produced by these fabrication techniques, they require further subsequent machining to facilitate precise dimensions to the part. Hence the need for accurate machining of composites has increased enormously. The mechanism behind machining of composite is different from metals. According to Ramkumar *et al.* (2004), machining of composites can be different to metals as it is anisotropic, inhomogeneous, and mostly it is prepared in laminate form before going through the machining process.

In addition, machinability of composites is influenced by fibre and matrix properties, fibre orientation and the type of weave. On top of that, machining of composites will bring more undesirable results, such as rapid tool wear, rough surface finish of finished product, and a defective sub-surface layer with cracks and delamination (Palanikumar and Karthikeyan, 2006).

2.11 Factors Influencing Surface Finish of Turned Composites

There are much fewer investigations into turning of composites than turning of metals. According to El-Sonbaty *et al.* (2004), increasing the volume fibre fraction, V_f of GFREC can improve the surface finish but in the same time cutting speed and feed have a vice versa effect. Wang and Zhang (2003) had investigated unidirectional fibre reinforced polymer (FRP) composite and the result shown the surface finish is greatly influenced by the fibre orientation. Takeyama and Lijima (1988) had examined the surface finish on machining of GFRP composites and found that the higher the cutting speed, the rougher and the more damaged the machined surface is. Ramulu *et al.* (1994) also achieved better surface finish at high velocity whereas Birhan (2008) discovered that surface finish will decrease of increase of cutting speed and increased with the increase of feed rate. He also discovered that the surface finish decreased with the increase of tool nose radius. In addition, Spur and Wunsch (1988) realized that during turning of GFRP composites, surface finish increased with the increase of feed rate but it was not dependent on the cutting velocity.

Table 2.2: Factors affecting surface roughness and major investigators

Major Factors	Investigators	Material Studied
<u>A) Inhomogeneous and anisotropic material</u>		
1. Fibre orientation angle	1. Bhatnagar <i>et al.</i> (1995) 2. Jahanmir <i>et al.</i> (1997) 3. Sakuma and Seto (1983) 4. Wang and Zhang (2003)	FRP Composite FRP Composite GFRP Composite FRP Composite
2. Fibre volume fraction, V_f	1. Palanikumar and Karthikeyan (2006) 2. El-Sonbaty <i>et al.</i> (2004)	Al/SiC-MMC Composite GFR/epoxy Composite
3. Manufacturing technique i) Hand Lay Up	1. Davim and Mata (2005) 2. Palanikumar <i>et al.</i> (2006)	FRP Composite FRP Composite
ii) Filament Winding	1. Davim and Mata (2005) 2. Palanikumar <i>et al.</i> (2006)	FRP Composite FRP Composite
4. Type of Fibre	1. Jahanmir <i>et al.</i> (1998)	FRP Composite
<u>B) Cutting Parameter</u>		
1. Feed Rate	1. Birhan (2008) 2. Hocheng <i>et al.</i> (1997) 3. Palanikumar and Karthikeyan (2006) 4. Palanikumar <i>et al.</i> (2006) 5. El-Sonbaty <i>et al.</i> (2004) 6. Spur and Wunsch (1988)	GFRP Composite Graphite/Aluminium Composite Al/SiC-MMC Composite FRP Composite GFR/epoxy Composite GFRP Composite
2. Cutting Speed	1. Birhan (2008) 2. Hocheng <i>et al.</i> (1997) 3. Palanikumar and Karthikeyan (2006) 4. Palanikumar <i>et al.</i> (2006) 5. El-Sonbaty <i>et al.</i> (2004) 6. Spur and Wunsch (1988)	GFRP Composite Graphite/Aluminium Composite Al/SiC-MMC Composite FRP Composite GFR/epoxy Composite GFRP Composite

<u>C) Tool</u>		
1. Tool Wear	1. Birhan (2008) 2. Bhatnagar <i>et al.</i> (1995) 3. Sakuma and Seto (1983)	GFRP Composite FRP Composite GFRP Composite
2. Built up Edge	1. Palanikumar and Karthikeyan (2006)	FRP Composite

*1 -*4 sequence of most importance factor influence surface finish

A good surface finish is required for improving the physical properties, fatigue strength, corrosion resistance and aesthetic appeal of the product. It is vital to find out the factors that will influence surface finish. From the literatures survey that has been carried out, the major factors influencing surface finish during turning of composites are feed rate, fibre orientation, hand layup technique and tool wear.

The feed rate is the cutting parameter that has the highest influence on surface finish. An increase in feed rate will increase the heat generation and hence, tool wears which results in higher surface finish. Tool wear will decrease the cutting tool life and subsequently increase the cost of machining of the turned parts. In the mean time surface finish will fluctuate for different angle of fibre orientation. The higher the orientation angle, the rougher the surface finish will be generated whereas for the manufacturing technique, hand layup process is proven to be producing better surface finish than the filament winding process in machining of composites.

2.12 Chapter Summary

The early and latest researches on dynamic model of rotating beam/shaft have been reviewed including regenerative chatter modelling in turning operation. Some of the limitation of previous chatter models (manufacturing engineer models) are none of them consider moving loads in their dynamics

model. Moving loads should be considered because they are variable in both space and time as the cutter moves along the work piece and majority of the engineering structures are subjected to time and space varying loads.

In addition, in the past studies, most studies of dynamic model of turning operation have generally assumed the work piece to be rigid and no deformation was considered. In those studies, the stability of the cutting process was analysed by merely the dynamic equation of tools. The turning tool usually is represented with a single or two degree of freedom for spring mass system working over a rigid work piece. Real cutting tools have multiple degrees of freedom and in addition to horizontal and vertical displacements, tools can twist and bend.

However, in practice the work piece does have deformation when there is an external force exerting on it. Such deformation will change the chip thickness and have an effect on the critical chip thickness of stability. Although work piece vibrations impact both cutting instability and product quality including surface finishing, most models developed for investigating surface roughness do not consider work piece vibrations at all.

In this project, the research is focussed on developing a new mathematical model considering both the work piece and cutting tools as flexible. The mathematical model as well will consider moving loads with regenerative chatter for the development of dynamic model in turning operation. The development on this dynamic model will be discussed in detail later in chapter 3. Furthermore, the effect of the deflection dependence of the moving cutting forces with regenerative chatter on the dynamic behaviour of the system at various travelling speeds will also be investigated.

Besides, it is also concluded the most factors contributing to the surface finish quality are the cutting parameters which is the cutting speed, depth of cut and feed rate. Generally in machining, by changing the cutting parameters, one should be more careful and consider the cutting condition used is within recommended range to prevent unstable cutting condition.

Chapter 3

Dynamic Model of Turning Operation

3.1 Introduction

A dynamic model is defined as a time varying process but rather than the state of the process at some time t_o is dependent on the evolution of the state of the process over the time interval $[0, t_o]$ (Enders *et al.*, 1999). It is also used to express and model the behaviour of the system over time. In this research, a new mathematical model for turning metal work pieces which consider the work piece as a flexible work piece and cutting tools as a flexible cutting tool with the regenerative chatter effects is developed by combining concept of both dynamic models from two main groups of researchers; structural dynamicists and manufacturing engineers. Previously, most studies of dynamic models of turning operation generally assumed the work piece to be rigid and have therefore, ignored work piece deformation. However, in practice, the work piece undergoes deformation as a result of an external force by the cutting tool. This deformation affects and changes the chip thickness. There are no dynamic models found previously that considered the work piece and cutting tools as flexible and therefore there is a need to do this research. The details of the development of mathematical formulation of this dynamic model are thoroughly discussed and explained in the following topics.








3.2 Development of Mathematical Formulation of Rotating Beam Subjected to Three Directional Moving Loads with Regenerative Chatter

The turned work piece is modelled as a circular beam which is subjected to three directional forces moving along x axis and is rotating about its longitudinal axis, x as shown earlier in Figure 2.6. During turning, as the cutter travels along the work piece, the deformations produced in the y and z directions by the moving cutting forces are denoted by v and w . The three directional moving cutting forces are acting on the surface of the beam and they have been translated to the neutral axis of the beam as shown in Figure 2.6.

3.2.1 Boundary Conditions

Boundary condition is a value of constant integration which is determined by evaluating the functions for shear, moment, slope or displacement at a particular point on the beam and usually the value of the function is known. Several possible boundary conditions that are often used to solve beam (or shaft) deflection problems are listed in Table 3.1. For example, if the beam is supported by a roller or pin (refer to Table 3.1 - 1, 2, 3, 4), then it is required to set the displacement to zero at these points. Furthermore, if these supports are located at the ends of the beam (refer to Table 3.1 - 1, 2), the internal moment in the beam must also be zero. Besides, at a fixed support (refer to Table 3.1 - 5), the slope and displacement are both zero, whereas the free-ended beam has both zero moment and zero shear force. Lastly, if two segments of a beam are connected by an internal pin or hinge, the moment must be zero at this connection.

Table 3.1: Possible boundary conditions (Hibbeler, 2011)

1	
	$\Delta = 0$ $M = 0$ Roller
2	
	$\Delta = 0$ $M = 0$ Pin
3	
	$\Delta = 0$ Roller
4	
	$\Delta = 0$ Pin
5	
	$\theta = 0$ $\Delta = 0$ Fixed end
6	
	$V = 0$ $M = 0$ Free end
7	
	$M = 0$ Internal pin or hinge

On lathe, the work piece is clamped to a chuck at one end and is supported at the tailstock on the other end. Thus, the clamped end mimics the fixed support while the tailstock simply represents pin support. The value of v and w will depends not only on time, t but also the position along the work piece, x . It is assumed that the deflections of the work piece are

$$v(x, t) = \sum_{i=1}^n \varphi_i(x) \alpha_i(t) = \boldsymbol{\varphi}^T \boldsymbol{\alpha} \quad (3.1)$$

$$w(x, t) = \sum_{i=1}^n \varphi_i(x) \beta_i(t) = \boldsymbol{\varphi}^T \boldsymbol{\beta} \quad (3.2)$$

where $\boldsymbol{\phi}^T = \{\phi_1, \phi_2, \dots, \phi_n\}$ is a spatial function that satisfies the clamped-pinned boundary conditions of the work piece and i th mode is for the stationary beam and $\boldsymbol{\alpha}^T = \{\alpha_1, \alpha_2, \dots, \alpha_n\}$ and $\boldsymbol{\beta}^T = \{\beta_1, \beta_2, \dots, \beta_n\}$ with $\alpha_i(t)$ and $\beta_i(t)$ is the corresponding modal coordinate. Different boundary conditions mentioned previously are reflected by $\phi_i(x)$. The biggest deformations produced by the moving cutting force on the work piece are denoted by v (in y direction) and only included inside the dynamic model developed. The derivation of deflection equation (3.3) is denoted as (3.4) and (3.5) respectively.

$$v(x, t) = \boldsymbol{\phi}^T(x) \boldsymbol{\alpha}(t) \quad (3.3)$$

Taking partial differentiation with respect to time, t and distance along the work piece give rise to

$$\frac{\partial v}{\partial t} = \boldsymbol{\phi}^T(x) \dot{\boldsymbol{\alpha}}(t) \quad (3.4)$$

and taking partial differentiation with respect to distance along the work piece, x by one and two times gives

$$\frac{\partial v}{\partial x} = \boldsymbol{\phi}'^T(x) \boldsymbol{\alpha}(t) \quad (3.5)$$

$$\frac{\partial^2 v}{\partial x^2} = \boldsymbol{\phi}''^T(x) \boldsymbol{\alpha}(t) \quad (3.6)$$

and by multiplying equation (3.4) and (3.5) give rise to

$$\frac{\partial^2 v}{\partial x \partial t} = \boldsymbol{\phi}'^T(x) \dot{\boldsymbol{\alpha}}(t) \quad (3.7)$$

The second largest deflection, w is in z direction and can be written as

$$w(x, t) = \boldsymbol{\phi}^T(x) \boldsymbol{\beta}(t) \quad (3.8)$$

Taking partial differentiation with respect to time, t and distance along the work piece give rise to

$$\frac{\partial w}{\partial t} = \boldsymbol{\phi}^T(x) \dot{\boldsymbol{\beta}}(t) \quad (3.9)$$

and taking partial differentiation with respect to distance along the work piece, x by one and two times gives

$$\frac{\partial w}{\partial x} = \boldsymbol{\phi}'^T(x) \boldsymbol{\beta}(t) \quad (3.10)$$

$$\frac{\partial^2 w}{\partial x^2} = \boldsymbol{\phi}''^T(x) \boldsymbol{\beta}(t) \quad (3.11)$$

and by multiplying equation (3.9) and (3.10) give rise to

$$\frac{\partial^2 w}{\partial x \partial t} = \boldsymbol{\phi}'^T(x) \dot{\boldsymbol{\beta}}(t) \quad (3.12)$$

3.2.2 Energy Method

In general, the energy of a vibrating system is partly potential and partly kinetic. The kinetic and potential energies of beam are established based on the following assumptions. Beam has homogeneous and isotropic material properties, the elastic and centroid axes in the cross section of a beam coincide, thus the effects due to eccentricity are not considered. The work performed by the external loads during this displacement is equated to internal work. Based on Rayleigh beam theory, the kinetic energy of the beam can be written as (adapted from Chen and Ku (1997))

$$\begin{aligned}
T = & \frac{1}{2} \int_0^l \left\{ \rho A \left[\left(\frac{\partial v}{\partial t} \right)^2 + \left(\frac{\partial w}{\partial t} \right)^2 \right] \right. \\
& \left. + \rho I \left\{ \left[\left(\frac{\partial^2 v}{\partial x \partial t} \right)^2 + \left(\frac{\partial^2 w}{\partial x \partial t} \right)^2 \right] + 2\Omega \left(\frac{\partial^2 v}{\partial x \partial t} \frac{\partial w}{\partial x} - \frac{\partial^2 w}{\partial x \partial t} \frac{\partial v}{\partial x} \right) + 2\Omega^2 \right\} \right\} dx
\end{aligned} \tag{3.13}$$

By substituting equations (3.4), (3.5), (3.7), (3.9), (3.10) and (3.12) into equation (3.13);

$$\begin{aligned}
T = & \frac{\rho A}{2} \left[\dot{\alpha}^T(t) \int_0^l \boldsymbol{\varphi}(x) \otimes \boldsymbol{\varphi}^T(x) dx \dot{\alpha}(t) + \dot{\beta}^T(t) \int_0^l \boldsymbol{\varphi}(x) \otimes \boldsymbol{\varphi}^T(x) dx \dot{\beta}(t) \right] \\
& + \frac{\rho I}{2} \left[\dot{\alpha}^T(t) \int_0^l \boldsymbol{\varphi}'(x) \otimes \boldsymbol{\varphi}'^T(x) dx \dot{\alpha}(t) + \dot{\beta}^T(t) \int_0^l \boldsymbol{\varphi}'(x) \otimes \boldsymbol{\varphi}'^T(x) dx \dot{\beta}(t) \right] \\
& + \rho I \Omega \left[\dot{\alpha}^T(t) \int_0^l \boldsymbol{\varphi}'(x) \otimes \boldsymbol{\varphi}'^T(x) dx \dot{\beta}(t) - \dot{\beta}^T(t) \int_0^l \boldsymbol{\varphi}'(x) \otimes \boldsymbol{\varphi}'^T(x) dx \dot{\alpha}(t) \right]
\end{aligned}$$

Based on Chen and Ku (1997), the kinetic energy of the beam used can be obtained as below;

$$\begin{aligned}
T = & \frac{\rho A}{2} \left[\dot{\alpha}^T(t) \mathbf{A} \dot{\alpha}(t) + \dot{\beta}^T(t) \mathbf{A} \dot{\beta}(t) \right] + \frac{\rho I}{2} \left[\dot{\alpha}^T(t) \mathbf{B} \dot{\alpha}(t) + \dot{\beta}^T(t) \mathbf{B} \dot{\beta}(t) \right] \\
& + \rho I \Omega \left[\dot{\alpha}^T(t) \mathbf{B} \dot{\beta}(t) - \dot{\beta}^T(t) \mathbf{B} \dot{\alpha}(t) \right]
\end{aligned} \tag{3.14}$$

where

$$\mathbf{A} = \int_0^l \boldsymbol{\varphi}(x) \boldsymbol{\varphi}^T(x) dx, \quad \mathbf{B} = \int_0^l \boldsymbol{\varphi}'(x) \boldsymbol{\varphi}'^T(x) dx$$

and ρ is mass density, A is the cross sectional area, $I = \frac{\pi r^4}{4}$ for a circular cross-section, and Ω is the rotational speed of the work piece.

The strain energy of the beam, V is the same as the work done in deforming the beam. The strain energy of the Rayleigh beam theory is adapted from Chen and Ku (1997) and is presented in equation (3.15).

$$V = \frac{1}{2} \int_0^l EI \left[\left(\frac{\partial^2 v}{\partial x^2} \right)^2 + \left(\frac{\partial^2 w}{\partial x^2} \right)^2 \right] dx - \frac{1}{2} \int_s^l P_x \left[\left(\frac{\partial v}{\partial x} \right)^2 + \left(\frac{\partial w}{\partial x} \right)^2 \right] dx \quad (3.15)$$

By substituting equations (3.5), (3.6), (3.10) and (3.11) into equation (3.15), the strain energy of the beam can then be formed as below

$$V = \frac{EI}{2} [\boldsymbol{\alpha}^T(t) \mathbf{C} \boldsymbol{\alpha}(t) + \boldsymbol{\beta}^T(t) \mathbf{C} \boldsymbol{\beta}(t)] - \frac{P_x}{2} [\boldsymbol{\alpha}^T(t) \mathbf{B}l(t) \boldsymbol{\alpha}(t) + \boldsymbol{\beta}^T(t) \mathbf{B}l(t) \boldsymbol{\beta}(t)] dx \quad (3.16)$$

where E is Young's modulus of the beam and P_x is the axial force and

$$\mathbf{C} = \int_0^l \boldsymbol{\varphi}''(x) \times \boldsymbol{\varphi}''^T(x) dx, \quad \mathbf{B}l(t) = \int_s^l \boldsymbol{\varphi}'(x) \times \boldsymbol{\varphi}'^T(x) dx$$

Note $\mathbf{B}l(t)$ is time varying matrices. In equation (3.14) and (3.16), the dot and dash represent derivatives with respect to t and x respectively.

3.2.3 Lagrange's Equation

In order to derive the equation of motion of vibration of a rotating work piece in turning operations by using Lagrange's equations, the first step is to establish the kinetic and potential energy equations as mentioned in section 3.2.2.

Lagrange's equations for n degree of freedom system, can be stated as

$$\frac{d}{dt} \left(\frac{\partial T}{\partial \dot{q}_j} \right) - \frac{\partial T}{\partial q_j} + \frac{\partial V}{\partial q_j} = Q_j^{(n)}, \quad j = 1, 2, \dots, n \quad (3.17)$$

where $\dot{q}_j = \partial q_j / \partial t$ is the generalized velocity and $Q_j^{(n)}$ is the non-conservative generalized force or external force corresponding to the generalized

coordinate q_j . By using this formula into the problem, q can be replaced by α and the formula can be rewritten as follow;

$$\frac{d}{dt} \left(\frac{\partial T}{\partial \dot{\alpha}} \right) - \frac{\partial T}{\partial \alpha} + \frac{\partial V}{\partial \alpha} = Q \quad (3.18)$$

From the kinetic energy of the beam derived in equation (3.14);

$$T = \frac{\rho A}{2} \left[\dot{\alpha}^T(t) \mathbf{A} \dot{\alpha}(t) + \dot{\beta}^T(t) \mathbf{A} \dot{\beta}(t) \right] + \frac{\rho I}{2} \left[\dot{\alpha}^T(t) \mathbf{B} \dot{\alpha}(t) + \dot{\beta}^T(t) \mathbf{B} \dot{\beta}(t) \right] \\ + \rho I \Omega \left[\dot{\alpha}^T(t) \mathbf{B} \dot{\beta}(t) - \dot{\beta}^T(t) \mathbf{B} \dot{\alpha}(t) \right]$$

The partial derivative of T with respect to $\dot{\alpha}$ give

$$\frac{\partial T}{\partial \dot{\alpha}} = (\rho A \mathbf{A} + \rho I \mathbf{B}) \dot{\alpha} \quad (3.19)$$

and by differentiating T with respect to $\dot{\alpha}$

$$\frac{d}{dt} \frac{\partial T}{\partial \dot{\alpha}} = (\rho A \mathbf{A} + \rho I \mathbf{B}) \ddot{\alpha} \quad (3.20)$$

The partial derivative of T with respect to $\dot{\alpha}$ give

$$\frac{\partial T}{\partial \alpha} = -2\Omega \rho I \mathbf{B} \dot{\beta} \quad (3.21)$$

From the strain energy of the beam (equation (3.16));

$$V = \frac{EI}{2} \left[\alpha^T(t) \mathbf{C} \alpha(t) + \beta^T(t) \mathbf{C} \beta(t) \right] - \\ \frac{P_x}{2} \left[\alpha^T(t) \mathbf{B} l(t) \alpha(t) + \beta^T(t) \mathbf{B} l(t) \beta(t) \right] dx$$

and differentiating V with respect to α gives

$$\frac{\partial V}{\partial \alpha} = (EIC - P_x \mathbf{B}l(t))\alpha \quad (3.22)$$

while Q is the generalize cutting force component in y direction

$$Q = P_y \boldsymbol{\varphi}(s) - P_x r \boldsymbol{\varphi}' \quad (3.23)$$

Lagrange's equations give rise to the following equation of motion.

$$\rho(A\mathbf{A} + I\mathbf{B})\ddot{\alpha} + 2\rho\Omega I\mathbf{B}\dot{\beta} + (EIC - P_x \mathbf{B}l(t))\alpha = P_y \boldsymbol{\varphi}(s) - P_x r \boldsymbol{\varphi}'(s) \quad (3.24)$$

Lagrange's equations is also being used in which q is replaced with β for developing equation of motion in z direction and it can be rewritten as below;

$$\frac{d}{dt} \left(\frac{\partial T}{\partial \dot{\beta}} \right) - \frac{\partial T}{\partial \beta} + \frac{\partial V}{\partial \beta} = Q \quad (3.25)$$

From the kinetic energy of the beam derived in equation (3.14);

$$T = \frac{\rho A}{2} \left[\dot{\alpha}^T(t) \mathbf{A} \dot{\alpha}(t) + \dot{\beta}^T(t) \mathbf{A} \dot{\beta}(t) \right] + \frac{\rho I}{2} \left[\dot{\alpha}^T(t) \mathbf{B} \dot{\alpha}(t) + \dot{\beta}^T(t) \mathbf{B} \dot{\beta}(t) \right] \\ + \rho I \Omega \left[\dot{\alpha}^T(t) \mathbf{B} \dot{\beta}(t) - \dot{\beta}^T(t) \mathbf{B} \dot{\alpha}(t) \right]$$

The partial derivative of T with respect to $\dot{\beta}$ give

$$\frac{\partial T}{\partial \dot{\beta}} = (\rho A \mathbf{A} + \rho I \mathbf{B}) \dot{\beta} \quad (3.26)$$

and by differentiating T with respect to $\dot{\beta}$

$$\frac{d}{dt} \frac{\partial T}{\partial \dot{\beta}} = (\rho A \mathbf{A} + \rho I \mathbf{B}) \ddot{\beta} \quad (3.27)$$

The partial derivative of T with respect to β , give

$$\frac{\partial T}{\partial \beta} = 2\Omega\rho I\mathbf{B}\dot{\alpha} \quad (3.28)$$

From the kinetic energy of the beam;

$$V = \frac{EI}{2} [\dot{\alpha}^T(t) \mathbf{C} \alpha(t) + \dot{\beta}^T(t) \mathbf{C} \beta(t)] - \frac{P_x}{2} [\dot{\alpha}^T(t) \mathbf{B}l(t) \alpha(t) + \dot{\beta}^T(t) \mathbf{B}l(t) \beta(t)] dx$$

and differentiating V with respect to α , gives

$$\frac{\partial V}{\partial \beta} = (EIC - P_x \mathbf{B}l(t))\beta \quad (3.29)$$

while Q is the generalize cutting force component in z direction

$$Q = P_z \varphi(s) \quad (3.30)$$

Lagrange's equations give rise to the following equation of motion.

$$\rho(A\mathbf{A} + I\mathbf{B})\ddot{\beta} - 2\rho\Omega I\mathbf{B}\dot{\alpha} + (EIC - P_x \mathbf{B}l(t))\beta = P_z \varphi(s) \quad (3.31)$$

Equation (3.22) and (3.23) are governing differential equations derived for such turning operation mechanism and takes form of a delay differential equation (DDE) and this will be discussed in section 3.3.2.2. By assembling equation (3.24) and (3.31) in a matrix form leads to

$$\begin{bmatrix} \rho(A\mathbf{A} + I\mathbf{B}) & 0 \\ 0 & \rho(A\mathbf{A} + I\mathbf{B}) \end{bmatrix} \begin{bmatrix} \ddot{\alpha} \\ \ddot{\beta} \end{bmatrix} + \begin{bmatrix} 0 & 2\rho\Omega I\mathbf{B} \\ -2\rho\Omega I\mathbf{B} & 0 \end{bmatrix} \begin{bmatrix} \dot{\alpha} \\ \dot{\beta} \end{bmatrix} + \begin{bmatrix} (EIC - P_x \mathbf{B}l(t)) & 0 \\ 0 & (EIC - P_x \mathbf{B}l(t)) \end{bmatrix} \begin{bmatrix} \alpha \\ \beta \end{bmatrix} = \begin{bmatrix} P_y \varphi(s) - P_x r \varphi'(s) \\ P_z \varphi(s) \end{bmatrix}$$

α and β are column vector. Note that mass, stiffness and damping matrix in equation (3.24) and (3.31) are all time dependant and therefore the time integration is complicated and difficult to solve.

3.2.4 Three Directional Moving Cutting Forces with Regenerative Chatter Mechanism

The diagram of a typical cylindrical turning process is shown in Figure 2.2. The cutting tool moves parallel to the spindle and removes a skin from the blank, hence reducing the diameter of the work piece. Note that from Figure 2.2, for a semi orthogonal cutting operation in lathe turning, the force component can be measured in three directions and the force relationships are relatively simple. The component of the force acting on the rake face of the tool, normal to the cutting edge is called the main cutting force, P_y . This usually is the largest of the three components and acts in the direction of cutting velocity. The force component acting on the tool which parallel to the direction of feed, is referred to as a feed force, P_x . This force acts tangential to the main cutting forces, P_y . The third force component tend to push the tool away from the work in a radial direction, is the smallest of the force components in simple turning and it is usually ignored.

The turning cutting force, P has three components, P_x which determines the direct load on the feed direction, the radial component P_z , which is decisive for the deflections affecting the accuracy of the machined surface and the tangential force P_y which has the direction of the cutting speed. It is tangential to the cut surface. The cutting or tangential force acts downward on the tool tip allowing deflection of the work piece upward. It supplies the energy required for the cutting operation. Meanwhile, the axial or feed force acts in the longitudinal direction. It is also called the feed force because it is in the feed direction of the tool. This force tends to push the tool away from the chuck. The radial or thrust force acts in the radial direction. In the development of this dynamic model of turning process, the regenerative mechanism is included inside the three

directional moving cutting forces equation. If the regenerative chatter mechanism is to be modelled accurately, then the vibrations of the tool should also be included in the time delay. In turning process, the time delay is basically determined by the rotation of the work piece but it is also affected by the current and the delayed position of the tool. The cutting forces with regenerative chatter are derived from experimental data obtained during turning of several work pieces and take the form of

$$P_x = K_x f^{q_x} h \quad (3.32)$$

$$P_y = K_y f^{q_y} h \quad (3.33)$$

$$P_z = K_z f^{q_z} h \quad (3.34)$$

where K_x , K_y and K_z , are the cutting force coefficients, f is feed rate (m/rev), q_x , q_y and q_z are the exponents determined from Han *et al.* (2012) and h is the instantaneous depth of cut which can be expressed as

$$h = h_o - v(t) + v(t - \tau) \quad (3.35)$$

The moving cutting force in turning operation not only depends upon the present tool position, $v(t)$ but also delayed position of the tool, $v(t - \tau)$. Substituting equation (3.1) into equation (3.35) leads to

$$h = h_o - \boldsymbol{\varphi}^T s(t) \boldsymbol{\alpha}(t) + \boldsymbol{\varphi}^T s(t - \tau) \boldsymbol{\alpha}(t - \tau) \quad (3.36)$$

and the corresponding cutting force components with instantaneous depth of cut are shown below in equations (3.37), (3.38) and (3.39).

$$P_x = K_x f^{q_x} [h_o - \boldsymbol{\varphi}^T s(t) \boldsymbol{\alpha}(t) + \boldsymbol{\varphi}^T s(t - \tau) \boldsymbol{\alpha}(t - \tau)] \quad (3.37)$$

$$P_y = K_y f^{q_y} [h_o - \boldsymbol{\varphi}^T s(t) \boldsymbol{\alpha}(t) + \boldsymbol{\varphi}^T s(t - \tau) \boldsymbol{\alpha}(t - \tau)] \quad (3.38)$$

$$P_z = K_z f^{q_z} [h_o - \boldsymbol{\varphi}^T s(t) \boldsymbol{\alpha}(t) + \boldsymbol{\varphi}^T s(t - \tau) \boldsymbol{\alpha}(t - \tau)] \quad (3.39)$$

Later, section 3.3.2.2 explains how to solve a simple tutorial of delay differential equation and by employing this method of steps technique for solving the three directional moving cutting force equations with regenerative chatter mechanism.

From equation (3.24);

$$\rho(AA + IB)\ddot{\alpha} + 2\rho\Omega IB\dot{\beta} + (EIC - P_x B l(t))\alpha = P_y \varphi(s) - P_x r \varphi'(s)$$

and we have

$$\begin{aligned} P_Y \varphi(s) - P_X r \varphi'(s) = & h_o (K_y f^{qy} \varphi[s(t)] - K_x f^{qx} r \varphi'[s(t)]) \\ & + \varphi^T[s(t)] \alpha(t) (-K_y f^{qy} \varphi[s(t)] + K_x f^{qx} r \varphi'[s(t)]) \\ & + \varphi^T[s(t - \tau)] \alpha(t - \tau) (K_y f^{qy} \varphi[s(t)] - K_x f^{qx} r \varphi'[s(t)]) \end{aligned} \quad (3.40)$$

Substituting equation (3.24) into equation (3.40) leads to

$$\begin{aligned} \rho(AA + IB)\ddot{\alpha}(t) = & -2\rho\Omega IB\dot{\beta}(t) + \alpha(t) (-K_y f^{qy} \varphi[s(t)] \varphi^T[s(t)] + \\ & K_x f^{qx} r \varphi'[s(t)] \varphi^T[s(t)] - (EIC - P_x B l(t))) + \\ & \alpha(t - \tau) (K_y f^{qy} \varphi[s(t)] \varphi^T[s(t - \tau)] - \\ & K_x f^{qx} r \varphi'[s(t)] \varphi^T[s(t - \tau)]) + h_o (K_y f^{qy} \varphi[s(t)] - \\ & K_x f^{qx} r \varphi'[s(t)]) \end{aligned} \quad (3.41)$$

with

$$\begin{aligned} \mathbf{D} &= \text{inv}(\rho(AA + IB)) \\ \mathbf{U}_1 &= -K_y f^{qy} \varphi[s(t)] \varphi^T[s(t)] + K_x f^{qx} r \varphi'[s(t)] \varphi^T[s(t)] - (EIC - P_x B l(t)) \\ \mathbf{U}_2 &= -2\rho\Omega IB \\ \mathbf{U}_3 &= K_y f^{qy} \varphi[s(t)] \varphi^T[s(t - \tau)] - K_x f^{qx} r \varphi'[s(t)] \varphi^T[s(t - \tau)] \\ \mathbf{U}_4 &= h_o (K_y f^{qy} \varphi[s(t)] - K_x f^{qx} r \varphi'[s(t)]) \end{aligned}$$

Note that \mathbf{U}_1 and \mathbf{U}_3 are all time varying matrices and later will be computed in the Matlab software as shown in Appendix A2. α and β are column vector.

From equation (3.31);

$$\rho(A\mathbf{A} + I\mathbf{B})\ddot{\boldsymbol{\beta}} - 2\rho\Omega I\mathbf{B}\dot{\boldsymbol{\alpha}} + (E I\mathbf{C} - P_x \mathbf{B}l(t))\boldsymbol{\beta} = P_z \boldsymbol{\varphi}(s)$$

Substituting equation (3.33) into equation (3.41) leads to

$$\begin{aligned} \rho(A\mathbf{A} + I\mathbf{B})\ddot{\boldsymbol{\beta}}(t) &= 2\rho\Omega I\mathbf{B}\dot{\boldsymbol{\alpha}}(t) - K_z f^{qz} \boldsymbol{\varphi}[s(t)]\boldsymbol{\varphi}^T s(t)\boldsymbol{\alpha}(t) \\ &\quad - (E I\mathbf{C} - P_x \mathbf{B}l(t))\boldsymbol{\beta}(t) + K_z f^{qz} \boldsymbol{\varphi}[s(t)]\boldsymbol{\varphi}^T s(t-\tau)\boldsymbol{\alpha}(t-\tau) + \\ &\quad K_z f^{qz} h_o \boldsymbol{\varphi}[s(t)] \end{aligned} \quad (3.42)$$

with

$$\mathbf{D} = \text{inv}(\rho(A\mathbf{A} + I\mathbf{B}))$$

$$\mathbf{V}_1 = -K_z f^{qz} \boldsymbol{\varphi}[s(t)]\boldsymbol{\varphi}^T s(t)$$

$$\mathbf{V}_2 = 2\rho\Omega I\mathbf{B}$$

$$\mathbf{V}_3 = K_z f^{qz} \boldsymbol{\varphi}[s(t)]\boldsymbol{\varphi}^T s(t-\tau)$$

$$\mathbf{V}_4 = K_z f^{qz} h_o \boldsymbol{\varphi}[s(t)]$$

$$\mathbf{V}_5 = -(E I\mathbf{C} - P_x \mathbf{B}l(t))$$

$\mathbf{V}_1, \mathbf{V}_3$ and \mathbf{V}_5 are all time varying matrices and later will be computed as well in the Matlab software as shown in Appendix A2. α and β are column vector. The system above can be represented in the matrix form as:

$$\begin{aligned} \begin{bmatrix} \dot{\alpha}(t) \\ \ddot{\alpha}(t) \\ \dot{\beta}(t) \\ \ddot{\beta}(t) \end{bmatrix} &= \begin{bmatrix} 0 & \mathbf{I} & 0 & 0 \\ \mathbf{U}_2 * \mathbf{D} & 0 & 0 & \mathbf{U}_4 * \mathbf{D} \\ 0 & 0 & \mathbf{I} & 0 \\ 0 & \mathbf{V}_4 * \mathbf{D} & \mathbf{V}_2 * \mathbf{D} & 0 \end{bmatrix} \begin{bmatrix} \alpha(t) \\ \dot{\alpha}(t) \\ \beta(t) \\ \dot{\beta}(t) \end{bmatrix} + \\ &\quad \begin{bmatrix} 0 & 0 & 0 & 0 \\ \mathbf{U}_3 * \mathbf{D} & 0 & 0 & 0 \\ 0 & 0 & 0 & 0 \\ 0 & 0 & \mathbf{V}_3 * \mathbf{D} & 0 \end{bmatrix} \begin{bmatrix} \alpha(t-\tau) \\ \dot{\alpha}(t-\tau) \\ \beta(t-\tau) \\ \dot{\beta}(t-\tau) \end{bmatrix} + \begin{bmatrix} 0 \\ \mathbf{U}_1 * \mathbf{D} \\ 0 \\ \mathbf{V}_1 * \mathbf{D} \end{bmatrix} \end{aligned}$$

3.2.5 Improved Dynamic Model by Adapting Insperger's Cutting Force Model

Insperger (2008) studied the regenerative delay in turning operation and the model developed considered work piece as rigid and the cutting tool as flexible. The Insperger's cutting force model is being adopted in current dynamic model because of the cutting tool is assumed to be flexible. In practice, cutting tools have multiple degrees of freedom and in addition to horizontal and vertical displacements, tools can twist and bend. The cutting tool is assumed to experience bending motion in directions x and y , while the work piece is assumed to be rigid. The cutting forces are given in the form of

$$F_x = K_x w h^q \quad (3.43)$$

$$F_y = K_y w h^q \quad (3.44)$$

$$F_z = K_z w h^q \quad (3.45)$$

where K_x, K_y and K_z are the cutting force coefficients, w is the depth of cut, q is an exponent ($q = 0.75$ is a typical empirical value for this parameter) and h is the chip thickness which can be given as

$$h = f \cdot f \cdot s \cdot \tau - X(t) + X(t - \tau) \quad (3.46)$$

and $f \cdot f \cdot s$ is the speed of the feed and τ is the time delay. The moving cutting force in turning operation not only depends on the present cut $X(t)$, but also relies on the previous cut of the tool, $X(t - \tau)$. Figure 3.1 depicted the difference of coordinate system between the current dynamic model with Insperger's coordinate system.

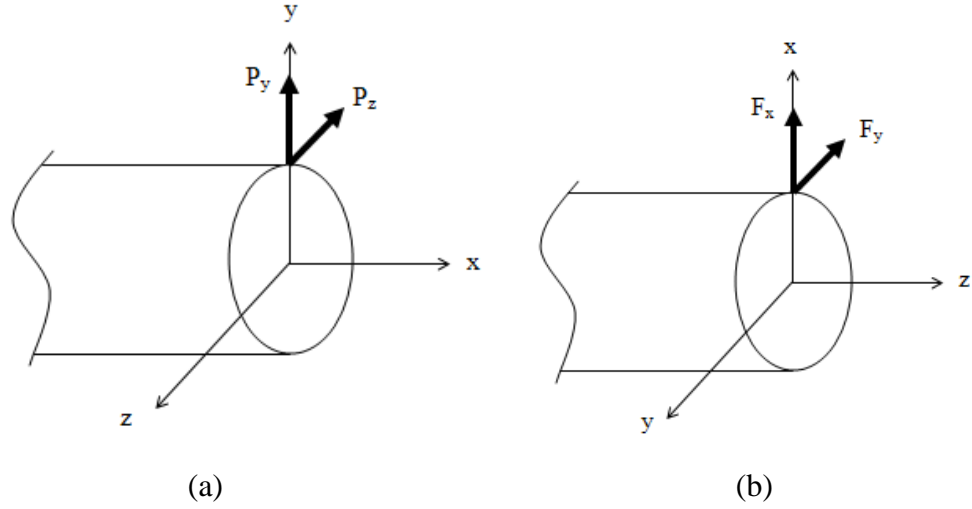


Figure 3.1: Comparison between current dynamic model coordinate system and Insperger's coordinate system (a) current dynamic model coordinate system (b) Insperger's coordinate system

The generalization between current dynamic model coordinate system and Insperger's coordinate system is done by matching Insperger's cutting forces to the current cutting forces used as depicted in Table 3.2 below;

Table 3.2: Matching table for both coordinate systems

Current cutting forces	Insperger's cutting forces
P_x	F_z
P_y	F_x
P_z	F_y

The new corresponding cutting force equations with instantaneous depth of cut are shown below in equations (3.47), (3.48) and (3.49)

$$P_x = K_y w [f \cdot f \cdot s * \tau + X(t - \tau) - X(t)]^q \quad (3.47)$$

$$P_y = K_z w [f \cdot f \cdot s * \tau + X(t - \tau) - X(t)]^q \quad (3.48)$$

$$P_z = K_x w [f \cdot f \cdot s * \tau + X(t - \tau) - X(t)]^q \quad (3.49)$$

So now

$$\begin{aligned}
P_Y \boldsymbol{\varphi}(s) - P_X r \boldsymbol{\varphi}'(s) = & w * f.f.s * \tau (K_z \boldsymbol{\varphi}[s(t)] - K_y r \boldsymbol{\varphi}'[s(t)]) \\
& + w * X(t)(-K_z \boldsymbol{\varphi}[s(t)] + K_y r \boldsymbol{\varphi}'[s(t)]) + w * X(t - \tau)(K_z \boldsymbol{\varphi}[s(t)] - \\
& K_y r \boldsymbol{\varphi}'[s(t)])
\end{aligned} \tag{3.50}$$

From equation (3.24),

$$\rho(AA + IB)\ddot{\boldsymbol{\alpha}} + 2\rho\Omega IB\dot{\boldsymbol{\beta}} + (EIC - P_x \mathbf{B}l(t))\boldsymbol{\alpha} = P_y \boldsymbol{\varphi}(s) - P_x r \boldsymbol{\varphi}'(s)$$

where axial load, $P_x \mathbf{B}l(t)$ is negligible.

By comparing and adopting Insperger's cutting force model (Insperger, 2008) into the current dynamic model of a rotating beam subjected to three directional moving cutting forces with regenerative chatter model, the new improved equation of motion of the beam in y direction can be derived as below:

$$\begin{aligned}
\rho(AA + IB)\ddot{\boldsymbol{\alpha}} + 2\rho\Omega IB\dot{\boldsymbol{\beta}} + EIC\boldsymbol{\alpha} = & w * f.f.s * \tau (K_z \boldsymbol{\varphi}[s(t)] - K_y r \boldsymbol{\varphi}'[s(t)]) + \\
& w * X(t)(-K_z \boldsymbol{\varphi}[s(t)] + K_y r \boldsymbol{\varphi}'[s(t)]) + w * X(t - \tau)(K_z \boldsymbol{\varphi}[s(t)] - K_y r \boldsymbol{\varphi}'[s(t)])
\end{aligned} \tag{3.51}$$

with

$$\begin{aligned}
\mathbf{D} &= \text{inv}(\rho(AA + IB)) \\
\mathbf{U}_1 &= -EIC \\
\mathbf{U}_2 &= -2\rho\Omega IB \\
\mathbf{U}_3 &= w * (-K_z \boldsymbol{\varphi}[s(t)] + K_y r \boldsymbol{\varphi}'[s(t)]) \\
\mathbf{U}_4 &= w * (K_z \boldsymbol{\varphi}[s(t)] - K_y r \boldsymbol{\varphi}'[s(t)]) \\
\mathbf{U}_5 &= w * f.f.s * \tau (K_z \boldsymbol{\varphi}[s(t)] - K_y r \boldsymbol{\varphi}'[s(t)])
\end{aligned}$$

Note that all matrices are later computed in the Matlab software as shown in Appendix A2.

From equation (3.31), the new improved equation of motion of beam in z direction can be derived as below;

$$\rho(AA + IB)\ddot{\boldsymbol{\beta}} + 2\rho\Omega IB\dot{\boldsymbol{\alpha}} + (EIC - P_x \mathbf{B}l(t))\boldsymbol{\beta} = P_z \varphi(s)$$

where axial load, $P_x \mathbf{B}l(t)$ is negligible and yields

$$\begin{aligned} \rho(AA + IB)\ddot{\boldsymbol{\beta}} + 2\rho\Omega IB\dot{\boldsymbol{\alpha}} + (EIC - P_x \mathbf{B}l(t))\boldsymbol{\beta} = & w * f.f.s * \tau (K_x \boldsymbol{\varphi}[s(t)]) \\ & - w * X(t)(K_x \boldsymbol{\varphi}[s(t)]) + w * X(t - \tau)(K_x \boldsymbol{\varphi}[s(t)]) \end{aligned} \quad (3.52)$$

with

$$\mathbf{D} = \text{inv}(\rho(AA + IB))$$

$$\mathbf{V}_1 = -EIC = \mathbf{U}_1$$

$$\mathbf{V}_2 = 2\rho\Omega IB = -\mathbf{U}_2$$

$$\mathbf{V}_3 = -w * K_x \boldsymbol{\varphi}[s(t)]$$

$$\mathbf{V}_4 = w * K_x \boldsymbol{\varphi}[s(t)]$$

$$\mathbf{V}_5 = w * f.f.s * \tau (K_x \boldsymbol{\varphi}[s(t)])$$

All matrices are later computed in the Matlab software and shown in Appendix A2.

3.2.6 Cutting Tool Equation of Motions

The vibrations of the tool should also be included in the developed dynamic model to ensure the model accuracy. The cutting tools are often modelled as a lumped vibration system having one or two degrees of freedom for describing motions of the cutting tool where the cutting force is described as a function of relative vibrations during the current and previous passes.

Equation of motion of cutting tool in x direction can be derived as

$$m\ddot{\mathbf{X}}(t) + C_X\dot{\mathbf{X}}(t) + K_X\mathbf{X}(t) = P_X \quad (3.53)$$

Substituting equation (3.47) into equation (3.53) gives rise to

$$m\ddot{\mathbf{X}}(t) + C_X\dot{\mathbf{X}}(t) + K_X\mathbf{X}(t) = K_y w [f.f.s * \tau + X(t - \tau) - X(t)]^q$$

and

$$\ddot{\mathbf{X}}(t) = (-C_X\dot{\mathbf{X}}(t) + \mathbf{X}(t)(-K_y w - K_X) + K_y w X(t - \tau) + K_y w * f.f.s * \tau)/m \quad (3.54)$$

with

$$\mathbf{W}_1 = -C_X/m$$

$$\mathbf{W}_2 = (-K_y w - K_X)/m$$

$$\mathbf{W}_3 = K_y w/m$$

$$\mathbf{W}_4 = (K_y w * f.f.s * \tau)/m$$

Equation of motion of cutting tool in z direction is

$$m\ddot{\mathbf{Z}}(t) + C_Z\dot{\mathbf{Z}}(t) + K_Z\mathbf{Z}(t) = P_Z \quad (3.55)$$

Substituting equation (3.47) into equation (3.55) leads to

$$m\ddot{\mathbf{Z}}(t) + C_Z\dot{\mathbf{Z}}(t) + K_Z\mathbf{Z}(t) = K_x w [f.f.s * \tau + X(t - \tau) - X(t)]^q$$

and

$$\ddot{\mathbf{Z}}(t) = (-C_Z\dot{\mathbf{Z}}(t) + X(t)(-K_x w) + K_x w X(t - \tau) - K_Z\mathbf{Z}(t) + K_x w * f.f.s * \tau)/m \quad (3.56)$$

with

$$\begin{aligned}
\mathbf{P}_1 &= -C_Z/m \\
\mathbf{P}_2 &= -K_x w/m \\
\mathbf{P}_3 &= K_x w/m = -\mathbf{P}_2 \\
\mathbf{P}_4 &= -K_Z/m \\
\mathbf{P}_5 &= K_x w * f.f.s * \tau/m
\end{aligned}$$

By assembling equations (3.51), (3.52), (3.54) and (3.56), it can be represented in a matrix form as below;

$$\begin{bmatrix} \dot{\alpha}(t) \\ \ddot{\alpha}(t) \\ \dot{\beta}(t) \\ \ddot{\beta}(t) \\ \dot{X}(t) \\ \ddot{X}(t) \\ \dot{Z}(t) \\ \ddot{Z}(t) \end{bmatrix} = \begin{bmatrix} 0 & \mathbf{I} & 0 & 0 & 0 & 0 & 0 & 0 & 0 \\ \mathbf{U}_1 * \mathbf{D} & 0 & 0 & \mathbf{U}_2 * \mathbf{D} & \mathbf{U}_3 * \mathbf{D} & 0 & 0 & 0 & 0 \\ 0 & 0 & 0 & \mathbf{I} & 0 & 0 & 0 & 0 & 0 \\ 0 & \mathbf{V}_2 * \mathbf{D} & \mathbf{V}_1 * \mathbf{D} & 0 & \mathbf{V}_3 * \mathbf{D} & 0 & 0 & 0 & 0 \\ 0 & 0 & 0 & 0 & 0 & \mathbf{I} & 0 & 0 & 0 \\ 0 & 0 & 0 & 0 & \mathbf{W}_2 * \mathbf{F} & \mathbf{W}_1 * \mathbf{F} & 0 & 0 & 0 \\ 0 & 0 & 0 & 0 & 0 & 0 & 0 & \mathbf{I} & 0 \\ 0 & 0 & 0 & 0 & \mathbf{P}_2 * \mathbf{F} & 0 & \mathbf{P}_4 * \mathbf{F} & \mathbf{P}_1 * \mathbf{F} & 0 \end{bmatrix} \begin{bmatrix} \alpha(t) \\ \dot{\alpha}(t) \\ \beta(t) \\ \dot{\beta}(t) \\ X(t) \\ \dot{X}(t) \\ Z(t) \\ \dot{Z}(t) \end{bmatrix} \\
+ \begin{bmatrix} 0 & 0 & 0 & 0 & 0 & 0 & 0 & 0 & 0 \\ 0 & 0 & 0 & 0 & \mathbf{U}_4 & 0 & 0 & 0 & 0 \\ 0 & 0 & 0 & 0 & 0 & 0 & 0 & 0 & 0 \\ 0 & 0 & 0 & 0 & \mathbf{V}_4 & 0 & 0 & 0 & 0 \\ 0 & 0 & 0 & 0 & 0 & 0 & 0 & 0 & 0 \\ 0 & 0 & 0 & 0 & \mathbf{W}_3 & 0 & 0 & 0 & 0 \\ 0 & 0 & 0 & 0 & 0 & 0 & 0 & 0 & 0 \\ 0 & 0 & 0 & 0 & \mathbf{P}_3 & 0 & 0 & 0 & 0 \end{bmatrix} \begin{bmatrix} \alpha(t-\tau) \\ \dot{\alpha}(t-\tau) \\ \beta(t-\tau) \\ \dot{\beta}(t-\tau) \\ X(t-\tau) \\ \dot{X}(t-\tau) \\ Z(t-\tau) \\ \dot{Z}(t-\tau) \end{bmatrix} + \begin{bmatrix} 0 \\ \mathbf{U}_5 \\ 0 \\ \mathbf{V}_5 \\ 0 \\ \mathbf{W}_4 \\ 0 \\ \mathbf{P}_5 \end{bmatrix}$$

3.3 Elastic Boundary Condition

The usual first step in performing a dynamic analysis is determining the natural frequencies and mode shapes of the structure. These results characterize the basic dynamic behaviour of the structure and are an indication of how the structure will respond to dynamic loading. The natural frequencies of a structure are the frequencies at which the structure naturally tends to vibrate if it is subjected to a disturbance. The deformed shape of the structure at a specific natural frequency of vibration is termed its mode shape. Each mode shape is associated with a specific natural frequency.

Natural frequencies and mode shapes are functions of the structural property and boundary conditions. A cantilever beam has a set of natural frequencies and associated mode shapes. If the structural properties change, the natural frequencies change, but the mode shapes may not necessarily change. For example, if the elastic modulus of cantilever beam is changed, the natural frequencies change but the mode shapes remain the same. If the boundary conditions change, then the natural frequencies and mode shapes both change.

For a cantilever beam, the free vibration solution can be found using the method of separation of variables as $w(x, t) = W(x)T(t)$ and the solution of $W(x)$ is assumed to be

$$W(x) = Ce^{sx} \quad (3.57)$$

The function $W(x)$ is known as the normal mode or characteristic function of the beam, where C and s are constants. The auxiliary equation is

$$s^4 - \beta^4 = 0 \quad (3.58)$$

The roots of this equation are

$$s_{1,2} = \pm \beta, \quad s_{3,4} = \pm i\beta \quad (3.59)$$

Hence the solution of equation $\frac{d^4 W(x)}{dx^4} - \beta^4 W(x) = 0$ becomes

$$W(x) = C_1 e^{\beta x} + C_2 e^{-\beta x} + C_3 e^{i\beta x} + C_4 e^{-i\beta x} \quad (3.60)$$

Equation (3.60) can also be expressed as

$$W(x_n) = C_1 \cos(\beta x_n) + C_2 \sin \beta x_n + C_3 \cosh \beta x_n + C_4 \sinh(\beta x_n) \quad (3.61)$$

where C_1 , C_2 , C_3 , and C_4 are different constants. The value of β can be found from any beam boundary conditions. ω_n is the n th natural frequency of the beam and is given by

$$\omega_n = (\beta_n l)^2 \sqrt{\frac{EI}{\rho A l^4}} \quad (3.62)$$

For any beams, there will be an infinite number of normal modes with one natural frequency associated with each normal mode. The other collaborator group from Dalian University of Technology (DUT) in China has done the modal testing for boundary work piece in lathe in order to determine its natural frequencies and mode shapes. Table 3.3 below shows the measured mode shapes Z , measured frequencies ω_n , and β_n can be calculated from equation (3.62) with known length, $l = 0.55$ m, radius $r = 18.5$ mm, Young's Modulus $E = 2.07 \times 10^{11}$ Pa, and density, $\rho = 7817.4$ kg/m³.

Table 3.3: Tabulated measured mode shapes, frequencies and β_n

Measured mode shapes, Z	ω (Hz)	ω (rad/s)	β_n
1Z	243	1526.81403	5.661339609
2Z	253	1589.645883	5.77665368
3Z	318	1998.052928	6.476339858
4Z	336	2111.150263	6.657109641
5Z	1.31E+03	8230.972752	13.14473148
6Z	1.42E+03	8922.123136	13.68548658
7Z	1.74E+03	10932.74243	15.14923474
8Z	1.86E+03	11686.72467	15.66291327
9Z	2.72E+03	17090.26404	18.94089616
10Z	2.92E+03	18346.9011	19.624902
11Z	3.07E+03	19289.37889	20.12265396
12Z	3.35E+03	21048.67078	21.02027893
13Z	4.59E+03	28839.82056	24.60494586
14Z	4.73E+03	29719.4665	24.97736621

These four values of β_n (5.77665368, 6.657109641, 13.14473148 and 13.68548658) are corresponding to its measured mode shapes at 2Z, 4Z, 5Z and

6Z. These values are chosen as it is depicted the first, second, third and fourth bending mode shape of the beam. Figure 3.2 illustrates one of the chosen values of β_n , 5.77665368 which show the beam first bending mode shape.

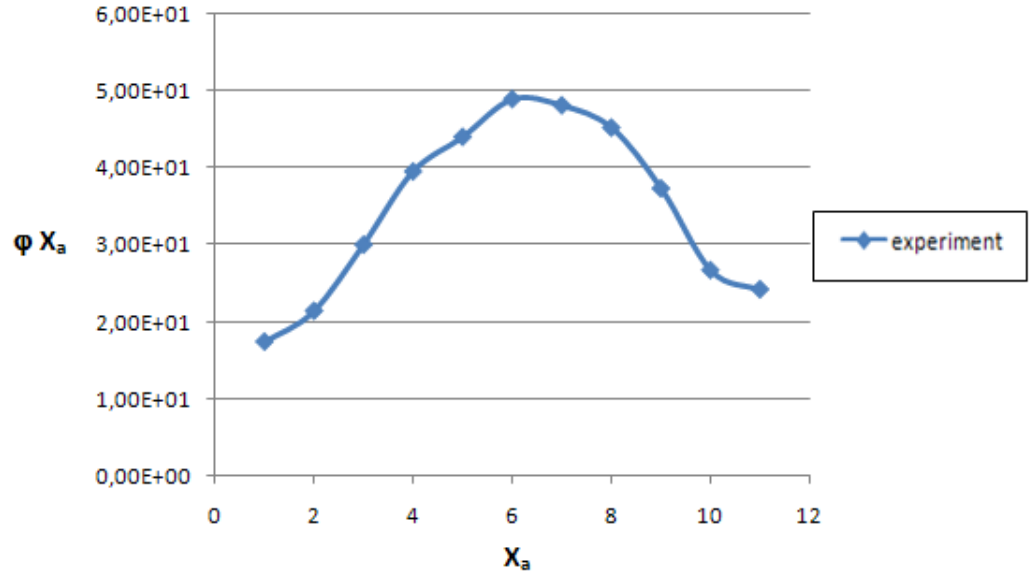


Figure 3.2: Example of one value of β_n showing the beam first bending mode shape

Later, $\beta_2, \beta_4, \beta_5$ and β_6 are substituted into equation (3.61) to calculate their corresponding C_1, C_2, C_3 , and C_4 . Curve fitting is employed in order to determine the value of C_1, C_2, C_3 and C_4 from the experimental data provided. Curve fitting is a process of constructing a curve that has the best fit to a series of data points. Experimental data provided the values for one or more measured quantities for specific values of set quantities. The linear regression formula is shown in Equation (3.63) below

$$\sigma^2 = \frac{1}{N} \sum_1^N [y_n - f(x_n)]^2 \quad (3.63)$$

σ is the root mean square which is the distance between the experiment mode shape and new fitted mode shape and it should be minimised

$$f(x_n) = C_1 \cos(\beta x_n) + C_2 \sin \beta x_n + C_3 \cosh \beta x_n + C_4 \sinh(\beta x_n) \quad (3.64)$$

Substitute equation (3.64) into equation (3.63) leads to

$$\sigma^2 = \frac{1}{N} \sum_1^N [y_n - C_1 \cos(\beta x_n) - C_2 \sin \beta x_n - C_3 \cosh \beta x_n - C_4 \sinh(\beta x_n)]^2 \quad (3.65)$$

Taking partial differentiation about σ^2 in respect of each of the constant C_1 , C_2 , C_3 and C_4 gives

$$\begin{aligned} \frac{\partial(\sigma^2)}{\partial C_1} &= \frac{2}{N} \sum_1^N [\cos(\beta x_n)] [y_n - C_1 \cos(\beta x_n) - C_2 \sin(\beta x_n) \\ &\quad - C_3 \cosh(\beta x_n) - C_4 \sinh(\beta x_n)]^2 \end{aligned}$$

$$\begin{aligned} \frac{\partial(\sigma^2)}{\partial C_2} &= \frac{2}{N} \sum_1^N [\sin(\beta x_n)] [y_n - C_1 \cos(\beta x_n) - C_2 \sin \beta x_n \\ &\quad - C_3 \cosh \beta x_n - C_4 \sinh(\beta x_n)]^2 \end{aligned}$$

$$\begin{aligned} \frac{\partial(\sigma^2)}{\partial C_2} &= \frac{2}{N} \sum_1^N [\sin(\beta x_n)] [y_n - C_1 \cos(\beta x_n) - C_2 \sin \beta x_n \\ &\quad - C_3 \cosh \beta x_n - C_4 \sinh(\beta x_n)]^2 \end{aligned}$$

$$\begin{aligned} \frac{\partial(\sigma^2)}{\partial C_3} &= \frac{2}{N} \sum_1^N [\cosh(\beta x_n)] [y_n - C_1 \cos(\beta x_n) - C_2 \sin(\beta x_n) \\ &\quad - C_3 \cosh(\beta x_n) - C_4 \sinh(\beta x_n)]^2 \end{aligned}$$

$$\begin{aligned} \frac{\partial(\sigma^2)}{\partial C_4} &= \frac{2}{N} \sum_1^N [\sinh(\beta x_n)] [y_n - C_1 \cos(\beta x_n) - C_2 \sin(\beta x_n) \\ &\quad - C_3 \cosh(\beta x_n) - C_4 \sinh(\beta x_n)]^2 \end{aligned}$$

and in the matrix form and it can be expressed as

$$\frac{2}{N} \sum_1^N \begin{bmatrix} (\cos(\beta x_n))^2 & \sin(\beta x_n) \cos(\beta x_n) & \cosh(\beta x_n) \cos(\beta x_n) & \sinh(\beta x_n) \cos(\beta x_n) \\ \cos(\beta x_n) \sin(\beta x_n) & (\sin(\beta x_n))^2 & \cosh(\beta x_n) \sin(\beta x_n) & \sinh(\beta x_n) \sin(\beta x_n) \\ \cos(\beta x_n) \cosh(\beta x_n) & \sin(\beta x_n) \cosh(\beta x_n) & (\cosh(\beta x_n))^2 & \sinh(\beta x_n) \cosh(\beta x_n) \\ \cos(\beta x_n) \sinh(\beta x_n) & \sin(\beta x_n) \sinh(\beta x_n) & \cosh(\beta x_n) \sinh(\beta x_n) & (\sinh(\beta x_n))^2 \end{bmatrix} \begin{bmatrix} C_1 \\ C_2 \\ C_3 \\ C_4 \end{bmatrix}$$

$$= \frac{2}{N} (y_n) \sum_1^N \begin{bmatrix} \cos(\beta x_n) \\ \sin(\beta x_n) \\ \cosh(\beta x_n) \\ \sinh(\beta x_n) \end{bmatrix}$$

The matrix is then computed in Matlab software. The details of the computation programme generated in Matlab software is shown in Appendix A13 - Calculation of C_1 , C_2 , C_3 and C_4 variables.

The new fitted mode shape can be calculated by substituting C_1 , C_2 , C_3 , C_4 and β_n , respectively into the equation (3.61). These new C_1 , C_2 , C_3 , and C_4 are constant and will also be used for the chuck-tailstock numerical simulation. Table 3.4 below shows the example calculation for fitting the mode shape of 2Z.

Table 3.4: Example calculation for fitting the mode shape of 2Z

x_a	β_n	$x_a \beta_n$	C_a	$C_1 \cos x_a$ β_n	$C_2 \sin x_a$ β_n	$C_3 \cosh x_a$ β_n	$C_4 \sinh x_a$ β_n	$\Phi_1 x_a$
0	5.777	2.88	12.28	-11.89	10.01	83.22	-65.79	21.52
0.05		2.59	40.01	-10.52	20.63	62.49	-49.16	30.64
0.10		2.31	9.23	-8.28	29.54	47.019	-36.67	38.47
0.15		2.02	-7.34	-5.35	36.00	35.49	-27.25	44.17
0.20		1.73		-1.98	39.48	26.94	-20.13	47.17
0.25		1.44		1.55	39.69	20.66	-14.70	47.20
0.30		1.15		4.95	36.60	16.11	-10.50	44.31
0.35		0.86		7.95	30.49	12.92	-7.19	38.88
0.40		0.57		10.29	21.85	10.82	-4.48	31.61
0.45		0.28		11.77	11.39	9.62	-2.15	23.44
0.50		0		12.28	0	9.23	0	15.56

where x_a is the length of the work piece and $\phi_1 x_a$ is the new fitted mode shape. The new fitted theoretical (marked by red) and measured (marked by blue) mode shapes for the chuck-tailstock is shown in Figure (3.3) below

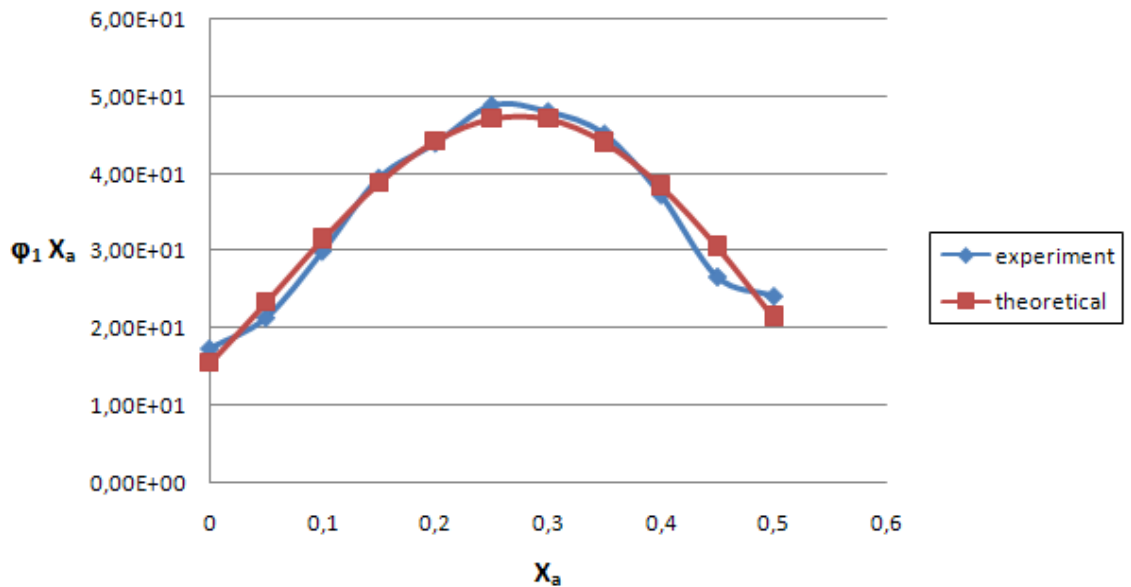


Figure 3.3: Graph of new fitted theoretical (marked by red) and measured (marked by blue) mode shapes for the chuck-tailstock

3.4 Methodology for Chatter Analysis / Numerical Integration Methods in Vibration Analysis

When the differential equation of motion of a vibrating system cannot be integrated in a closed form, a numerical approach must be used. Several numerical methods are available for the vibration problems such as (1) Runge-Kutta method, (2) Houbolt method, (3) Wilson method, and (4) Newmark method. In Runge-Kutta methods, the current displacement is expressed in terms of the previously determined values of displacement, velocity and the resulting equations are solved to find the current displacement.

Meanwhile, the most general approach for the solution of the dynamic response of structural systems is the direct numerical integration of the dynamic

equilibrium equations. This involves, after the solution is defined at time zero, the attempt to satisfy dynamic equilibrium at discrete points in time. Most methods use equal time intervals at Δt , $2\Delta t$, $3\Delta t$,..... $N\Delta t$. Many different numerical techniques have previously been presented; however, all approaches can fundamentally be classified as either explicit or implicit integration methods. Explicit methods do not involve the solution of a set of linear equations at each step. Basically, these methods use the differential equation at time “ t ” to predict a solution at time “ $t + \Delta t$ ”. For most real structures, which contain stiff elements, a very small time step is required in order to obtain a stable solution. Therefore, all explicit methods are conditionally stable with respect to the size of the time step. Implicit methods attempt to satisfy the differential equation at time “ t ” after the solution at time “ $t - \Delta t$ ” is found. These methods require the solution of a set of linear equations at each time step; however, larger time steps may be used. Implicit methods can be conditionally or unconditionally stable.

Numerical methods such as Runge-Kutta and delay differential methods require the use of a time step. The accuracy of the solution always depends on the size of the time step. Numerical integration methods have two fundamental characteristics. First is to satisfy the governing differential equation at all time, t but only at discrete time intervals Δt apart. Second, a suitable type of variation of the displacement x , velocity \dot{x} , and acceleration \ddot{x} are assumed within each time interval Δt . The values of x and \dot{x} are known to be x_0 and \dot{x}_0 , respectively at time $t = 0$ and the solution of the problem is required from $t = 0$ to $t = T$.

There are two most common analyses used in numerical integration for vibrating system which are frequency response analysis and time domain analysis. Each of this analysis will be explained in section 3.4.1 and 3.4.2.

3.4.1 Frequency Response Analysis

Frequency response analysis is the response characteristics of the system when subjected to sinusoidal inputs. The input frequency is varied, and the output characteristics are computed or represented as a function of the frequency. Frequency response analysis provides useful insights into the stability and performance characteristics of the dynamic system.

Estimating the frequency response for a physical system generally involves exciting the system with an input signal, measuring both input and output time histories, and comparing the two through a process such as the Fast Fourier Transform (FFT). The important aspect of this analysis is that the frequency content of the input signal must cover the frequency range of interest or the results will not be valid for the portion of the frequency range not covered.

Representation of a frequency response for a dynamic system using the transfer function is very useful in control theory as well as in vibration testing for measuring the dynamic response and for system identification. For example, for a system whose parameters such as mass (m), damping constant (c) and spring stiffness (k) are unknown, the transfer function can be determined experimentally by measuring the response or output due to a known input. Once the transfer function is determined, it provides a complete description of the dynamic characteristics of the system.

In vibration testing, the measured vibration response (due to a known input or forcing function) could be the displacement, velocity or more commonly the acceleration. The transfer function corresponding to the acceleration response can be defined as the ratio of $\frac{s^2 X(s)}{F(s)}$ where $F(s)$ is the Laplace's Transform of the input and $s^2 X(s)$ is the Laplace's Transform of the acceleration.

3.4.2 Transient Response Analysis

Transient response analysis is the most general method for computing forced dynamic response. The purpose of a transient response analysis is to compute the behaviour of a structure subjected to time varying excitation/load. The transient excitation is explicitly defined in the time domain. All of the forces applied to the structure are known at each instant in time. Forces can be in the form of applied forces and/or enforced motions. The important results obtained from transient analysis are typically displacements, velocities, and acceleration of grid points, and forces and stresses in elements.

Depending upon the structure and the nature of loading, two different numerical methods can be used for dynamic transient analysis; direct and modal. The direct method performs a numerical integration on the complete coupled equation of motion. The modal method utilizes the mode shapes of the structure to reduce and uncouple the equation of motion; the solution is then obtained through the summation of the individual modal responses. In transient response, structural response is computed by solving a set of couple equations using direct numerical integration. Initial displacement or/and velocities in direct transient response need to be imposed.

Introduction of Runge-Kutta method and delay differential equations are given in the following section. In the beginning, the current model developed employs a Runge-Kutta method. In Runge-Kutta method, the matrix equation of motion is used to express acceleration vector. This method requires initial conditions such as a displacement or velocity and it is a time domain analysis.

3.4.2.1 Runge-Kutta Method

Runge-Kutta method is by far the most commonly used methods in most engineering applications today. They were developed around 100 years ago (relatively new in terms of math history since Newton was in the 17th century

and Euler was in the early of 18th century), and are an extension of the same math Euler developed. In Euler's work, he seemed to favour employing Taylor series to all sorts of different. It is a first order of Taylor polynomial expansion, so its accuracy is limited, and if the derivatives of the function are not good it will lead to some serious error.

Runge-Kutta method includes an additional calculation of slope in the middle of each time step, and takes a weighted average of the values to evaluate the function. This helps reduce the error as it goes from time step to time step, and can result in some very accurate results. These methods are named RK2 (2 terms model) and it is very basic, and equivalent to the Midpoint MATLAB's ODE45 routine switches between an RK4 and RK5 based on which is providing a better result, hence the name ODE45. Runge-Kutta method works by several evaluations of an ODE at different points, then averaging those values:

$$k_{1,n} = h * f(t_n, y_n) \quad (3.51)$$

$$k_{2,n} = h * f\left(t_n + \frac{h}{2}, y_n + \frac{k_{1,n}}{2}\right) \quad (3.52)$$

$$y_{n+1} = y_n + \left(\frac{k_1 + k_2}{2}\right) \quad (3.53)$$

k_1 and k_2 are Euler's Method and by evaluating the function at the midpoint, using previous calculation of y in k_1 . Then, average these values to get (more accurate) estimation for y_{n+1} . The RK4 works exactly like the RK2 except for two points, there are more k terms, and the average is weighted traditionally in the middle. Here is the iterative function in general:

$$k_1 = h * f(t_n, y_n)$$

$$k_2 = h * f\left(t_n + \frac{h}{2}, y_n + \frac{k_1}{2}\right)$$

$$k_3 = h * f\left(t_n + \frac{h}{2}, y_n + \frac{k_2}{2}\right)$$

$$k_4 = h * f(t_n + h, y_n + k_3)$$

$$y_{n+1} = y_n + \left(\frac{k_1 + 2k_2 + 2k_3 + k_4}{6}\right)$$

Notice that the first two terms are exactly the same as RK2. The third term k_3 is calculated exactly the same way as k_2 , but with k_2 as y -value instead of k_1 . This is just a refinement method for k_2 's value. k_4 evaluates y at $(t + h)$ using k_3 's approximation for y , and then the weighted average is taken where the middle values are more weighted than the ends.

Runge-Kutta method is self starting and stable for multi-degree of freedom systems. But it needs a value of displacement, $x(t = 0)$ or velocity, $\dot{x}(t = 0)$ to calculate the time step. In contrast, using a Delay Differential Equation (DDE) will automatically recognize the time step since it is a self generated algorithm and have smaller time steps. Runge-Kutta method always depends on the initial conditions. Hence, it is much easier and quicker in terms of programming to adopt DDE methods.

3.4.2.2 Delay Differential Equations (DDE)

In a system of ordinary differential equations (ODEs) $y'(t) = f(t, y(t))$, the derivative of the solution depends on the solution at the present time, t . In a system of delay differential equations (DDEs), the derivative also depends on the solution at earlier times.

$$y'(t) = f(t, y(t)), f(t, y(t - \tau_1)), f(t, y(t - \tau_2)) \dots, f(t, y(t - \tau_k)) \quad (3.54)$$

where the delays, τ_j are positive constants. In evaluating the DDEs of equation (3.54), $y(t - \tau_k)$ may represent values of the solution at points prior to the

initial point. In particular, when evaluating DDEs at point $t = a$, we must have a value of $y(a - \tau)$. The given initial data must include not only $y(a)$ but also a ‘history’: the values $y(t)$ for all t in the interval $[a - \tau, a]$.

The method of steps is a technique for solving DDEs by reducing them to a sequence of ODEs. The detailed procedure of how the method work for $y'(t) = y(t - 1)$ in the first two steps with history $S(t) = 1$ for $0 \leq t \leq 1$ is shown in Table 3.5.

Table 3.5: A technique of solving DDEs by reducing to a sequence of ODEs.

T	$t-1$	$y(t - 1)$	$y'(t) = y(t - 1)$	$y(t)$
$0 \leq t \leq 1$	$-1 \leq t \leq 0$	1	$y'(t) = 1$	$\int y' = \int 1 dt$ $y(t) = t + c$ <p>Initial value $y(0) = 1$</p> $y(0) = c = 1$ $y(t) = t + 1$ $y(1) = 2$
$1 \leq t \leq 2$	$0 \leq t \leq 1$	$y(t) = t + 1$ $y(t - 1) = t$	$y'(t) = t$	$\int y' = \int t dt$ $y(t) = \frac{t^2}{2} + c$ <p>Initial value $y(1) = 2$</p> $y(1) = c + \frac{1}{2} = 4$ $c = \frac{3}{2}$ $y(t) = \frac{t^2 + 3}{2}$ $y(2) = \frac{7}{2}$

To show how it goes and to illustrate the propagation of discontinuities, $y'(t) = y(t-1)$ with history $S(t) = 1$ equation is solved for $0 \leq t$. On the interval, $0 \leq t \leq 1$, the function $y(t-1)$ in $y'(t) = y(t-1)$ has the known value $S(t-1) = 1$ because $t-1 \leq 0$. The DDE on this interval reduces to the ODE $y'(t) = 1$ with initial value $y(0) = S(0) = 1$ to obtain $y(t) = t+1$ for $0 \leq t \leq 1$. The solution of DDE exhibits typical discontinuity in its first derivative at $t = 0$ because it is 0 to the left origin and 1 to the right. Now that solution $t \leq 1$ has been obtained, DDE on the interval $1 \leq t \leq 2$ can be reduced to ODE $y' = (t-1) + 1 = t$ with initial value $y(1) = 2$ and solving this Initial Value Problem finds $y(t) = 0.5t^2 + 1.5$. The first derivative is continuous at $t = 1$, but there is a discontinuity in the second derivative. The subsequent steps are similar to those in the above table but are not given as they become increasingly tedious though not very difficult to do in theory. Therefore, numerical methods are usually used to solve the delay differential equations.

3.5 Chapter Summary

A new mathematical model for turning metal work pieces which consider both work piece and cutting tools as flexible with its moving load cutting force and regenerative chatter effects is developed. In the past, most studies of dynamic model of turning operation generally assumed the work piece to be rigid and ignored the work piece deformation. It only considers cutting tool deflection but practically, the work piece also suffers from deformation as a result of an external force by the cutting tool which affects and changes the chip thickness. No dynamic models established before that considered the work piece and cutting tools as flexible. Hence, the development of such mathematical formulation was initiated and thoroughly explained.

The development of the dynamic models starts by identifying suitable boundary conditions. Since the work piece is clamped to a chuck and is supported at the tailstock on the other end, a clamp-pinned boundary condition has been assumed for the work piece. The energy method is then employed as

the energy of a vibrating system of a turning process is partly potential and partly kinetic. The equation of motion of vibration of a rotating work piece in turning operations is then derived using Lagrange's equations. Three directional moving cutting forces with regenerative chatter mechanism is next included in the dynamic model developed. The improved dynamic model is later generated by adopting Insperger's cutting force model. Lastly, the cutting tool equation of motions for new improved dynamic model is also established and computed in Matlab software.

A method to analyse the chatter is then performed by utilizing a frequency response analysis and transient response analysis. In order to perform these analyses, a Runge-Kutta method has been used initially. But, since a Runge-Kutta needs a value of displacement, $x(t = 0)$ or velocity, $\dot{x}(t = 0)$ to calculate the time step and always depends on the initial conditions, a more suitable method should be used. A Delay Differential equation has been selected to replace a Runge-Kutta method since it is a self generated algorithm where the time step will be automatically recognized. By considering this, a quicker and efficient dynamic model could be generated.

Chapter 4

Experimental Modal Analysis

4.1 Introduction

Generally there are three major objectives of this experimental observation in the field of structural dynamics, especially for:

- (1) measurement of essential material properties under dynamic loading
- (2) determining the nature and extent of vibration response levels in operation
- (3) verifying theoretical models and predictions of various dynamic phenomena

The third objective mentioned above can be accomplished by performing experimental modal analysis (EMA). EMA is a process of measuring (often out of normal service environment) and analysing dynamic properties of structures under a known vibrational excitation. It is also known as Modal Testing. In this chapter, an introductory overview of experimental modal analysis is described. Brief explanation on the basic system of vibration measurement is also included. Since the aim is to understand the dynamics of turned metal, a cylindrical metal work piece is employed and described. Modal testing results carried out by the student and her collaborators on work pieces are presented and discussed.

Modal testing is defined as the study of the dynamic characteristics of a mechanical structure. Another definition of modal testing is a technique used to determine a structure's vibration characteristics such as natural frequencies, mode shapes and mode participation factors. Some of the benefits of modal analysis are allowing the design to avoid resonance vibration or to vibrate as a specified frequency, giving an engineer an idea of how the design will respond to different types of dynamic loads and helping in calculating solution control (time-step etc.) for other dynamic analysis. It is employed to create a mathematical model of a physical structure based on measured vibration data. These vibration data are not only response levels but also the excitations on the structure measured, thus permitting a relationship to be defined between them. These measured responses and excitations are usually presented in time domain before being transformed into frequency domain to reveal frequency response functions (FRFs) or impulse response functions (IRFs). The response model can also be obtained theoretically by direct analysis, as explained in the following.

The theoretical route to vibration analysis is shown in Figure 4.1. This illustrates the three stages through which a typical theoretical vibration analysis progresses (Ewins, 2000); spatial model, modal model and response model. Generally, a mathematical model is constructed to describe the structure's physical characteristics, usually in terms of its mass, stiffness and damping properties and this is referred to as the spatial model. Then, a theoretical modal analysis of the spatial model is performed which leads to a description of structure's behaviour as a set of vibration modes in the form of its modal properties (natural frequencies, modal damping factors and mode shapes) called modal model. The modal model always describes the normal modes of the structure, in which the structure vibrates naturally without any external excitations. The third stage (response model) is then executed to describe how the structure will respond under given excitation conditions by constructing a set of FRFs within the applicable range of frequency.

In the mean time, the experimental route to vibration analysis is commenced in the reverse direction of the theoretical route in which the FRFs are measured to create the response model, and the modal model consisting of

natural frequencies, modal damping and mode shapes can then be defined. Lastly, the spatial model can be obtained providing enough measurements to characterise the physical structure. Therefore it is essential to include enough degrees of freedom (DOFs) in the measurement and also to cover most of the vibration modes within a specified frequency range.

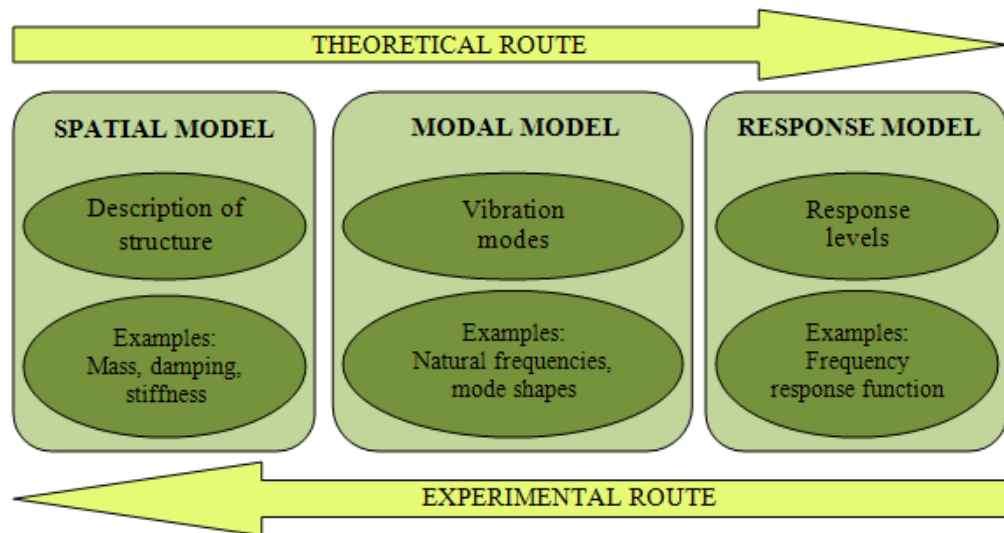


Figure 4.1: Route to vibration analysis

Generally, there are four essential steps or phases in a modal test. The first step is a test planning phase. It is important to ensure that the correct equipment is used for the various transductions, signal processing and analysis tasks. Another very important requirement of a modal test is to ensure that all the necessary parameters are measured. This means ensuring that all those quantities which are required for the eventual application are included in the list of quantities to be measured and, likewise, that unnecessary data are excluded from the list. Another aspect of test planning concerns the choice of response measurement locations. This choice is governed by the eventual application and it should be noted that the set of degrees of freedoms (DOFs) required for a clear visual interpretation of animated mode shape displays is not necessarily the optimum set for a more quantitative application such as model validation, updating or modification.

Following planning, the next phase is concerned with the preparation of the structure for test and the acquisition of the raw data that will be used to construct the model of the structure's dynamics. It must be emphasized here that the second most important feature of these measured data (after ensuring their completeness, i.e. that the correct ones are measured) is their accuracy. The main concern in this respect is to guard against the incursion of systematic errors, such as those caused by incorrect use of the equipment or installation of the transducers. These errors are much more difficult to detect and to eradicate than are those of a more random nature, such as arise due to noise, and once embedded in the data will seriously degrade the effectiveness of the model constructed.

Next is the measurement phase. The essential feature of the measurement phase in a modal test is that a controlled excitation forcing must be applied and measured together with the resulting responses at as many points as are necessary. The ensuing measured data will be presented in the form of response functions which are a series of ratios between responses and excitations, either characterized by functions which describe the responses to an arbitrary harmonic excitation (FRFs) or to an impulsive excitation (IRFs). The properties of the Fourier transform enable converting raw data from any of these excitation patterns into the required format of FRF or IRF by suitable signal processing.

Immediately following the data acquisition and processing phase, comes the interpretation or analysis-of-response-functions task. Here, the measured data are subjected to a process which seeks to determine the specific parameters of a generic mathematical model which makes this particular model exhibit the same dynamic behaviour as that measured in the test. The model in question is usually a modal model so that the analysis task is one of determining the modal properties of the system which most closely described the dynamic behaviour observed in the tests. This analysis is often achieved using a curve-fitting approach in which the coefficients in a specified polynomial function are established by requiring a minimum difference between the measured curve(s) and the curve(s) regenerated using the polynomial expression. This is not the only means of deriving the modal model but is by far the most common.

The final phase in the modal testing process is referred to as modeling. In the modeling phase a number of steps are taken. First, when the modal analysis has been carried out in a one-function-at-a-time way, users are confronted with a set of modal parameters which will most likely contain some inconsistencies. These inconsistencies will be manifested by the fact that there are many duplicate estimates for the natural frequency and damping factor for most of the modes. A different value for each from each individual FRF and these multiple values are not compatible with the type of multiple degree of freedoms (MDOF) linear system which forms the basis of modal model. Thus, it is necessary to extract from these multiple estimates a single value for the natural frequency and damping factor for each mode. Such a process is done automatically in the course of the global type of modal analysis (in which all FRFs are analysed in a single step, rather than individually, as is the case with other analysis strategies). While it is a simple matter to compute an average value from several different estimates, this should only be accepted as a reasonable value if the variance of the individual estimates is small and their differences are random in nature. Otherwise, the significance of the variation should not be ignored. It probably indicates a non-trivial error or problem with the original data set or with their modal analyses. There are other checks which must be undertaken on the resulting model, such as verification that the modes are suitably real, and not complex, except in the specific conditions where modal complexity can be justified. There are a number of checks that can be applied to the measured data and to their extracted models to test the statistical and physical reliability of the final results and these checks should be routinely applied to ensure that the appropriate quality is maintained throughout all the stages of the test.

4.2 Basic Components of Experimental Modal Analysis (EMA)

The basic components of EMA are described in this section. A typical layout for measurement system used for single-point excitation is illustrated in Figure 4.2, which includes the three main elements of EMA; excitation of

structure, mechanism of sensing and data acquisition and processing mechanisms.

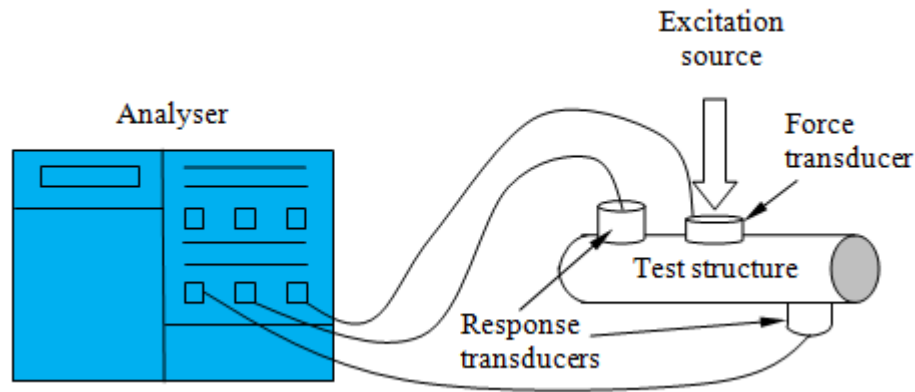


Figure 4.2: General layout of EMA

4.2.1 Excitation of Structure

There are numerous types of mechanisms available for excitation of a structure, which can be classified into contacting and non-contacting types. The first type involves connecting an exciter (such as electromagnetic or electro-hydraulic shaker) that remains attached to the structure during the modal test. Such a system causes some constraining and mass loading effects of the structure. The connecting excitation mechanism, also known as the shaker, is established by a system that applies the excitation, generally in the form of a driving force $f(t)$, at a given coordinate of the test structure. The excitation signals can be any of the wide variety of signal forms including harmonic, impulsive, random, transient, periodic and others. It must be chosen to match the requirements of the test. In addition, a power amplifier and signal generator are required to provide a large enough input for the measurement. The excitation is usually measured by a force transducer located at the connection between the shaker and the structure under investigation.

The second type consists of excitation devices that are either in contact for a short period (i.e. an impact hammer) or have no contact at all (i.e. an electromagnetic device) with the test structure while the excitation is being applied. The impact hammer is a complete excitation mechanism by which a force transducer attached to its head. By using this type of technique, a connection between the excitation device and the test structure is unnecessary thus mass loading effects can be avoided. Furthermore, the device does not require a signal generator and a power amplifier. The impact hammer as shown in Figure 4.3 is used to hit the structure in order to excite a wide range of frequencies, which depends on the properties of the hammer tip. The magnitude of impact is determined by the mass of the hammer head and the velocity of the impact introduced by the operator. In addition, the frequency range is defined by the stiffness of the contacting surfaces and the mass of the hammer head. The stiffer the materials, the higher the effective frequency range and vice versa. That is why the impact hammer normally comes with a set of different tips and heads that are interchangeable to manage appropriate impact magnitudes and frequency ranges. Although the impact hammer is simple and does not add mass loading to the structure, it is often incapable of transforming sufficient energy to the structure to obtain adequate response signals in the frequency range of interest. Nonetheless, impact hammer remains a popular and useful excitation device, as it generally is much faster to use than shakers.

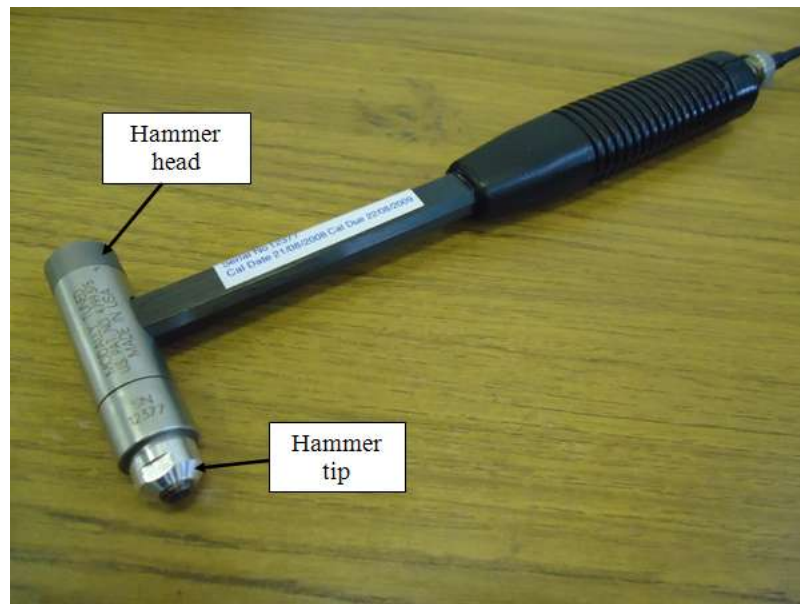


Figure 4.3: Impact Hammer

4.2.2 Mechanism of Sensing

Mechanism of sensing or transduction is used for measurement of force excitation (by means of force transducers) or acceleration response (by means of accelerometers as depicted in Figure 4.4) in modal testing. These transducers generate electric signals that are proportional to the physical parameters to be measured such as force or accelerations. It is very important that each set of transducer or accelerometer is properly calibrated in terms of both magnitude and phase over the frequency range of interest. If the signals are weak, amplifiers may be needed to boost the signals into a signal strong enough to be measured by the analyser. There are two main factors to be considered when attaching and locating the accelerometer on the test structure. Firstly, there are various methods to attach the accelerometers to the surface of a structure under test includes using a stud, magnet, a layer of wax and even hand-held. The use of wax is the simplest and easiest way, thus is widely applied in modal testing. Secondly, it is important to correctly position the accelerometers so that they are not located too close to a node of vibration modes. Besides, the location of the

measurement points must be selected properly in order to capture the actual mode shapes of the test structure.

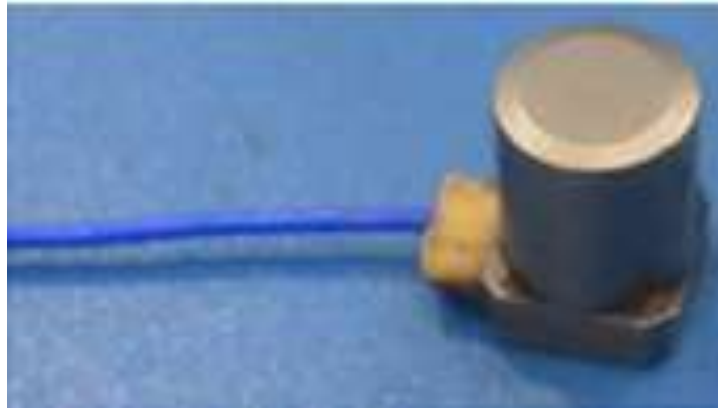


Figure 4.4: Accelerometer

4.2.3 Data Acquisition and Processing Mechanism

The purpose of a data acquisition and processing system is to measure the excitation and response signals transmitted by the excitation and sensing mechanisms using sophisticated devices called analysers. A spectrum analyser which is also known as Fast Fourier Transform (FFT) analyser is commonly used in modal testing because it can directly provide measurement of the FRFs. This is done by converting the analogue time domain signals developed by the transducers into digital frequency domain information that can afterwards be processed by digital computers.

4.3 Experimental Modal Analysis of Metal and Composite Work piece

Modal testing was performed by conducting the main aspects of experimental modal analysis, including excitation of the structure, measurement of the response as well as data acquisition and processing on the work piece.

The experiments were carried out using a LMS Test Lab package in which an impact hammer was used to excite the work piece and several accelerometers were employed to measure the vibration response at multiple locations. The experimental setups are described and the measured data is given in the following subsections

4.3.1 Free-free Boundary

Modal testing with free-free boundary condition was conducted for metal and composite work piece as a long cylindrical as illustrated in Figure 4.5. The free-free boundary condition is achieved by using a pair of strings to hang the cylindrical work piece during testing. A PCB impact hammer (Figure 4.6 (a)) and two Kistler accelerometers (Figure 4.6 (b)) were used in the test. The cylindrical work piece is tested using one hammer point and two measurement points as depicted in Figure 4.5. The locations of the hammer and measurement points were carefully chosen so that they are not near any nodal points. The responses were measured using a 12-channels LMS system (Figure 4.6 (c)) and were extracted using a LMS PolyMAX curve-fitting procedure.

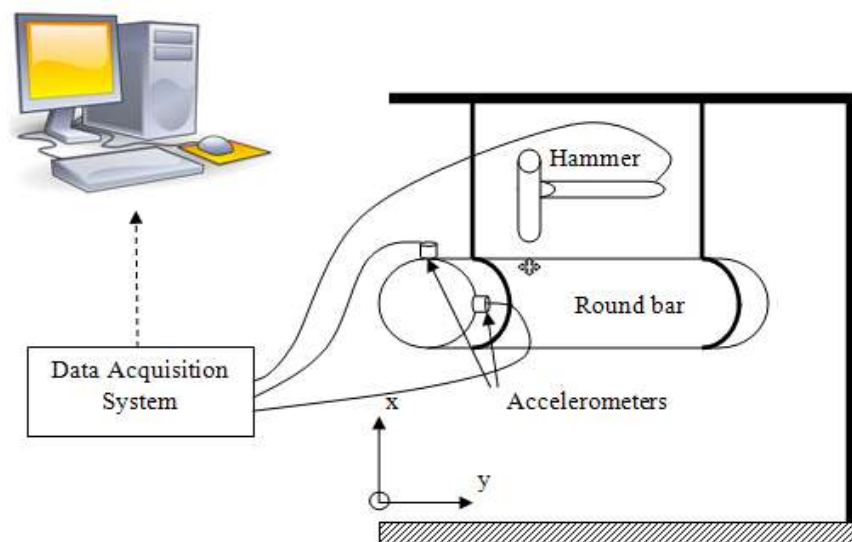


Figure 4.5: Experimental set up for the cylindrical metal work piece of free-free boundary

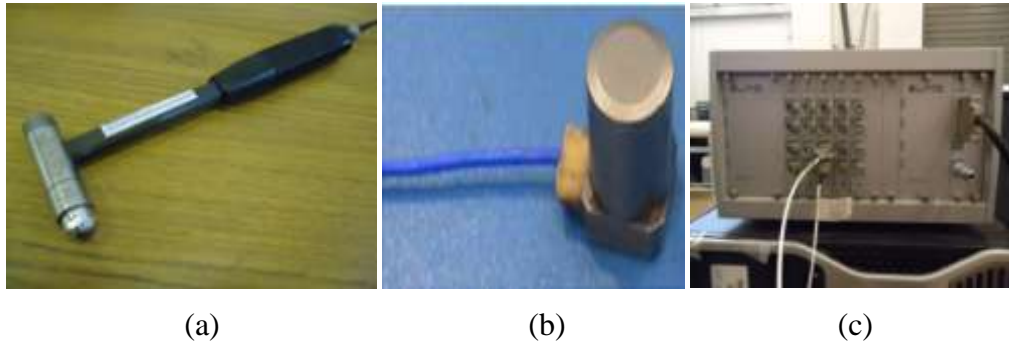


Figure 4.6: Apparatus used for modal testing (a) PCB impact hammer (b) Kistler accelerometer (c) 12-channels LMS system

The cylindrical metal work piece used is cut into 500 mm length with diameter of 50 mm and the distance between measurement points of each equally space node is 12 mm as illustrated in Figure 4.7. Its nominal material properties are given in Table 4.1.

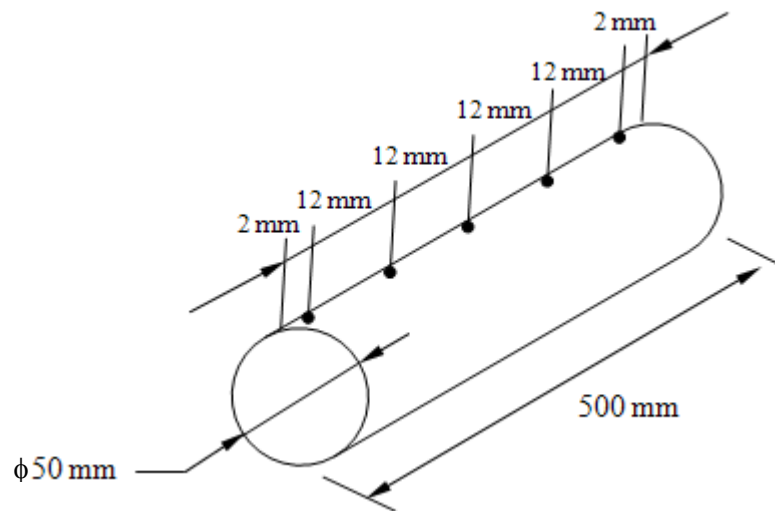


Figure 4.7: A cylindrical metal work piece with its five measured locations

Table 4.1: Nominal material properties of cylindrical metal work piece

Properties	Value
Young's Modulus, E	210 GPa
Mass density, ρ	7850 kg/m ³

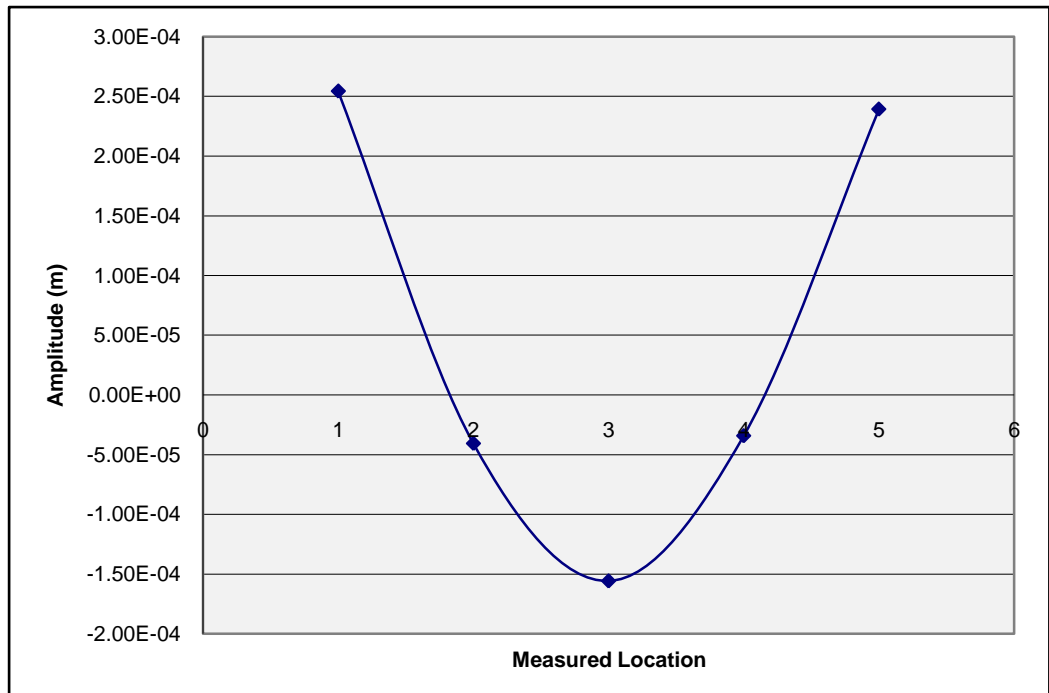
The three measured natural frequencies are shown in Table 4.2 and their mode shapes respectively are depicted in Figure 4.8. The theoretical frequency, ω_n can be calculated by using equation 4.1 below where I is the moment of inertia, ρ is a mass density, l is a length, A is the cross-sectional area of the work piece and $\beta_1 l = 4.730041$, $\beta_2 l = 7.853205$, $\beta_3 l = 10.995608$ (Rao, 1995).

$$\omega_n = (\beta_n l)^2 \sqrt{\frac{EI}{\rho A l^4}} \quad (4.1)$$

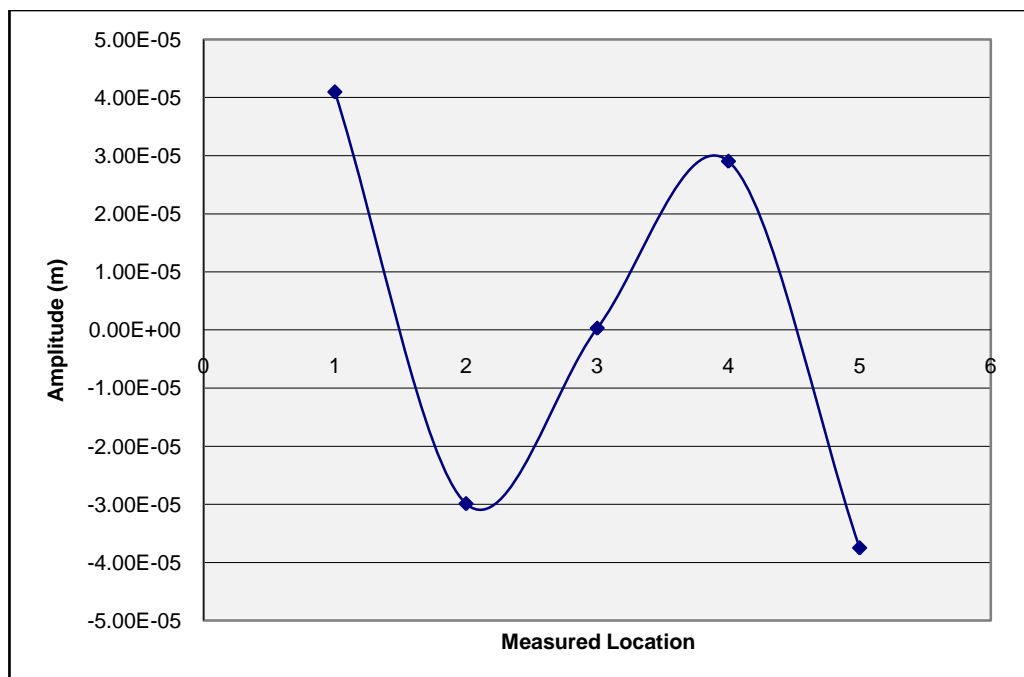
It was found that from the modal test results shown in Table 4.2, the results were as expected in which the tested frequencies were quite close to the theoretical frequencies. It is also observed that from the resultant measured mode shapes, it appeared following the same classical beam mode shapes for free-free boundary as predicted.

Table 4.2: The three measured natural frequencies of the cylindrical metal work piece

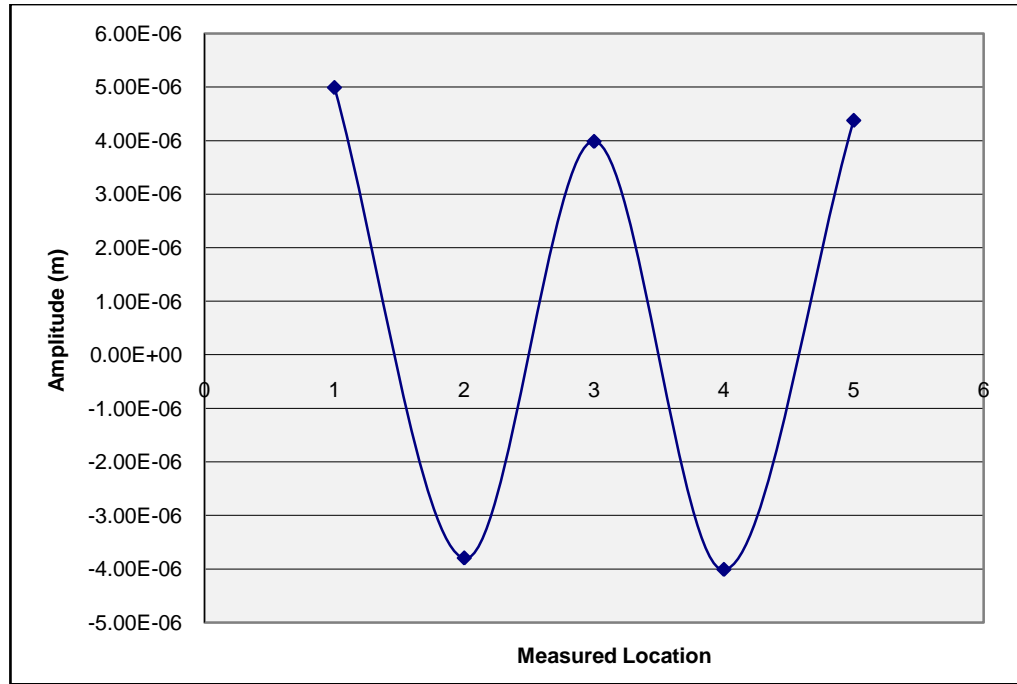
Order of Fundamental Frequency	Tested Frequency (Hz)	Theoretical Frequency (Hz)
1	896.01	917.54
2	2368.04	2529.25
3	4400.17	4958.34



(a) Mode 1



(b) Mode 2



(c) Mode 3

Figure 4.8: The experimental mode shapes of the cylindrical metal work piece for free-free boundary

As for composite work piece, it is cut with the length of 500 mm similar to the metal work piece length but with slightly smaller diameter of 38 mm. The distance between measurement points of each node is 12 mm as depicted in Figure 4.7. Its nominal material properties are given in Table 4.3.

Table 4.3: Nominal material properties of cylindrical composite work piece

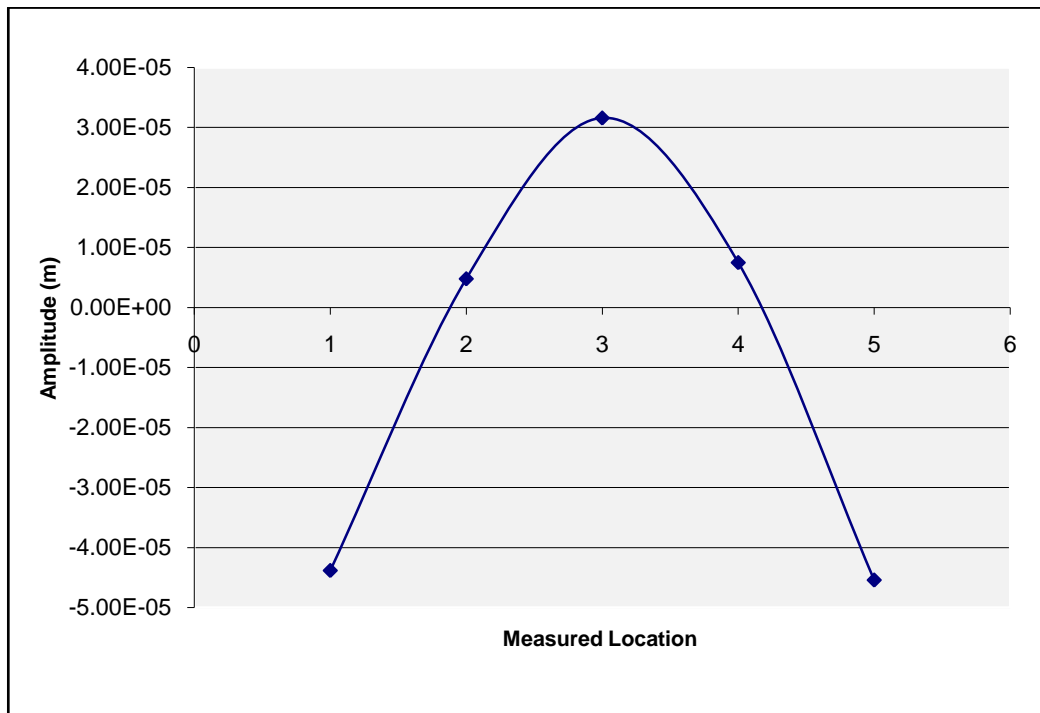
Properties	Value
Young's Modulus, E	36.75 GPa
Mass density, ρ	882 kg/m ³

The three measured natural frequencies are shown in Table 4.4 and their mode shapes respectively are depicted in Figure 4.9. It was found that from the modal test results shown in Table 4.4, the results were as expected where the tested frequencies were quite close to the theoretical frequencies. The resultant

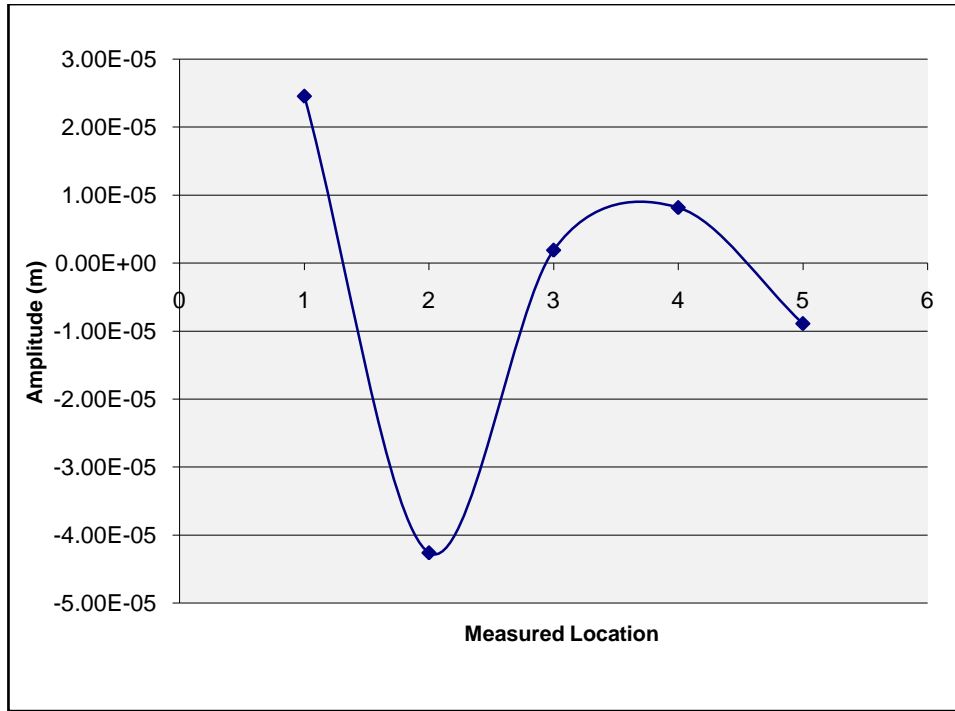
measured mode shapes were not following the classical beam mode shapes for free-free boundary.

Table 4.4: The three measured natural frequencies of the cylindrical composite work piece

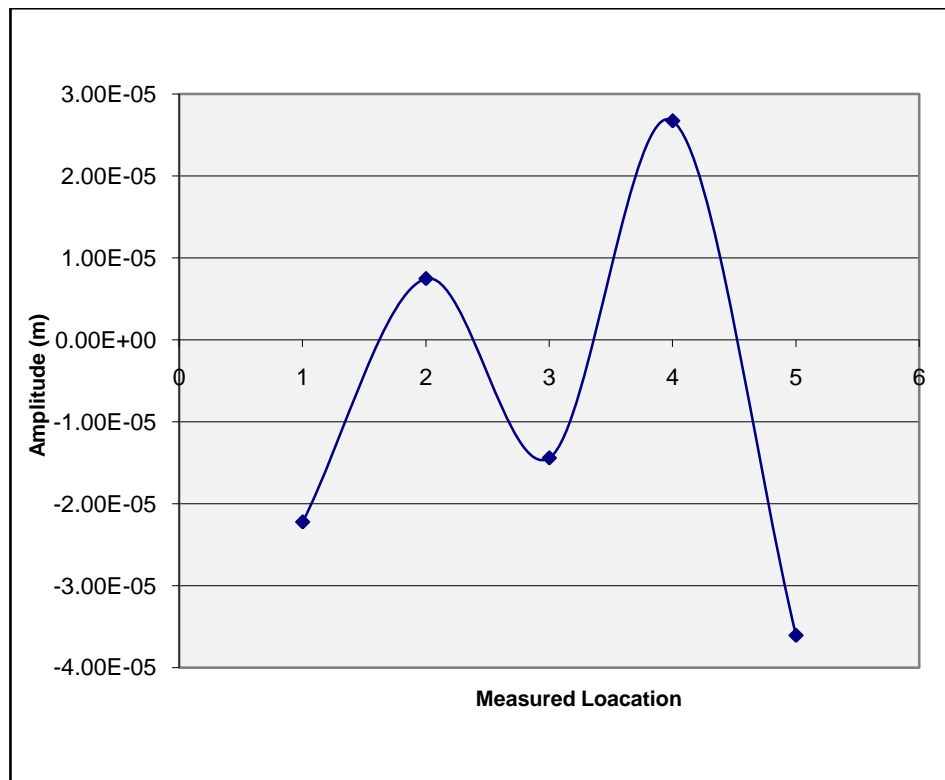
Order of Fundamental frequency	Tested frequency (Hz)	Theoretical frequency (Hz)
1	618.40	602.00
2	1630.02	1549.35
3	3017.91	2988.20



(a) Mode 1



(b) Mode 2



(c) Mode 3

Figure 4.9: The experimental mode shapes of the cylindrical composite work piece for free-free boundary

4.3.2 Clamped Pinned Boundary

Turning operation is performed on a lathe machine in which one end of the work piece is fixed to the spindle by a chuck and the other end pin mounted to the tails stock as shown in Figure 4.10. Due to this arrangement, the boundary condition of the work piece on a lathe machine is considered as a clamped-pinned. In this modal test, two methods of sensing mechanisms have been employed using Kistler accelerometers and Micro-epsilon laser sensor (Figure 4.11) to determine the natural frequencies and mode shapes of the round metal work piece. The accelerometers used in the experiments can be difficult to mount on different locations of the work piece being tested during turning. Laser displacement sensor is more practical to mount in measuring the vibration of the work piece during turning operation.

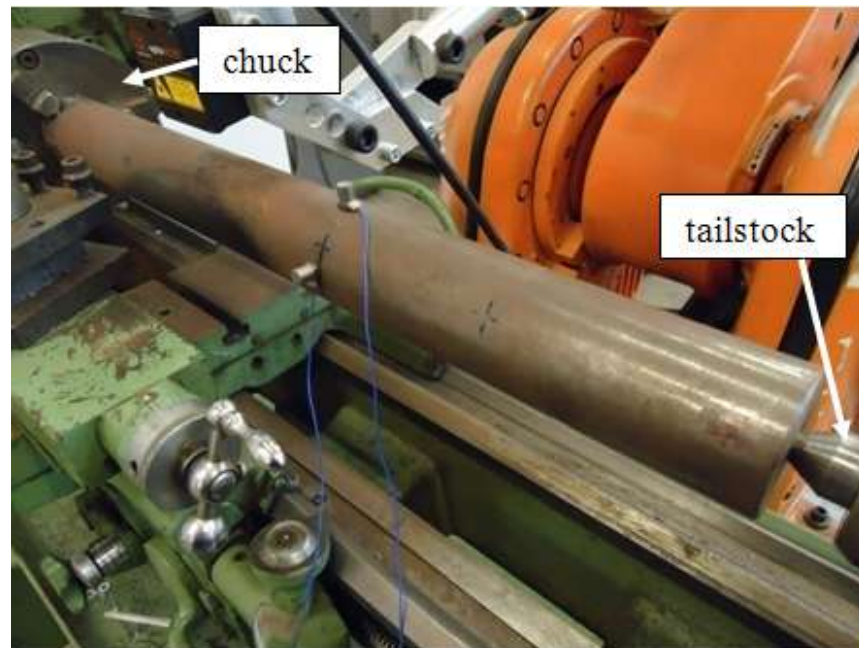


Figure 4.10: Modal test setup for cylindrical work piece in clamped-pinned boundary condition (in Dynamics laboratory in the University of Liverpool)

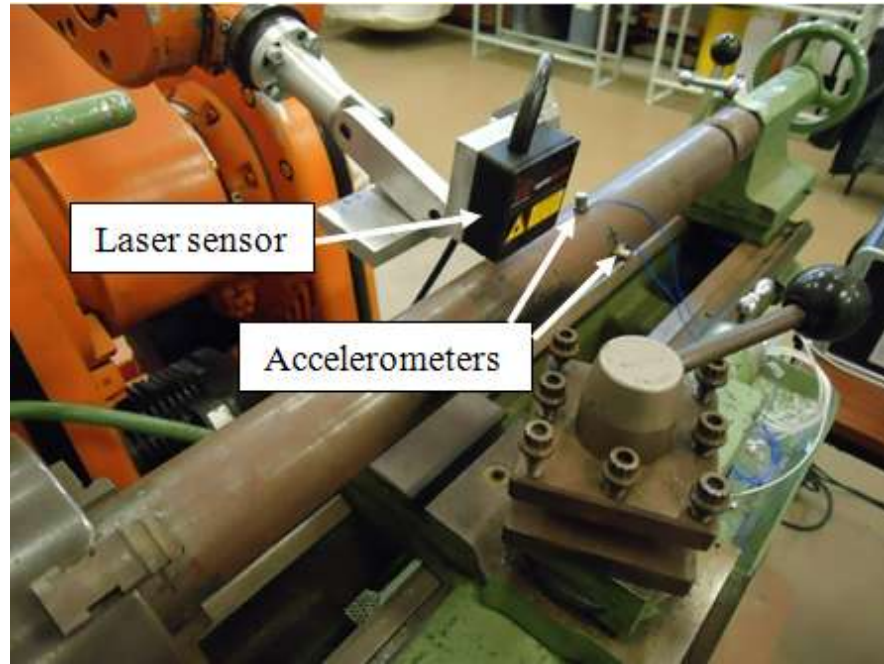
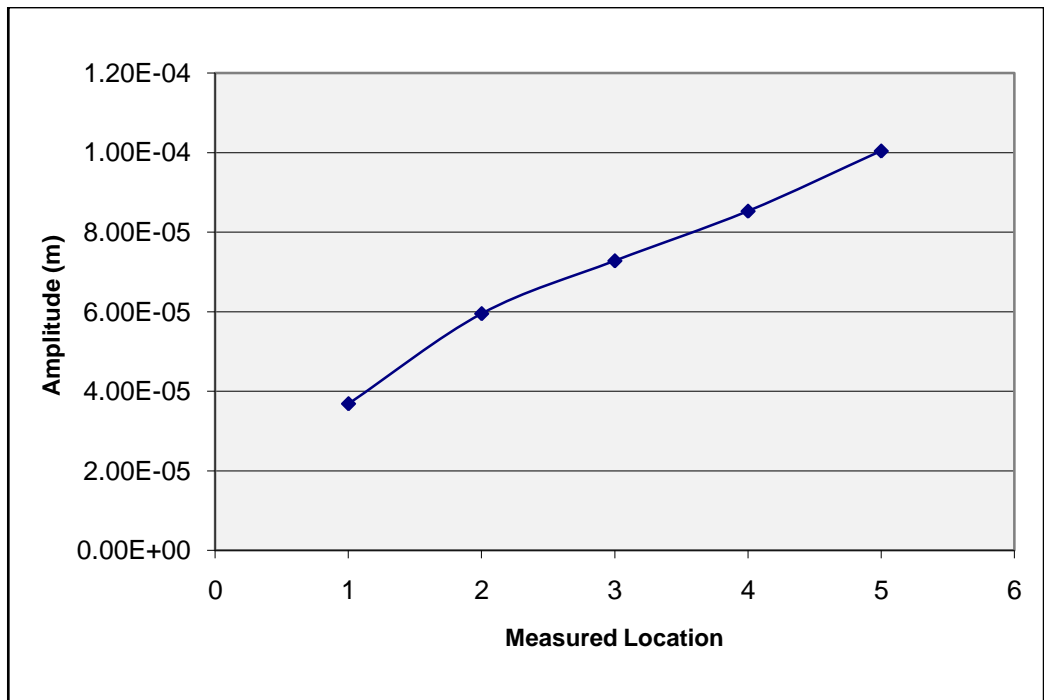


Figure 4.11: Kistler accelerometer and Micro-epsilon laser sensor (in Dynamics laboratory in the University of Liverpool)

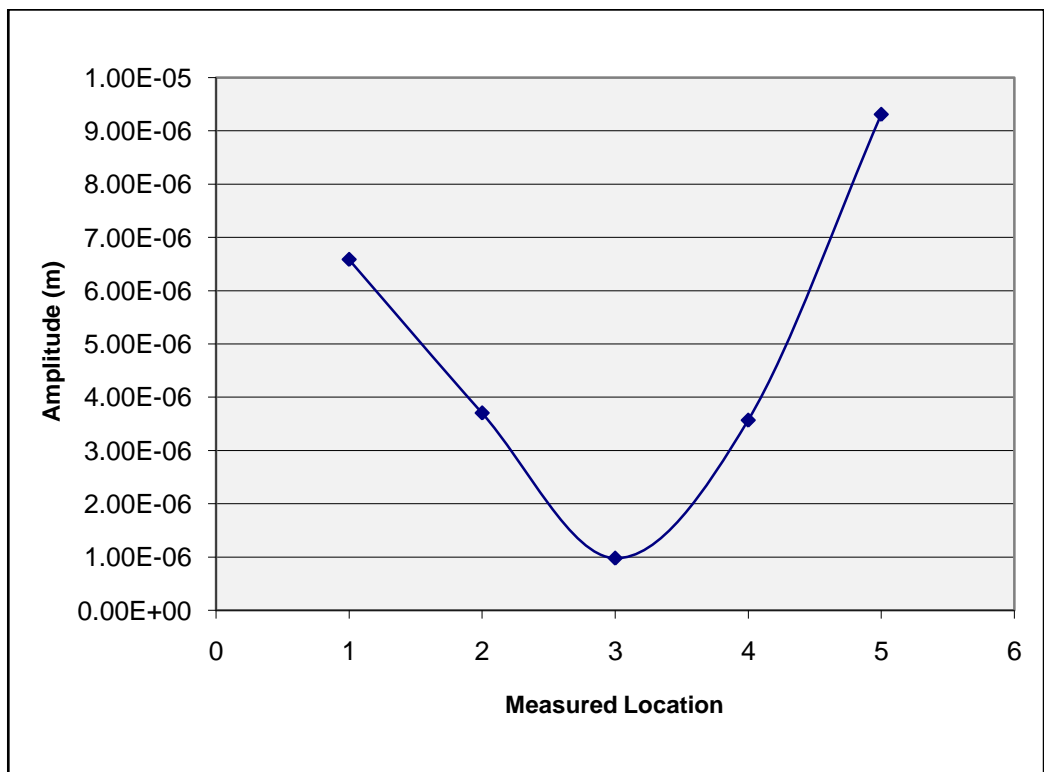
The three measured natural frequencies for clamped-pinned boundary are shown in Table 4.5 and their mode shapes are depicted in Figure 4.12. It was found that from the modal test results shown in Table 4.5, the results were not as expected in which the tested frequencies from both sensing mechanisms were lower than the theoretical frequencies. It is also observed that the resultant measured mode shapes were not symmetrical and not following the classical beam mode shapes for clamped-pinned boundary as envisaged.

Table 4.5: The three measured clamped-pinned natural frequencies of the cylindrical metal work piece

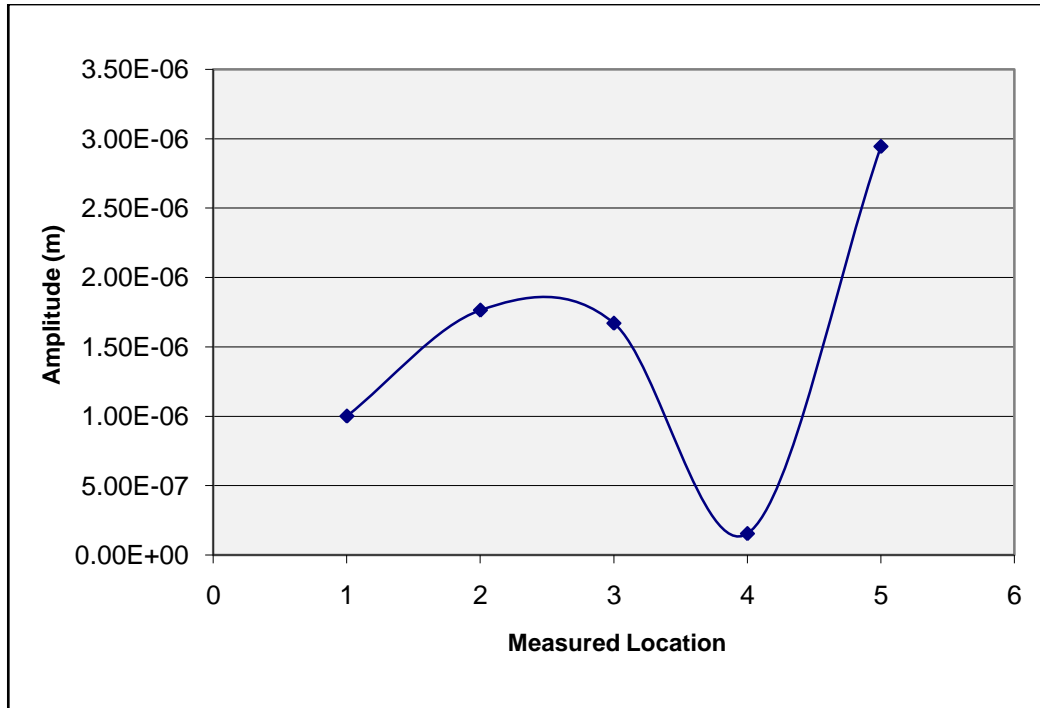
Order of Frequency	Tested Frequency (Accelerometer) (Hz)	Tested Frequency (Laser Sensor) (Hz)	Theoretical Frequency (Hz)
1	176.45	206.4	634.39
2	423.63	440.9	2055.82
3	842.83	716.5	4289.31



(a) Mode 1



(b) Mode 2



(c) Mode 3

Figure 4.12: The experimental mode shapes of the cylindrical metal work piece for clamp-pinned boundary

Hence, several runs of modal test have been conducted to redo the test in order to acquire the expected frequencies (closer to theoretical frequencies). But the outcomes are still the same. Due to this problem, the modal test for clamped-pinned boundary for composite work piece as well could not be carried out.

The large difference of these two frequencies might be due to the clamped-pinned boundary condition considered earlier. This is because the work piece that is held at chuck was not fixed enough thus allowing some movements. Another boundary condition should be considered to correct this discrepancy. A suitable boundary should be an elastic boundary condition where the rotational and vertical springs are considered at the clamped end. On the other hand, the work piece that is pin mounted at tails stock is considered as one vertical spring only.

In addition, it is also noticed that both sensing mechanisms worked successfully but the responses from the laser sensor were too noisy to be captured hence the expected natural frequencies and mode shapes could not be determined accurately. These were shown in Figure 4.13 below. Only readings from accelerometers were taken into account.

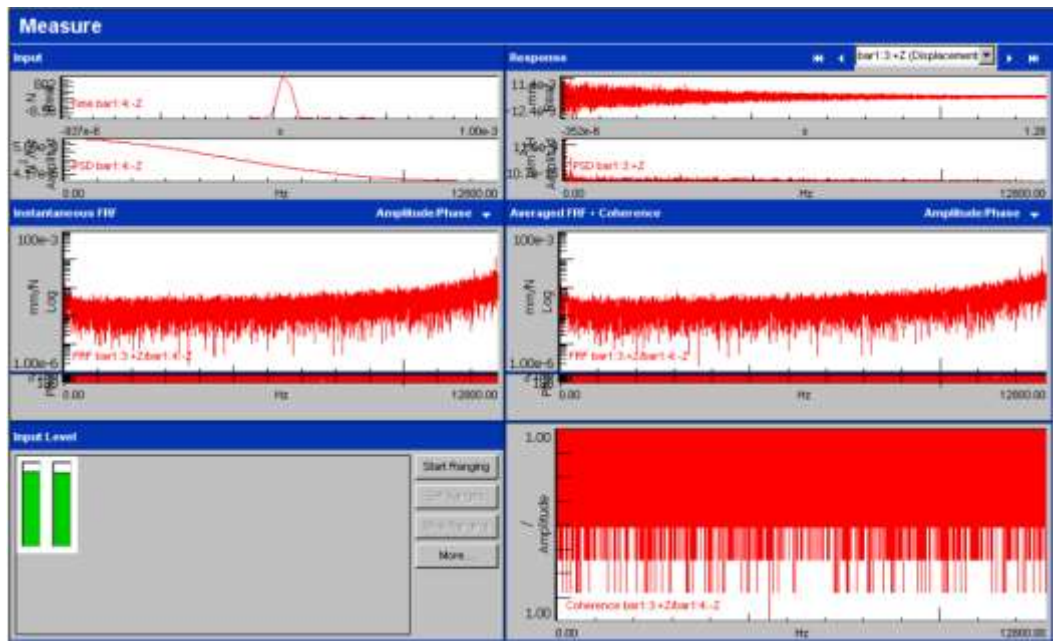


Figure 4.13: Responses from laser sensor showing the noise

To overcome these huge discrepancies between the two sets of frequencies, another modal test has been performed with better data acquisition and processing mechanism. It was done in collaboration with Dalian University of Technology (DUT) in China. The modal test is only done on the metal work piece. The results of the modal test done are described in the next subsection. The material and geometric properties of the cylindrical work piece used during the modal test are shown in the Table 4.6 below.

Table 4.6: Properties of the cylindrical metal work piece used in the DUT test

Properties	Values
Size	Length = 549.95, diameter = 37.03 mm
Material	Quenched and tempered steel 45
Weight	About 4.63 kg
Density of mass	7817.4 kg/m ³
Young's Modulus	210 GPa

The modal test for both free-free and clamped-pinned boundary condition was conducted for the metal work piece. The steps of performing the free-free boundary modal test are similar as the previous test. The three measured free-free boundary natural frequencies of the metal work piece are tabulated in Table 4.7 below. From the results, it shows that the tested frequencies were as expected where the values are close enough to the theoretical frequencies.

Table 4.7: Free-free boundary condition for cylindrical metal work piece

Order of Fundamental frequency	Tested frequency (Hz)	Theoretical frequency (Hz)
1	558	559.7
2	1506	1542.8
3	2872	3024.5

On the other hand, the clamped-pinned boundary modal test is also performed and the modal test setup is depicted in Figure 4.14. This test is essential to replace the clamped-pinned modal test done previously. The four measured clamped-pinned boundary natural frequencies of the metal work piece in y direction are illustrated in Table 4.8 below. It was found that the resultant tested frequencies were close enough with the theoretical frequencies as expected.

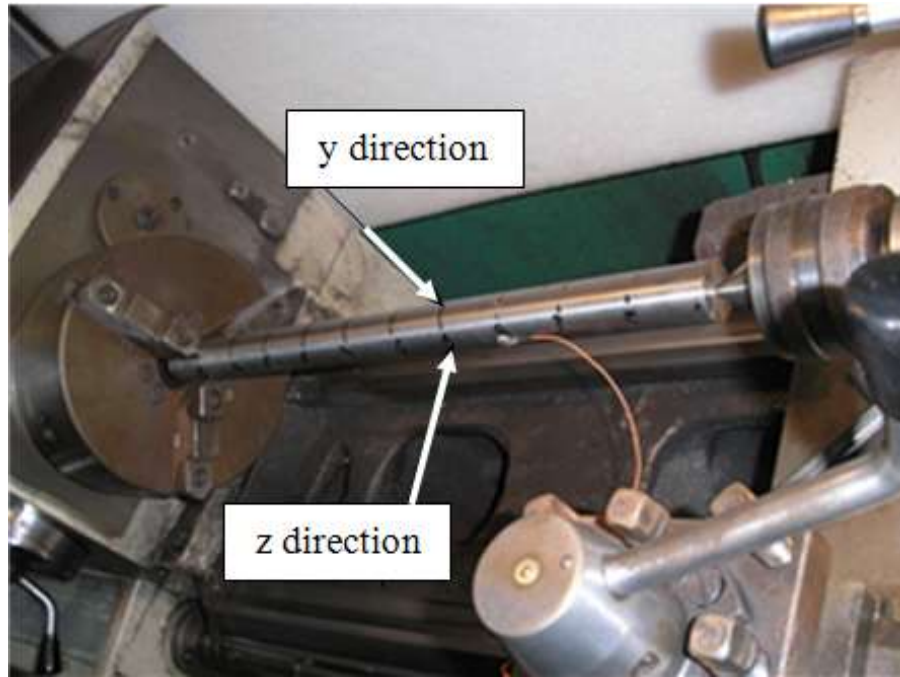


Figure 4.14: Modal test setup for clamped-pinned boundary in y and z direction
(in the Institute of Moulds, Dalian University of Technology)

Table 4.8: Clamped-pinned boundary condition for metal work piece
(y direction)

Order of Fundamental frequency	Tested frequency (Hz)	Theoretical frequency (Hz)
1	336	385.7
2	1310	1249.9
3	2720	2607.9
4	4590	4459.6

The clamped-pinned boundary modal test is also conducted in z direction as shown in Figure 4.14. The four measured clamped-pinned boundary natural frequencies of the metal work piece in z direction are shown in Table 4.9 below. It was found that the resultant tested frequencies were close enough to the theoretical frequencies as expected.

Table 4.9: Clamped-pinned boundary condition for metal work piece
(z direction)

Order of Fundamental frequency	Tested frequency (Hz)	Theoretical frequency (Hz)
1	337	385.7
2	1280	1249.9
3	2740	2607.9
4	4740	4459.6

4.4 Experimental Modal Analysis During Machining of Cylindrical Metal Work piece at DUT

This section explains the experimental setup and the procedures behind the vibration test of the turned metal work piece. This vibration test is done to monitor the occurrence of chatter and to determine the effect of varying some cutting parameters on chatter occurrence.

The schematic of the experimental setup is depicted in Figure 4.15 and the real lathe with the work piece under testing is pictured in Figure 4.16. The type of the metal work piece used is AISI 1045 steel with hardness of HB190. It is supported at one end by chuck on the lathe machine (CA6140) and the other end by a tailstock. A dry turning operation was done to determine the cutting forces and vibration. The tool holder used in the experiment is PSSNR2525M12 and the cutting tool employed is P10 quadrangle carbide inserts coated with optimal combination of MT-TiCN, Al_2O_3 , TiN and SNMG120404-PM with 0.4 mm nose radius. The cutting tool has a side cutting edge angle of $c_s = 45^\circ$, inclination angle of $i_a = 0^\circ$, and normal rake angle of $\gamma_n = 10^\circ$.

A data acquisition system (Brueel & Kjaer's PULSE-Type 3560E) which is equipped with 16 channels is adopted to measure the cutting force and vibration of the metal work piece. Two eddy-current transducers were used to measure the vibration of the shaft near the being-machined cross-section in the y direction and z direction. These two eddy-current transducers (3300 XL 8 mm

Proximity Transducer System) which are made by Bently Nevada are fixed on the tool carriage that is connected with a fixation apparatus. It is kept at a distance within 2 mm between the end of the eddy-current transducers and the machined surface of the work piece in the y and z directions. Meanwhile, the distance between the end eddy-current transducers and the tool tip in x direction is kept within 10 mm.

The dynamometer (YDX-III9702) which is made by the Institute of Sensing and Control at Dalian University of Technology is used to measure the dynamic cutting force. The dynamometer assembly is specifically designed and made to fit under the tool post. The cutter is synchronously driven with the dynamometer and the eddy-current transducers from the right-hand side of the work piece to the chuck. The sampling frequency is set to be 8 kHz.

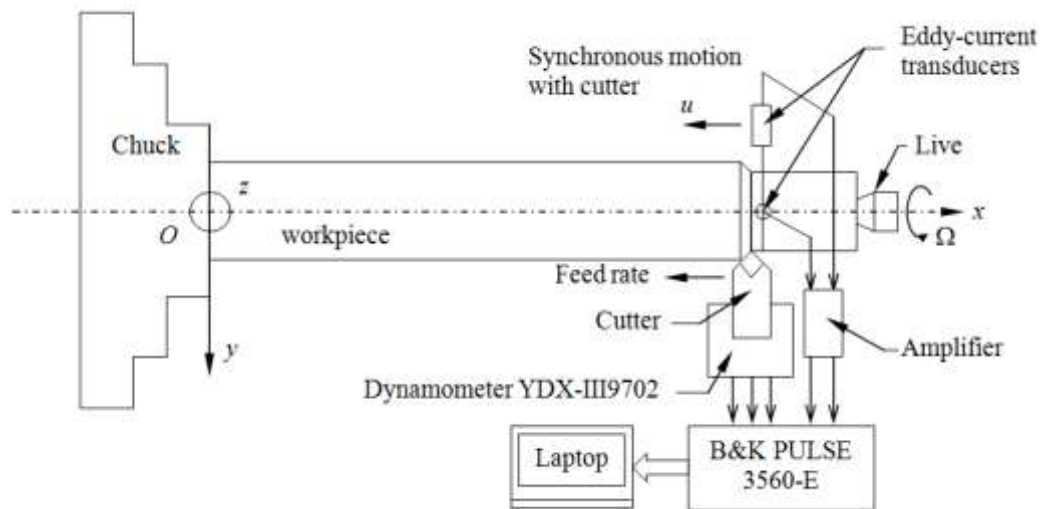


Figure 4.15: Schematic illustration of the vibration test set-up

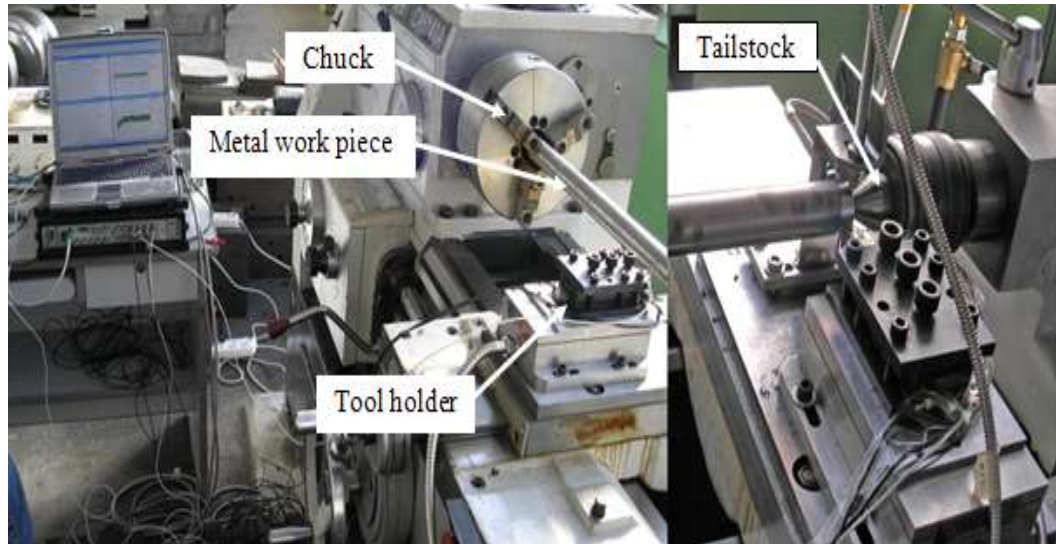


Figure 4.16: Two views of the experimental rig (Han *et al.*, 2012)

The cutting conditions used are shown in Table 4.10. The rotating speed, feed rate and depth of cut are carefully chosen in different values consistent with the previous numerical simulations under different cutting conditions.

Table 4.10: Cutting parameters and work piece characteristics

Experiment Number	Rotary speed, Ω (rev/min)	Depth of Cut, d (mm)	Feed Rate, f (mm/rev)	Diameter, D (mm)
1	1250	1.5	0.3	36.5
2	1000	3.0	0.2	35.0

Vibration of the work piece is due to the cutting force and its travel along the longitudinal direction and (relatively) in the circumferential direction in the turning operations. These two factors together affect vibration of work piece. Moreover, regenerative chatter may also occur. Suitable cutting condition and dimension of the shaft were used in the experiment.

The dynamometer was used to measure the dynamic cutting forces. Two eddy-current transducers measure the vibration of the shaft near the being-machined cross-section in the y and z direction. All sensors move simultaneously along longitudinal axis of the work piece with the tool carriage. Thus, the being-machined section of the shaft is tracked and its deflections are measured. During machining, the vibration response signal may not solely come from moving loads or the cutting forces. Other factors may contribute such as the vibration of the spindle of the lathe due to power transmitted via the gear and the tool carriage moving on its adjustable horizontal metal rail with clearance, and vibration of the tool holder may contributed to the vibration signal measured and sever to contaminate the true work piece vibration signal.

Therefore, a pre-test is performed with the shaft rotating and the cutter making one complete travel without cutting before each formal test of vibration in turning operation is conducted. The vibration signal of the pre-test is measured to analyze the effect of these variations on the measured signals. During turning operation, vibrations of the shaft subjected to three moving dynamic cutting forces were recorded at different cutting conditions. Two tests were performed in different cutting conditions as described in Table 4.10 in the dry run. The five channels of the 3560-E were simultaneously used for data acquisition which three channels for measuring the cutting force signals and another two channels for collecting vibration signals during each cut.

The dynamic response of the shaft in y and z direction is measured at the being machined position during the turning. The carriage moves the tool in a direction that is only nearly parallel to the longitudinal direction due to the deformation of the guide way. Thus, the deflection curves are dealt with according to the tested data from an empty turning before the formal turning process. All the results in this experiment are explained in the next chapter.

4.5 Chapter Summary

In this chapter, experimental modal analysis has been explained, and the theoretical and experimental routes of vibration analysis are described. Brief explanations of the three main aspects of the basic measurement system used in vibration analysis (i.e. excitation, transduction and data analysers) have also been included. It is important to have a good understanding of the concept of EMA before performing the modal test, as presented in the remainder of the chapter.

A cylindrical metal and composite work pieces have been utilised to be investigated in this research and their description have been included in this chapter. Modal testing has been conducted on each of the work piece in order to determine the natural frequencies and the mode shapes of each work piece. Two types of boundary conditions; free-free and clamp-pinned have been considered and results for the metal and composites work pieces for free-free boundary are encouraging. The tested frequencies for both work pieces were quite close to the theoretical frequencies and the resultant measured mode shapes appeared in line with the classical beam mode shapes as predicted.

In contrast, the results for the clamp-pinned boundary for metal work piece were not as expected. The tested frequencies were lower than the theoretical frequencies and the resultant measured mode shapes were not symmetrical and not following the classical beam mode shapes. Several attempts have been conducted to redo the test but similar results were produced. Hence, the modal test could not be carried out for composite work piece. The main problems encountered led to these discrepancies in metal work piece natural frequencies and mode shapes are due to the clamped pinned boundary condition considered earlier. The assumed boundary condition is not entirely correct as both supports (chuck and tailstock) are actually flexible. A suitable boundary should be considered (an elastic boundary condition) in the developed dynamic model (Chapter 3) and the simulated numerical results in Chapter 5 will be based on this boundary condition. In addition, the responses from the laser

sensor were too noisy to be captured thus the expected natural frequencies and mode shapes could not be determined.

To overcome these problems, another modal test has been performed with better data acquisition and processing mechanism with a collaboration from Dalian University of Technology (DUT) in China. The modal test is only done on the metal work piece for clamped-pinned boundary condition only. The results are promising where the tested frequencies were as expected (close enough to the theoretical) frequencies. The experimental data from this modal test will be employed in the dynamic model for numerical simulation purposes. It is done to ensure the accuracy of the numerical simulation and minimise the error respectively.

Chapter 5

Numerical Simulation Results

5.1 Overview

The aim of this chapter is to present the results for numerical simulation of the dynamic model developed in Chapter 3. Traditional design phases that include building and testing product prototypes are no longer practical and economical to be employed today due to demands of a reduced time-to-market among product manufacturers. In order to meet the demands, increasing use of the numerical analysis especially in the field of structural analysis should be attempted. Therefore, many efforts are given to the development of accurate analytical models for the prediction of the system's response to various excitations, boundary conditions and parameter changes. Consequently, development of numerical models for structural dynamics prediction has become more and more significant especially with the growing capabilities of computing facilities.

5.2 Parametric Studies

Cutting speed, depth of cut, and rotational speed are known to be the cutting parameters that influence the surface finish of turned work pieces (explained earlier in Chapter 2). From the dynamic model established, the effect of these cutting parameters is simulated to observe their influences on vibration and chatter occurrence of turned work piece. In this study, the effect of varying these main cutting parameters is investigated and the outcome from the simulation will be analyzed accordingly.

5.2.1 Clamped Pinned (Metal work piece)

5.2.1.1 Convergence Test

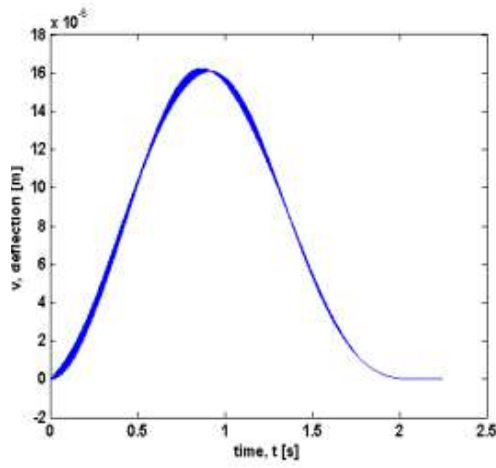
To start with, some preliminary simulation work has been done for clamped pinned boundary condition of metal work pieces. The convergence test has been performed to monitor the occurrence of chatter (up to five modes) and to determine the appropriate number of modes included in the simulation. As a result, four modes of the shaft are found to produce satisfactory results and hence used for the simulation. The geometric and material properties of the shaft (cylindrical metal work piece) used in this convergence test are length, $l = 0.5$ m, radius $r = 25$ mm, Young's Modulus $E = 2.07 \times 10^{11}$ Pa, and density, $\rho = 7850$ kg/m³ while the cutting parameters used are 0.2228 m/s for cutting speed, 3.00 mm for the depth of cut, 1250 rev/min for rotational speed and 0.3 mm/rev for the feed rate. By considering the clamped pinned boundary first, its modes are

$$\varphi_n(x) = \cosh\left(\frac{\lambda_n}{l}x\right) - \cos\left(\frac{\lambda_n}{l}x\right) - \sigma_n\left(\sinh\left(\frac{\lambda_n}{l}x\right) - \sin\left(\frac{\lambda_n}{l}x\right)\right) \quad (5.1)$$

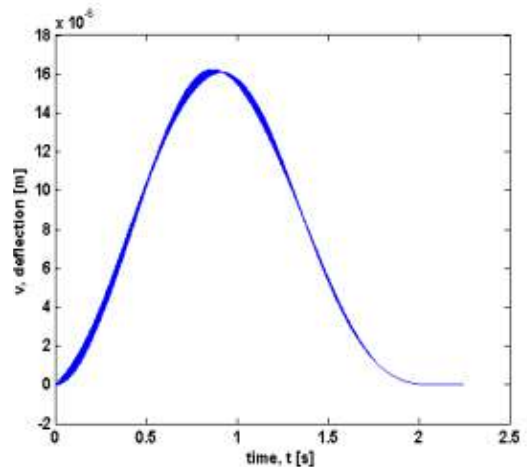
where $\lambda = [3.9266, 7.0686, 10.2102, 13.3518, 16.4934]$ and $\sigma = [1.000777304, 1.000001445, 1.0000000000]$. $\omega_n = (\lambda_n)^2 \sqrt{EI/\rho A} / 2\pi l^2$ ($n = 1, 2, 3...$) in rad/s is the natural frequency of the stationary shaft.

The numerical results of the dynamic responses of deflection, v and w at the moving cutter location (in the y and z direction respectively) are depicted in Figure 5.1 and Figure 5.2. Meanwhile the moving cutter starts from the pinned support and finishes at the clamped support. It is found that as the higher modes are included in the simulation, higher oscillation (chatter) starts to appear on top of the deflection (dynamic response) curve in both v (y) and w (z) direction as depicted in Figure 5.1 (c) and Figure 5.2 (c).

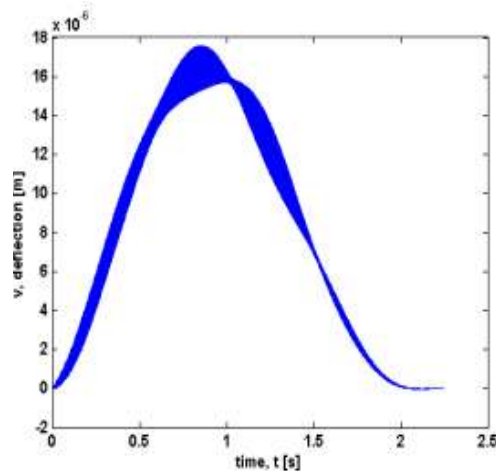
It is also observed that four modes of the shaft are sufficient and hence used during numerical simulation. It is necessary to include higher modes as they represent high frequency oscillation. The accuracy of the dynamic model also increases since at a certain mode, it starts to converge which can be seen from four modes. The more modes considered, the more accurate the results; but at certain points it is not necessary to include more than four modes. With four modes, there is high frequency oscillation on top of the static deflection.



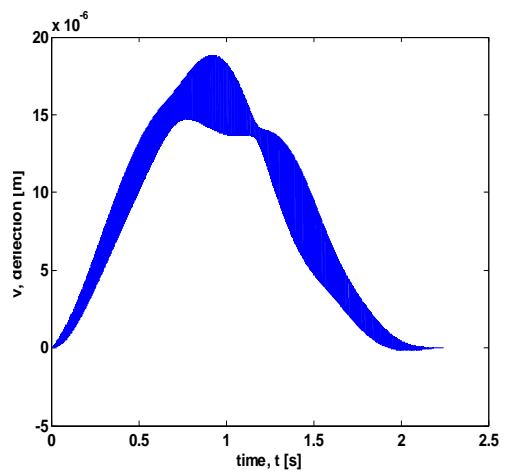
(a) One mode



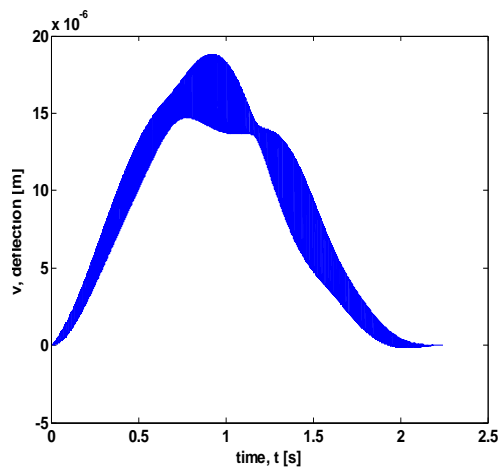
(b) Two modes



(c) Three modes

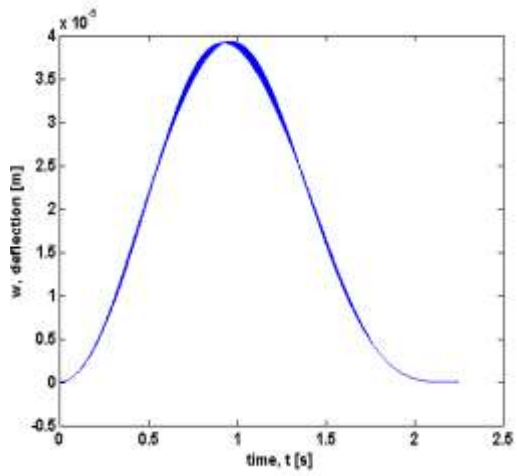


(d) Four modes

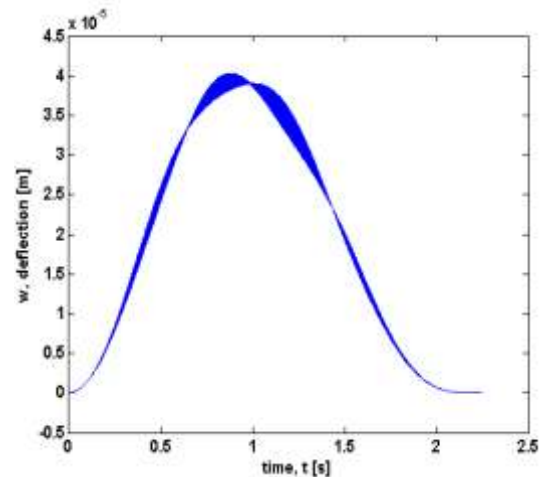


(e) Five modes

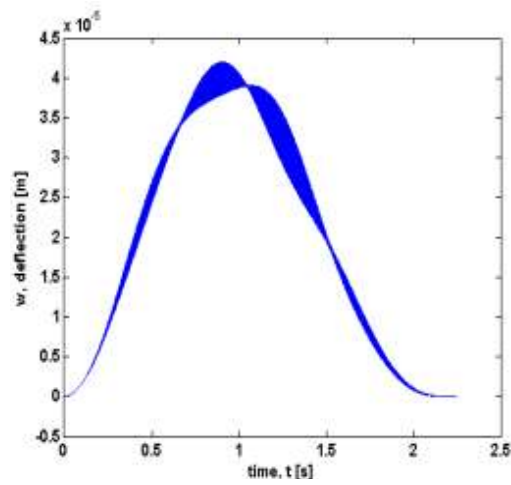
Figure 5.1: Dynamic response of deflection, v (y direction) with (a) one mode (b) two modes (c) three modes (d) four modes (e) five modes. Note that the unit for x axis is time, t (s) and y axis is the dynamic response, m.



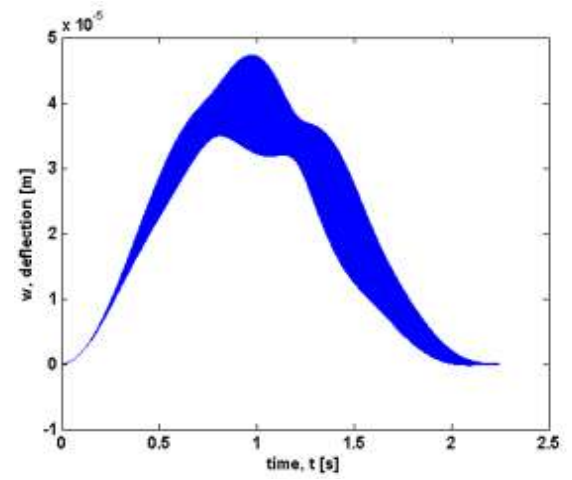
(a) One mode



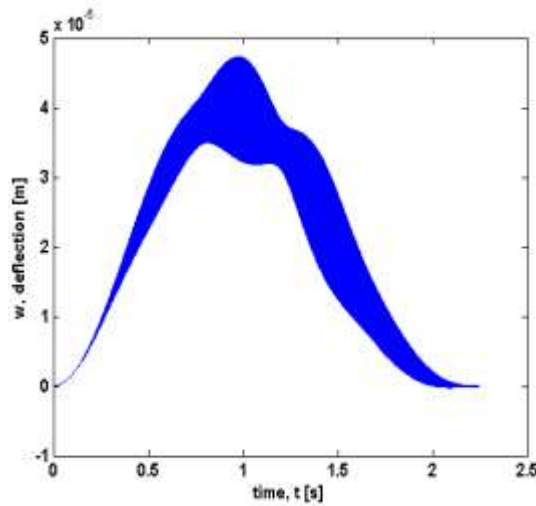
(b) Two modes



(c) Three modes



(d) Four modes



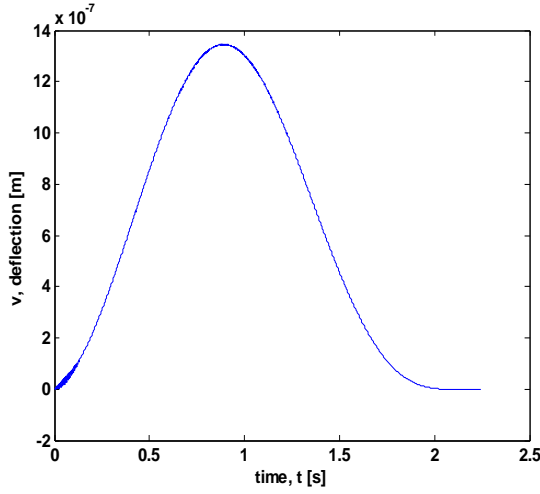
(e) Five modes

Figure 5.2: Dynamic response of deflection, w (z direction) with (a) one mode (b) two modes (c) three modes (d) four modes (e) five modes. Note that the unit for x axis is time, t (s) and y axis is the dynamic response, m.

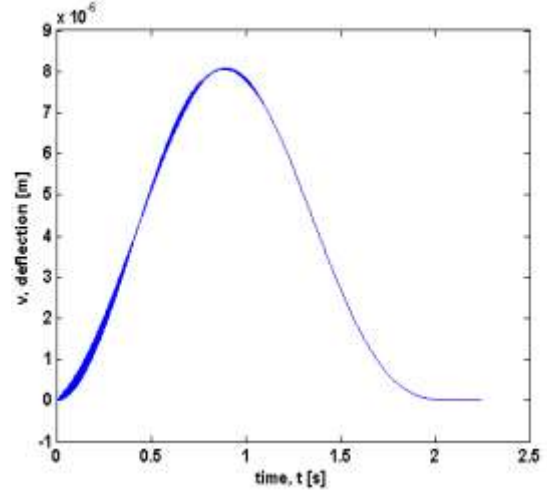
Further numerical simulation work is done on the model established to observe the effect of these main cutting parameters which are (i) the depth of cut – the thickness of the metal removed from the work piece, (ii) the cutting speed – the tangential velocity of the surface of work piece, and (iii) the rotational speed – the number of complete rotations or revolutions per time unit. Rotational speed is a cyclic frequency measured in hertz (rotations per second). These three parameters have been computed in dynamic model to investigate its influence on dynamic response and regenerative chatter. The numerical results of the dynamic response under these cutting parameters are shown in Figures 5.3 to 5.23. The effect of axial force, P_x (equation 3.31) is negligible and hence it is ignored during simulation of the dynamic model. The deflection, w in the z direction has a very similar pattern for different depth of cut, cutting speed and rotational speed with one mode and two modes only since there is no consideration of deflection, w in the instantaneous depth of cut formula, h (equation 3.27). More modes bring in some local features and the pattern of dynamic response is also different. Adding more modes does not change w as much as v .

5.2.1.2 Effect of Depth of Cut

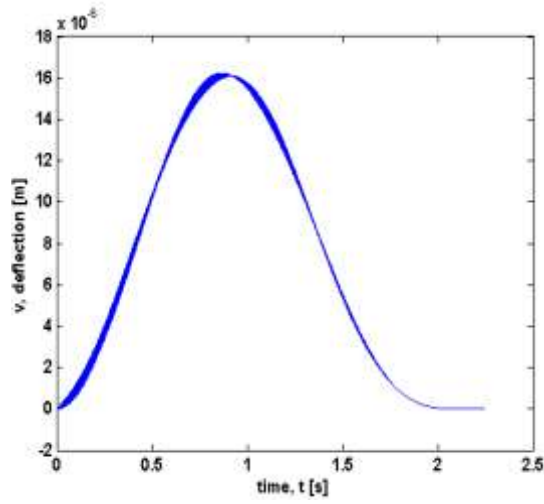
Figure 5.3 illustrates the dynamic responses of deflection, v in y direction for three different values of depth of cut which is 0.25 mm, 1.50 mm and 3.00 mm. Besides, the cutting speed, the rotational speed and the feed rate used are constant in which the cutting speed is 0.2228 m/s, the rotational speed is 1250 rev/min and the feed rate is 0.3 mm/rev. The graph shows that an increase in depth of cut increases the amplitudes and frequency of oscillation. The 3.00 mm depth of cut is prominent, as on top of nearly static deflection, high frequency oscillations begin to appear at the same time. Moreover, the magnitude shows almost double than 1.50 mm depth of cut. Figures 5.3 (b) indicates that the presence of chatter occurred at the beginning of pinned support. The deflection is not symmetrical due to the clamped pinned boundary condition as the fixed end is much stiffer than the other end.



(a) $h_c = 0.25$ mm

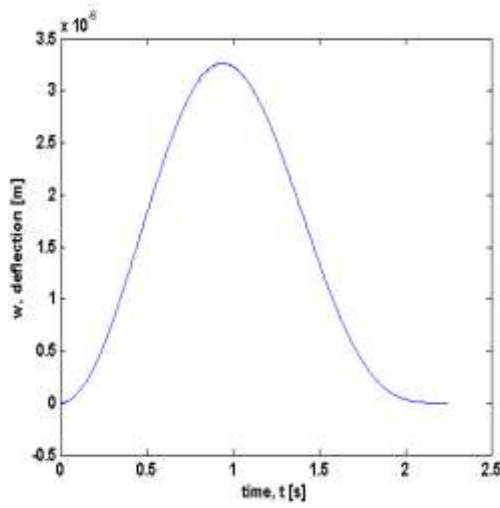


(b) $h_c = 1.50$ mm

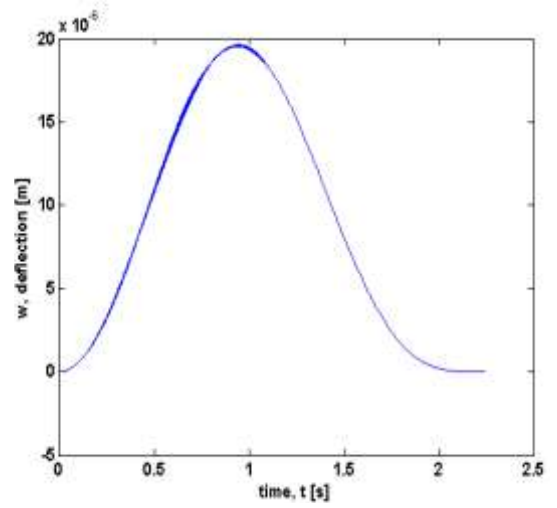


(c) $h_c = 3.00$ mm

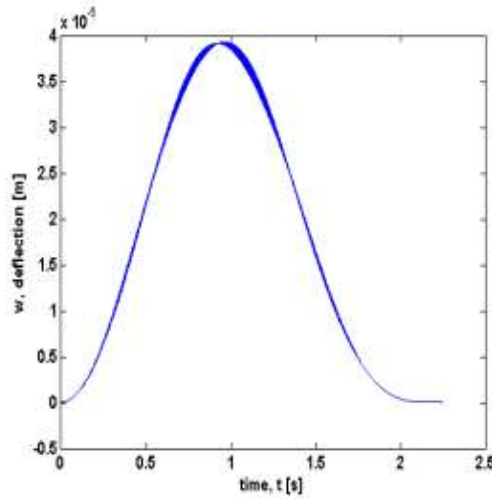
Figure 5.3: Dynamic response of deflection, v at different depths of cut with one mode (cutting speed = 0.2228 m/s, the rotational speed = 1250 rev/min and the feed rate = 0.3 mm/rev)



(a) $h_c = 0.25$ mm



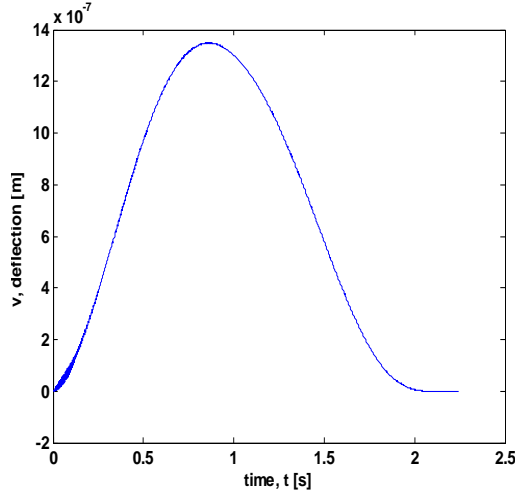
(b) $h_c = 1.50$ mm



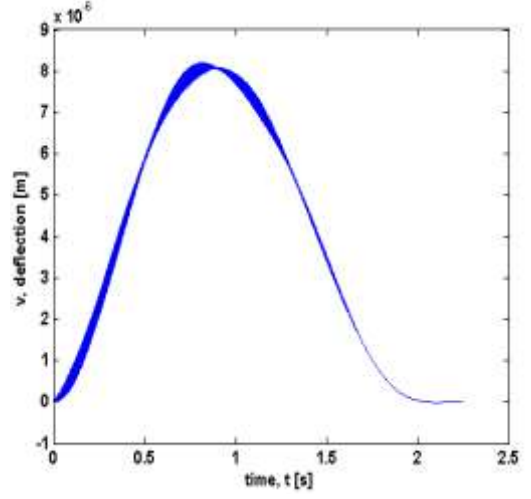
(c) $h_c = 3.00$ mm

Figure 5.4: Dynamic response of deflection, w at different depths of cut with one mode (cutting speed = 0.2228 m/s, the rotational speed = 1250 rev/min and the feed rate = 0.3 mm/rev)

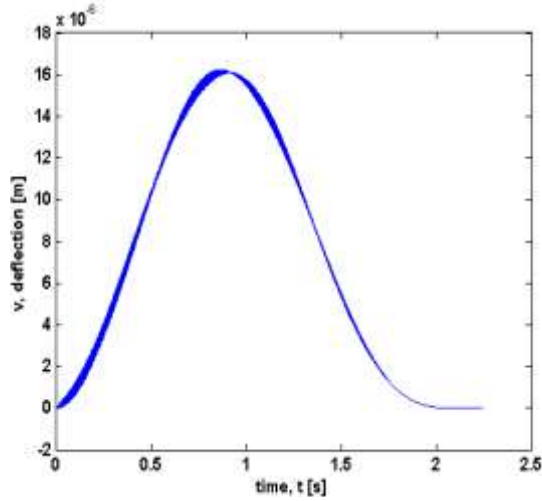
By using the same parameters in Figure 5.3, the dynamic responses of deflection, v using two modes are shown in Figure 5.5. Apparently, higher frequency components seem to have appeared in comparison with one mode. The high amplitude of oscillation is increased with the increase of number of modes.



(a) $h_c = 0.25$ mm

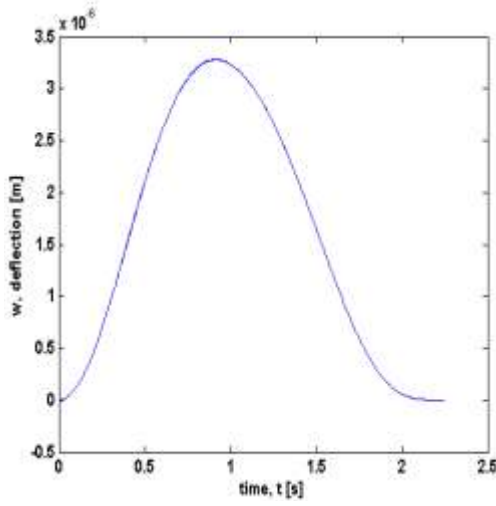


(b) $h_c = 1.50$ mm

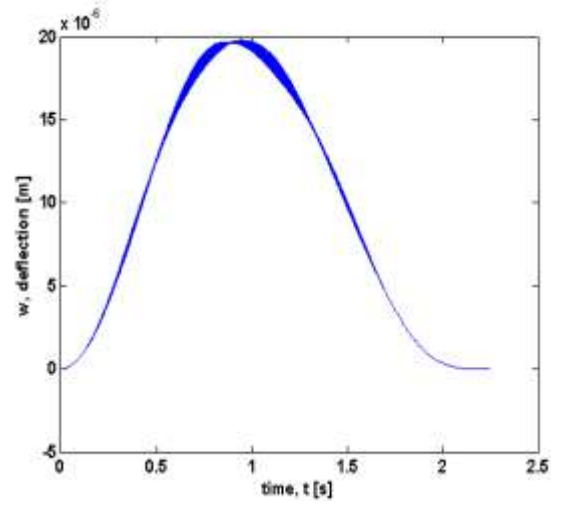


(c) $h_c = 3.00$ mm

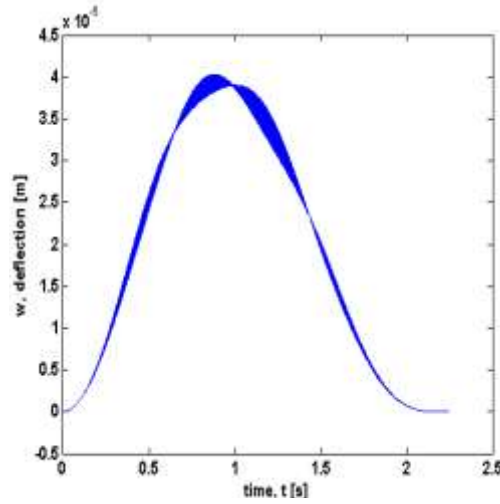
Figure 5.5: Dynamic response of deflection, v at different depths of cut with two modes (cutting speed = 0.2228 m/s, the rotational speed = 1250 rev/min and the feed rate = 0.3 mm/rev)



(a) $h_c = 0.25$ mm



(b) $h_c = 1.50$ mm



(c) $h_c = 3.00$ mm

Figure 5.6: Dynamic response of deflection, w at different depths of cut with two modes (cutting speed = 0.2228 m/s, the rotational speed = 1250 rev/min and the feed rate = 0.3 mm/rev)

Furthermore, the dynamic response, v obtained using three modes has a similar pattern as depicted in Figure 5.8. Figure 5.8 (a), 5.8 (b) and 5.8 (c) generate a same pattern but difference in amplitude due to a higher depth of cut used. Figure 5.8 (c) appeared to have higher amplitude than Figure 5.8 (a) and 5.8 (b) since the biggest depth of cut is used. Notice that in the whole Figure 5.8, at half through time, t the response in Figure 5.8 (c) begins to illustrate a beating

phenomenon. Beating phenomenon is when two harmonic motions, with frequencies and amplitudes close to one another, are added, and then resulting motion exhibits a phenomenon known as beats. It is different from chatter which chatter is a harmonic imbalance that occurs between the tool and the work piece because they are bouncing against each other. Chatter can easily be recognized by the noise associated with self-excited vibrations. It also can be seen from the appearance of the chips according to Tlustý (2000). The phenomenon of beating is often observed in machines, structures and electric houses. For example in machine and structures, the beating phenomenon occurs when the forcing frequency is close to the natural frequency of the system (Rao, 1995). The examples of two harmonic motions are represented as below;

$$x_1(t) = X \cos \omega t \quad (5.1)$$

$$x_2(t) = X \cos (\omega + \delta)t \quad (5.2)$$

where δ is a small quantity and the addition of these motions yields

$$x(t) = x_1(t) + x_2(t) = X [\cos \omega t + \cos (\omega + \delta)t] \quad (5.3)$$

Using the relation

$$\cos A + \cos B = 2 \cos \left(\frac{A+B}{2} \right) \cos \left(\frac{A-B}{2} \right) \quad (5.4)$$

and equation 5.3 can be rewritten as

$$x(t) = 2X \cos \frac{\delta t}{2} \cos \left(\omega + \frac{\delta}{2} \right) t$$

This equation is shown graphically in Figure 5.7.

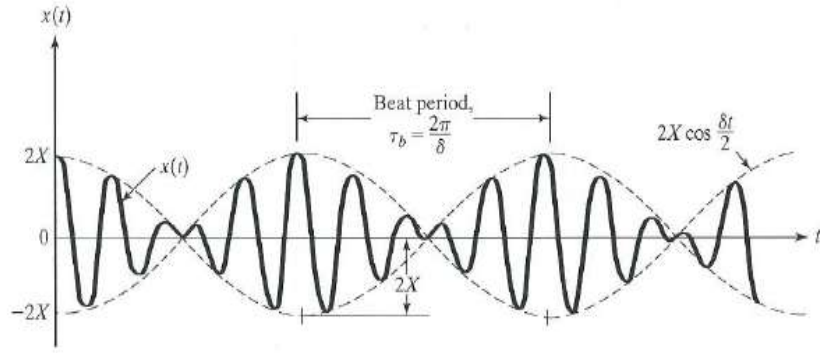
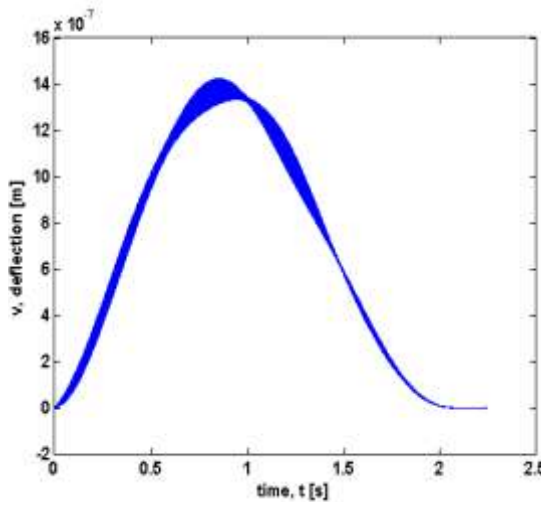
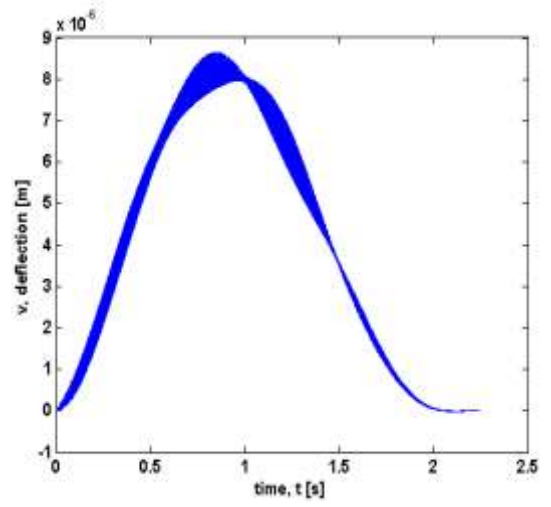


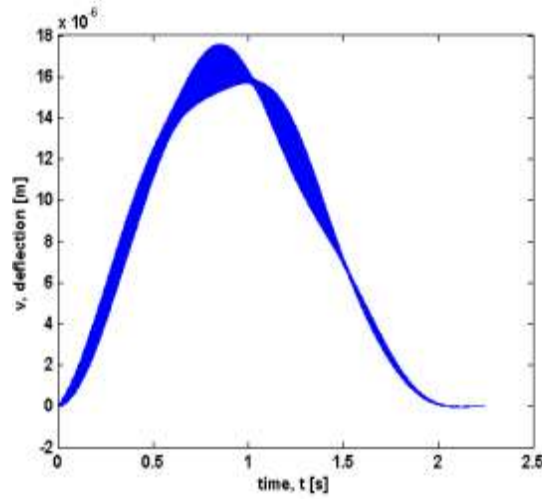
Figure 5.7: Phenomenon of beats (Rao, 1995)



(a) $h_c = 0.25$ mm

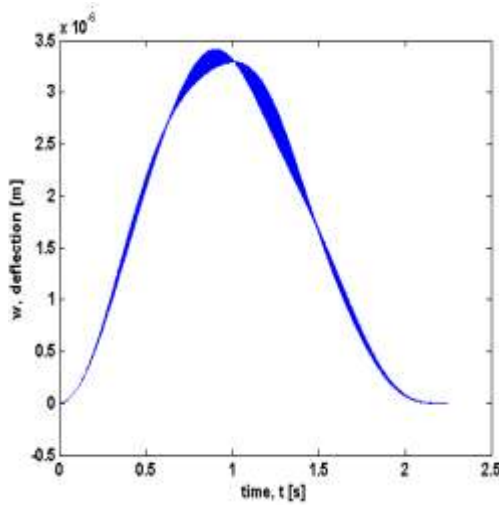


(b) $h_c = 1.50$ mm

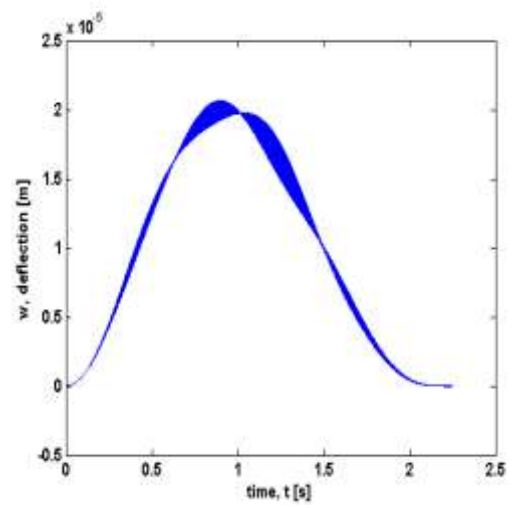


(c) $h_c = 3.00$ mm

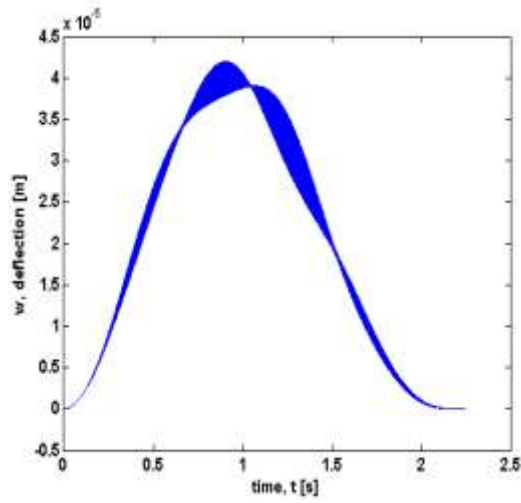
Figure 5.8: Dynamic response of deflection, v at different depths of cut with three modes (cutting speed = 0.2228 m/s, the rotational speed = 1250 rev/min and the feed rate = 0.3 mm/rev)



(a) $h_c = 0.25$ mm



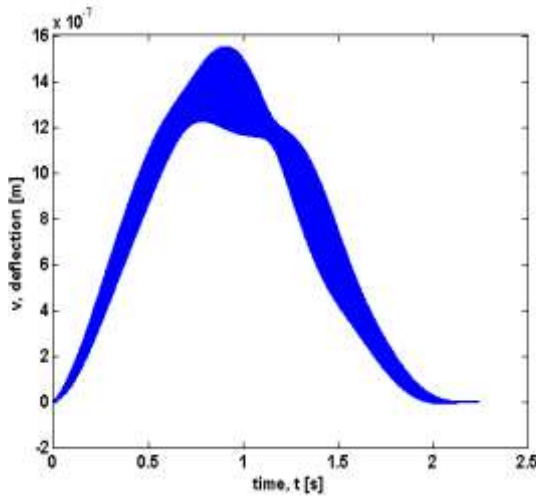
(b) $h_c = 1.50$ mm



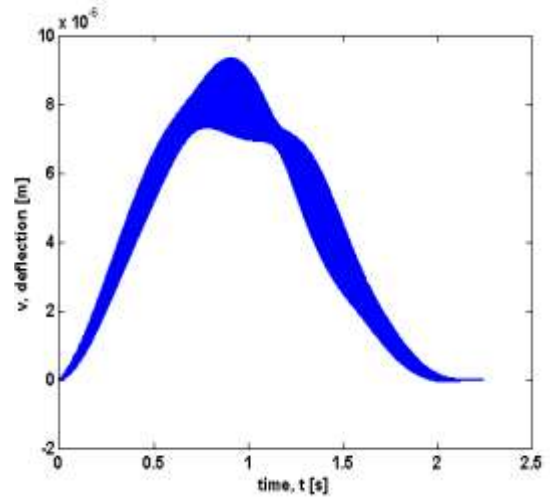
(c) $h_c = 3.00$ mm

Figure 5.9: Dynamic response of deflection, w at different depths of cut with three modes (cutting speed = 0.2228 m/s, the rotational speed = 1250 rev/min and the feed rate = 0.3 mm/rev)

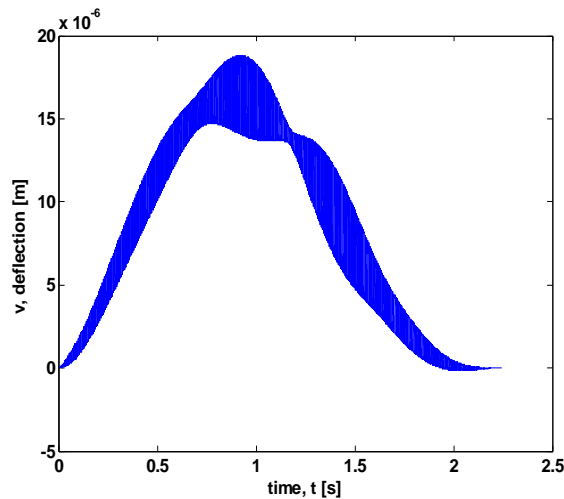
A slightly different pattern is produced when four modes are used. Again, Figure 5.10 (a), 5.10 (b) and 5.10 (c) generate a same pattern but difference in amplitude due to a higher depth of cut is used. Figure 5.10 (c) appeared to have higher amplitude than Figure 5.10 (a) and 5.10 (b). At half way through the time, t the mode shape in Figure 5.10 (c) begins to illustrate a beating phenomenon.



(a) $h_c = 0.25$ mm

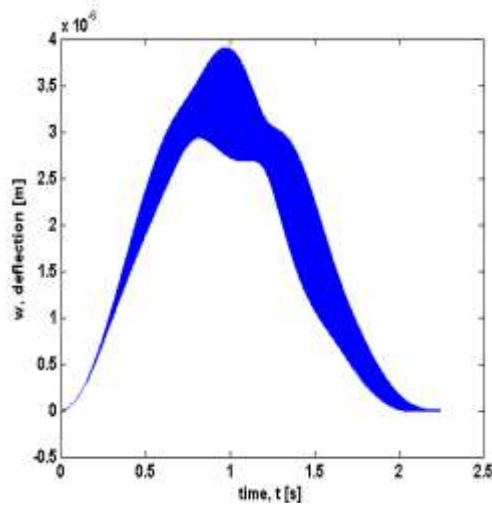


(b) $h_c = 1.50$ mm

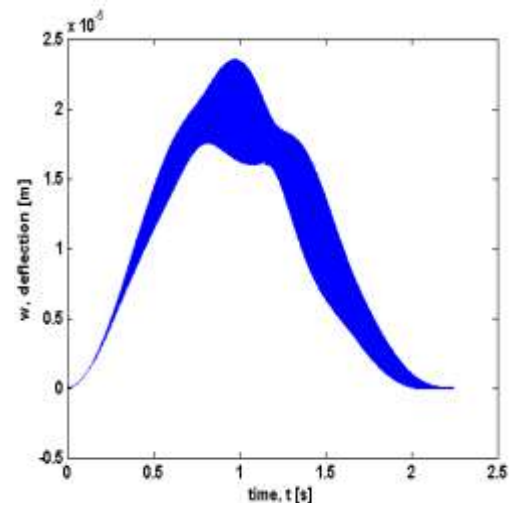


(c) $h_c = 3.00$ mm

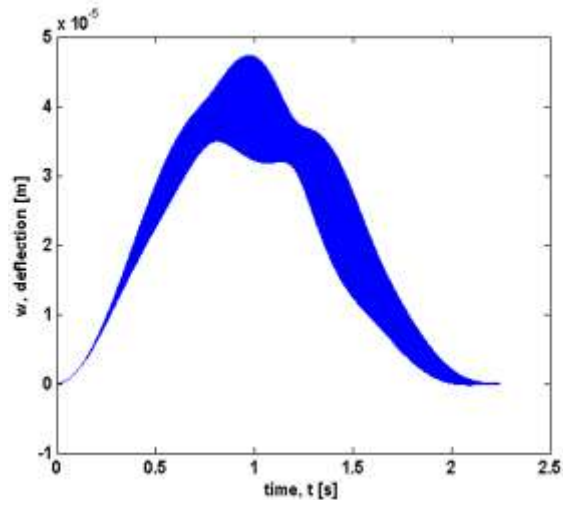
Figure 5.10: Dynamic response of deflection, v at different depths of cut with four modes (cutting speed = 0.2228 m/s, the rotational speed = 1250 rev/min and the feed rate = 0.3 mm/rev)



(a) $h_c = 0.25$ mm



(b) $h_c = 1.50$ mm

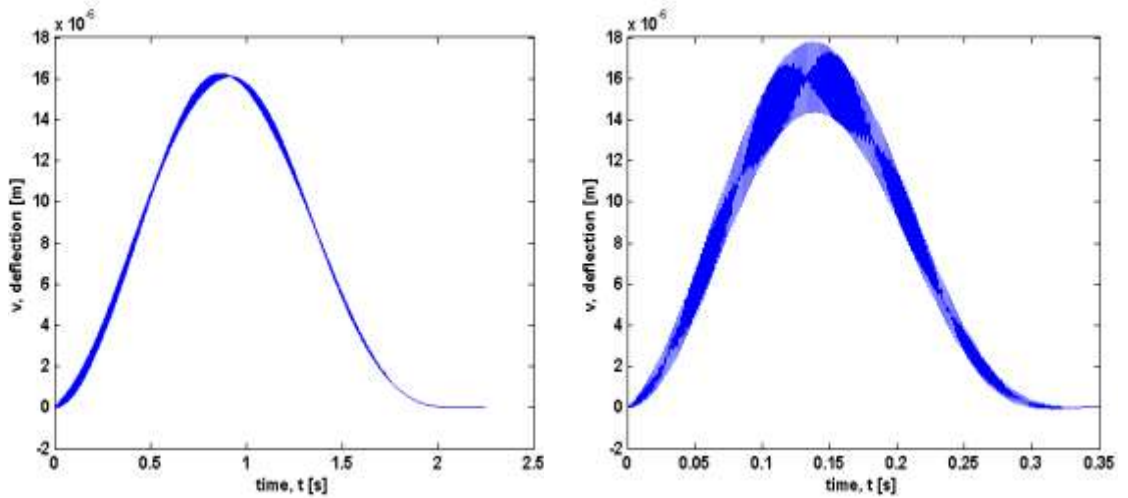


(c) $h_c = 3.00$ mm

Figure 5.11: Dynamic response of deflection, w at different depths of cut with four modes (cutting speed = 0.2228 m/s, the rotational speed = 1250 rev/min and the feed rate = 0.3 mm/rev)

5.2.2 Effect of Cutting Speed

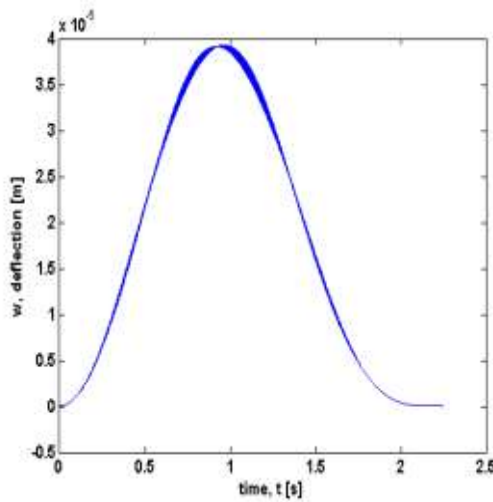
The next cutting parameter simulated in the dynamic model is the cutting speed. Figure 5.12 and Figure 5.13 show the dynamic response, v at two different cutting speeds in order to demonstrate its effect with one mode. The other cutting parameters are set to be constant which are the depth of cut of 3.00 mm, the rotational speed of 1250 rev/min and the feed rate of 0.3 mm/rev. From Figure 5.12 (b), high frequency oscillation appeared on top of the nearly static deflection and the mode illustrates a beating phenomenon. By comparing Figure 5.12 (a) and 5.12 (b), it can be seen that higher-frequency oscillation has bigger amplitude at a higher cutting speed. The finding is consistent with a conclusion by Tobias and Fishwick (1958) that a lower cutting speed would suppress chatter and therefore produce a better surface finish.



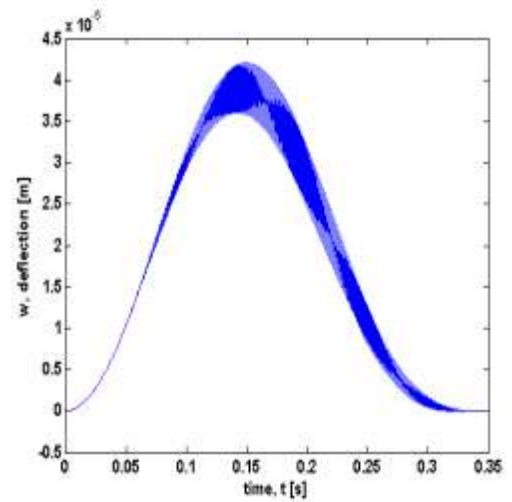
(a) cutting speed = 0.2228 m/s

(b) cutting speed = 1.4353 m/s

Figure 5.12: Dynamic response of deflection, v at different cutting speeds with one mode (depth of cut = 3.00 mm, rotational speed = 1250 rev/min and the feed rate = 0.3 mm/rev)



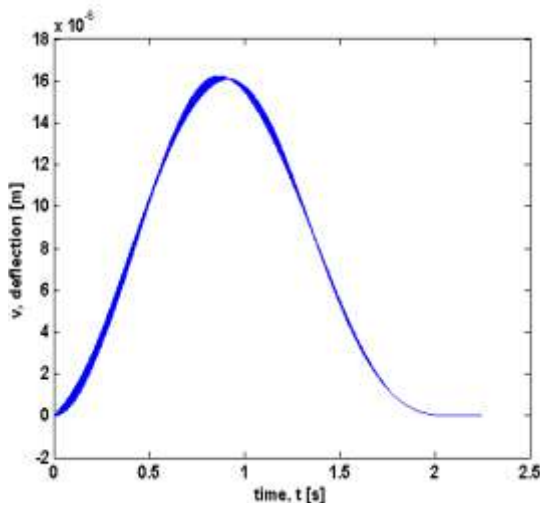
(a) cutting speed = 0.2228 m/s



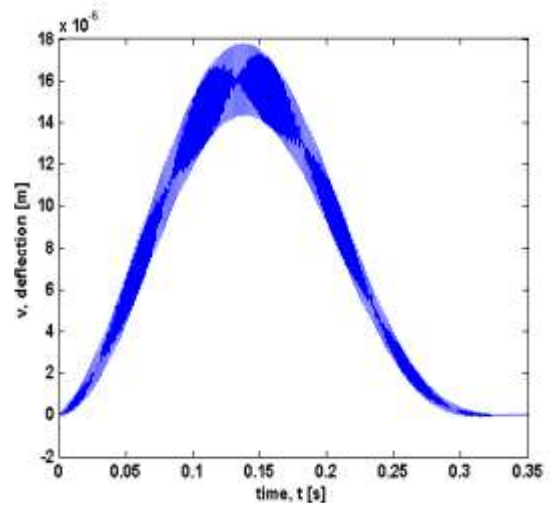
(b) cutting speed = 1.4353 m/s

Figure 5.13: Dynamic response of deflection, w at different cutting speeds with one mode (depth of cut = 3.00 mm, rotational speed = 1250 rev/min and the feed rate = 0.3 mm/rev)

The same cutting conditions are simulated with two modes and the results are shown in Figure 5.14 and Figure 5.15. Higher amplitude vibration becomes more pronounced with more modes. The deflection is skewed to the weaker support, which is the tailstock. The beating phenomenon is even greater at a higher cutting speed which is 1.4353 m/s. The results obtained with three and four modes are similar with two modes as illustrated in Figure 5.16 and Figure 5.17.

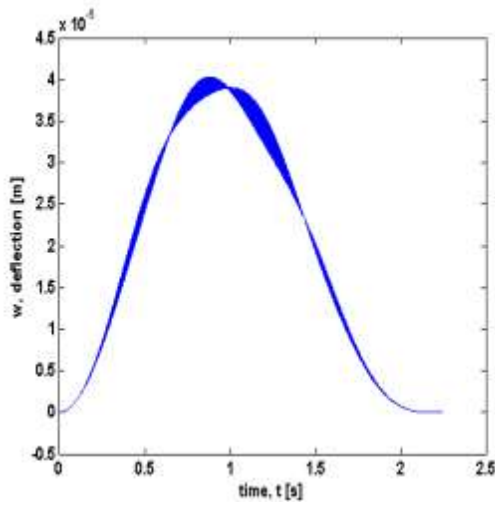


(a) cutting speed = 0.2228 m/s

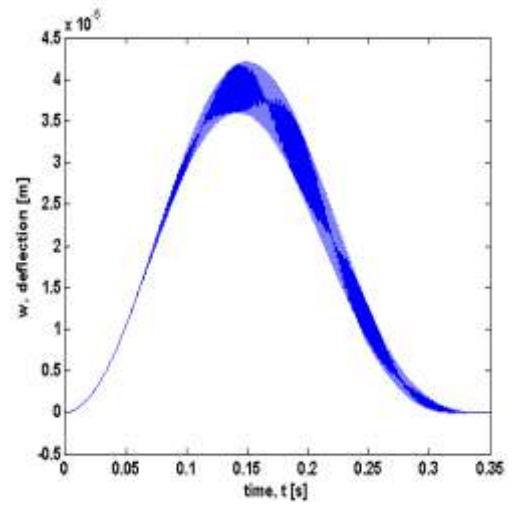


(b) cutting speed = 1.4353 m/s

Figure 5.14: Dynamic response of deflection, v at different cutting speeds with two modes (depth of cut = 3.00 mm, rotational speed = 1250 rev/min and the feed rate = 0.3 mm/rev)

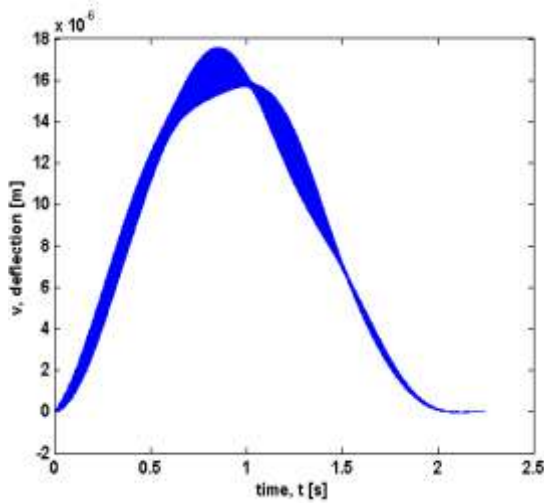


(a) cutting speed = 0.2228 m/s

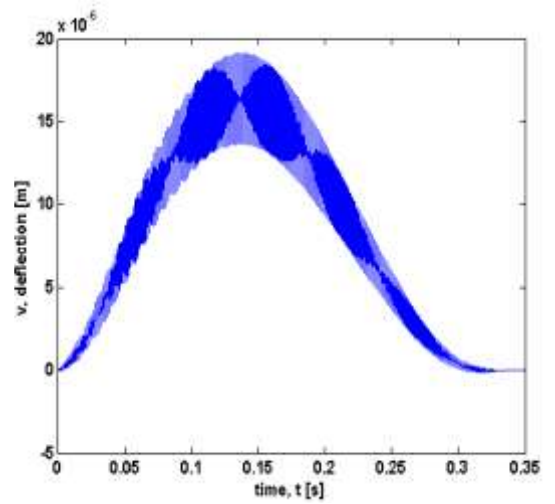


(b) cutting speed = 1.4353 m/s

Figure 5.15: Dynamic response of deflection, w at different cutting speeds with two modes (depth of cut = 3.00 mm, rotational speed = 1250 rev/min and the feed rate = 0.3 mm/rev)

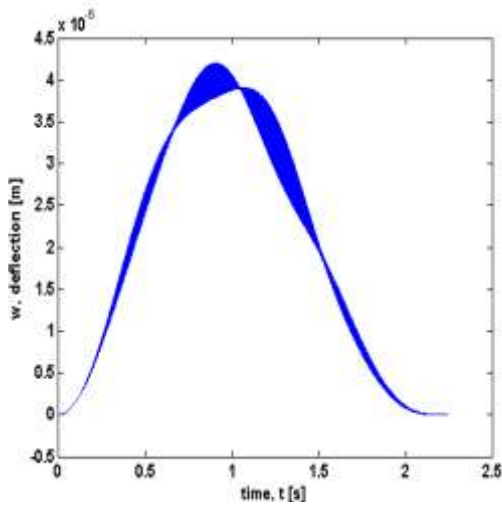


(a) cutting speed = 0.2228 m/s

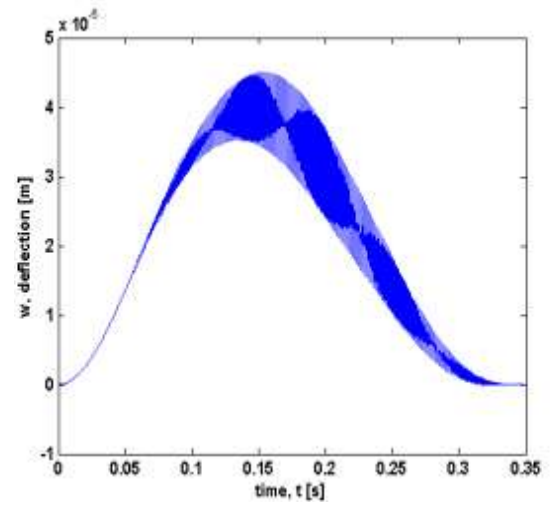


(b) cutting speed = 1.4353 m/s

Figure 5.16: Dynamic response of deflection, v at different cutting speeds with three modes (depth of cut = 3.00 mm, rotational speed = 1250 rev/min and the feed rate = 0.3 mm/rev)



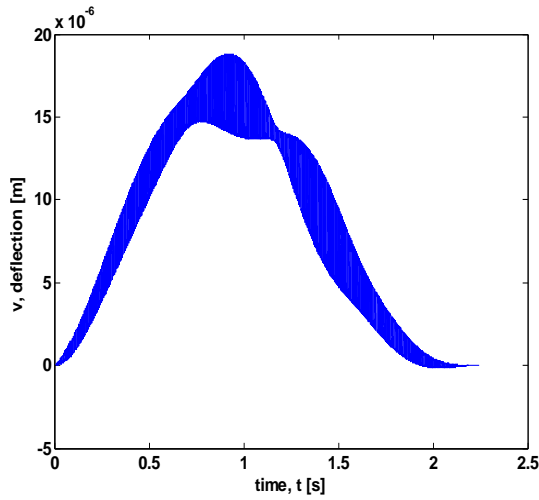
(a) cutting speed = 0.2228 m/s



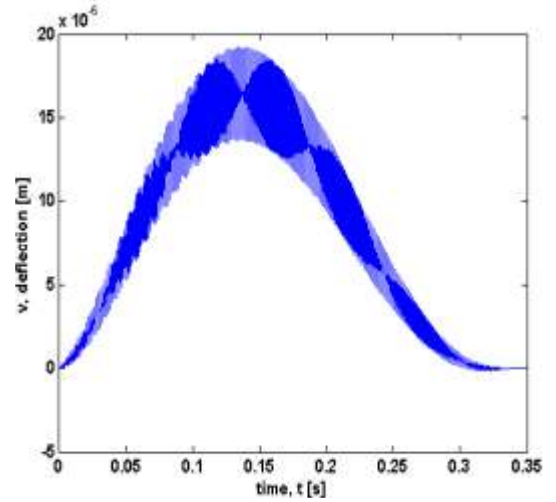
(b) cutting speed = 1.4353 m/s

Figure 5.17: Dynamic response of deflection, w at different cutting speeds with three modes (depth of cut = 3.00 mm, rotational speed = 1250 rev/min and the feed rate = 0.3 mm/rev)

A slightly different pattern is produced when four modes (Figure 5.18 and Figure 5.19) are used but the difference in amplitude is due to a high number of modes included in the simulation. Figure 5.18 (b) appeared to have higher amplitude with beating phenomenon than Figure 5.18 (a).

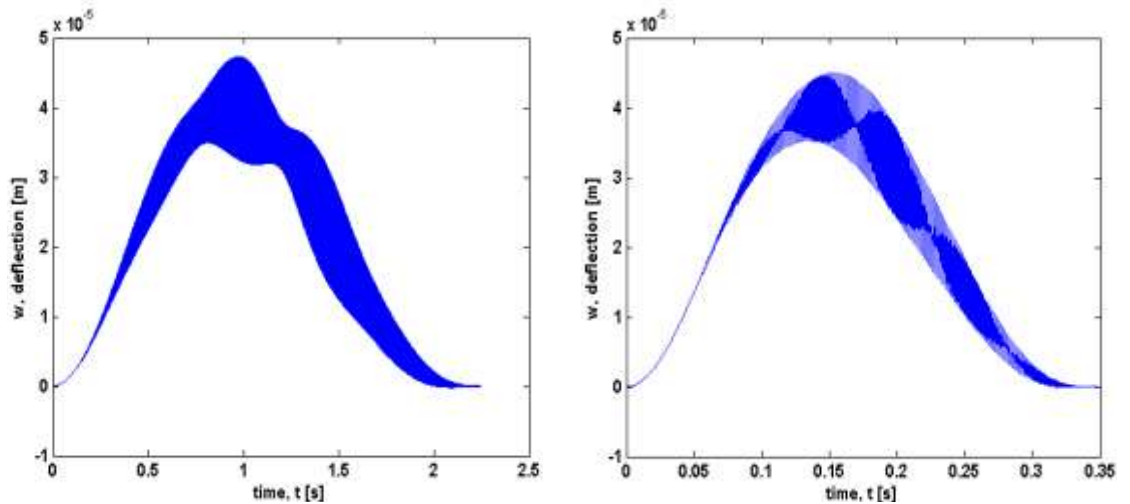


(a) cutting speed = 0.2228 m/s



(b) cutting speed = 1.4353 m/s

Figure 5.18: Dynamic response of deflection, v at different cutting speeds with four modes (depth of cut = 3.00 mm, rotational speed = 1250 rev/min and the feed rate = 0.3 mm/rev)



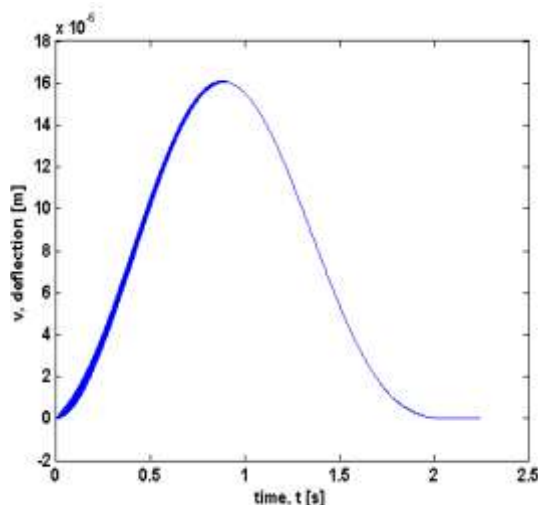
(a) cutting speed = 0.2228 m/s

(b) cutting speed = 1.4353 m/s

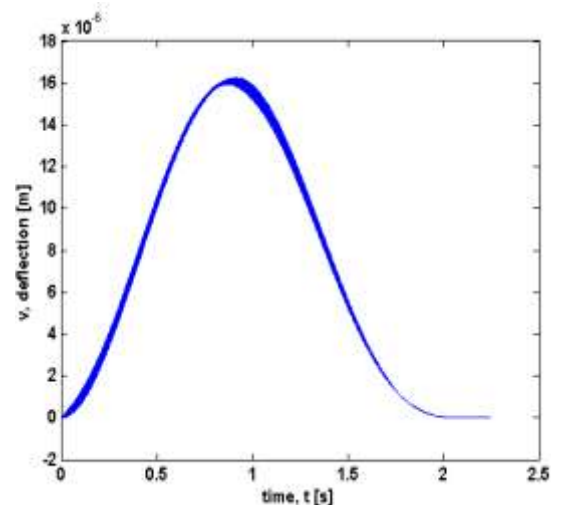
Figure 5.19: Dynamic response of deflection, w at different cutting speeds with four modes (depth of cut = 3.00 mm, rotational speed = 1250 rev/min and the feed rate = 0.3 mm/rev)

5.2.3 Effect of Rotational Speed

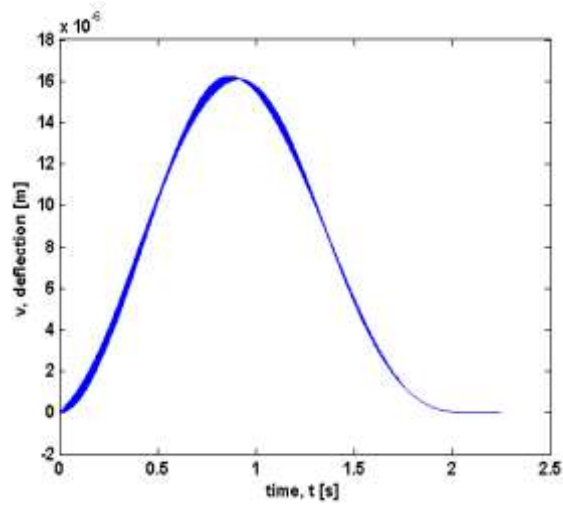
The last cutting parameter simulated in the dynamic model is the rotational speed. Figure 5.20 to Figure 5.25 illustrates the results of the effects of different rotational speeds on dynamic response, v and w , at three different rotational speeds in order to demonstrate its effect with one mode, two modes, three modes and four modes. Again, the other cutting parameters are set to be constant which are the depth of cut is 3.00 mm, the cutting speed is 0.2228 m/s and the feed rate is 3.00 mm. The results of the effects of different rotational speeds with one mode are illustrated in Figure 5.20. At lower rotational speed, the high oscillation only appears at the beginning of the mode shape. There is not much amplitude difference between the first, second and third modes. The rotational speed does not seem to have a big effect on the dynamic response especially on the amplitude of deflection.



(a) rotational speed = 230 rev/min

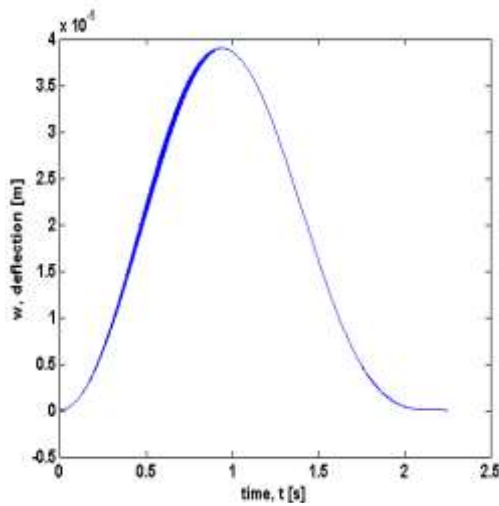


(b) rotational speed = 480 rev/min

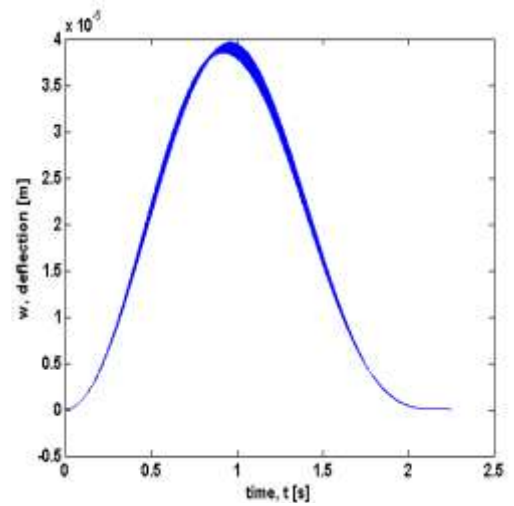


(c) rotational speed = 1250 rev/min

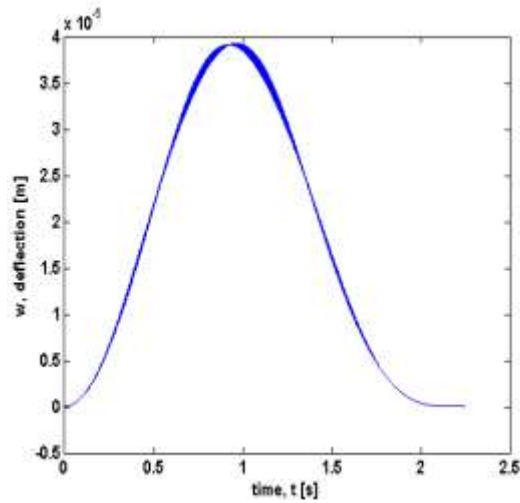
Figure 5.20: Dynamic response of deflection, v at different rotational speeds with one mode (depth of cut = 3.00 mm, cutting speed = 0.2228 m/s and the feed rate = 0.3 mm/rev)



(a) rotational speed = 230 rev/min



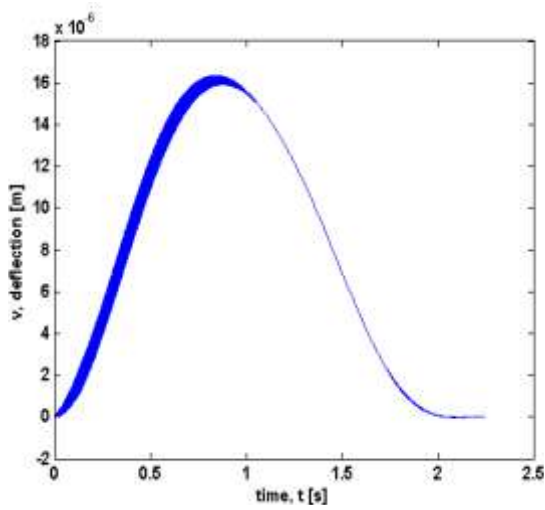
(b) rotational speed = 480 rev/min



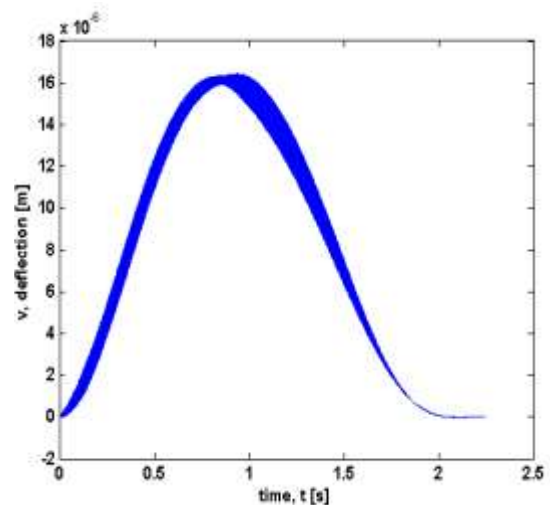
(c) rotational speed = 1250 rev/min

Figure 5.21: Dynamic response of deflection, w at different rotational speeds with one mode (depth of cut = 3 mm, cutting speed = 0.2228 m/s and the feed rate = 0.3 mm/rev)

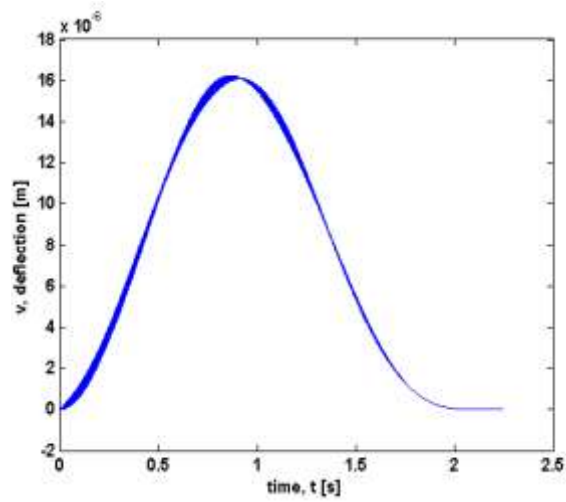
There are some differences in oscillation particularly in mode two. When two modes are used as shown in Figure 5.22, a higher rotational speed is seen to excite slightly greater high-frequency components. Therefore, increasing the rotational speed moderately promotes the occurrence of chatter.



(a) rotational speed = 230 rev/min

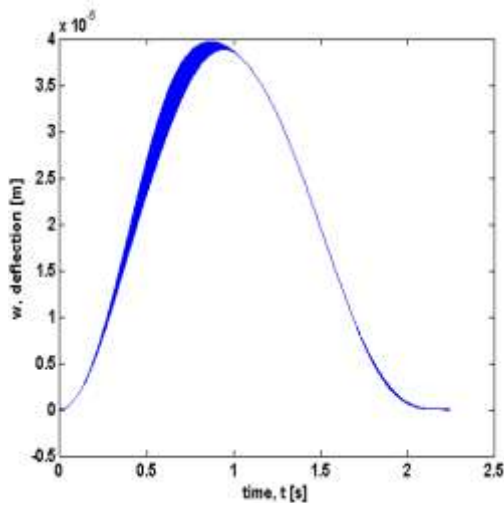


(b) rotational speed = 480 rev/min

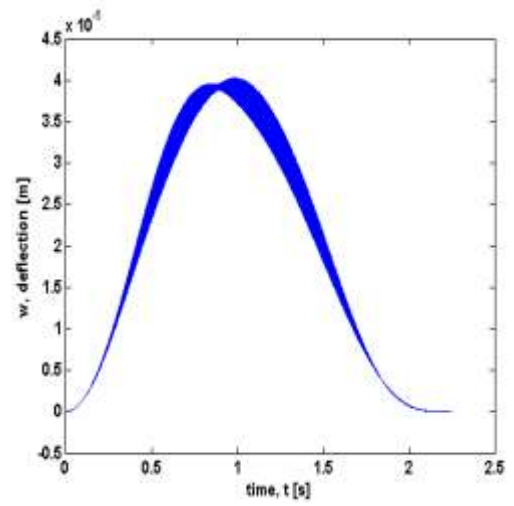


(c) rotational speed = 1250 rev/min

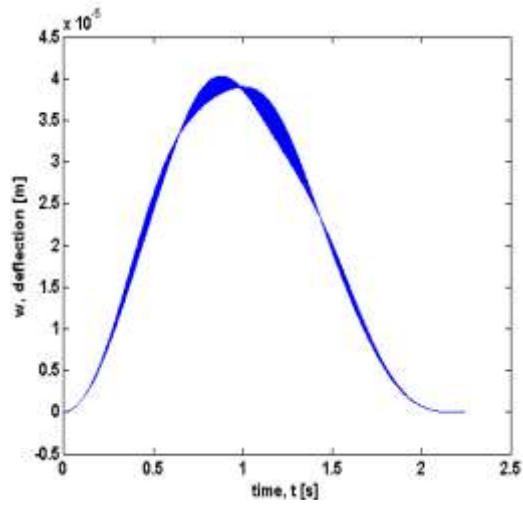
Figure 5.22: Dynamic response of deflection, v at different rotational speeds with two modes (depth of cut = 3.00 mm, cutting speed = 0.2228 m/s and the feed rate = 0.3 mm/rev)



(a) rotational speed = 230 rev/min



(b) rotational speed = 480 rev/min



(c) rotational speed = 1250 rev/min

Figure 5.23: Dynamic response of deflection, w at different rotational speeds with two modes (depth of cut = 3.00 mm, cutting speed = 0.2228 m/s and the feed rate = 0.3 mm/rev)

5.3 Elastic Boundary

5.3.1 Introduction

Initially, the assumed boundary conditions were a clamped and pinned to represent a chuck and a tailstock supports on lathe. Unfortunately, the dynamic responses, v and w illustrate a small magnitude of deflection which is not realistic to the actual lathe support (shown earlier in section 5.2). Thus, more suitable boundary conditions which replicate the actual lathe support should be adopted to ensure the accuracy of the dynamic response. This new boundary conditions employed are known as an elastic boundary condition since a chuck is more suitable to be represented by rotational spring and a tailstock as a linear spring.

5.3.2 Convergence test

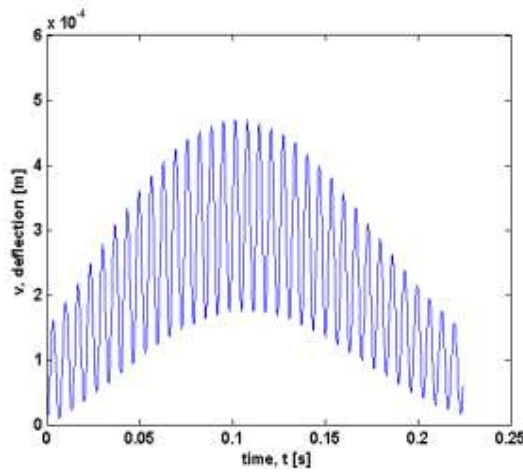
The convergence test has also been performed for the elastic boundary condition to monitor the occurrence of chatter (up to five modes) and to determine the appropriate number of modes included in the simulation. The properties of the shaft (cylindrical metal work piece) used in this convergence test are length, $l = 0.55$ m, radius $r = 18.5$ mm, Young's Modulus $E = 2.07 \times 10^{11}$ Pa, and density, $\rho = 7817.4$ kg/m³ while the cutting parameters used are 2.228 m/s for cutting speed, 1250 rev/min for rotational speed and 0.3 mm/rev for feed rate. By considering an elastic boundary, its normalized modes are

$$\varphi_n(x) = C_1 \cos(\beta_n x) + C_2 \sin(\beta_n x) + C_3 \cosh(\beta_n x) + C_4 \sinh(\beta_n x) \quad (5.1)$$

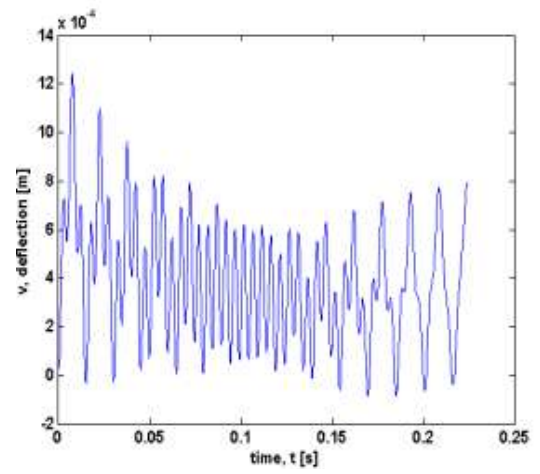
where $\beta_n = [5.777 \ 6.657 \ 13.145 \ 13.685]$ and $\omega_n = (\lambda_n)^2 \sqrt{EI/\rho A} / 2\pi l^2$ ($n = 1, 2, 3, \dots$) is the natural frequency of the stationary shaft.

The dynamic responses of deflection, v in y direction and w in the z direction are shown in Figure 5.24 and Figure 5.25 respectively. It was found that as the higher modes are included in the simulation, higher oscillation (chatter) starts to appear on top of the deflection (dynamic response) curve in both v (y) and w (z) direction as depicted in Figure 5.24 (c) and Figure 5.25 (c). The amplitude of the deflection increased with the increase number of mode used.

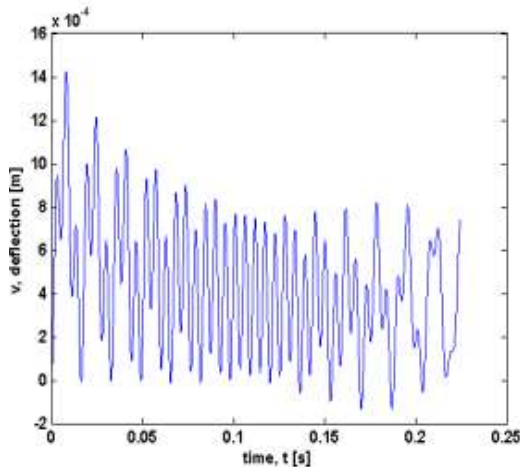
It is also noticed that four modes are adequate for numerical simulation since it will excite high frequency oscillation. Sometimes, it is not essential to include more than four modes because it will increase the computational workloads and also lengthen the iteration process. However, the more modes considered, the more accurate the results



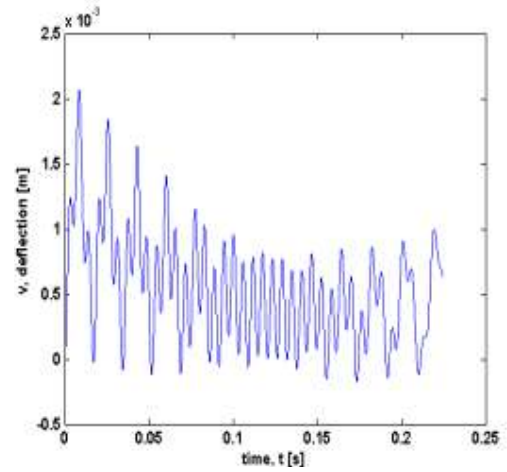
(a) One mode



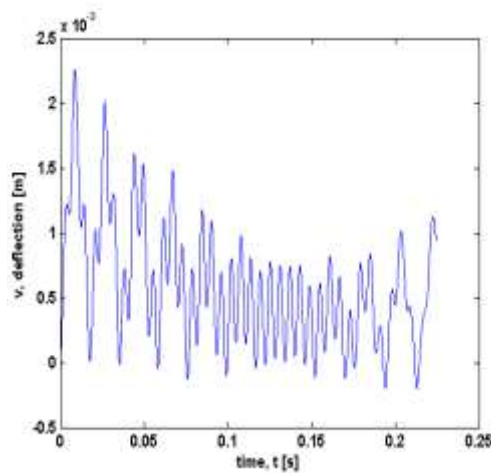
(b) Two modes



(c) Three modes

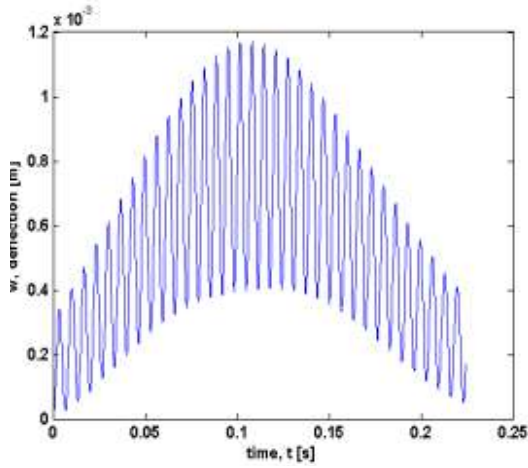


(d) Four modes

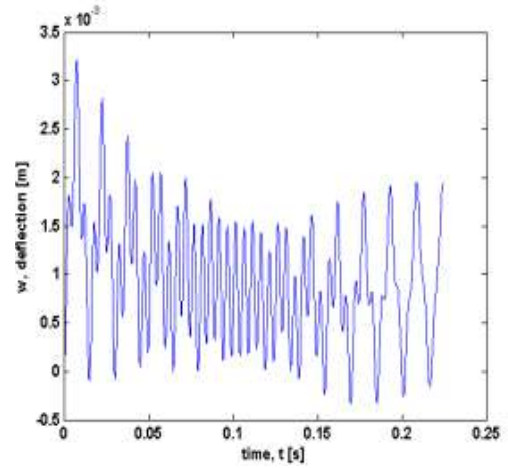


(e) Five modes

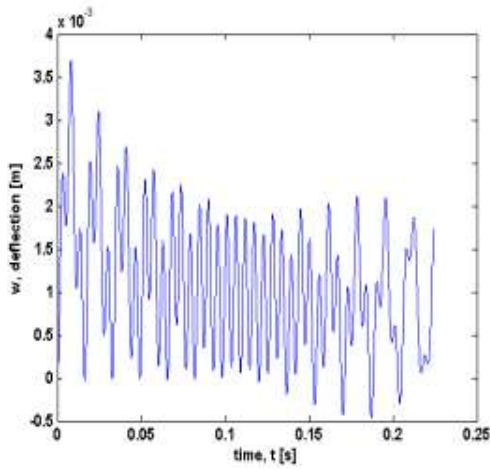
Figure 5.24: Dynamic response of deflection, v (y direction) with (a) one mode (b) two modes (c) three modes (d) four modes (e) five modes. Note that the unit for x axis is time, t (s) and y axis is the dynamic response, m.



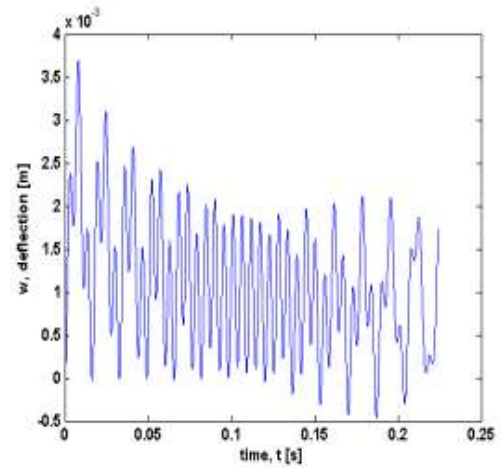
(c) One mode



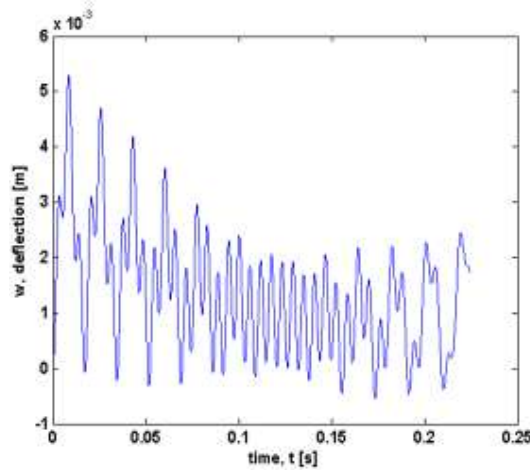
(b) Two modes



(e) Three modes



(d) Four modes

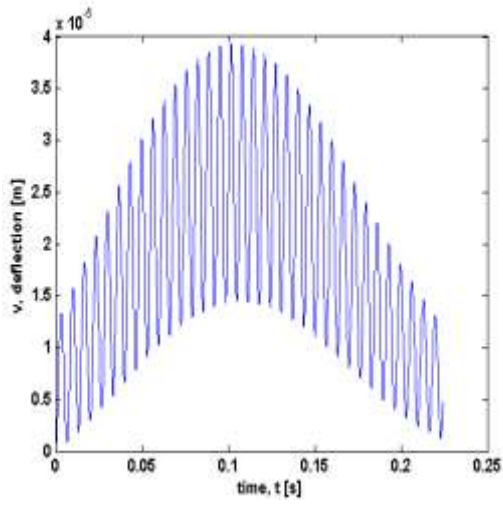


(e) Five modes

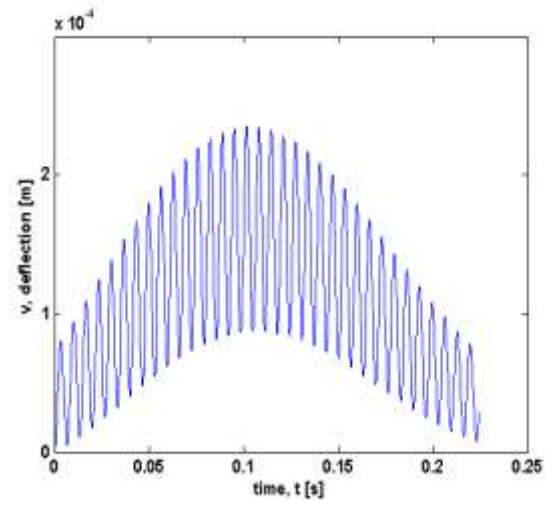
Figure 5.25: Dynamic response of deflection, w (z direction) with (a) one mode (b) two modes (c) three modes (d) four modes (e) five modes. Note that the unit for x axis is time, t (s) and y axis is the dynamic response, m.

5.3.3 Effect of Depth of Cut

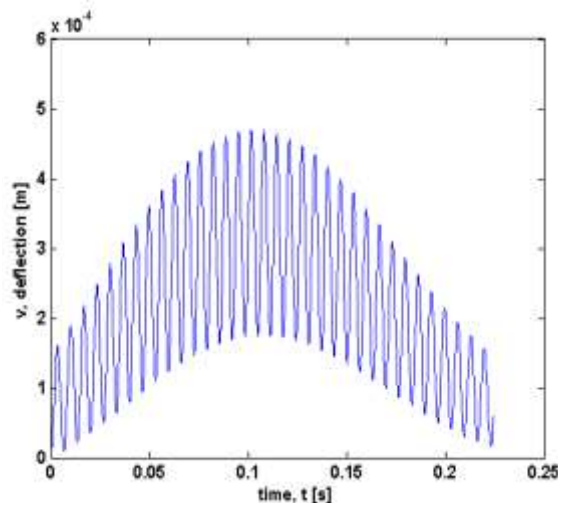
Figure 5.26 illustrates the dynamic responses of deflection, v in y direction for three different values of depth of cut which is 0.25 mm, 1.50 mm and 3.00 mm. Besides, the cutting speed, the rotational speed and the feed rate are constant in which the cutting speed is 2.228 m/s, the rotational speed is 1250 rev/min and the feed rate is 0.3 mm/rev. In elastic boundary conditions, the cutting speed used is slightly higher as compared with a clamped pinned boundary. This is done purposely to avoid any intensive computational works which somehow prolong and complicate the production of results. From the graph, it shows that an increase in depth of cut will increase the amplitudes and frequency of oscillation. The 3.00 mm depth of cut is prominent, as the magnitude of the oscillation becomes bigger. Figures 5.26 (c) and Figure 5.27 (c) indicate that the amplitude of oscillation is the highest among the three values of depth of cut.



(a) $h_c = 0.25$ mm

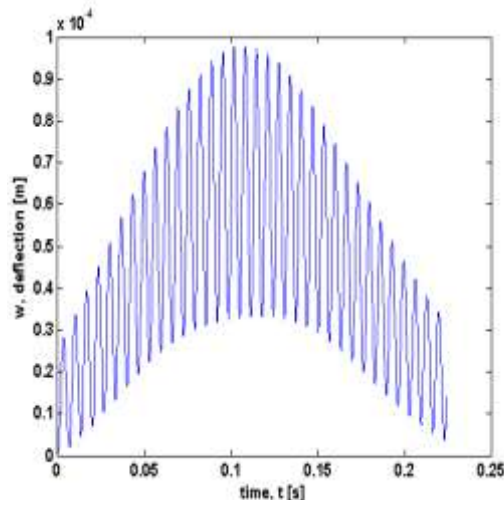


(b) $h_c = 1.50$ mm

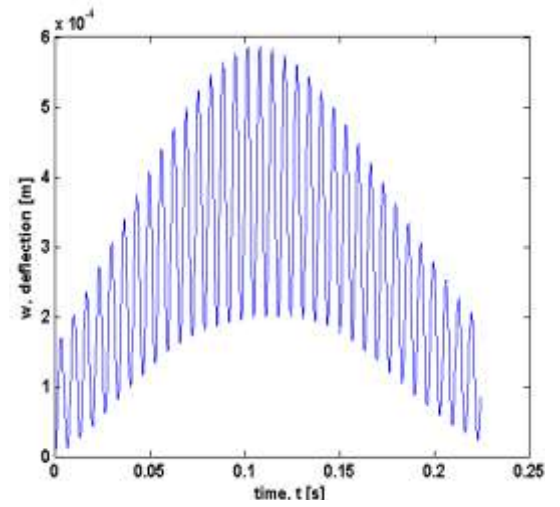


(c) $h_c = 3.00$ mm

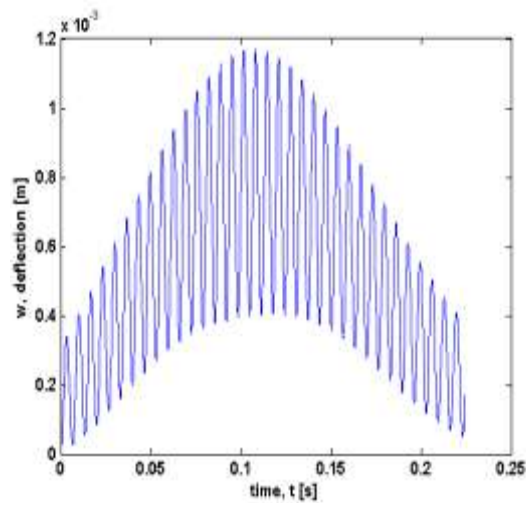
Figure 5.26: Dynamic response of deflection, v at different depths of cut with one mode (1250 rev/min, cutting speed = 2.228 m/s and feed rate is 0.3 mm/rev)



(a) $h_c = 0.25$ mm



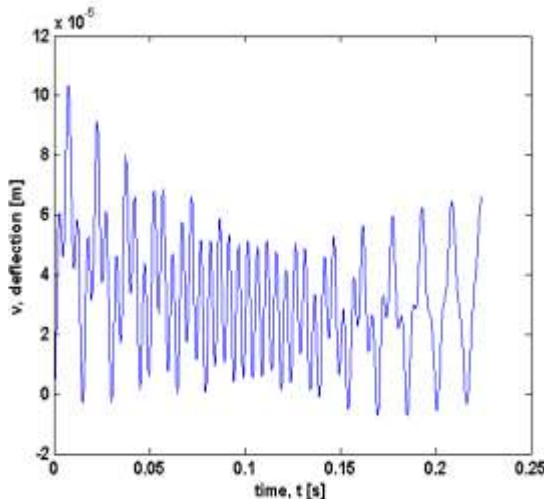
(b) $h_c = 1.50$ mm



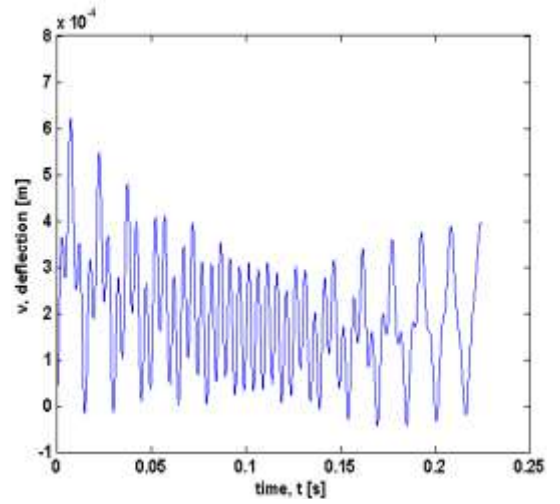
(c) $h_c = 3.00$ mm

Figure 5.27: Dynamic response of deflection, w at different depths of cut with one mode (1250 rev/min, cutting speed = 2.228m/s and feed rate is 0.3 mm/rev)

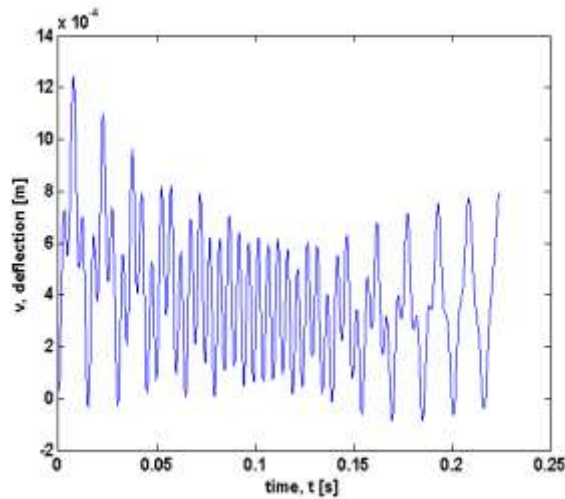
By using the same parameters in Figure 5.26, the dynamic responses of deflection, v using two modes are shown in Figure 5.28. Apparently, a different shape of deflection curve was observed and higher frequency components seem to have appeared in comparison with one mode. The high amplitude of oscillation is increased with the increase of number of modes.



(a) $h_c = 0.25$ mm

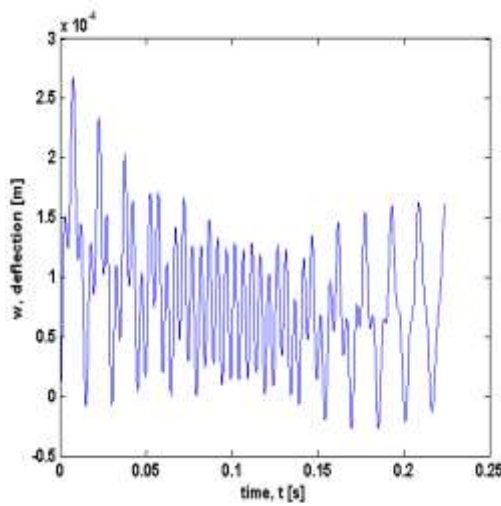


(b) $h_c = 1.50$ mm

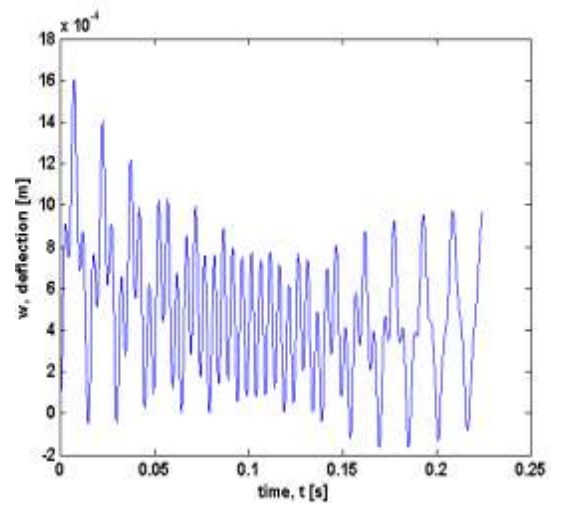


(c) $h_c = 3.00$ mm

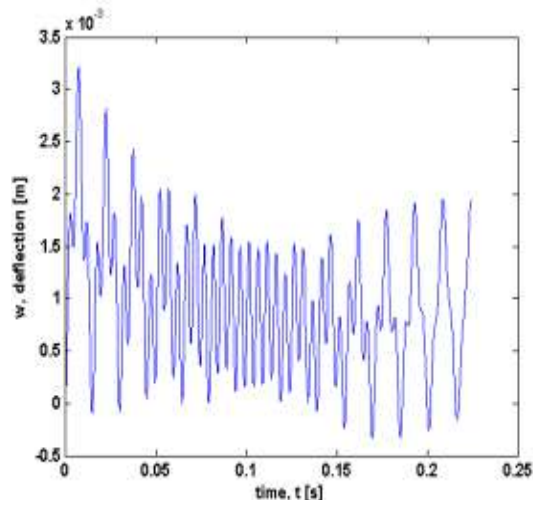
Figure 5.28: Dynamic response of deflection, v at different depths of cut with two modes (1250 rev/min, cutting speed = 2.228 m/s and feed rate is 0.3 mm/rev)



(a) $h_c = 0.25$ mm



(b) $h_c = 1.50$ mm

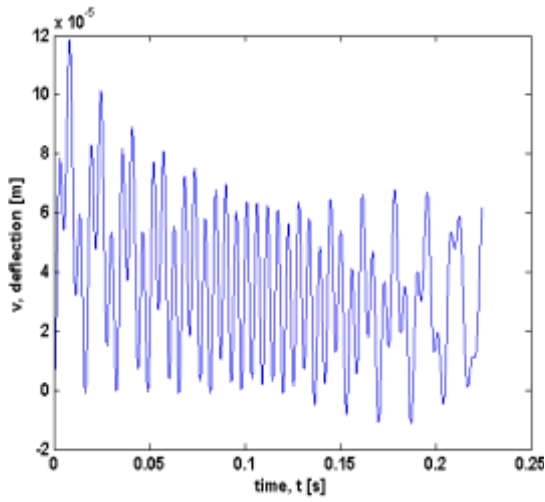


(c) $h_c = 3.00$ mm

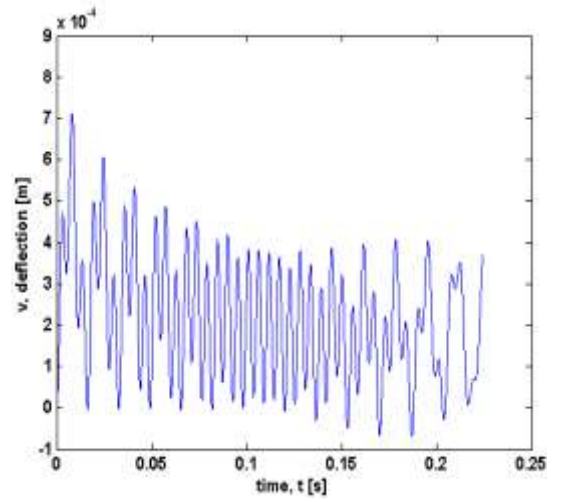
Figure 5.29: Dynamic response of deflection, w at different depths of cut with two modes (1250 rev/min, cutting speed = 2.228 m/s and feed rate is 0.3 mm/rev)

Furthermore, the dynamic response, v obtained using three modes and four modes have a similar pattern as depicted in Figure 5.30 to Figure 5.33. All of them generate the same pattern but slightly different in amplitude. For

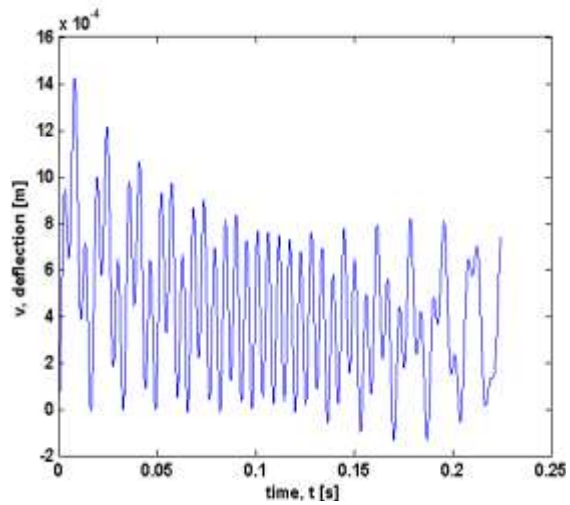
example, Figure 5.30 (c) appeared to have higher amplitude than Figure 5.30 (a) and 5.30 (b).



(a) $h_c = 0.25$ mm

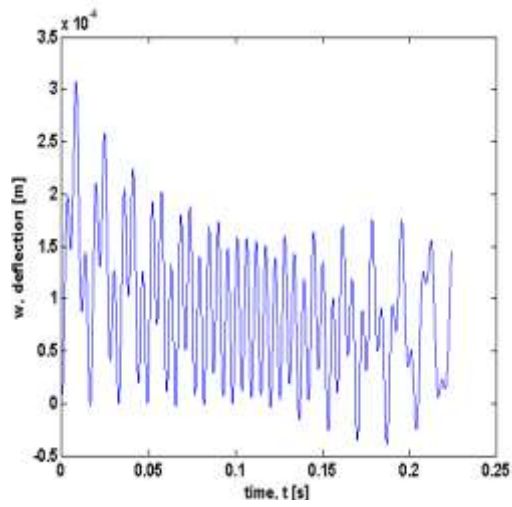


(b) $h_c = 1.50$ mm

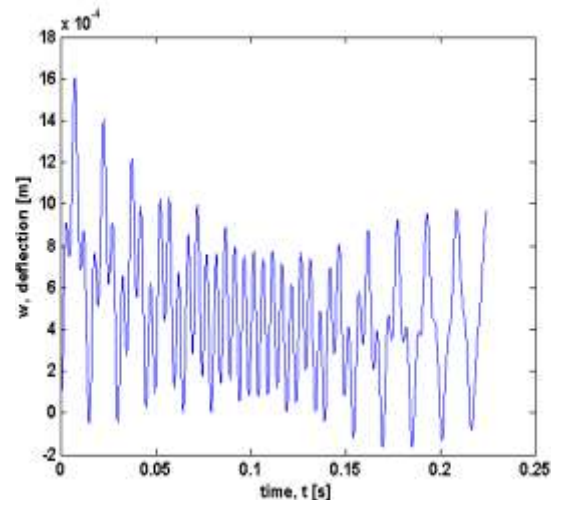


(c) $h_c = 3.00$ mm

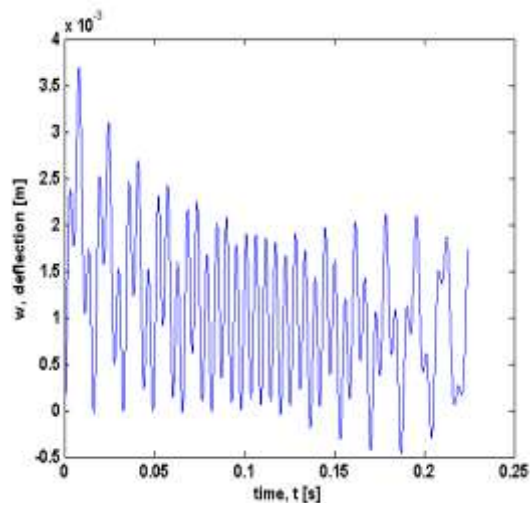
Figure 5.30: Dynamic response of deflection, v at different depths of cut with three modes (1250 rev/min, cutting speed = 2.228 m/s and feed rate is 0.3 mm/rev)



(a) $h_c = 0.25$ mm

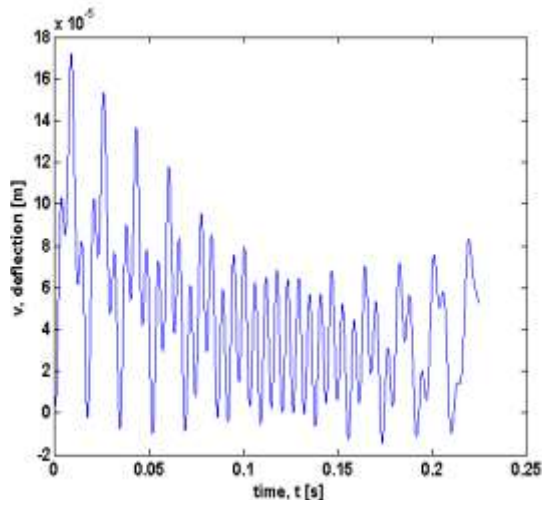


(b) $h_c = 1.50$ mm

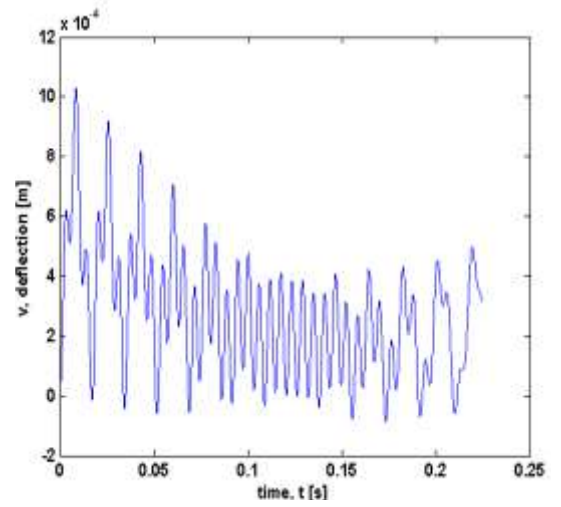


(c) $h_c = 3.00$ mm

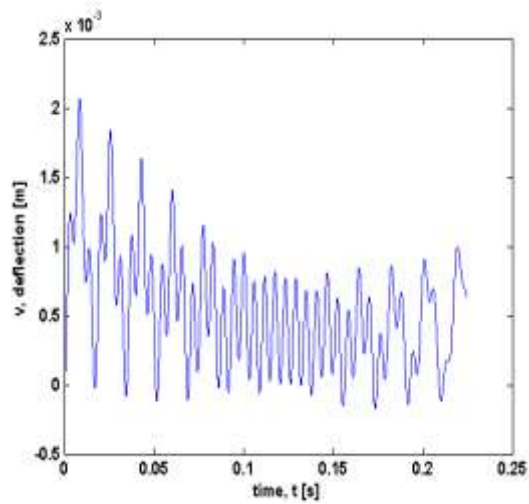
Figure 5.31: Dynamic response of deflection, w at different depths of cut with three modes (1250 rev/min, cutting speed = 2.228 m/s and feed rate is 0.3 mm/rev)



(a) $h_c = 0.25$ mm

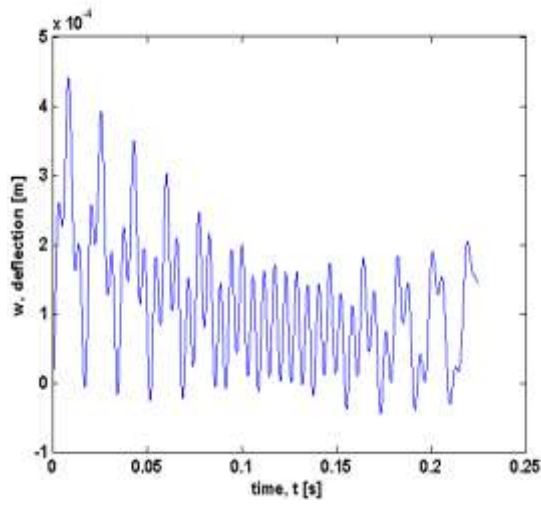


(b) $h_c = 1.50$ mm

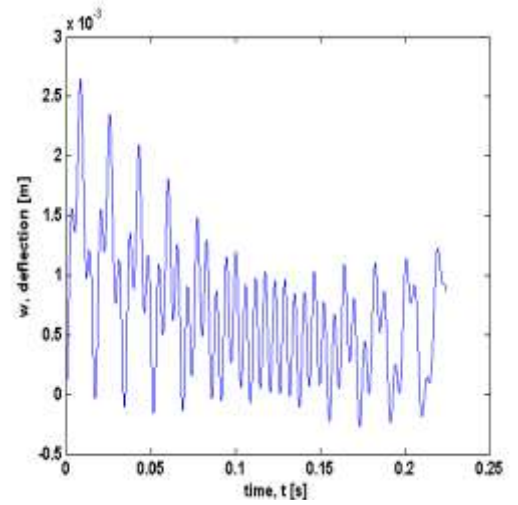


(c) $h_c = 3.00$ mm

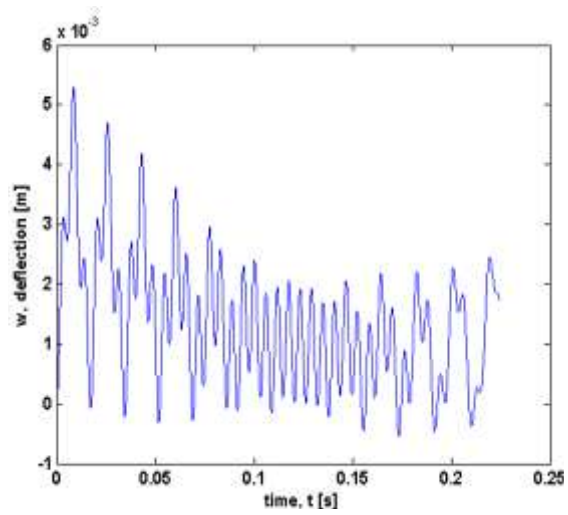
Figure 5.32: Dynamic response of deflection, v at different depths of cut with four modes (1250 rev/min, cutting speed = 2.228 m/s and feed rate is 0.3 mm/rev)



(a) $h_c = 0.25$ mm



(b) $h_c = 1.50$ mm



(c) $h_c = 3.00$ mm

Figure 5.33: Dynamic response of deflection, w at different depths of cut with four modes (1250 rev/min, cutting speed = 2.228 m/s and feed rate is 0.3 mm/rev)

5.3.4 Effect of Cutting Speed

The next cutting parameter investigated is cutting speed. Figure 5.34 shows the dynamic response, v at two different cutting speeds for one mode. The other cutting parameters are set to be constant which are the depth of cut is 3.00 mm, the rotational speed is 1250 rev/min and the feed rate is 0.3 mm/rev. By comparing Figure 5.34 (a) and 5.34 (b), it can be seen that higher-frequency oscillation has bigger amplitude at higher cutting speed.

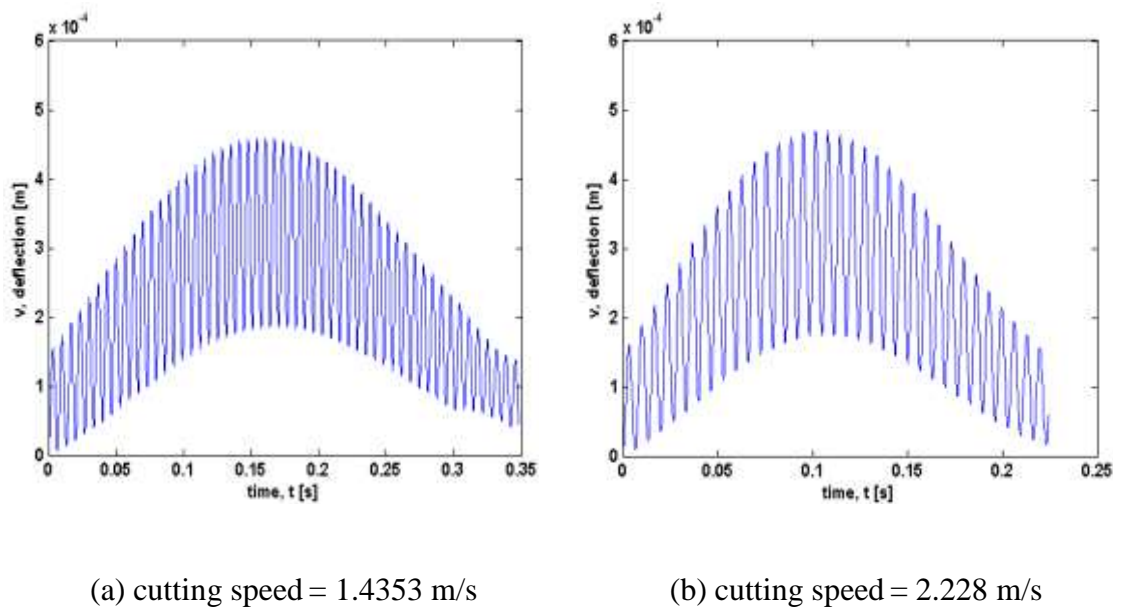
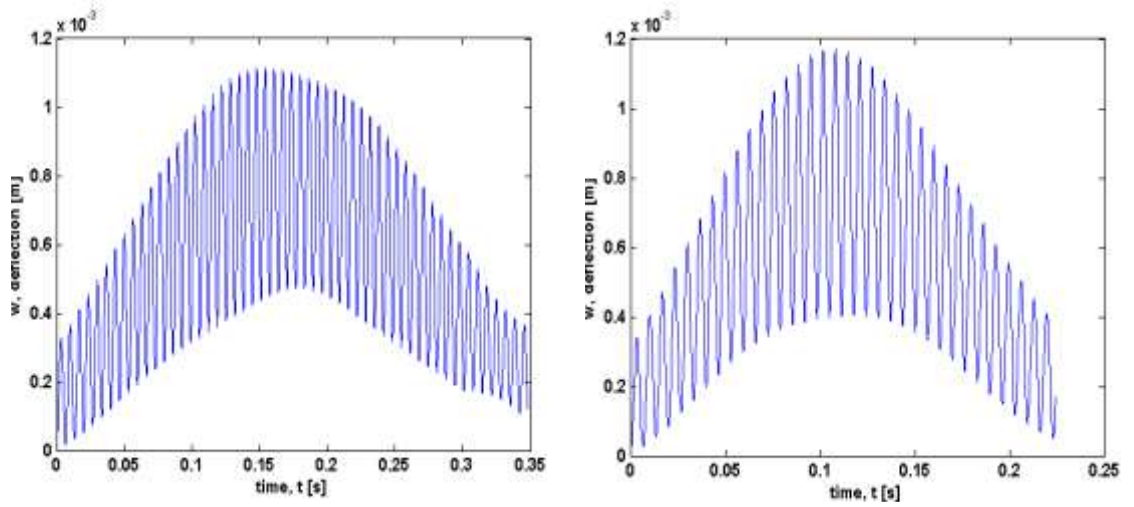


Figure 5.34: Dynamic response of deflection, v at different cutting speed with one mode (depth of cut = 3.00 mm, rotational speed = 1250 rev/min and feed rate is 0.3 mm/rev)

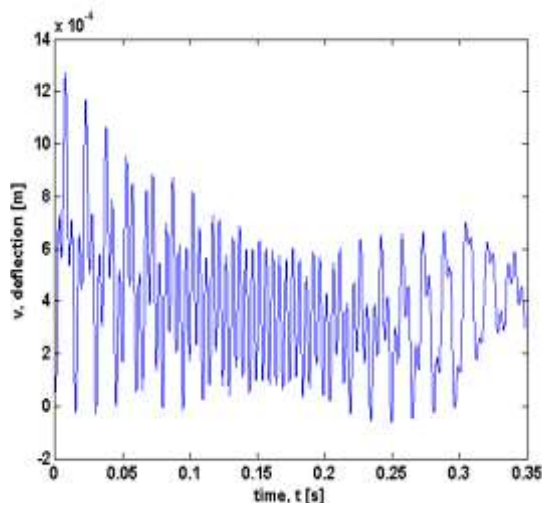


(a) cutting speed = 1.4353 m/s

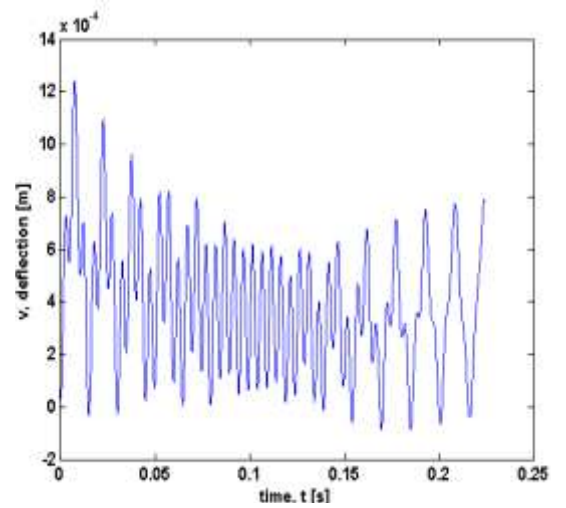
(b) cutting speed = 2.228 m/s

Figure 5.35: Dynamic response of deflection, w at different cutting speed with one mode (depth of cut = 3.00 mm, rotational speed = 1250 rev/min and feed rate is 0.3 mm/rev)

The same cutting conditions are simulated with two modes and the results are shown in Figure 5.36 and 5.37. The mode shapes have changed when a higher number of modes are used. Similar pattern and amplitude of vibration were produced for different cutting speeds. Higher amplitude vibration becomes more pronounced with more modes. The deflection is skewed to the weaker support, which is the tailstock. The beating phenomenon is even greater at a higher cutting speed which is 1.4353 m/s. The results obtained with three and four modes are similar with two modes as illustrated in Figure 5.38, 5.39, 5.40 and 5.41.

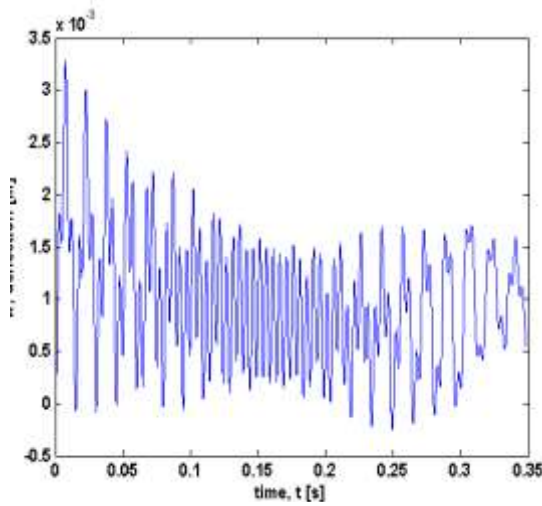


(a) cutting speed = 1.4353 m/s

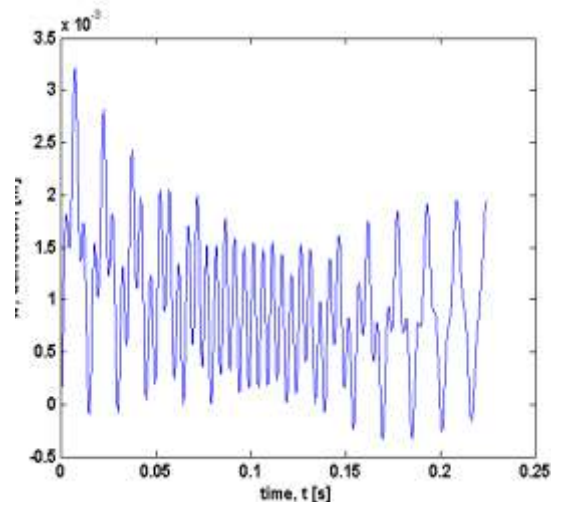


(b) cutting speed = 2.228 m/s

Figure 5.36: Dynamic response of deflection, v at different cutting speed with two modes (depth of cut = 3.00 mm, rotational speed = 1250 rev/min and feed rate is 0.3 mm/rev)

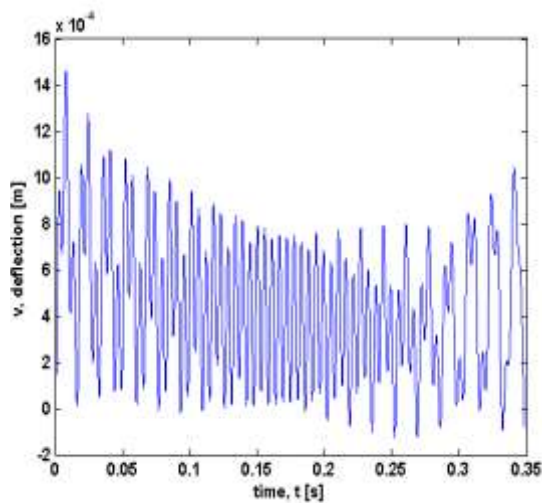


(a) cutting speed = 1.4353 m/s

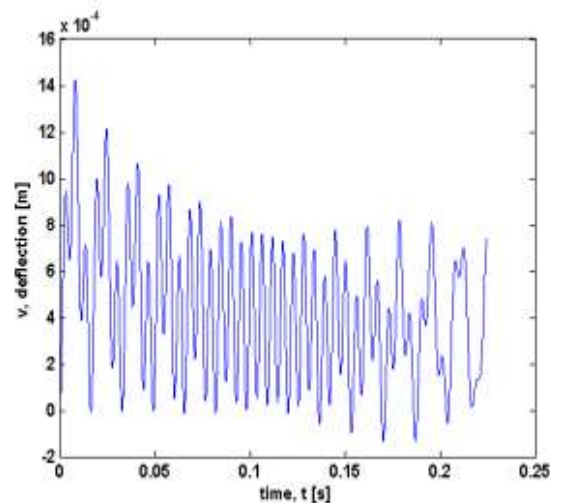


(b) cutting speed = 2.228 m/s

Figure 5.37: Dynamic response of deflection, w at different cutting speed with two modes (depth of cut = 3.00 mm, rotational speed = 1250 rev/min and feed rate is 0.3 mm/rev)

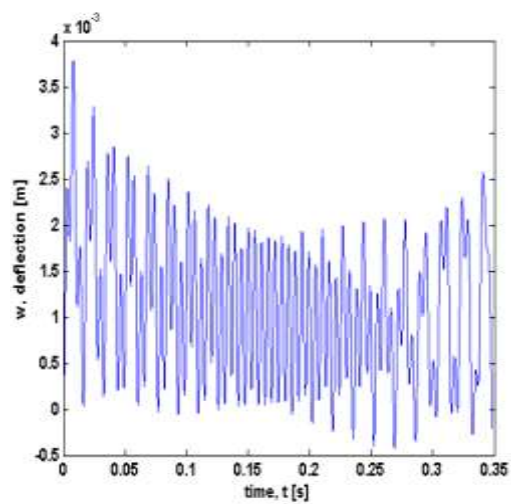


(a) cutting speed = 1.4353 m/s

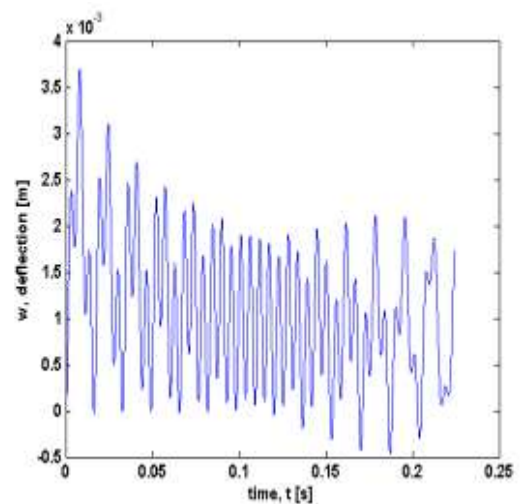


(b) cutting speed = 2.228 m/s

Figure 5.38: Dynamic response of deflection, v at different cutting speed with three modes (depth of cut = 3.00 mm and rotational speed = 1250 rev/min and feed rate is 0.3 mm/rev)

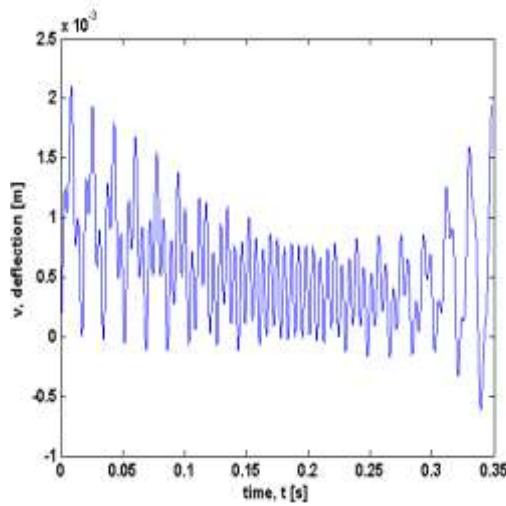


(a) cutting speed = 1.4353 m/s

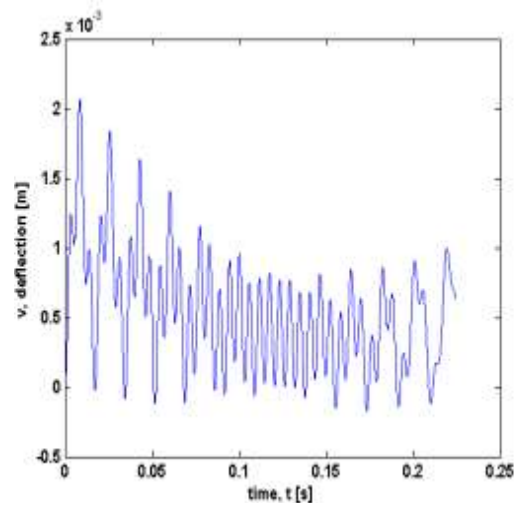


(b) cutting speed = 2.228 m/s

Figure 5.39: Dynamic response of deflection, w at different cutting speed with three modes (depth of cut = 3.00 mm, rotational speed = 1250 rev/min and feed rate is 0.3 mm/rev)

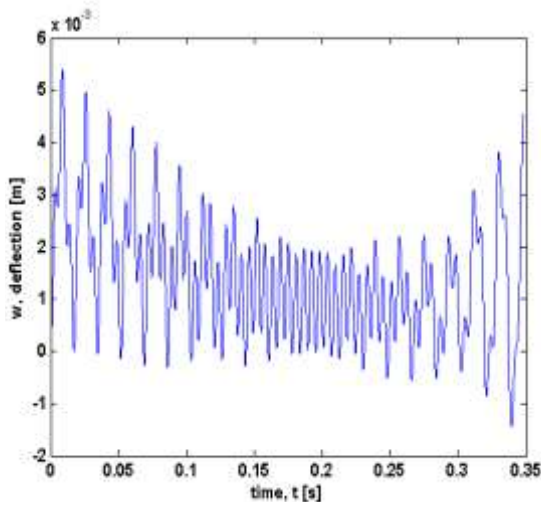


(a) cutting speed = 1.4353 m/s

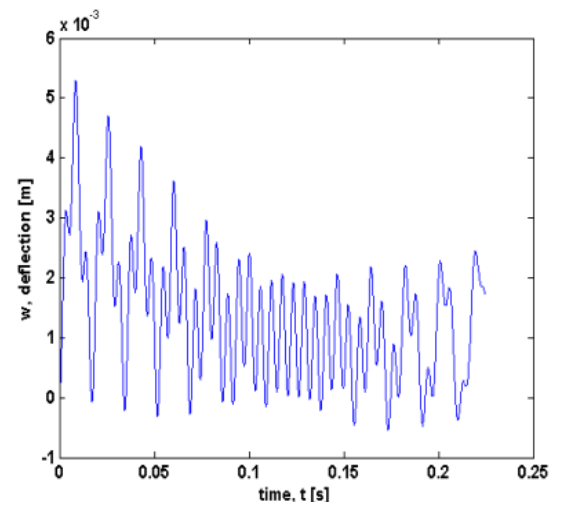


(b) cutting speed = 2.228 m/s

Figure 5.40: Dynamic response of deflection, v at different cutting speed with four modes (depth of cut = 3.00 mm, rotational speed = 1250 rev/min and feed rate is 0.3 mm/rev)



(a) cutting speed = 1.4353 m/s



(b) cutting speed = 2.228 m/s

Figure 5.41: Dynamic response of deflection, w at different cutting speed with four modes (depth of cut = 3.00 mm, rotational speed = 1250 rev/min and feed rate is 0.3 mm/rev)

5.3.4 Effect of Rotational Speed

The final cutting parameter examined is rotational speed. The results of the dynamic response, v at different rotational speeds are illustrated in Figure 5.42. In the simulation works, the other cutting parameters are set to be constant which are the depth of cut is 3.00 mm, the cutting speed is 2.228 m/s and the feed rate is 0.3 mm/rev. It is observed that there is not much amplitude difference between the first, second and third modes. A similar pattern is also produced for all rotational speed. The rotational speed does not seem to have a big effect on the dynamic response especially on the amplitude of vibration.

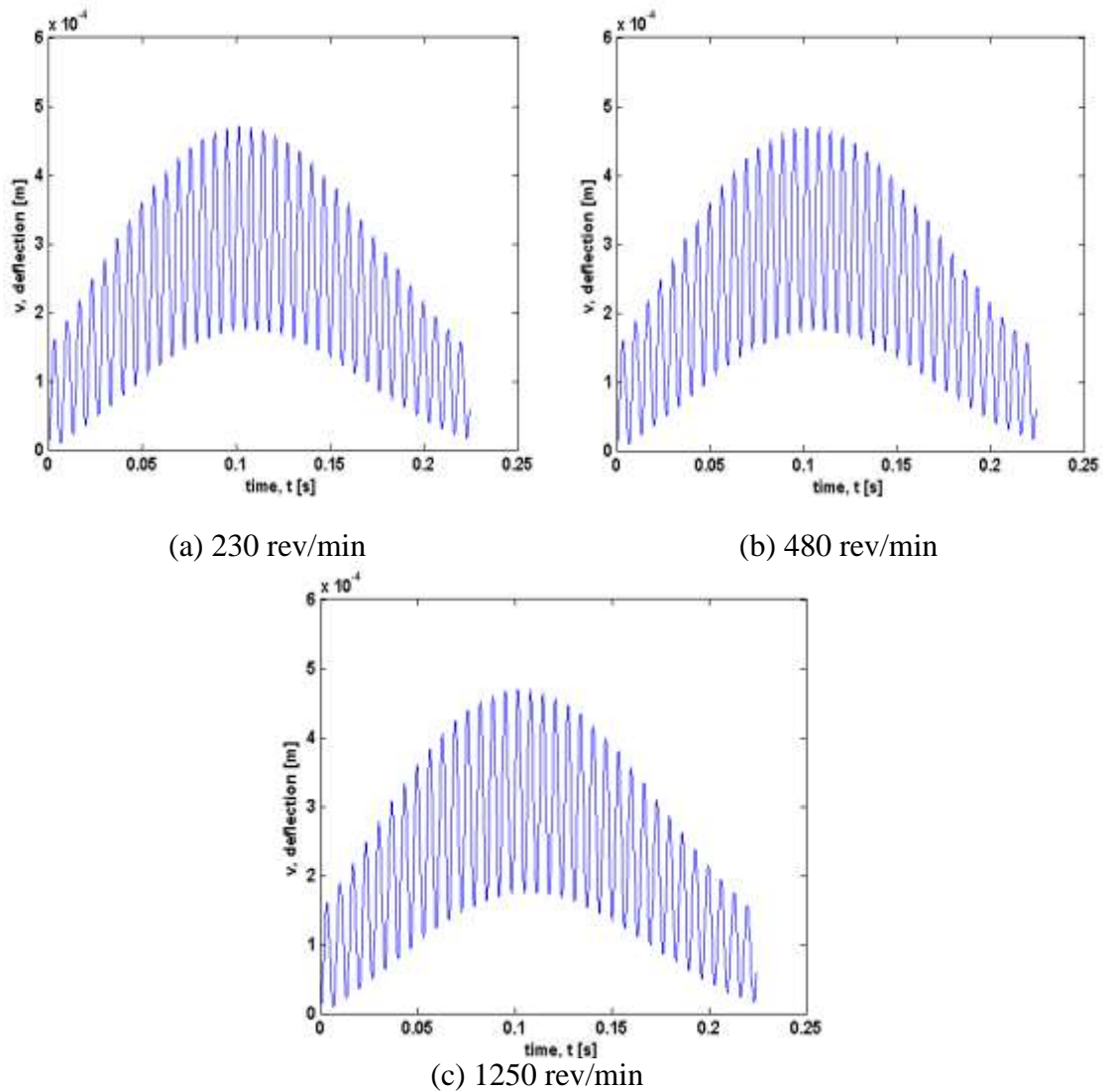
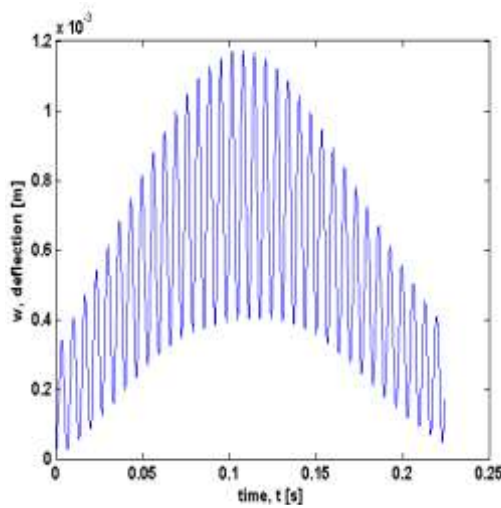
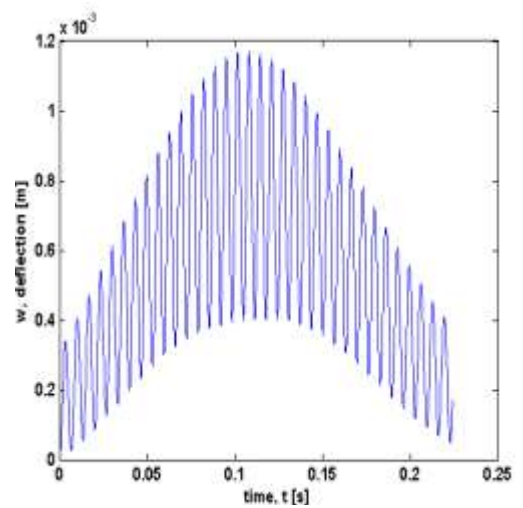


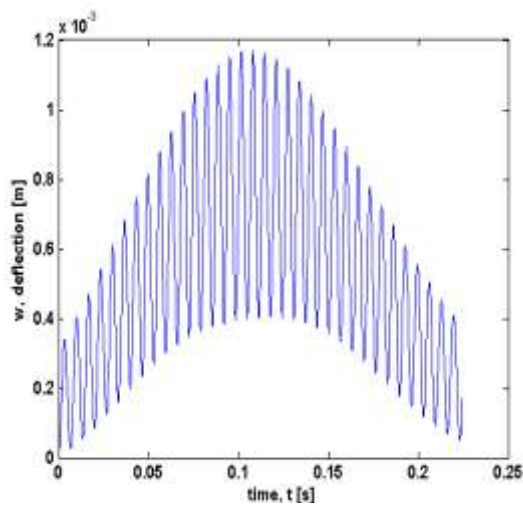
Figure 5.42: Dynamic response of deflection, v at different rotational speed with one mode (depth of cut = 3.00 mm, cutting speed = 2.228 m/s and feed rate = 0.3 mm/rev)



(a) 230 rev/min



(b) 480 rev/min

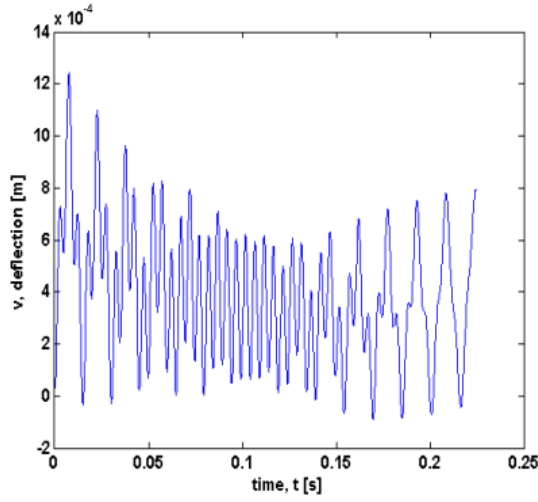


(c) 1250 rev/min

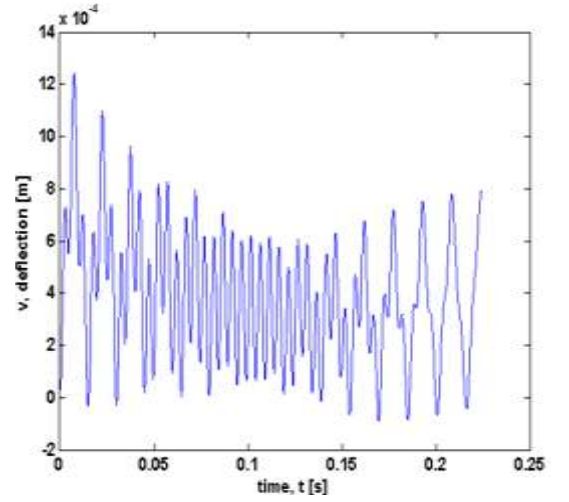
Figure 5.43: Dynamic response of deflection, w at different rotational speed with one mode (depth of cut = 3.00 mm, cutting speed = 2.228 m/s and feed rate = 0.3 mm/rev)

A different deflection curve has been produced when a higher number of modes are used. Figures 5.44 to 5.49 illustrate the deflection, v at depth of cut, 3.00 mm with two, three and four modes and these graphs demonstrate the effect of including more modes. There are some differences in amplitude of vibration

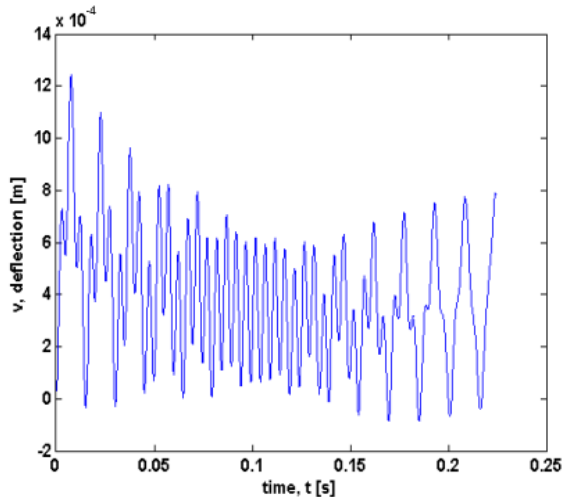
particularly in mode three and four. When three modes are used as shown in Figure 5.46, a higher number of modes used is seen to excite slightly greater amplitude of vibration. Therefore, increasing the number of modes moderately promotes the occurrence of chatter. The deflection, w obtained with three and four modes are shown in Figure 5.49 and 5.51 for comparison. Adding more modes does not change w as much as v .



(a) 230 rev/min

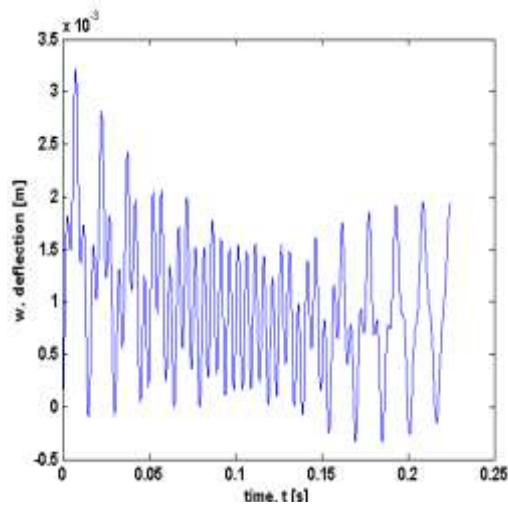


(b) 480 rev/min

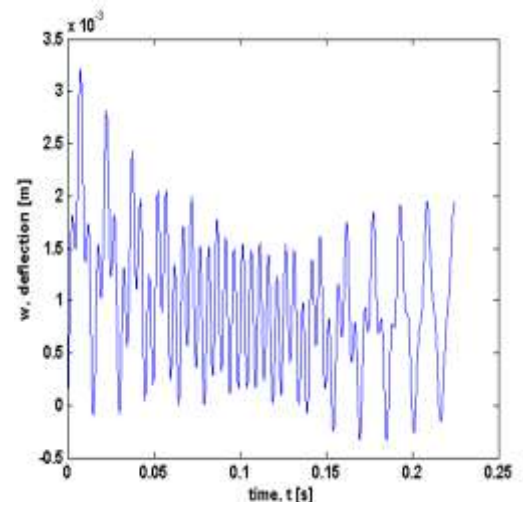


(c) 1250 rev/min

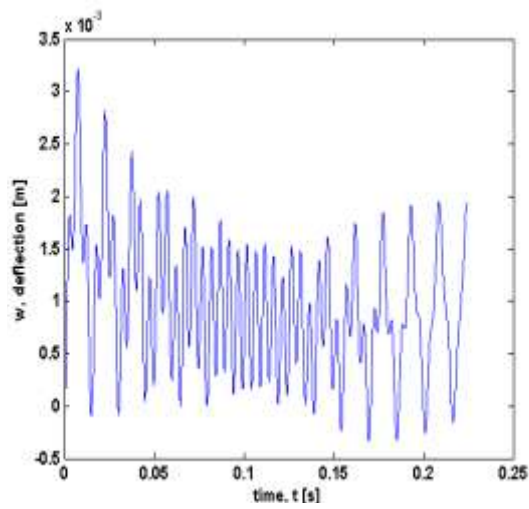
Figure 5.44: Dynamic response of deflection, v at different rotational speed with two modes (depth of cut = 3.00 mm, cutting speed = 2.228 m/s and feed rate = 0.3 mm/rev)



(a) 230 rev/min

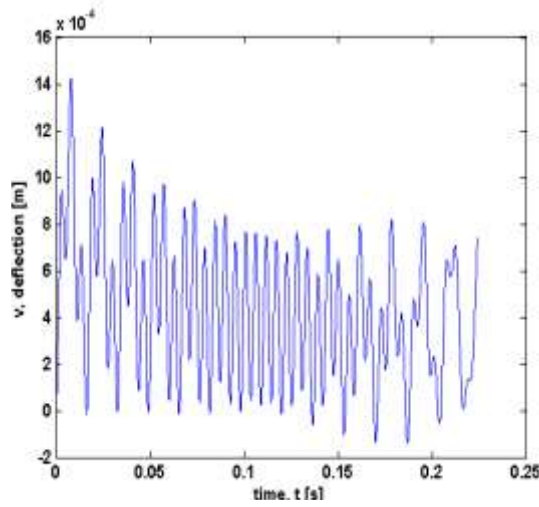


(b) 480 rev/min

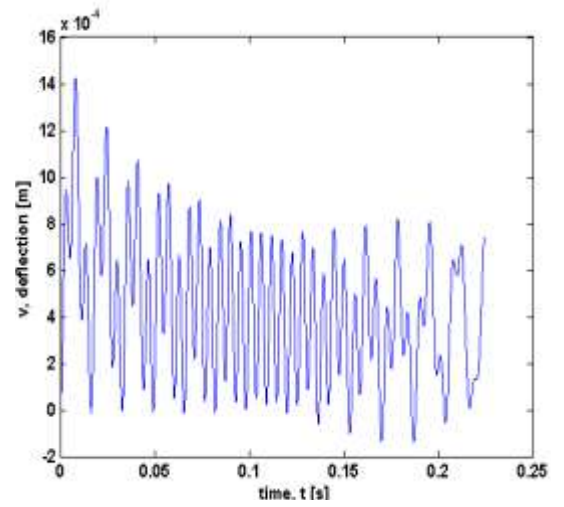


(c) 1250 rev/min

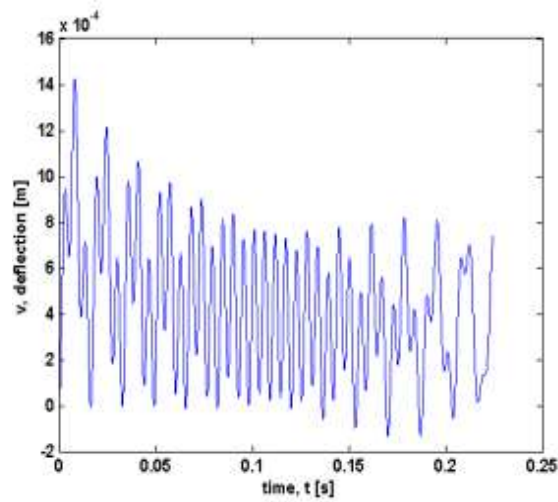
Figure 5.45: Dynamic response of deflection, w at different rotational speed with two modes (depth of cut = 3.00 mm, cutting speed = 2.228 m/s and feed rate = 0.3 mm/rev)



(a) 230 rev/min

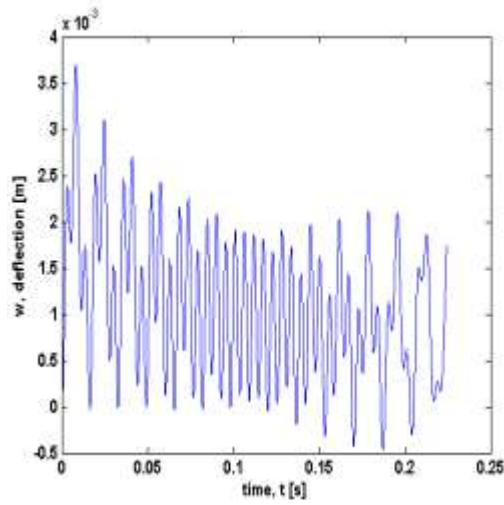


(b) 480 rev/min

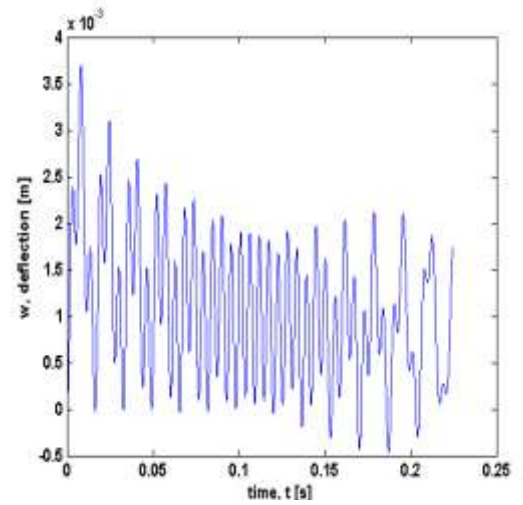


(c) 1250 rev/min

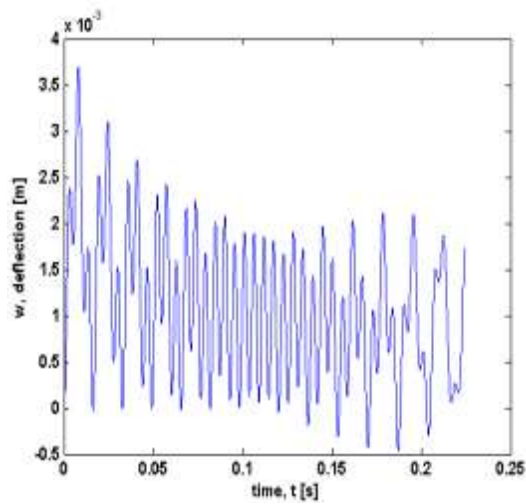
Figure 5.46: Dynamic response of deflection, v at different rotational speed with three modes (depth of cut = 3.00 mm, cutting speed = 2.228 m/s and feed rate = 0.3 mm/rev)



(a) 230 rev/min

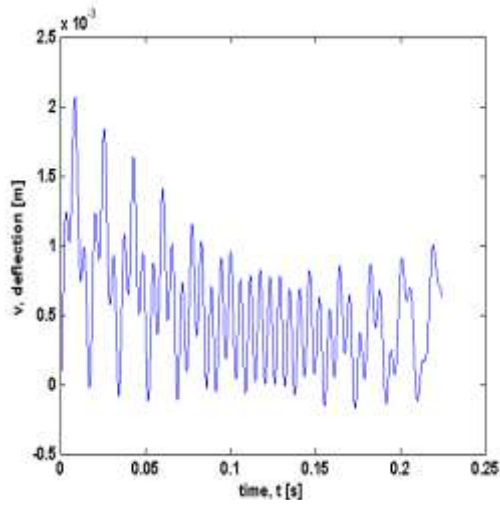


(b) 480 rev/min

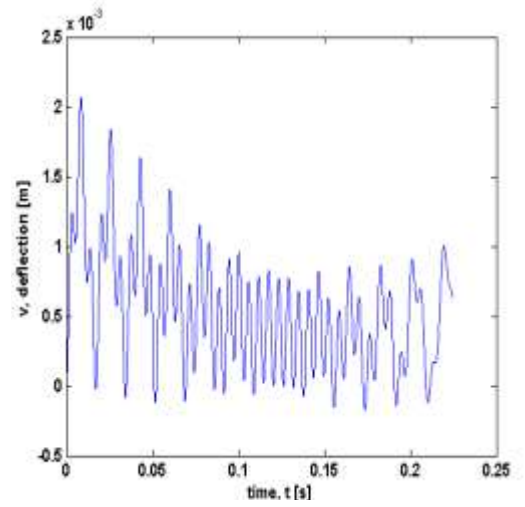


(c) 1250 rev/min

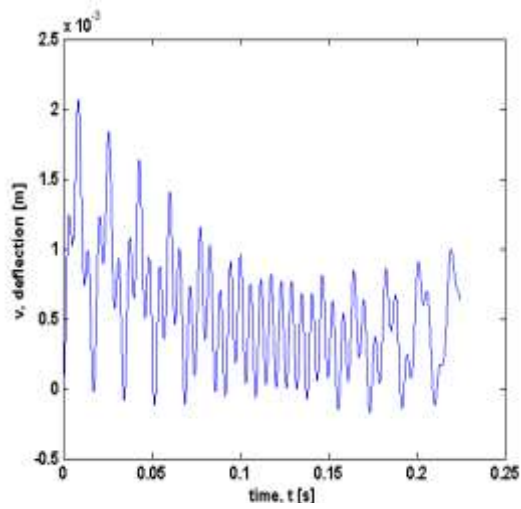
Figure 5.47: Dynamic response of deflection, w at different rotational speed with three modes (depth of cut = 3.00 mm, cutting speed = 2.228 m/s and feed rate = 0.3 mm/rev)



(a) 230 rev/min

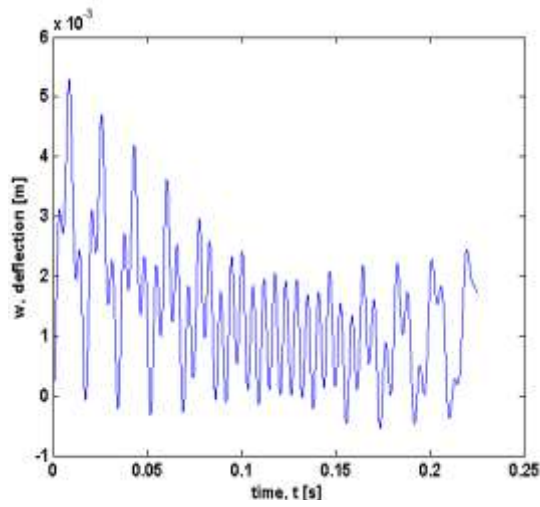


(b) 480 rev/min

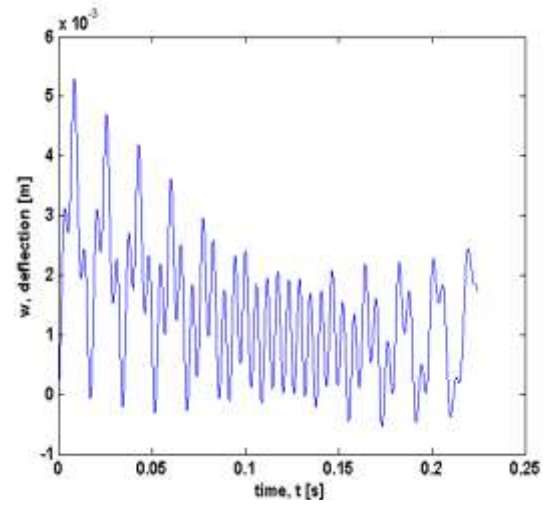


(c) 1250 rev/min

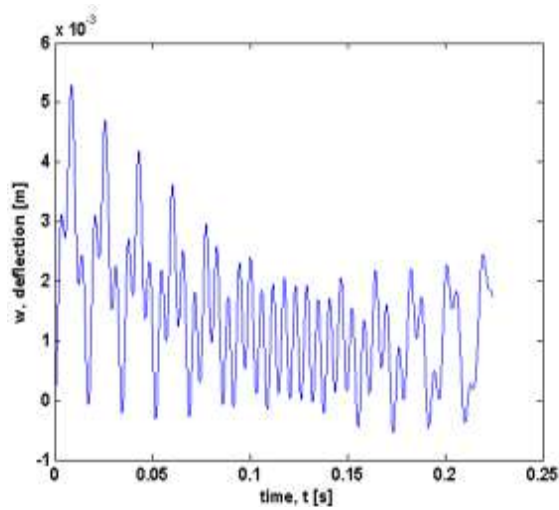
Figure 5.48: Dynamic response of deflection, v at different rotational speed with four modes (depth of cut = 3.00 mm, cutting speed = 2.228 m/s and feed rate = 0.3 mm/rev)



(a) 230 rev/min



(b) 480 rev/min



(c) 1250 rev/min

Figure 5.49: Dynamic response of deflection, w at different rotational speed with four modes (depth of cut = 3.00 mm, cutting speed = 2.228 m/s and feed rate = 0.3 mm/rev)

5.2.3 Clamped Pinned (Composite work piece)

A simulation work has also been done for clamped pinned boundary condition on composite work piece. It is done as a preliminary study to investigate several cutting parameters such as cutting, depth of cut, rotational speed and the feed rate on turned composite. The geometric and material properties of the work piece are length, $l = 0.5$ m, radius $r = 19$ mm, Young's Modulus $E = 36.75 \times 10^9$ Pa, and density, $\rho = 882$ kg/m³ while the cutting parameters used are 0.2228 m/s for cutting speed, 0.25 mm for the depth of cut, 1250 rev/min for rotational speed and 0.3 mm/rev for the feed rate. The numerical results of the dynamic response of deflection, v and w in both y and z direction under these cutting parameters are shown in Figures 5.50 and 5.51 below.

It can be seen that a similar deflection curve pattern is formed. At smaller depth of cut (0.25 mm), low frequency oscillations begin to appear thus indication of chatter presence. Similar to the metal work piece, the simulated deflection is not symmetrical due to the clamped pinned boundary condition. If a different depth of cut is being used for example a bigger depth of cut (3.00 mm), the result obtained will be the same as with metal work piece simulated earlier where higher frequency oscillations will be generated on top of the static deflection. Notice that the amplitude of the dynamic response, v and w for both of the depth of cuts (0.25mm and 3.0mm) is slightly bigger than metal work piece. This is true because of the nature of composite material itself is inhomogeneous.

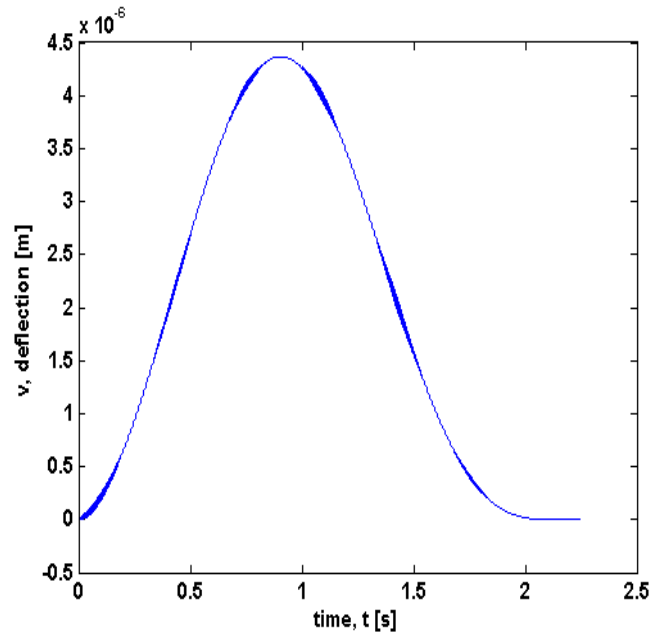


Figure 5.50: Dynamic response of deflection, v at one mode (depth of cut = 0.25 mm, cutting speed = 0.2228 m/s, rotational speed = 1250 rev/min and feed rate = 0.3 mm/rev)

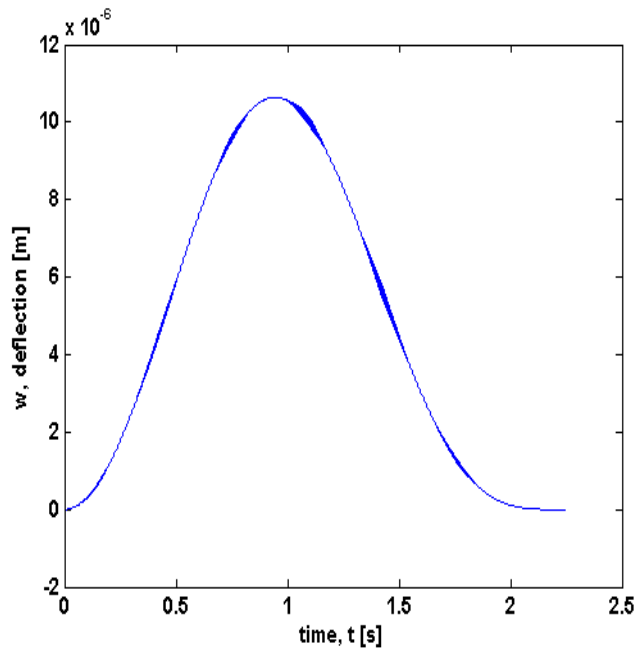


Figure 5.51: Dynamic response of deflection, w at one mode (depth of cut = 0.25 mm, cutting speed = 0.2228 m/s, rotational speed = 1250 rev/min and feed rate = 0.3 mm/rev)

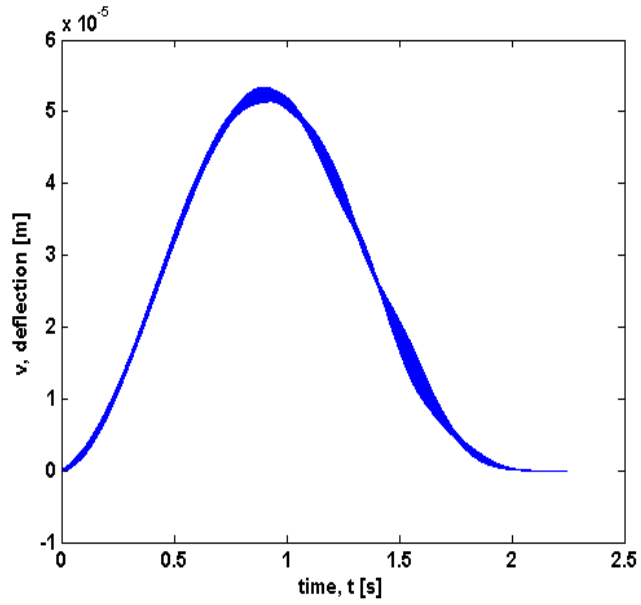


Figure 5.52: Dynamic response of deflection, v at one mode (depth of cut = 3.0 mm, cutting speed = 0.2228 m/s, rotational speed = 1250 rev/min and feed rate = 0.3 mm/rev)

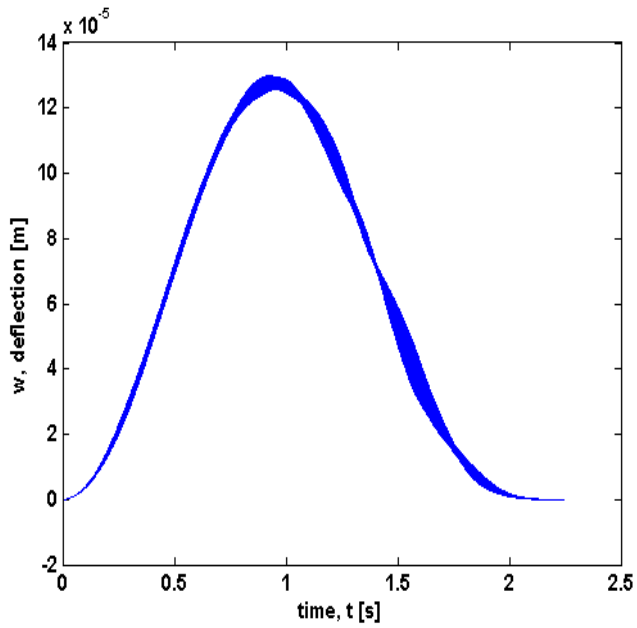


Figure 5.53: Dynamic response of deflection, w at one mode (depth of cut = 3.0 mm, cutting speed = 0.2228 m/s, rotational speed = 1250 rev/min and feed rate = 0.3 mm/rev)

5.3 Vibration Test During Turning Operation

As mentioned earlier in Chapter 4, due to the limitation of the equipment in performing vibration testing during turning operation at the University of Liverpool, the results from the other collaborator group from Dalian University of Technology (DUT) in China are employed to validate the dynamic model established.

The cutting parameters used during the turning operation are shown in Table 5.1. The rotating speed, feed rate and depth of cut are carefully chosen in different values consistent with the previous numerical simulations under different cutting conditions. The geometric and material properties of the work-piece are length, $l = 0.5$ m, Young's Modulus, $E = 2.07 \times 10^{11}$ Pa, and material density, $\rho = 7850$ kg/m³.

Table 5.1: Cutting parameters and work piece characteristics used during turning operation (Han *et al*, 2012)

Experiment	Rotational speed (rev/min)	Depth of cut, a_p (mm)	Feed rate, f (mm/rev)	Diameter, D (mm)
1	1250	1.5	0.3	36.5
2	1000	3.0	0.2	35.0

Figure 5.54 shows the photograph of the machined cylindrical metal work piece for experiment 1. The dynamic responses of the shaft (cylindrical metal work piece) in y and z directions are measured at the position being machined during the turning process as depicted in Figure 5.55.



Figure 5.54: The being machined work piece of experiment 1 (Han *et al*, 2012)

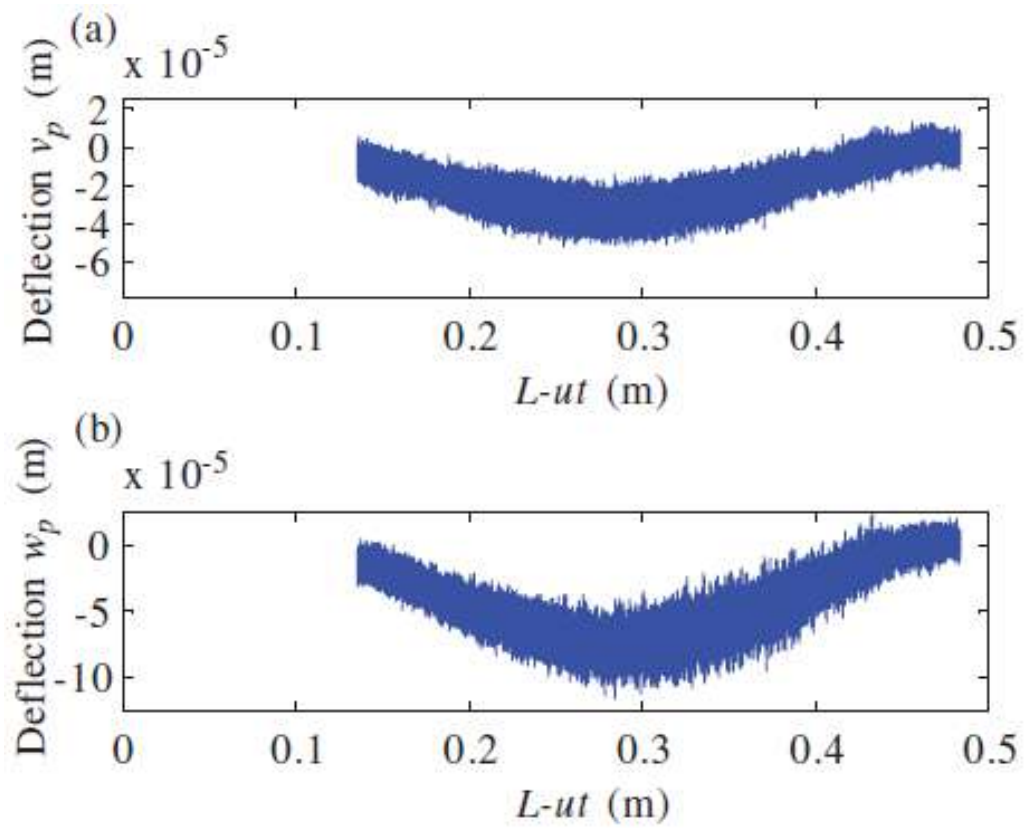


Figure 5.55: Deflections in time domain of experiment 1 (Han *et al*, 2012)

A higher depth of cut and a smaller feed rate are used in experiment 2 to observe the effect of varying the cutting parameters. The machined cylindrical metal work piece is shown in Figure 5.56, in which the phenomena of chatter can be clearly seen in the middle of the cylindrical metal work piece (marked as a dotted white line). Chatter is large amplitude irregular vibration, happening during machining shown in the large dynamic response. Moreover, higher oscillation appears in the dynamic response of the time domain as illustrated in Figure 5.57.



Figure 5.56: The being machined work piece of experiment 2 shown chatter occurrence (Han *et al*, 2012).

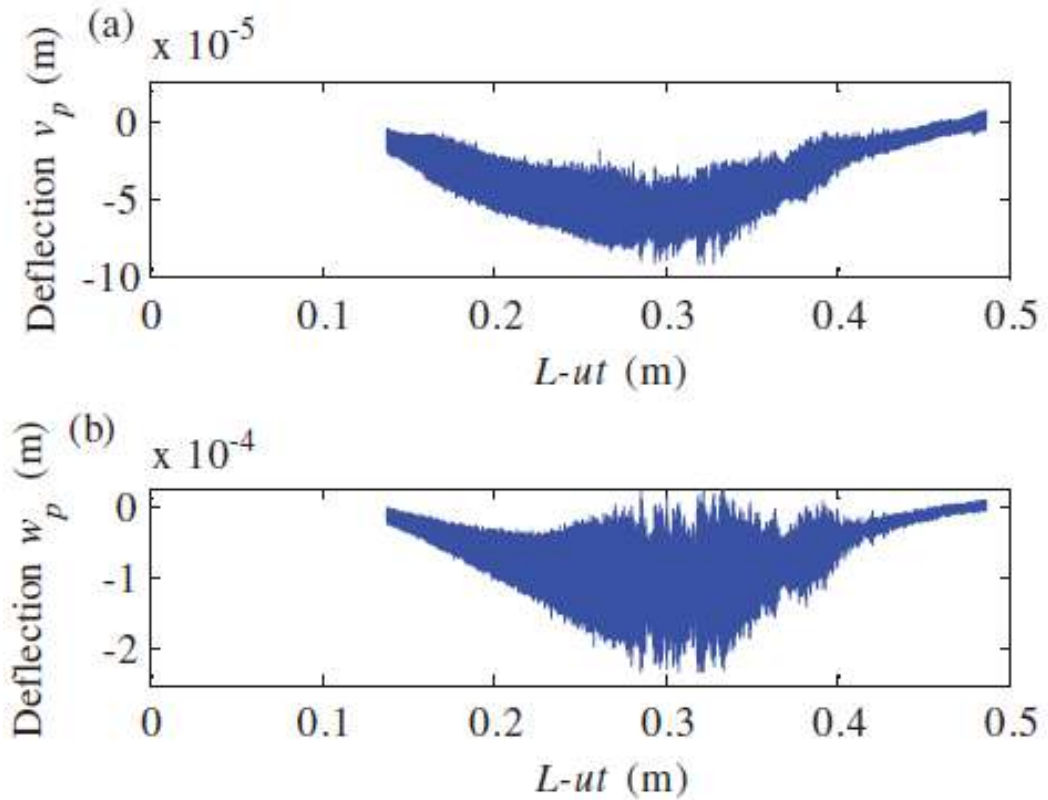


Figure 5.57: Deflections in time domain of experiment 2 (Han *et al*, 2012).

In comparison of the dynamic responses, v and w of the work piece, it can be seen that the deformation patterns are fairly similar between the experiment and the developed model. However, the measured deflections are greater than the developed model. It is believed that the dynamic model developed is stiffer. Examining all the numerical results, it may be concluded that the predicted and measured patterns of time histories of work piece vibration agree fairly well but the magnitudes are not so close to each other, in particular when the large vibration (chatter) is excited during experiments. Further improvement to the model is likely to come from a more accurate representation of the chuck and tail stock boundaries.

5.6 Chapter Summary

This chapter presents numerical simulation work of vibration of a metal work piece being turned. The work piece is modeled as a rotating Rayleigh beam and the cutting forces as three directional moving loads with regenerative chatter mechanism. The moving cutting forces with regenerative chatter introduce time delay in the dynamic model. The effects of depth of cut, cutting speed and rotational speed of the cutter on vibration and chatter occurrence are examined. The effect of using several numbers of modes is also investigated.

The results for all three cutting parameters simulated when an elastic boundary is considered generate a slightly different oscillation compared with clamped pinned boundary assumed earlier. The oscillations are much higher when elastic boundary is considered. The results are in line with the actual work piece where the chuck and tailstock also deform. The amplitude of vibration as well increases when the number of modes used in the simulation increases. Similar to clamped pinned boundary, four modes are sufficient and hence used during the numerical simulation. It is necessary to include higher modes as it will cover high frequency oscillation. The more modes considered, the more accurate the results; but at certain points it is not necessary to include more than four modes.

For both clamp pinned and elastic boundary conditions, an increase in depth of cut will increase the amplitudes and frequency of oscillation. The response at 3.00 mm depth of cut is significant as the magnitude of the oscillation becomes bigger. Most of the high amplitude of oscillation increases with the increase of number of modes. Moreover, higher cutting speed will generate a higher frequency oscillation hence bigger amplitude is obtained. On the other hand, for the effect of different rotational speed, it can be concluded that there is not much amplitude difference between the first, second and third modes. There are some differences in amplitude of vibration particularly in modes three and four. Therefore, increasing the number of modes moderately promotes the occurrence of greater response in simulation.

From the experiment done by the collaborating group in China, it can be seen that the deformation patterns are fairly similar between both the experiment and the developed model. However, the measured deflections are smaller than the developed dynamic model. It is believed that the theoretical model with clamped pinned boundary is much stiffer since the chuck is represented by a clamped boundary and the tail stock support is represented by a pinned boundary. In contrast, from the results gained when an elastic boundary is considered, the simulated deflection magnitude is bigger than the measured deflection during experiment. It can be concluded that the predicted and measured patterns of time histories of work piece vibration agree fairly well when an elastic boundary conditions are considered in the simulation works of the developed dynamic model.

In conclusion a dynamic model for a rotating Rayleigh beam subjected to a three directional moving cutting forces with regenerative chatter effect is successfully established.

Chapter 6

Analysis and Discussion

6.1 Parametric Studies

6.1.1 Clamped Pinned (Metal work piece)

The first simulation work done is to monitor the occurrence of chatter (up to five modes) and to determine the appropriate number of modes used in the simulation. Initially the boundary condition used was a clamp-pinned boundary as the work piece is held in chuck at one end and the other end was pinned down by a tailstock. This is also the boundary condition considered in papers on vibration in turning operation by other researchers. From the results shown earlier (Figure 5.1 (d) and Figure 5.2 (d)), when higher modes are used in the simulation, higher oscillation (chatter) starts to appear on top of the deflection (dynamic response) curve in both v (y) and w (z) directions. It is necessary to simulate higher modes as they will cover high frequency oscillation and the dynamic responses settle at four modes.

It is also observed that four modes are satisfactory to be used in the parametric studies since high frequency oscillation is present on the top of the deflection curve showing chatter occurrence. Furthermore, it also demonstrates

the effectiveness of the dynamic model developed in detecting chatter. It is necessary to include higher modes in the simulation as the more modes considered, the more accurate the results. However, at certain points more than four modes are not necessary as one of the aims of the numerical simulation is to define the appropriate number of modes and four modes are defined to be a starting point where the mode shape start to converge indicative of a stable system. Furthermore, more than four modes will produce similar results but if more than four modes are used, it will have more computational workloads. In addition, the deflection curve produced also shows the dynamic model developed works successfully at the initial stage since it truly represents the behaviour of the work piece during turning operation in which the deflection is generated as predicted.

The developed dynamic model is also simulated to investigate the effects of three main cutting parameters; the depth of cut, the cutting speed and the rotational speed on the chatter occurrence.

6.1.1.1 Effect of Depth of Cut

From the results illustrated earlier (Figure 5.3), it is noticed that the increase of depth of cut used during simulation results in the increase of amplitudes and frequency of oscillation. This condition is in fact reflecting the actual turning process where an increase of depth of cut will increase the chance of the occurrence of chatter on turned work piece. The 3.00 mm depth of cut used shows two features, a nearly static deflection and high frequency oscillations start to appear at the same time. The presence of chatter appears at the beginning of pinned support. In addition, the deflection curves produced are not symmetrical due to the clamped pinned boundary assumption earlier. The clamped support is much stiffer than the other pinned support. However, when the same parameters are used with a slightly higher mode; two, higher vibration magnitude appears. This is because higher modes will cover higher frequency oscillation during numerical simulation. As the number of modes increases, the

higher oscillation develops. A similar pattern is obtained for the dynamic response, v using three modes and four modes but with slightly higher vibration magnitude. The use of higher modes results in higher amplitude oscillation and a beating phenomenon also starts to develop. The beating phenomenon occurs when the forcing frequency is close to the natural frequency of the system. This phenomenon is often observed in machinery, structures and electric power houses.

6.1.1.2 Effect of Cutting Speed

The next cutting parameter simulated in the dynamic model is the cutting speed in which the effect of two different cutting speeds is examined with one mode. Only two values of cutting speeds are simulated because it took more than 24 hours to run for each mode shape before the analysis stops for the smallest cutting speed (0.0062 m/s). From the results shown (Figure 5.5 (b)), high frequency oscillation is observed on top of the nearly static deflection due to the use of high cutting speed. Since the depth of cut used is quite high (3.00 mm), it promotes frequency oscillation to increase for higher cutting speed used. If the two graphs from Figure 5.5 (a) and 5.5 (b) are compared, it can be seen that higher-frequency oscillation has bigger amplitude at a higher cutting speed. A lower cutting speed would suppress chatter as mentioned by Tobias and Fishwick (1958) and this is true only if smaller values of depth of cut are used.

When the same cutting conditions are simulated with two modes (Figure 5.6), higher amplitude vibration becomes more prominent with more modes. By simulating higher modes, higher frequency oscillation is found. Both of the dynamic response (v and w) should be in the middle of the work piece, but since the work piece has its own inertia, the deflection is skewed to the weaker support, which is the tailstock. The beating phenomenon is even greater at a higher cutting speed of 1.4353 m/s. It occurs when the excitation frequency is close to the natural frequency of the system and the cutting speed influences the excitation frequency. The results obtained with three and four modes are similar

to two modes since from two modes, it already shows convergence of displacement in both directions, y and z .

6.1.1.3 Effect of Rotational Speed

The rotational speed does not seem to have a big impact on the dynamic response of the shaft. At lower rotational speed, the high oscillation only appears at the beginning of the mode shape (Figure 5.20). Small difference of amplitude is noticed between the first, second and third mode but slight dissimilarity is observed in oscillation particularly in two modes. When higher modes are used (two modes), higher rotational speed excites slightly greater high-frequency components. It is because dynamic response starts to settle and converges and hence increasing the rotational speed moderately promotes the occurrence of chatter.

Since there is no consideration of deflection, w in the instantaneous depth of cut formula, h , the deflection, w in the z direction has a very similar pattern for different depth of cut, cutting speed and rotational speed with one mode and two modes only. In addition, the use of higher modes (bigger than two) during numerical simulation brought in some local features but the pattern of dynamic response remains somewhat similar. It is because the dynamic response starts to settle and converges at four modes. In conclusion, for the effect of rotational speed at 3.00 mm depth of cut, including more modes does not change deflection, w in z direction as much as deflection, v in y direction.

6.1.2 Elastic Boundary (Chuck tailstock – Metal work piece)

Since there are some problems encountered using the clamped pinned boundary condition assumed earlier which led to some discrepancies in metal work piece natural frequencies and mode shapes, a suitable boundary should be

considered, in this case an elastic boundary condition because in practice both supports (chuck and tailstock) are actually flexible. This boundary condition is then employed in the developed dynamic model (Chapter 3) and the simulated numerical results (Chapter 5).

The convergence test has been performed initially for the elastic boundary condition. It is done to monitor the occurrence of chatter (up to five modes) and to determine the appropriate number of modes included in the simulation. The properties of the shaft (cylindrical metal work piece) used is similar to the one that is being used for a clamp pinned boundary. The only difference is the cutting parameters used especially for cutting speed where a slightly higher value is used (2.228 m/s). A higher value is selected in order to avoid longer computational workloads. The classical normalized modes are used for an elastic boundary (shown in Equation 3.61).

From the results shown earlier, it can be seen that as the higher modes are included in the simulation, higher oscillation (chatter) starts to appear on top of the deflection (dynamic response) curve in both v (y) and w (z) direction. It is required to simulate higher modes as this will cover high frequency oscillation. The amplitude of the deflection as well increases when the number of modes used in the simulation increases. It is also observed that four modes of the shaft are adequate. It is necessary to include higher modes as it will stimulate high frequency oscillation. The more modes are considered, the more accurate the results are but it is also time consuming.

6.1.2.1 Effect of Depth of Cut

Same values of depth of cut are used which are 0.25 mm, 1.50 mm and 3.00 mm and a same constant value of the cutting speed and the rotational speed are employed. From the results it can be seen that an increase in depth of cut will increase the amplitudes and frequency of oscillation. The 3.00 mm depth of cut is significant as the magnitude of the oscillation becomes bigger. The same

parameters are simulated for two modes and it appears that a different shape of deflection curve is observed and higher frequency components seem to have appeared in comparison with one mode. Most of the high amplitude of oscillation is increased with the increase of number of modes. A similar pattern of deflection curve is also obtained but slightly different in amplitude for three and four modes. Higher amplitude was obtained when a higher depth of cut is used.

6.1.2.2 Effect of Cutting Speed

The two different cutting speeds are next simulated to demonstrate its effect with one mode. A constant value of depth of cut (3.00 mm) and rotational speed (1250 rev/min) were employed. From the results it appears that higher-frequency oscillation has bigger amplitude at a higher cutting speed. The same cutting conditions are also simulated for two modes and it can be seen that the mode shapes have changed when a higher number of modes were used. Similar pattern and amplitude of vibration were produced for different cutting speed and higher amplitude vibration becomes more distinct with more modes. The deflection is slanted to the weaker support, which is the tailstock. The beating phenomenon is even greater at a higher cutting speed (1.4353 m/s). The results obtained for three and four modes are similar with two modes.

6.1.2.3 Effect of Rotational Speed

There are different rotational speeds simulated which are 230 rev/min, 480 rev/min and 1250 rev/min. It is observed that a similar pattern is generated for all rotational speeds and there is not much amplitude difference between the first, second and third modes. It can be said that a variation of rotational speed does not seem to have a big effect on the dynamic response especially on the amplitude of vibration. However, a different pattern has been obtained when a higher number of modes are used. There are some differences in amplitude of

vibration particularly in modes three and four. A higher number of modes (three or more modes) are seen to stimulate slightly greater amplitude of vibration. Therefore, increasing the number of modes moderately promotes the occurrence of chatter. In addition, adding more modes does not change w as much as v .

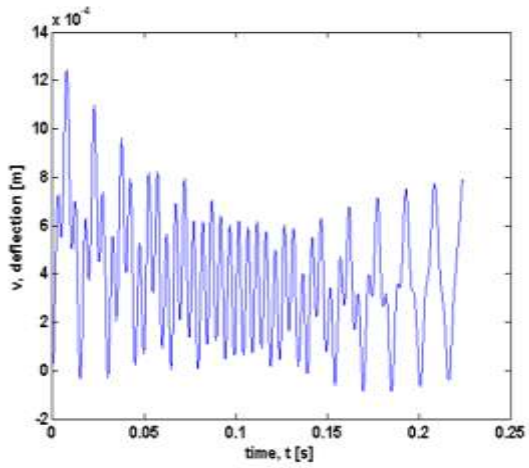
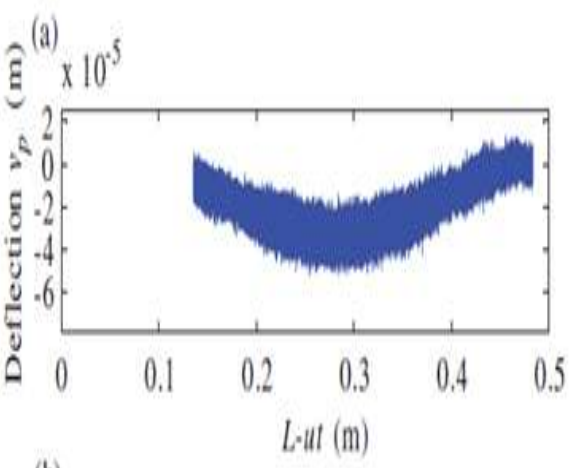
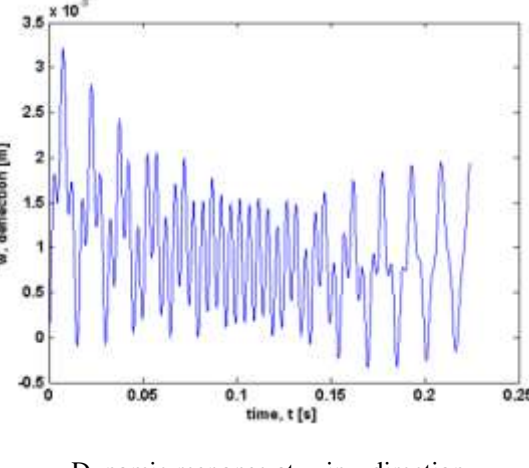
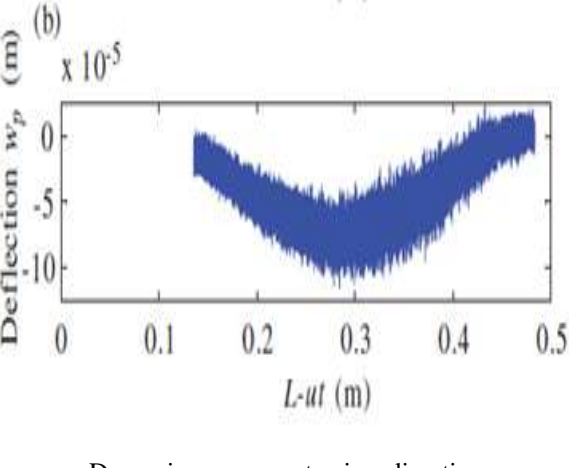
6.2 Validation Between Numerical and Experimental Results

The experiments were conducted with a collaborator at Dailan University of Technology (DUT) in China and the results were employed to validate the dynamic model established. Variation of cutting parameters including the rotating speed, feed rate and depth of cut are carefully chosen in different values consistent with the previous numerical simulations under different cutting conditions in order to investigate the effect of varying the cutting parameters. The phenomena of chatter can be clearly seen at the middle of the cylindrical metal work piece. Moreover, higher oscillation appears in the dynamic response of the time domain.

It can be observed that the deformation patterns are fairly similar between both the experiments and the developed model of clamped pinned and elastic boundary conditions. In the beginning, the theoretical deflections of clamped pinned are greater from the experiment as compared with the developed clamped pinned dynamic model. It might be due to the fact that the initial boundary condition assumed earlier in the theoretical dynamic model is much stiffer at the chuck and more flexible at the tail stock support. In contrast, from the results gained when an elastic boundary is employed, the simulated theoretical deflection magnitude is slightly greater than the measured deflection during experiment. The results are more realistic since both the chuck and tailstock were assumed to be flexible support. Practically the work piece and cutting tool suffer from deflection. It can be concluded that the predicted and measured patterns of time histories of work piece vibration agree fairly well when an elastic boundary conditions are considered in the simulation works of

the developed dynamic model. Note that in Table 6.1 below both of the x -axis of theoretical and experiment graphs represent the moving cutting coordinates. For the theoretical x -axis, it can be calculated by dividing the length of the work piece over cutting speed while in the experiment x -axis, it is simply the length of the work piece subtracted with the product of cutting speed and time.

Table 6.1: Comparison between theoretical and experimental of dynamic responses at both v and w

Theoretical (Chuck-tailstock)	Experimental
 <p>Dynamic response at v in y direction</p>	 <p>Dynamic response at v in y direction</p>
 <p>Dynamic response at w in z direction</p>	 <p>Dynamic response at w in z direction</p>

Chapter 7

Conclusion and Future Work

7.1 Summary of Findings of the Investigation

This thesis presents a study of vibration of work pieces in turning operation modelled as a rotating beam with clamped pinned and elastic supports subjected to three directional moving loads with regenerative chatter mechanism. From the literature reviews done, some of the limitation of previous chatter models (manufacturing engineer models) are that none of them consider moving loads in their dynamics model. Moving loads (cutting forces) should be considered because they are variable in both space and time as the cutter moves along the work piece (a large number of the engineering structures are subjected to time and space varying loads). The moving cutting forces also consider the regenerative chatter effect.

In addition, most studies of dynamic model of turning operation previously have generally assumed the work piece to be rigid and no deformation of work piece is considered. However, in practice the work piece does have deformation when there is an external force exerting on it. Such deformation will change the chip thickness and have an effect on the critical chip thickness and dynamic stability. Although work piece vibrations impact

both cutting instability and product quality including surface finish, most models developed for investigating surface roughness do not consider work piece vibrations at all. Therefore, in this project, the research is focussed on developing a new mathematical model considering both the work piece and cutting tools as flexible. Besides, it is also concluded that the most significant factors contributing to the surface finish quality are the cutting parameters which are the cutting speed, depth of cut and feed rate. One should be more careful in considering the cutting condition used is within recommended range to prevent unstable cutting condition.

The development of the dynamic models was initiated by identifying suitable boundary conditions. The energy method is then employed since the energy of a vibrating system of a turning process is partly potential and partly kinetic. The equation of motion of vibration of a rotating work piece in turning operations is then derived using Lagrange's equations. Three directional moving cutting forces with regenerative chatter mechanism is next included in the dynamic model developed. The improved dynamic model is later generated by adapting Insperger's cutting force model. Lastly, the cutting tool equation of motions for new improved dynamic model is also established and computed in Matlab software. A method to analyse chatter is also established by utilizing a dynamic transient response analysis. Runge-Kutta method has been used initially but since Runge-Kutta always depends on the initial conditions, a Delay Differential equation was selected to replace the Runge-Kutta method since it is a self generated algorithm where the time step will be automatically recognized.

In order to investigate the effect of the cutting parameters, the numerical simulation work is performed to observe the influence of these cutting parameters on the chatter occurrence. Numerical results of the deflection of the beam for these three different cutting parameters (depth of cut, cutting speed and rotational speed) are obtained. It is found that the cutting force model of regenerative chatter which introduces time delay in a dynamic model leads to an interesting dynamic behaviour in the vibration of rotating beams and a sufficient number of modes must be included to sufficiently represent the dynamic behaviour. The effects of depth of cut, the cutting speed and rotational speed on

the vibration and chatter occurrence are examined and obtained. Simulated numerical examples are presented as well.

During the simulation work, two types of boundary conditions are considered; clamped pinned and chuck tailstock (elastic boundary). The results for all three cutting parameters are simulated when an elastic boundary is considered producing a slightly different oscillation as compared with a clamped pinned boundary assumed earlier. The oscillations are much higher when elastic boundary is considered. The results are in line with the actual practice where the work piece suffers from deformation. The amplitude of vibration increases as well when higher numbers of modes are used in the simulation. Similar to clamped pinned boundary, four modes are sufficient and hence used during numerical simulation. It is necessary to include higher modes as it will excite high frequency oscillation. The more modes considered, the more accurate the results; but it is not necessary to include more than four modes.

These three different cutting parameters are vital and definitely influence the dynamic responses of deflection in the y and z directions. The depth of cut is seen to be the most influential on the magnitude of the deflection. For both clamp pinned and elastic boundary conditions, an increase in depth of cut will increase the amplitudes and frequency of oscillation. The 3.00 mm depth of cut is significant as the magnitude of the oscillation becomes bigger. Most of the high amplitude of oscillation increased with the increase of number of modes. Moreover, higher cutting speed will generate a higher-frequency oscillation hence bigger amplitude is obtained. The mode shape pattern changes when a higher number of modes are used. Higher amplitude vibration becomes more pronounced with more modes. Besides, for the effect of different rotational speed, there is not much amplitude difference between the first, second and third modes. A similar pattern of mode shapes is gathered for all rotational speeds. The rotational speed does not seem to have a big influence on dynamic response especially on the amplitude of vibration. In addition, a different pattern has been produced when a higher number of modes are used. There are some differences in amplitude of vibration particularly in mode three and four. When three modes are used, a higher number of modes used are seen to excite slightly greater

amplitude of vibration. Therefore, increasing the number of modes moderately promotes the occurrence of chatter.

Several turning experiments are conducted to demonstrate the existence of vibration and chatter during machining operations. The deformation patterns obtained are reasonably comparable between both the experiment and the developed model. However, the measured deflections are larger from the experiment. It is due to the theoretical model developed is stiffer since the chuck is represented by a clamped boundary and the tail stock support is represented by a simple support. On the contrary, the simulated deflection magnitude gained when an elastic boundary is considered produces a slightly greater magnitude of deflection to the measured deflection during experiment. It can be concluded that the predicted and measured patterns of time histories of work piece vibration agree fairly well when an elastic boundary conditions are considered in the simulation work of the developed dynamic model. These have been both theoretically predicted and experimentally validated.

Lastly, a dynamic model for a rotating Rayleigh beam subjected to a three directional moving cutting forces with regenerative chatter effect is successfully established. The use of established information from the parametric studies on turning operation can be of assistance to the operators in choosing the optimum acceptable turning cutting conditions that will prevent instability and consequent deterioration of the quality of the turned components.

7.2 Contribution to New Knowledge

The main original contributions delivered by this research are listed as follows:

- 7.2.1 The mathematical model developed considered work piece and cutting tools as a flexible work piece and flexible cutting tools. Without doubt, this dynamic model of vibration of work piece in turning operation is

more realistic than previous ones as the dynamic model has multiple-degrees-of-freedom and considers the vibration of the cutter with regenerative chatter. In reality the work piece does have deformation when there is an external force exerting on it. Such deformation will change the chip thickness and have an effect on the critical chip thickness of stability.

- 7.2.2 The work piece is modelled as a rotating Rayleigh beam and the cutter provides a three-dimensional moving load with time delay based on the introduction of regenerative chatter mechanism.
- 7.3.3 Elastic boundary condition is employed in the developed mathematical model to mimic the actual chuck and tailstock support for the work piece on lathe machines.

7.3 Recommendations for Further Investigation

The following suggestions can be made for future research:

- 7.3.1 Acquire better mechanism of sensing to capture deflection during turning process since the previous laser sensor used was too noisy to capture the expected natural frequencies and mode shapes. The used of laser displacement sensor is more practical to mount in measuring the vibration of the work piece during turning operation.
- 7.3.2 Performing experimental modal analysis on composite work pieces since one of the initial aim of this research is to reduce vibration and chatter during turning operation by means of numerical and experimental studies. These can be achieved by pursuing several main objectives of this research. First is to understand what affect the vibration and noise during turned metal in a quantitative manner and then find ways of alleviating this problem by parametric studies.

- 7.3.3 Next is the development of the mathematical model which then will be validated against the experimental results. The validated model will be used to simulate structural modifications in order to identify means of design improvements and vibration reduction.
- 7.3.4 Machine the composite work pieces using turning process as this research is emphasis on turning process.

7.4 List of Publications

7.4.1 Journal Paper

- Han, X., Ouyang, H., Wang, M., **Hassan, N.**, Mao, Y., 2012, Self-excited Vibration of Workpieces in a Turning Process, *Proc. IMechE Part C: J. Mechanical Engineering Science*, 226(8) 1958-1970.

7.4.2 Conference Paper

- **Hassan, N.**, Ouyang, H., 2011, A Dynamic Chatter Model For Turning Processes With A Moving Regenerative Cutting Force, *International Conference on Structural Engineering Dynamics*, Tavira, Portugal.

References

- Al-Regib, E., Ni, J., Lee, S. H., 2003, Programming spindle speed variation for machine tool chatter suppression, *International Journal of Machine Tools & Manufacture*, 43 (12): 1229-1240.
- Altintas, Y., 2000, *Manufacturing Automation: Metal Cutting Mechanics, Machine Tool Vibrations, and CNC Design*, Cambridge University Press, Cambridge.
- Altintas, Y., Chan, P. K., 1992, In process detection and suppression of chatter in milling, *Int J Mach Tools Manuf*, 32, 329–347.
- Argento, A., Morano, H. L., 1995, A Spinning Beam Subjected to a Moving Deflection Dependent Load. 2: Parametric Resonance, *J. Sound Vib.*, 182 (4), pp. 617–622.
- Argento, A., Scott, R. A., 1992, Dynamic Response of a Rotating Beam Subjected to an Accelerating Distributed Surface Force, *J. Sound Vib.*, 157 (2), pp. 221–231.
- Azouzi, R., Guillot, M., 1997, On-line prediction of surface finish and dimensional deviation in turning using neural network based sensor fusion, *International Journal of Machine Tools and Manufacture*, 37 (9), pp. 1201–1217.

- Basavarajappa, S., Chandramohan, G., Rao, K. V. N., Radhakrishnan, R., Krishnaraj, V., 2006, Turning of particulate metal matrix composites – review and discussion, *Proc. IMechE*, Vol. 220, pp.1189-1203.
- Bhatnagar, N., Ramakrishnan, N., Naik, N. K., Komandur, R., 1995, On the machining of fiber reinforced plastic (FRP) composite laminates, *Int. J. Mach. Tools Manufacturing*, 35 (5), pp.701-716.
- Birhan, I., 2008, Experimental investigations of surface roughness in orthogonal turning of unidirectional glass-fiber reinforced plastic composites, *The International Journal of Advanced Manufacturing Technology*, 37 (1-2), pp 42-48.
- Budak, E., 2006, Analytical Methods for High Performance Milling-Part II: Dynamics and Stability, *International Journal of Machine Tools & Manufacture*, 46, pp. 1489-1499.
- Budak, E., Wiercihroch, M., 2001, Sources of nonlinearities, chatter generation and suppression in metal cutting, *Philosophical Transactions of the Royal Society of London, Part A*, 359, pp. 663-693.
- Chandiramani, N.K., Pothala, T., 2006, Dynamics of 2-DOF regenerative chatter during turning, *J. Sound Vib.*, 290, p. 448–464.
- Chen, C. K., Tsao, Y. M., 2006, A stability analysis of regenerative chatter in turning process without using tailstock, *International Journal of Advanced Manufacturing Technology*, 29, pp. 648-654.
- Chen, C. K., Tsao, Y. M., 2006, A stability analysis of turning a tailstock supported flexible work piece, *International Journal of Machine Tools & Manufacturing*, 46, pp. 18-25.
- Chen, L. W., Ku, D. M., 1997, Dynamic stability of a cantilever shaft-disk system, *ASME Journal of Vibration and Acoustics*, 119 (1), pp. 326-329.

- Chen, M., Knopse, C. R., 2007, Control approaches to the suppression of machining chatter using active magnetic bearings, *IEEE Trans Control Systems Technology*, 15 (2), pp. 220-232.
- Chiou, R. Y., Liang, S. Y., 1997, Chatter stability of a slender cutting tool in turning with tool wear effect, *International Journal of Machine Tools & Manufacture*, 38, pp. 315-327.
- Dassanayake, A. V., Suh, C. S., 2008, On nonlinear cutting response and tool chatter in turning operation, *Commun Nonlinear Sci Numer Simul*, 13 (5): 979-1001.
- Davim, J. P., Mata, F., 2005, A new machinability index in turning fiber reinforced plastics, *Journal of Material Processing Technology*, 170, pp. 436-440.
- Delio, T., Tlustý, J., Smith, S., 1992, Use of audio signal for chatter detection and control, *ASME J Eng Industry*, 114, 146–157
- Doolan, P., Phadke, M., Wu, S., 1975, Computer design of a vibration free face-milling cutter, *ASME J Eng Industry*, 97, 925
- El-Saeidy, F. M. A., 2000, Finite Element Dynamic Analysis of a Rotating Shaft With or Without Nonlinear Boundary Conditions Subjected to a Moving Load, *Nonlinear Dyn.*, 21 (4), pp. 377–407.
- El-Sonbaty, I., Khashaba, U. A., Machaly, T., 2004, Factors affecting the machinability of GFR/epoxy composites, *Composite Structures*, 63, pp. 329-338.
- Enders, W. J., Sutherland, J. W., DeVor, R. E., Kapoor, S. G., 1999, A dynamic model of the cutting force system in the turning process
- Engelhardt, R., Lin, S., DeVor, R., Kapoor, S., 1989, A verification of the use of variable spindle speed for vibration reduction in face milling, *Proc NAMRC*, pp. 115–122

- Erturka, A., Ozguvena, H. N., Budak, E., 2006, Analytical Modeling of Spindle-Tool Dynamics on Machine Tools Using Timoshenko Beam Model and Receptance Coupling for the Prediction of Tool Point FRF, *Int. J. Mach.Tools Manuf.*, 46, pp. 1901–1912.
- Ewins, D. J., 2000, *Modal testing: theory, practice and application*, Research Studies Press Ltd., Hertfordshire, England, 2nd edition.
- Faassen, R. P. H., Wouw, N. V., Oosterling, J. A. J., Nijmeijer, H., 2003, Prediction of regenerative chatter by modelling and analysis of high-speed milling, *International Journal of Machine Tools & Manufacture*, 43, 1437–1446
- Frangoudis, S., Nicolescu, M., Rashid, A., 2013, Experimental analysis of a machining system with adaptive dynamic stiffness, *Journal of Machine Engineering*, Vol. 13, No. 1.
- Fu, H., De Vor, R., Kappor, S., 1984, The optimal design of tooth spacing in face milling via a dynamic force model, *Proc 12th NAMRC*, pp. 291–297
- Ganguli, A. Deraemaeker, A., Preumont, A., 2007, Regenerative chatter reduction by active damping control. *Journal of Sound and Vibration*, 300 (3-5):847-862.
- Han, R. P. S., Zu, J. W. Z., 1992, Modal Analysis of Rotating Shafts: A Body-Fixed Approach, *J. Sound Vib.*, 156 (1), pp. 1–16.
- Han, S. M., Benaroya, H., Wei, T., 1999, Dynamics of transversely vibrating beams using four engineering theories, *J of Sound and Vibration*, 225 (5), pp. 935-988.
- Han, X., Ouyang, H., Wang, M., Hassan, N., Mao, Y., 2012, Self-excited vibration of workpieces in a turning process, *Proc IMechE Part C: J Mechanical Engineering Science*, 226 (8) 1958-1970.

- Hanna, N. H., Tobias, S.A., 1969, The nonlinear dynamic behavior of a machine tool structure. *Int J Mach Tool Design Res*, 9 (3), pp. 293–307.
- Hibbeler, R. C., 2011, *Mechanics of Materials*, Eighth Edition, Singapore, Prentice Hall.
- Hocheng, H., Yen, S. B., Yen, B. K., 1997, Fundamental turning characteristic of a tribiology-favored graphite/aluminium alloy composite material, *Composites Part A*, pp. 883-890.
- Hoshi, T., Sakisaka, N., Moriyama, I., Sato, M., 1977, Study for practical application of fluctuating speed cutting for regenerative chatter control, *Annals of the CIRP*, 25, 175–179
- Huang, C. Y., Junz Wang, J. J., 2009, *ASME International Mechanical Engineering Congress and Exposition*, Volume 10: Mechanical Systems and Control, Parts A and B
- Huang, S. C., Chen, J. S., 1990, Dynamic Response of Spinning Orthotropic Beams Subjected to Moving Harmonic Forces, *J. Chin. Soc. Mech. Eng.*, 11, pp. 63–73.
- Huang, S. C., Hsu, B. S., 1990, Resonant Phenomena of a Rotating Cylindrical Shell Subjected to a Harmonic Moving Load, *J. Sound Vib.*, 136, pp. 215–228.
- Inamura, T., Sata, T., 1974, Stability analysis of cutting under varying spindle speed, *J Faculty of Eng*, The University of Tokyo (B) XXXIII (1)
- Insperger, T., Barton, D. A. W., Stepan, G., 2008, Criticality of Hopf bifurcation in state dependent delay model of turning processes, *International Journal of Non-Linear Mechanics*, 43 (2), pp. 140-149.
- Jahanmir, S., Ramulu, M., Koshy, P., 1998, *Machining of ceramics and composites*, Marcel Dekker Inc., New York, pp. 238-243.

- Jen, M. U., Magrab, E. B., 1996, The Dynamic Interaction of the Cutting Process, Workpiece and Lathe's Structure in Facing, *ASME J. Manuf. Sci. Eng.*, 118, pp. 348–358.
- Kashyzadeh, K. R., Ostad-Ahmad-Ghorabi, M. J., 2012, Study of Chatter Analysis in turning tool and control methods – A Review, *International Journal of Emerging Technology and Advanced Engineering*, Volume 2, Issue 4.
- Kato, S., Marui, E., 1974, On the Cause of Regenerative Chatter Due to Work piece Deflection, *ASME J. Eng. Ind.*, 96, pp. 179–186.
- Katz, W. R., Lee, C., A. G., Scott, R. A., 1988, The Dynamic Response of a Rotating Shaft Subject to a Moving Load, *J. Sound Vibration.*, 122(1), pp. 131-148.
- Katz, W. R., Lee, C., Ulsoy, A. G., Scott, R. A., 1987, The Dynamic Response of a Rotating Shaft Subject to a Moving Load, *J. Sound Vib.*, 122, pp. 134-148.
- Katz, W. R., Lee, C., Ulsoy, A. G., Scott, R. A., 1989, Turning of Slender Workpieces Modeling and Experiments, *Mechanical Systems and Signal Processing*, 3(2), pp. 195-205.
- Koeingsberger, F., Thusty, J., 1970, *Machine Tool Structures*, Vol. 1, Pergamon Press, New Jersey.
- Lacerda, H. B., Lima, V. T., 2004, Evaluation of Cutting Forces and Prediction of Chatter Vibrations in Milling, *J. of the Braz. Soc. of Mech. Sci. & Eng.*, Vol. XXVI, No. 1.
- Lambert, B. K., Taraman, K. A. , 1974, Surface roughness model for a turning operation, *International Journal of Production Research*, 12, pp. 691–703.
- Lee, A. C., Liu, C. S., 1991, Analysis of chatter vibration in the end milling process, *Int J Mach Tools and Manuf*, 31 (4), 471–479.

- Lee, C., Katz, W. R., Ulsoy, A. G., Scott, R. A., 1987, Modal Analysis of a Distributed Parameter Rotating Shaft, *J. Sound Vib.*, 122, pp. 119-130.
- Lin, C. S., Devor, R. E., Kapoor, S. G., 1990, The effects of variable speed cutting on vibration control in face milling, ASME, *J Eng Industry*, 112, 1–11.
- Lin, S. C., 1990, A Method to Analyze the Stability of Machine Tool, *CIRP Annal*, 44, pp. 253–265.
- Lu, W. F., Klamecki, B. E., 1990, Prediction of Chatter in Turning With a Modified Chatter Model, *Proceedings of ASME WAM*, PED-Vol. 44, pp.237–252.
- Marui, E., Ema, S., Kato, S., 1983, Chatter Vibration of Lathe Tools Part1: General Characteristics of Chatter Vibration, *ASME J. Eng. Ind.*, 105, pp.100–106.
- Merrit, H. E., 1965, Theory of self-excited machine-tool chatter, *ASME J Eng Ind*, 87 (4): 447-454.
- Miller, J. C., De Vor, R. E., Southerland, J. W., 1983, Surface roughness characteristics for turning 380 and 390 aluminum casting alloys, *Proceedings of North American Manufacturing Research Conference*, pp. 282–288.
- Mital, A., Mehta, M., 1988, Surface finish prediction models for fine turning, *International Journal of Production Research*, 26 (12).
- Nishitani, H., Imai, R., 1983, Effect of surface roughness of heat-treatment materials for S45C and SCM435 steels on rotary bending fatigue strength, *Trans. JSME (A)*, 49 (442), pp. 693–698.
- Otta, H., Kono, K., 1997, On Chatter Vibrations of Machine Tool or Work Due to Regenerative Effect and Time Lag, *J Eng Ind*, 96 (4), 1974.

- Ouyang, H., 2011, Moving-load dynamic problems: A tutorial (with a brief overview), *J Mechanical Systems and Signal Processing*, 25 (6), pp. 2039–2060.
- Ouyang, H., Wang, M. J., 2007, Dynamics of a rotating shaft subject to a three-directional moving load, *Journal of Vibration and Acoustics-Transactions of the ASME*, 129 (3), pp. 386-389.
- Ozel, T., Karpaz, Y., 2005, Predictive model surface roughness and tool wear in hard turning using regression and neural networks, *International Journal of Machine Tools and Manufacture*, 45 (4–5), pp. 467–479.
- Palanikumar, K., Karthikeyan, R., 2006, Optimal machining conditions for turning of particulate metal matrix composites using taguchi and response surface methodologies', *Machining Science and Technology*, 10, pp. 417-433.
- Palanikumar, K., Karunamoorthy, L., Karthikeyan, R., 2006, Assessment of factors influencing surface roughness on the machining of glass fiber-reinforced polymer composites, *Materials and Design*, 27, pp. 861-871,.
- Petropoulos, P. G., 1974, Statistical basis for surface roughness assessment in oblique finish turning of steel components, *International Journal of Production Research*, 12, pp. 345–360.
- Ramkumar, J., Aravindan, S., Malhotra, S. K., Krishnamoorthy, R., 2004, An enhancement of the machining performance of GFRP by oscillatory assisted drilling, *Int J Adv Manuf Technology*, 23, pp.240–244.
- Ramulu M, Arola D, Colligan K., 1994, Preliminary investigation of effects on the surface integrity of fiber reinforced plastics, *Eng Syst Anal ASME PD*, 64 (2), pp. 93–101.
- Rao, S. S., 1995, *Mechanical Vibrations*, Third Edition. Reading, MA, Addison-Wesley Publishing Company

- Rayleigh, J. W. S., 2003. *The Theory of Sound*, Two volumes, Dover Publications Inc., ISBNs: 978-0-486-60292-9 & 978-0-486-60293-6, New York.
- Risbood, K. A., Dixit, U. S., Sahasrabudhe, A. D., 2003, Prediction of surface roughness and dimensional deviation by measuring cutting forces and vibrations in turning process, *Journal of Materials Processing Technology*, 132 (1–3), pp. 203–214.
- Sakuma, K., Seto, M., 1983, Tool wear in cutting glass fibre-reinforced plastics, *Bulletin of the JSME*, 26 (218), pp.1420-1427.
- Sekar, M., Srinivas, J., Kotaiah, K., R., Yang, S., H., 2009, Stability analysis of turning process with tailstock-supported workpiece, *International Journal of Advanced Manufacturing Technology*, 43, pp.862–871.
- Sexton, J. S., Stone, R. J., 1978, The stability of machining with continuously varying spindle speed, *Annals of CIRP*, 24, 321–326
- Sexton, J. S., Stone, R. J., 1980, An investigation of the transient effects during variable speed cutting, *J Mech Eng Sci*, 22 (3), 107–118
- Shabana, A. A., 1996, *Theory of Vibration: An Introduction*, Springer
- Shawky, A. M., Elbestawi, M. A., 1998, Model-Based Predictive Control of Workpiece Accuracy in Bar Turning, *ASME J. Manuf. Sci. Eng.*, 120, pp.57–67.
- Sheu, G. J., Yang, S. M., 2005, Dynamic Analysis of a Spinning Rayleigh Beam, *Int. J. Mech. Sci.*, 47 (2), pp. 157–169.
- Shi, H. M., Tobias, S. A., 1984, Theory of finite amplitude machine instability. *Int J Mach Tool Design Res*, 24 (1), pp. 45–69.
- Sims, N. D., 2007, Vibration absorbers for chatter suppression: a new analytical tuning methodology, *Journal of Sound and Vibration*, 301: 592–607.

- Singh, D., Rao, P. V., 2007, A surface roughness prediction model for hard turning process, *International Journal of Advanced Manufacturing Technology*, 32: 1115-1124.
- Slavicek, J., 1965, The effect of irregular tooth pitch on stability in milling, *Proc 6th MTDR Conf*, pp. 15–22.
- Smith, S., Tlustý, J., 1992, Stabilizing chatter by automatic spindle speed regulation, *Annals of the CIRP*, 41, 433–436.
- Soliman, S., Ismail, F., 1997, Chatter suppression by adaptive speed modulation, *Int J Mach Tools Manuf*, 37 (3), 355–369.
- Spur, G., Wunsch, U. E., 1988, Turning of fiber reinforced plastics, *Manufacturing Review*, 1 (2):124–129.
- Stepan, G., Nagy, T. K., 1997, Nonlinear regenerative machine tool vibrations, *ASME Design Engineering Technical Conference*, p. 1–11.
- Stephenson, D. A., Agapiou, J. S., 1996, *Metal Cutting Theory and Practice*, Dekker, New York
- Stoferle, T., Grab, H., 1972, Vermeiden von Ratterschwingungen durch Periodische Drehzahländerung, *Werkstatt und Betrieb*, 105, 727–730.
- Stone, B. J., 1970, The effect on the chatter behavior of machine tools of cutters with different helix angles on adjacent teeth, *Proc 11th MTDR*, pp. 169–180
- Sundaram, R. M., Lambert, B. K., 1981, Mathematical models to predict surface finish in fine turning of steel, Parts I and II, *International Journal of Production Research*, 19, pp. 547–564.
- Takemura, T., Kitamura, T., Hoshi, T., 1974, Active suppression of chatter by programmed variation of spindle speed, *Annals of CIRP*, 23, 121–122
- Takeyama, H., Lijima, 1988, Machinability of glass fiber reinforced plastics and application of ultrasonic machining, *Ann CIRP*, 37 (1), pp.93-96.

- Tarng, Y. S., Kao, J. Y., Lee, E. C., 2000, Chatter suppression in turning operations with a tuned vibration absorber. *Journal of Materials Processing Technology*, 105 (1-2): 55-60.
- Tarng, Y., Hsieh, Y., Li, T., 1996, Automatic selection of spindle speed for suppression of regenerative chatter in turning, *Int J Adv Manuf Technol*, 11, 12–17
- Taylor, F. W., 1907, On the art of cutting metals, *Transactions of ASME*.
- Timoshenko, S. P., 1921, On the correction for shear of the differential equation for transverse vibrations of bars of uniform cross-section, *Philosophical Magazine*, 744.
- Timoshenko, S. P., 1922, On the transverse vibrations of bars of uniform cross-section, *Philosophical Magazine*, 125.
- Thusty, G., 2000, *Manufacturing Processes and Equipment*, Upper Saddle River, N.J.
- Thusty, J., Polacek, M., 1963, The stability of machine tool against self-excited vibration in machining, *Proceeding of International Production Engineering Research Conference*, 465-471.
- Thusty, J., Zaton, W., Ismail, F., 1983, Stability lobes in milling, *Annals of the CIRP*, 2, 309–313
- Tobias, S. A., 1965, *Machine tool vibration*, Blackie and Sons Ltd., London.
- Tobias, S. A., Fishwick, W., 1958, *Theory of Regenerative Machine Tool Chatter*, *Engineering*, 250.
- Tobias, S. A., Fishwick, W., 1958, The chatter of lathe tools under orthogonal cutting conditions, *Transactions of The American Society of Mechanical Engineers* 80, 1079-1088.

- Vanherck, P., 1967, Increasing milling machine productivity by use of cutter with non-constant cutting-edge pitch, *Proc Adv MTDR Conf*, No. 8, pp. 947–960
- Wang, M., Fei, R., 1999, Improvement of machining stability using a tunable-stiffness boring bar containing an electrorheological fluid, *Smart Material and Structure*, 8, 511.
- Wang, X. M., Zhang, L. C., 2003, An experimental investigation into the orthogonal cutting of unidirectional fibre reinforced plastics, *International Journal of Machine Tools & Manufacture*, 43, pp.1015-1022.
- Weck, M., Verhang, E., Gather, M., 1975, Adaptive control for face-milling operations with strategies for avoiding chatter vibrations and for automatic cut distribution, *Annals of the CIRP*, 24/1,405–409
- William, J. B., 2006, *Engineering Vibrations*, Taylor and Francis.
- Xavior, M. A., Adithan, M., 2009, Determining the influence of cutting fluids on tool wear and surface roughness during turning of AISI 304 austenitic stainless steel, *Journal of Materials Processing Technology*, 209 (2), pp. 900–909.
- Yilmaz, A., Al-Regib, E., Ni, J., 1999, Machine-tool chatter suppression by multi-level random spindle speed variation, *Symposium on Recent Advances in Machine Tool*, ASME, Mechanical Engineering Congress and Exposition, Nashville, Tennessee.
- Zhang, H., 1996, Chatter modeling, analysis and control for CNC machining systems, *PhD dissertation*, The University of Michigan
- Zibdeh, H. S., Juma, H. S., 1999, Dynamic Response of a Rotating Beam Subjected to a Random Moving Load, *J. Sound Vib.*, 223 (5), pp. 741–758.

Appendix A1 - Calculation of deflection, v and w for clamp-pinned boundary

```
function ddeow

l = 0.5 ;

comega = 1250/60;%230/60;%480/60;%1200/60; %1250/60 % Rotation
speed of the shaft(rev/s);

h0 = 2 * pi / comega ;%mine

speed = 0.2228; %86.12/60;

tend = l/speed;

sol = dde23(@ddeowde,h0,@ddeowhist,[0,tend]);

t = sol.x;

n2 = length(sol.x);

for j = 1:n2

    v(j) = 0;
    w(j) = 0;

    for i = 1: nm

        v(j) = v(j) + phi(i,l,lambda,sgma,s(t(j)))*sol.y(i,j);
        %w(j) = w(j) + phi(i,l,lambda,sgma,s(t(j)))*sol.y(i+2*nm,j);
        %s(t) is the cutter location starting from the right
        hand side at t=0;

    end
end

plot(sol.x,v)

set(gca,'fontsize',12,'fontweight','b','FontName','Times
Roman');
ylabel('v, deflection [m]');
xlabel('time, t [s]');
```

Appendix A2 – Derivation of Delay Differential equation for clamp-pinned boundary

```

function dydt = ddeowde(t,y,Z)% This is time integration as well
    and don't need Runge Kutta method

% all of A,B, C, D B2,B3 should be inside this function.

l = 0.5 ; E = 2.07 * 10^11 ; ro = 7850; % mine ro = 7700 ;
    steel

r = 0.025; A = pi * r * r ; I = 0.25 * A * r * r ; nm = 1;

%hc = 0.00254 ; ac = 0.003 ; % intended cut depth or h(t) and
    width of cut

hc = 0.003;%0.003;%0.00025;%0.0015 ;

ac = 0.00025; % xiangou value

Kx = 5.243175675e+6;
Ky = 7.322206549e+6;
Kz = 2.60201192e+8;
f = 0.3/1000; % Nominal Feed rate(m/rev); %exp1 % exp2 - 0.2,
    exp3 - 0.3

Ax = Kx * f^0.37; % Xiangou cutting force coefficient

Ay = Ky * f^0.4; % Xiangou cutting force coefficient

Az = Kz * f^0.73; % Xiangou cutting force coefficient

cx = Ax/ac; % to make the cutting force coefficient the same

cy = Ay/ac; % to make the cutting force coefficient the same

cz = Az/ac; % to make the cutting force coefficient the same

sigma = [ 1.000777304 1.000001445 ] ;

for i =3 : nm
    sigma (i) = 1;
end

lambda = [3.92660231 7.06858275 10.21017612 13.35176878
    16.49336143 ] ;

```

```

for i = 6 : nm
    lambda (i) = (4*i+1)*pi/4;
end

for i = 1 : nm
    omega(i) = ((lambda(i)^2)/(2*pi*l^2)) * sqrt(( E * I) / (ro
    * A));
end

comega = 1250/60;%230/60;%480/60%1200/60; %1250/60    % Rotation
    speed of the shaft(rev/s); xiangou

a = 0; b = 1; n = 20;    h = (b-a)/n ;

h0 = 2 * pi / comega ; %mine

B = zeros(nm,nm) ; C = B ; D = B;

for i = 1: nm;

    area_A = 0;
    for m = 1 :n
        xl = a + (m - 1)*h;          xu = xl + h; % i for
phi(x)and i for phi(x)transpose
        area_A = area_A + 0.5 * h * (
        phi(i,l,lambda,sgma,xl)^2 + phi(i,l,lambda,sgma,xu)^2 );
    end
    D(i,i) = ro*A*area_A ; % diagonal elements for mass

    for j = 1: nm;

        area_B = 0; area_C = 0;
        for m = 1 :n
            xl = a + (m - 1)*h;          xu = xl + h;

%Trapezium Numerical Integration
            area_B = area_B + 0.5* h
            *(phi_1d(i,l,lambda,sgma,xl)*... % i for phi(x)and j for
            phi(x)transpose
            phi_1d(j,l,lambda,sgma,xl)
            +
            phi_1d(i,l,lambda,sgma,xu)*phi_1d(j,l,lambda,sgma,xu)); % the
            reason it has two term 1 for lower bound (xl) and 1 for upper
            bound (xu)

            area_C = area_C + 0.5* h
            *(phi_2d(i,l,lambda,sgma,xl)*...
            phi_2d(j,l,lambda,sgma,xl)
            +
            phi_2d(i,l,lambda,sgma,xu)*phi_2d(j,l,lambda,sgma,xu));

        end
        B(i,j) = area_B;    C(i,j) = area_C; % off-diagonal
        elements such as damping and stiffness
        D(i,j) = D(i,j) + ro*I*B(i,j) ;
    end
end

```



```

B2 = 2 * comeqa * ro * I * B ; C1 = E * I * C ; D =
    D\eye(size(D)); %D = inv(D) ;

for i=1:nm
    for j=1:nm

        sum_phi(i,j) = phi(i,l,lambda,sgma,s(t)) *
        phi(j,l,lambda,sgma,s(t)); %
        sum_phi_1(i,j) = phi_1d(i,l,lambda,sgma,s(t)) *
        phi(j,l,lambda,sgma,s(t));
        sum_phi_2(i,j) = phi(i,l,lambda,sgma,s(t)) *
        phi(j,l,lambda,sgma,s(t-h0));%for ode23
        sum_phi_3(i,j) = phi_1d(i,l,lambda,sgma,s(t)) *
        phi(j,l,lambda,sgma,s(t-h0));%for ode23

    end
    U4(i) = ac*hc*(cy*phi(i,l,lambda,sgma,s(t)) -
    cx*r*phi_1d(i,l,lambda,sgma,s(t)));
    V4(i) = cz*ac*hc*phi(i,l,lambda,sgma,s(t));
end

U1 = -(C1)+ac*(-cy*sum_phi+cx*r*sum_phi_1); % without the
    effect of Px
U2 = -B2;
U3 = ac*(cy*sum_phi_2-cx*r*sum_phi_3);

V1 = -cz*ac*sum_phi;% without the effect of Px
V2 = B2;
V3 = cz*ac*sum_phi_2;
V5 = -(C1);% without the effect of Px

M = [zeros(nm) eye(nm) zeros(nm) zeros(nm); D*U1 zeros(nm)
    zeros(nm) D*U2;
    zeros(nm) zeros(nm) zeros(nm) eye(nm); D*V1 D*V2 D*V5
    zeros(nm)];

N = [zeros(nm) zeros(nm) zeros(nm) zeros(nm); D*U3 zeros(nm)
    zeros(nm) zeros(nm);
    zeros(nm) zeros(nm) zeros(nm) zeros(nm); D*V3 zeros(nm)
    zeros(nm) zeros(nm)];

O = [zeros(nm, 1); D*U4'; zeros(nm, 1); D*V4'];

ylag = Z(:,1);

dydt = M*y + N*ylag + O;

```

Appendix A3 – Time delay function

```
function z = ddeowhist(t)

nm = 1;

z = zeros(4*nm,1);
```

Appendix A4 – Determination of mode shape function for clamp-pinned boundary

```
function [func] = phi(i, l, lambda, sigma, x)

func = cosh(x * (lambda(i)/l)) - cos(x * (lambda(i)/l)) - ...
      sigma(i) * (sinh(x * (lambda(i)/l)) - sin(x *
(lambda(i)/l)));
```

Appendix A5 – First derivation of mode shape function for clamp-pinned boundary

```
function [func] = phi_1d (i, l, lambda, sigma, x)

func = lambda (i)/l * ( sinh(x * (lambda (i)/l)) + ...
    sin(x * (lambda (i)/l)) - sigma (i) * (cosh( x* (lambda
    (i)/l)) - ...
    cos(x * (lambda (i)/l))));
```

Appendix A6 – Second derivation of mode shape function for clamp-pinned boundary

```
function [func] = phi_2d (i, l, lambda, sigma, x)

func = (lambda (i)/l)^2 * ( cosh(x * (lambda (i)/l)) + ...
    cos(x * (lambda (i)/l)) - sigma (i) * (sinh(x * (lambda
    (i)/l)) + ...
    sin(x * (lambda (i)/l)))));
```

Appendix A7 – Calculation of cutting speed

```
function [func] = s(t)

    l = 0.5 ;

    speed = 0.2228;

    func = l - speed * t ;

    if t < 0
        func = l ;
    end
```

Appendix A8 - Calculation of deflection, v and w for elastic boundary

```
function ddeowelastic

clear all; clc;

global nm c1 c2 c3 c4 beta_n h0 ac hc cy cx r cz C1 B2 D l
speed

l = 0.5;

E = 2.07 * 10^11 ; ro = 7817.4; % mine ro = 7700 ; steel

r = 0.0185; A = pi * r * r ; I = 0.25 * A * r * r ; nm = 1;

beta_n = [5.661 6.476 13.685 15.663 18.941];

c1 = [3.1915 -105.7214 3.0913 81.3933 108.5319];
c2 = [105.9489 165.8741 -78.8856 -802.2749 137.3669];
c3 = [58.5381 66.2404 -28.3929 -325.8367 55.932];
c4 = [-56.2174 -49.8974 28.2829 325.2055 -55.9587];
% x = 0:l/20:l;
% plot(x, c1(1)*cos(beta_n(1)*x)+c2(1)*sin(beta_n(1)*x)+ ...
%      c3(1)*cosh(beta_n(1)*x)+c4(1)*sinh(beta_n(1)*x))
% figure
% plot(x, c1(2)*cos(beta_n(2)*x)+c2(2)*sin(beta_n(2)*x)+ ...
%      c3(2)*cosh(beta_n(2)*x)+c4(2)*sinh(beta_n(2)*x))
% figure
% plot(x, c1(3)*cos(beta_n(3)*x)+c2(3)*sin(beta_n(3)*x)+ ...
%      c3(3)*cosh(beta_n(3)*x)+c4(3)*sinh(beta_n(3)*x))
% figure
% plot(x, c1(4)*cos(beta_n(4)*x)+c2(4)*sin(beta_n(4)*x)+ ...
%      c3(4)*cosh(beta_n(4)*x)+c4(4)*sinh(beta_n(4)*x))
% figure
% plot(x, c1(5)*cos(beta_n(5)*x)+c2(5)*sin(beta_n(5)*x)+ ...
%      c3(5)*cosh(beta_n(5)*x)+c4(5)*sinh(beta_n(5)*x))

%hc = 0.00254 ; ac = 0.003 ; % intended cut depth or h(t) and
width of cut\

hc = 0.003;%0.003;%0.00025;%0.0015 ;

ac = 0.0003; % xiangou value

Kx = 5.243175675e+6;
Ky = 7.322206549e+6;
Kz = 2.60201192e+8;
f = 0.3/1000; % Nominal Feed rate(m/rev); %exp1 % exp2 - 0.2,
exp3 - 0.3

Ax = Kx * f^0.37; % Xiangou cutting force coefficient
```

```

Ay = Ky * f^0.4; % Xiangou cutting force coefficient

Az = Kz * f^0.73; % Xiangou cutting force coefficient

% Px = cx * hc * ac ;

cx = Ax/ac; % to make the cutting force coefficient the same
with Xiangou

cy = Ay/ac; % to make the cutting force coefficient the same
with Xiangou

cz = Az/ac; % to make the cutting force coefficient the same
with Xiangou

comega = 1250/60;%230/60;%480/60%1200/60; %1250/60 % Rotation
speed of the shaft(rev/s); xiangou

speed = 2.228; %xiangou

a = 0; b = 1; n = 50; h = (b-a)/n ;

h0 = 2 * pi / comega ; %mine

B = zeros(nm,nm) ; C = B ; D = B;

for i = 1: nm;

    area_A = 0;
for m = 1 :n
    xl = a + (m - 1)*h; xu = xl + h; % i for
    phi(x)and i for phi(x)transpose
    area_A = area_A + 0.5 * h * ( phi(i, c1, c2, c3, c4,
    beta_n, xl)^2 + phi(i, c1, c2, c3, c4, beta_n, xu)^2 );
end
    D(i,i) = ro*A*area_A ; % diagonal elements for mass

for j = 1: nm;

    area_B = 0; area_C = 0;
for m = 1 :n
    xl = a + (m - 1)*h; xu = xl + h;

%Trapezium Numerical Integration
    area_B = area_B + 0.5* h *(phi_1d(i, c1, c2, c3,
    c4, beta_n, xl)*... % i for phi(x)and j for phi(x)transpose
    phi_1d(j, c1, c2, c3, c4, beta_n, xl) +
    phi_1d(i, c1, c2, c3, c4, beta_n, xu)*phi_1d(j, c1, c2, c3,
    c4, beta_n, xu)); % the reason it has two term 1 for lower
    bound (xl) and 1 for upper bound (xu)

    area_C = area_C + 0.5* h *(phi_2d(i, c1, c2, c3,
    c4, beta_n, xl)*...
    phi_2d(j, c1, c2, c3, c4, beta_n, xl) +
    phi_2d(i, c1, c2, c3, c4, beta_n, xu)*phi_2d(j, c1, c2, c3,
    c4, beta_n, xu));

```



```

end
    B(i,j) = area_B;    C(i,j) = area_C; % off-diagonal
    elements such as damping and stiffness
    D(i,j) = D(i,j) + ro*I*B(i,j) ;
end
end

B2 = 2 * comeaga * ro * I * B ; C1 = E * I * C ; D =
    D\eye(size(D)); %D = inv(D) ;

tend = 1/speed;

sol = dde23(@ddeowdeelastic,h0,@ddeowhist,[0,tend]);

t = sol.x;

n2 = length(sol.x);

for j = 1:n2

    v(j) = 0;
    w(j) = 0;

    for i = 1: nm

        v(j) = v(j) + phi(i, c1, c2, c3, c4, beta_n,
            s(t(j)))*sol.y(i,j);
        %w(j) = w(j) + phi(i, c1, c2, c3, c4, beta_n,
            s(t(j)))*sol.y(i+2*nm,j);
        %s(t) is the cutter location starting from the right hand side
        at t=0;

    end
end

plot(sol.x,v)

set(gca,'fontsize',12,'fontweight','b','FontName','Times
    Roman');
ylabel('v, deflection [m]');
xlabel('time, t [s]');

```

Appendix A9 - Derivation of Delay Differential equation for elastic boundary

```
%the boundary condition is fixed end (chuck) and simply
supported (tailstock)

%function dydt = ddeowde(t,y)

function dydt = ddeowdeelastic(t,y,Z)% This is time integration
as well and don't need Runge Kutta method

display(t)

global nm c1 c2 c3 c4 beta_n h0 ac hc cy cx r cz C1 B2 D l speed

sum_phi = zeros(nm,nm);
sum_phi_1 = zeros(nm,nm);
sum_phi_2 = zeros(nm,nm);
sum_phi_3 = zeros(nm,nm);
U4 = zeros(1,nm);
V4 = zeros(1,nm);

for i=1:nm % this is about mode size which is nm
for j=1:nm

    sum_phi(i,j) = phi(i, c1, c2, c3, c4, beta_n, s(t)) *
    phi(j, c1, c2, c3, c4, beta_n, s(t)); %
    sum_phi_1(i,j) = phi_1d(i, c1, c2, c3, c4, beta_n, s(t))
    * phi(j, c1, c2, c3, c4, beta_n, s(t));
    sum_phi_2(i,j) = phi(i, c1, c2, c3, c4, beta_n, s(t)) *
    phi(j, c1, c2, c3, c4, beta_n, s(t-h0));%for ode23
    sum_phi_3(i,j) = phi_1d(i, c1, c2, c3, c4, beta_n, s(t))
    * phi(j, c1, c2, c3, c4, beta_n, s(t-h0));%for ode23

end

    U4(i) = ac*hc*(cy*phi(i, c1, c2, c3, c4, beta_n, s(t))-
    cx*r*phi_1d(i, c1, c2, c3, c4, beta_n, s(t)));% a row vectors
    V4(i) = cz*ac*hc*phi(i, c1, c2, c3, c4, beta_n, s(t));%
    a row vectors
end

U1 = (-(C1)+ac*(-cy*sum_phi+cx*r*sum_phi_1)); % without the
effect of Px
%U1 = (-(C1-Px*B3)+ac*(-cy*sum_phi+cx*r*sum_phi_1));
U2 = -B2;
U3 = ac*(cy*sum_phi_2-cx*r*sum_phi_3);

% beta double dot with v(x,t)= phiT(x)* ALPHA(t)
V1 = -cz*ac*sum_phi;% without the effect of Px
%V1 = (-Px*B3)-cz*ac*sum_phi); % with the effect of Px
```

```

V2 = B2;
V3 = cz*ac*sum_phi_2;
V5 = -(C1);% without the effect of Px
%V5 = -(C1-Px*B3)% with the effect of Px

% beta double dot with v(x,t)= phiT(x)* ALPHA(t)
M = [zeros(nm) eye(nm) zeros(nm) zeros(nm); D*U1 zeros(nm)
      zeros(nm) D*U2;
      zeros(nm) zeros(nm) zeros(nm) eye(nm); D*V1 D*V2 D*V5
      zeros(nm)];

N = [zeros(nm) zeros(nm) zeros(nm) zeros(nm); D*U3 zeros(nm)
      zeros(nm) zeros(nm);
      zeros(nm) zeros(nm) zeros(nm) zeros(nm); D*V3 zeros(nm)
      zeros(nm) zeros(nm)];

O = [zeros(nm, 1); D*U4'; zeros(nm, 1); D*V4'];

ylag = Z(:,1);

dydt = M*y + N*ylag + O;

%dydt = M*y + O;

```

Appendix A10 – Determination of mode shape function for elastic boundary

```
function [func] = phi(i, c1, c2, c3, c4, beta_n, x) %any
    boundary from Rao's book - elastic boundary

func = c1(i)*cos(beta_n(i)*x) + c2(i)*sin(beta_n(i)*x) +
    c3(i)*cosh(beta_n(i)*x) + c4(i)*sinh(beta_n(i)*x);

func = 0.01 * func ;
```

Appendix A11 – First derivation of mode shape function for elastic boundary

```
function [func] = phi_1d(i, c1, c2, c3, c4, beta_n, x) %any
    boundary from Rao's book - elastic boundary

func = beta_n(i)*(-c1(i)*sin(beta_n(i)*x) +
    c2(i)*cos(beta_n(i)*x) + c3(i)*sinh(beta_n(i)*x) +
    c4(i)*cosh(beta_n(i)*x));

func = 0.01 * func ;
```

Appendix A12 – Second derivation of mode shape function for elastic boundary

```
function [func] = phi_2d(i, c1, c2, c3, c4, beta_n, x) %any
    boundary from Rao's book - elastic boundary

func = beta_n(i)^2*(-c1(i)*cos(beta_n(i)*x) -
    c2(i)*sin(beta_n(i)*x) + c3(i)*cosh(beta_n(i)*x) +
    c4(i)*sinh(beta_n(i)*x));

func = 0.01 * func ;
```

Appendix A13 – Calculation of C_1 , C_2 , C_3 and C_4 variables

```
clear all; clc;

n = 11;

beta_n = 5.777; %[ 5.661 5.777 6.476 6.657 13.145 13.685 15.149
15.663 18.941 19.625 20.123 21.020 24.605 24.977 ];elastic
boundary corresponding to each mode

%y_n = [5.50E+01 7.14E+01 9.55E+01 1.16E+02 1.22E+02 1.23E+02
1.20E+02 1.07E+02 9.53E+01 7.65E+01 6.23E+01];;%xiangou's test
data - 1z
y_n = [2.42E+01 2.67E+01 3.73E+01 4.52E+01 4.81E+01 4.89E+01
4.40E+01 3.95E+01 3.00E+01 2.14E+01 1.74E+01];;%xiangou's test
data - 2z
%y_n = [2.98E+02 2.99E+02 2.93E+02 2.69E+02 2.57E+02 2.26E+02
1.86E+02 1.20E+02 5.91E+01 -1.34E+00 -3.47E+01];;%xiangou's
test data - 3z
%y_n = [4.81E+01 3.09E+01 5.79E+01 6.06E+01 5.00E+01 2.10E+01
1.92E+00 -8.99E+00 -2.02E+01 -1.39E+01 -4.87E+00];;%xiangou's
test data - 4z
%y_n = [-4.89E+02 2.06E+02 7.19E+02 8.05E+02 5.45E+02 -1.10E+01
-5.80E+02 -9.10E+02 -8.64E+02 -5.97E+02 -3.13E+02];;%xiangou's
test data - 5z
%y_n = [-9.27E+01 -1.32E+01 5.04E+01 7.61E+01 6.19E+01 1.69E+01
-3.65E+01 -7.47E+01 -7.73E+01 -5.66E+01 -2.99E+01];;%xiangou's
test data - 6z
%y_n = [-2.75E+01 -5.85E+01 1.13E+01 5.97E+01 5.29E+01 3.29E+01
-3.67E+01 -6.03E+01 -5.34E+01 -4.21E+01 -1.79E+01];;%xiangou's
test data - 7z
%y_n = [-1.57E+03 -9.09E+02 -1.18E+02 6.32E+02 7.60E+02 4.63E+02
-1.15E+02 -6.64E+02 -8.58E+02 -6.09E+02 -2.69E+02];;%xiangou's
test data - 8z
%y_n = [-2.83E+02 -3.88E+01 1.36E+02 1.28E+02 1.61E+01 -1.40E+02
-1.75E+02 -6.05E+01 1.14E+02 1.97E+02 1.63E+02];;%xiangou's
test data - 9z
%y_n = [-8.93E+02 -1.58E+02 4.20E+02 4.18E+02 3.37E+01 -4.90E+02
-5.60E+02 -1.01E+02 4.92E+02 6.62E+02 4.80E+02];;%xiangou's
test data - 10z
%y_n = [-1.26E+03 -2.16E+01 7.41E+02 4.27E+02 -2.04E+02 -
8.06E+02 -6.23E+02 1.79E+02 8.58E+02 7.88E+02
3.91E+02];;%xiangou's test data - 11z
%y_n = [-2.12E+03 -2.00E+02 1.06E+03 6.48E+02 -2.76E+02 -
1.20E+03 -8.56E+02 3.83E+02 1.26E+03 9.21E+02
1.27E+02];;%xiangou's test data - 12z
%y_n = [3.24E+02 -1.12E+02 -1.97E+02 1.26E+02 2.82E+02 1.18E+02
-1.76E+02 -1.99E+02 1.28E+02 3.03E+02 1.98E+02];;%xiangou's
test data - 13z
%y_n = [3.30E+02 -1.64E+02 -2.28E+02 1.77E+02 3.01E+02 5.42E+01
-2.81E+02 -1.83E+02 1.83E+02 3.35E+02 1.82E+02];;%xiangou's
test data - 14z
```

```

x_n = [0.50 0.45 0.40 0.35 0.30 0.25 0.20 0.15 0.10 0.05 0];
    %length of the workpiece, 0.54995/11 to match xiangou's test
    data - 1 mode
%x_n = [0 0.05 0.10 0.15 0.20 0.25 0.30 0.35 0.40 0.45 0.50];

sum_A = zeros(4,4); sum_B = zeros(4,1);

for j = 1 : n

    A = [cos(beta_n*x_n(j))^2
sin(beta_n*x_n(j))*cos(beta_n*x_n(j))
cosh(beta_n*x_n(j))*cos(beta_n*x_n(j))
sinh(beta_n*x_n(j))*cos(beta_n*x_n(j));
cos(beta_n*x_n(j))*sin(beta_n*x_n(j))
sin(beta_n*x_n(j))^2
cosh(beta_n*x_n(j))*sin(beta_n*x_n(j))
sinh(beta_n*x_n(j))*sin(beta_n*x_n(j));
cos(beta_n*x_n(j))*cosh(beta_n*x_n(j))
sin(beta_n*x_n(j))*cosh(beta_n*x_n(j))
cosh(beta_n*x_n(j))^2
sinh(beta_n*x_n(j))*cosh(beta_n*x_n(j));
cos(beta_n*x_n(j))*sinh(beta_n*x_n(j))
sin(beta_n*x_n(j))*sinh(beta_n*x_n(j))
cosh(beta_n*x_n(j))*sinh(beta_n*x_n(j))
sinh(beta_n*x_n(j))^2];

    B = [y_n(j)*cos(beta_n*x_n(j)); y_n(j)*sin(beta_n*x_n(j));
y_n(j)*cosh(beta_n*x_n(j)); y_n(j)*sinh(beta_n*x_n(j))];

sum_A = sum_A+A;    sum_B = sum_B+B;

end
%x = [C1; C2; C3; C4];

x = sum_A\sum_B

```